THE TORSIONAL BEHAVIOUR OF TRIANGULAR STRAND STEEL WIRE ROPES FOR DRUM WINDERS

Gerhard Rebel

A thesis submitted to the Faculty of Engineering, University of the Witwatersrand, in fulfilment of the requirements for the degree of Doctor of Philosophy.

Johannesburg
1997

CONTACT DETAILS

Author Contact Details, December 2002 :

Dr Gerhard Rebel
6 Calcot Court
Calcot
Reading
RG31 7RW
United Kingdom

Tel : +44-118-942-3238

Email : gerhard@bgisl.com

School of Mechanical, Industrial and Aeronautical Engineering

University of the Witwatersrand, Johannesburg :

http://www.wits.ac.za/fac/engineering/mech/index.htm

The University of the Witwatersrand owes its origins to the South African School of Mines which was founded in Kimberley in 1896. The School moved to Johannesburg in 1903 as the Transvaal Technical Institute and became the University of the Witwatersrand in 1922. In the same year Professor John Orr, who had been Professor of Mechanical and Electrical Engineering at the School of Mines since 1898, became the first De Beers Professor of Mechanical Engineering at the University. Professor Orr resigned his professorship in 1925 to organise technical education on the Witwatersrand, and later became the Director of the Witwatersrand Technical College. In the 1930's, in recognition of his contributions, his name was given to a Chair of Mechanical Engineering, and subsequently to a wing of the laboratory building.

In 1926, another distinguished Scot, Dr WJ Walker, succeeded Professor Orr, holding the Chair of Mechanical Engineering until 1952. Professor Walker established the laboratory and contributed significantly to engineering education in this country. He founded the Engineers' Association of South Africa to raise the status of professional engineers.

In 1960 the South African Institution of Mechanical Engineers launched a fund-raising campaign to endow two additional chairs in the Department. The Transvaal Industries Chair of Applied Mechanics was established in 1963 and the Chair of Fluid Mechanics, endowed by De Beers, was established in 1964. A further Chair, of Industrial Engineering, was established in 1970 and has been linked with the name of Barlows for many years.

One of the major developments in departmental activities was the introduction in 1962 of a part-time postgraduate coursework programme in Industrial Engineering leading to the Graduate Diploma in Engineering degree. In 1971 an Aeronautical Engineering degree was offered for the first time as an alternative to the Mechanical Engineering degree, with sponsorship from the aeronautical industry and the establishment of the Jack Davison Chair. In the same year the Department was converted into a School of Mechanical Engineering with three Branches and a rotating chairmanship.

Over the past few years, due to generous sponsorship from industry, additional Chairs were established and others were re-designated. Industry sponsored Chairs are now the Boart Longyear, Murray and Roberts, and Anglo American Corporation Chairs of Mechanical Engineering, the Eskom Chair of Design, and the Barlows Chair of Industrial Engineering.

Today the School awards on average some 80 BSc(Eng) and 40 postgraduate degrees and diplomas each year. The School enjoys formal international recognition of its degrees, through accreditation by the Engineering Council of the UK represented by the Institution of Mechanical Engineers, the Institution of Electrical Engineers (Manufacturing Division) and the Royal Aeronautical Society. The degrees are also accredited by the Engineering Council of South Africa.

Private Bag 3
WITS
2050
South Africa

Tel : +27-11-717-7323
Fax : +27-11-339-7997
Email : hjacobson@mech.wits.ac.za

Project Supervisor :

Prof H David Chandler

BSc(Leeds) MSc(Glasgow) PhD (CNAA), CEng, MIM

Reader in Mechanics of Materials and Associate Professor
Research Interests: Deformation and fracture in metals and composites, rheological properties of dense minerals slurries.

Background: Previously worked for United Steel in the UK (1961-1963). Was Research Assistant at Rugby College of Engineering and Technology (now part of Coventry University) in the UK (1969-1972) and Lecturer in Mechanical Engineering, University of Natal, Durban (1972-1973).

Papers: Has published numerous papers and attended local and international conferences on creep and deformation of metals, rheology of mineral slurries,

corrosion of glass fibres, mechanical properties of bio-materials and conformation of protein structures.

Email : hchand@mech.wits.ac.za
Office Telephone Number : +27-11-717-7340

School of Mechanical, Industrial and Aeronautical Engineering
University of the Witwatersrand, Johannesburg

REPORTS OF THESIS EXAMINERS

Published : 8/11/1997

EXAMINER A :

The thesis is concerned with an investigation into the torsional behaviour of steel wire ropes. This is a subject of current importance in the local context since the mines here are at present very deep and increasing shaft depths are being contemplated. In vertical shaft service, there is a tendency for conveyance ropes to twist as well as to elongate. Such twisting has implications for service life since fatigue resistance is lowered, there is a tendency for rope kinking and hence local weakening to occur etc.. As shaft depths are increased, problems arising from torsional behaviour increase and so a better understanding of such problems is required by the industry.

Mr. Rebel's work can be considered in three main sections :

(i) Development and commissioning of a tension - torsion test rig.

(ii) Obtaining test results both from laboratory measurements and from mine shafts.

(iii) Developing a model to predict in-shaft behaviour from laboratory tests and using it to determine likely rope behaviour in projected deeper shaft applications.

In all three aspects, Mr. Rebel's work is outstanding and novel in character. As far as the testing rig is concerned, this was based on an earlier design but has been greatly improved. In all probability, Mr. Rebel's rig (which belongs to the CSIR and will be used by them for future testing) is unique and is currently, probably the best machine in the world for this type of work.

Mr. Rebel then identified the test programmes required to produce critical results for behaviour estimation. A comprehensive laboratory testing programme was carried out in parallel to obtaining data on ropes in service. The data collected is probably unique in the South African context and useful since it should give operators a better guide as to how ropes are behaving in deep shafts. Finally, a model was developed to predict in-service torsional behaviour from the laboratory programme. Previous models have over-predicted twisting behaviour by a factor of five. The new model is based on the realisation that inter-wire friction effects and consequent hysteresis behaviour must be treated as a first order effect rather than ignored as has been the case in earlier modelling attempts. Very good correlations were obtained, using laboratory tests and the new model for twisting behaviour to calculate behaviour of long ropes, with the in-shaft behaviour observed.

With projected increases in shaft depths in the next few years, Mr. Rebel's work will provide a key element in rope selection and design. Candidate ropes can be tested on the machine designed and built during this work according to the testing programme developed. The model developed by Mr. Rebel can then be used to predict in-shaft performance with a good degree of confidence.

EXAMINER B :

The candidate has carried out an investigation of the torsional properties of triangular strand wire rope such as commonly used for deep shaft hoisting in South African hard rock mining. Using a mathematical model of the highly non-linear behaviour of triangular strand ropes he has analysed the torsional deformations in hoisting ropes, at installation, as they change during loading of a conveyance, and as they change during the service life of the rope.

The candidate has shown a detailed understanding of prior work, carried out both in South Africa and elsewhere, that relates to both rope torsional behaviour and to rope rotation in mine hoist systems. The experimental work to characterise rope has involved the development of special testing techniques and procedures. These results have then been used as input to an analysis of rope deformation taking full account of the non-linear characteristics, the analytical method developed includes many novel features. Having verified the model through comparison with measurements of rope rotation in a number of different shafts, the candidate has gone on to investigate the influence of different variables on deformation in shafts of greater depth than currently in use.

Throughout the thesis the candidate has given a full justification of assumptions made, and considered sources of error, and accounted for discrepancies between predictions and measurements.

The work which has been performed in this investigation constitutes a major contribution to knowledge and understanding of deep hoisting using triangular strand ropes. The South African mining industry is on the brink of committing to shafts of far greater depth than are in current use, anywhere in the world. The greatest area of uncertainty in this development is the behaviour of the rope, and in terms of extending hoisting depth with triangular strand ropes, the torsional response is the key factor. The outcome of this investigation provides a significant step towards resolving many of the questions raised. It is very important that the work which has been done here is refined and developed: the mining industry and research community must co-operate to take full advantage of the opportunity provided.

This is an excellent piece of work and the candidate thoroughly deserves the award of the degree. The thesis is well presented and with such a small number of trivial typographical errors (none of which impair the meaning) that in my view it should be accepted without amendment.

Issues which should be given further consideration include:

- The possible effects of service degradation on torsional properties (especially the no-slip to full-slip transition); the influence of lubricant on torsional behaviour (there is a degree of confusion as to what the lubrication policy was during the bedding in process);

- Whether any higher degree of consistency would result from the adaptation of the rope test facility to operation with full closed loop control for both tension and rotation.

- The causes for such a different response from the ropes constructed from galvanised wire.

- The apparent scale effect showing lower rotation from smaller diameter wires (which could well be simply the effect of a higher wire to rope diameter ratio giving higher torsional stiffness).

- The influence of torsional cycling on fatigue degradation (which could be beneficial).

- The effects of operating with long lay length on fatigue degradation, and so the impact on service endurance of letting out turns during maintenance (this could serve to motivate a change in maintenance policy, providing extended life for existing installations).

- Recommendations for detailed recording of turns let out during maintenance.

- The impact of rope construction variables (such as plastication) on torsional behaviour.

It has been both a pleasure and a privilege to be an external examiner of this thesis. I sincerely hope that every effort will be made to promote and pursue this work which has considerable potential value to industry as a tool to establish the ultimate limits to the depths to which triangular strand hoisting rope can safely and economically operate.

EXAMINER C :

Examiners review of the doctor's thesis prepared by Mr. Gerhard Rebel under the title "The Torsional Behaviour of Triangular Strand Steel Wire Ropes for Drum Winders"

1 General valuation at the thesis

The discussed thesis contains 318 typescript pages in total, including 29 tables, 198 figures and photographs and list of references containing 106 items. The thesis is preceded by the declaration, abstract, acknowledgements as well as specification of notations, symbols and units. The whole has been divided in 8 chapters, the first of which contain the introduction, analysis of bibliography, description of the development of laboratory tests, and the subsequent ones : method of conducting the experiments, modelling studies of torsional rope behaviour, results of measurements and calculations, discussion of the results, summary and recommendations. Included in the thesis are four appendices containing the discussion of: effect of the rope lay length changes on rope tensile properties, ie. breaking strength, torque, modulus of elasticity of the rope, changes of the rope lay between the pulley and drum and the point of fastening of the rope in the suspension, results of in-service measurements of the torque changes, as well as the graphical method to determine the rope lay lengths in the mine.

The present review does not contain a synopsis of the thesis limiting itself to its merits and drawbacks and the final assessment in the view of the requirements contained in the INFORMATION FOR GUIDANCE OF EXAMINERS OF A THESIS FOR THE DEGREE OF DOCTOR OF PHILOSOPHY.

The general valuation of the thesis is high.

2 Analysis of the thesis

2.1 Assessment of correctness of the subject

The subject of the examined doctor's thesis is the torsional behaviour of triangular strand steel wire ropes used in shaft drum winders at great depths (from 1000 to 2500 m). The subject is important and up-to-date, and very interesting both in theoretical and practical respect. The use of triangular strand lang's lay hoisting ropes in great-depth shafts creates serious problems both in respect of durability and safety of rope operation. Keeping this in mind it is to be said that the subject of the thesis has been selected correctly.

2.2 Substantive evaluation of the thesis

The Author has carried out a very detailed analysis of home and foreign bibliography, showing his many-sided orientation in the subject of torsional behaviour of ropes and in proper evaluation and classification of the discussed sources.

The principal merit of the thesis is a large and systematic range of tests conducted and an extensive analysis of their results. This constitutes a nearly monographic character in relation to-date publications in the subject which in their majority, were narrow-ranged and based on fragmentary measuring material. On analysing the obtained results, the Author has demonstrated good knowledge and skill in using matrix calculus and methods of statistical analysis of the measurements results as well as approximation of the obtained functional relationships with empirical equations.

A great achievement of the thesis there is the development of a new method of modelling the torsional behaviour of the rope. The Author has elaborated mathematical models enabling for mutual connection of such parameters as the torque, length of lay, number of rotations, torsional stillness, length of rope, load value, state of twist. The models can serve various analyses (both qualitative and quantitative), depending on the changes of individual parameters. Of interest there are the matrix relationships (5.3), page 109, between the load torque and twist of the rope. The results of analysis have been presented on pages 104 to 135. The Author has carried out verification of the proposed method using the results of laboratory and in-mine measurements obtained with the use of triangular strand ropes with the diameter range from 25 to 54 mm.

He has presented an extensive analysis of the results of calculations in Chapter 6. On page 142, a joint effect has been presented in a graphical form of the length of hanging rope and the degree of its twist (untwist, twist) on the change of the torque and torsional stillness of the rope. In Chapter 7, the Author has presented a detailed discussion of the obtained results and considerations. It follows from this, that the results of the thesis are not only of cognitive but also of utilitarian value, which has allowed the Author to formulate in conclusion several recommendations being of validity for mine practice.

The thesis is characterised by exceptionally careful elaboration. Beautiful also is its extremal form (type, drawings, montage) and accurate proof-reading.

3 Questions open to discussion

3.1 The volume of the thesis is too extensive, it contains more than 300 pages. Without any loss to its scientific value, the thesis could have contained approximately 150 pages.

3.2 The thesis does not contain a distinctly formulated point - may be it does not have to. In our country the doctor's thesis should contain the point placed after the review of bibliography.

4 Concluding remarks

After making a detailed analysis of Mr. Gerhard Rebel's thesis, I state the following :

4.1 The thesis constitutes an original solution of the problem of torsional behaviour of mine hoisting triangular strand ropes in mine drum winders and shafts of great depth. The method points at a high Author's knowledge and proficiency in methods of testing.

4.2 The Author has carried out a wide range of properly planned theoretical and experimental investigations. In the laboratory tests, he was using his own original method to measure the torque, elongation diameter and length of lay of the ropes. In the in-mine tests he applied a video technique not used so far.

4.3 The thesis constitutes an important contribution to the progress of knowledge in the domain of steel wire ropes and shaft hoisting. The modelling method of triangular strand ropes has also been presented which points at the possibility to use them in shafts of depths greater than 2500 m. However, the defined requirements must be met in relation to operation (rope maintenance) as well as manufacture of triangular strand ropes of great lengths.

DECLARATION

I declare that this thesis is my own unaided work. It is being submitted for the Degree of Doctor of Philosophy in the University of the Witwatersrand, Johannesburg. It has not been submitted before for any degree or examination in any other University.

GRebel.

Gerhard Rebel

First day of July 1997.

ABSTRACT

The torsional behaviour of Lang's lay triangular strand ropes will probably limit their application in ultra deep (2500 m - 4000 m) single lift shafts. These ropes have traditionally been used on the majority of South African drum winding systems and it would be beneficial if their application could be extended as far as possible. An improved understanding of the macroscopic factors which may lead to construction instability is however required. The objective of this study has been the determination and verification of a model to predict the static torsional behaviour of triangular strand ropes operating on drum winders. Rope lay length changes at installation; alterations in lay length with service period; rope rotation during conveyance loading and equilibrium rope torques were the primary variables of interest. A wire rope tension-torsion testing machine has been developed for conducting tests under constant twist, load and torque conditions. The relationship between load and torque, for constant twists, is used to determine the in-service lay length distributions. It has been found that the lay length at which a rope is manufactured significantly affects the in-shaft boundary conditions in the lay length analysis. Correct lay length distributions values, in the suspended rope section, are a prerequisite for the rotation calculations. The rotation analysis takes into account changes in rope torsional stiffness resulting from the no-slip to slip transition, between the rope wires, associated with twist displacements. This varying torsional stiffness characteristic is a function of the rope load and state of twisting (lay length). The hysteresis response during constant load tests, constitutes a first order effect, but it has been ignored in previous attempts at calculating in-service rope rotation. Consequently, far more rotations were forecast than is actually the case. With the new model, rope lay length and rotation predictions compare favourably with actual measured behaviour in existing shafts. The results of in-service lay length and rope rotation measurements, conducted in shafts up to 2500 m deep, are also presented. Parameters which have the greatest influence on the torsional behaviour of triangular strand ropes in vertical shafts have been identified and recommendations are made on how the depth limit of application for these ropes may be extended.

To my parents,

Mr and Mrs A.F.W. Rebel

for their support and encouragement

ACKNOWLEDGEMENTS

I would like to thank the following persons and organisations for their notable contribution to the study described in this thesis :

The CSIR Mine Hoisting Technology Division for allowing unlimited access to their laboratory test equipment, computer facilities and technical library and for financing the tension-torsion machine development project.

Prof. H.D. Chandler for his constructive guidance, advice and patience throughout the duration of the project.

The Engineering management of Gold Fields of South Africa and GENCOR Limited for arranging access to their mine shafts for the site measurements. Also the Engineering staff on the mines for their assistance in conducting the measurements.

GENCOR Limited, in particular Mr. D.E. Field for allowing me the time to complete this investigation.

The University of the Witwatersrand and the Foundation for Research Development for the financial support.

The staff of the Mechanical Engineering Laboratory of the University of the Witwatersrand for their assistance with the upgrading of the tension–torsion testing machine.

Mr. M. Borello for introducing me to the topic of drum winder rope torsional behaviour in 1993 and for this administrative and technical assistance during the tension-torsion machine development project.

Messrs M. Borello, D.B. Coward, R.A. Greer, R.E. Gundersen, G.F.K Hecker, T.C. Kuun, P.S. Laubscher and M.N. van Zyl for the valuable discussions on matters relating to the behaviour and operation of steel wire ropes and mine hoisting in general.

Haggie Rand Limited for supplying the rope samples for the laboratory testing, and for allowing access to their manufacturing records and technical library.

CONTENTS

	Page
DECLARATION	i
ABSTRACT	ii
ACKNOWLEDGEMENTS	iv
CONTENTS	v
LIST OF FIGURES	x
LIST OF TABLES	xvi
LIST OF SYMBOLS	xvii
LIST OF TERMS AND ABBREVIATIONS	xxiii
1 INTRODUCTION	1
1.1 Shaft and hoisting systems for gold mining in South Africa	1
1.2 Typical shaft and winder layout	10
1.3 The significance of hoisting depth as regards torsional behaviour	12
1.4 The effect of lay length on rope mechanical properties	16
1.5 Study objectives, scope and motivation	18
1.6 Thesis structure	21
2 LITERATURE REVIEW	24
2.1 Introduction	24
2.2 Triangular strand rope construction	26
2.3 Tension-torsion testing of wire ropes and strands	28
2.4 Wire rope torsional behaviour	39
2.5 In-service rope rotation measurement	53
2.6 Rope lay length measurement	54
2.7 Summary	56

3 DEVELOPMENT OF THE LABORATORY TESTING FACILITY 58

3.1 Torsion testing machine history and requirements 58
3.2 Torque-tension machine description 60

3.2.1 General layout 60
3.2.2 Electrical and hydraulic control system 63
3.2.3 Load and torque measurement 63
3.2.4 Elongation measurement 64
3.2.5 Diameter and lay length measurement 67

3.3 Control software 71
3.4 Examples of test variable control 74

4 EXPERIMENTAL APPROACH 78

4.1 Mine shaft measurements 78

4.1.1 Shaft measurement scope 78
4.1.2 Rope lay length measurements 84
4.1.3 Rope rotation measurements 86

4.2 Laboratory based rope tension-torsion tests 87

4.2.1 Scope of laboratory testing 87
4.2.2 Rope specimen preparation and installation 89
4.2.3 Transducer zero values and torque - rotation convention 92
4.2.4 Bedding in cycles 92
4.2.5 Constant twist tests 94
4.2.6 Constant load tests 96

5 MODELLING OF ROPE TORSIONAL RESPONSE 100

5.1 Rope lay lengths in design and manufacture 100
5.2 Rope installation on a drum winder 106
5.3 Installation equilibrium conditions 108
5.4 The effect of rope maintenance on lay length variations 119
5.5 Rope torsional stiffness properties 124
5.6 Response of a rope to changes in conveyance load 133
5.7 Calculation of rope rotation during conveyance loading 134

6 MEASURED AND CALCULATED RESULTS 137

6.1 Presentation of results 137
6.2 Detailed results for shaft E, 46 mm rope at 2403 m 138
6.3 Summary of the results for ropes S1 to S12 and S14 to S22 148

6.3.1 Shaft A, 41 mm ropes at 1071 m 148
6.3.2 Shaft B, 41 mm ropes at 1529 m 152
6.3.3 Shaft C, 46 mm ropes at 1426 m 155
6.3.4 Shaft D, 46 mm ropes at 1426 m 157
6.3.5 Shaft F, 48 mm ropes at 2196 m 159
6.3.6 Shaft G, 49 mm ropes at 1126 m 162
6.3.7 Shaft H, 49 mm ropes at 1068 m 165
6.3.8 Shaft J, 49 mm rope at 1599 m 167
6.3.9 Shaft K, 49 mm rope at 1935 m 169
6.3.10 Shaft L, 54 mm rope at 1887 m 171

6.4 Accuracy of the modelling approach 173

6.4.1 In-service lay length and rotation measurements 173
6.4.2 Installation lay lengths and loss of rotation 174
6.4.2 Torsion test lay length measurements 176
6.4.4 Empirical equation for torsion test lay lengths 177

6.5 Factors influencing the calculated results 179

6.5.1 The effect of galvanised wires on torsional hysteresis 179
6.5.2 Torsional stiffness variation with changes in lubrication 181
6.5.3 Reasons for considering the loading values of torque from the constant twist tests 183
6.5.4 Calculation of intermediate values of the torsional stiffness constants 185
6.5.5 Use of the average twisting up and untwisting torsional responses 189

6.6 Additional results regarding rope torsional behaviour in general 193

6.6.1 Rotation of the splice end during detachment from the conveyance 193
6.6.2 Rope rotation and lay length changes as a result of load release 194
6.6.3 Calculation of rope rotation during winder emergency braking 195

7 DISCUSSION 199

7.1 The importance of considering torsional hysteresis 199
7.2 Effects of in-service rotation boundary conditions 202
7.3 Factors influencing in-service torsional behaviour and the implications for future shaft systems 204

7.3.1 Selection of shaft parameters for analysis 205
7.3.2 Rope diameter 208
7.3.3 Rope weight per unit length 211
7.3.4 Influence of conveyance weight to payload ratio 213
7.3.5 Manufactured lay length 214
7.3.6 Total installed rope length 216
7.3.7 Parameters which have the greatest effect on the static rope torsional behaviour 217

7.4 The limit of triangular strand rope application and possible solutions 219

8 CONCLUSIONS AND RECOMMENDATIONS 223

8.1 Torsional properties of triangular strand ropes 223
8.2 Modelling of rope torsional behaviour 224
8.3 In-service torsional behaviour 224
8.4 Recommendations relating to modelling of rope torsional behaviour 226
8.5 Recommendations relating to the operation of triangular strand ropes 226
8.6 Recommendations relating to the design and manufacture of triangular strand ropes 227

APPENDICES

A : THE EFFECT OF LAY LENGTH ON ROPE TENSILE PROPERTIES 228

A.1 Equipment 229
A.2 Tensile test results 230
A.3 Torsion test results for calculating failure torque 233
A.4 Comments relating to the tensile test results 235
A.5 Rope modulus calculation 236

B : VARYING TWIST BETWEEN THE SHEAVE WHEEL AND DRUM CONNECTION POINT 241

C : IN-SERVICE ANALYSIS DETAILS 246

C.1 Analysis details for shaft A, ropes S1 to S4 247
C.2 Analysis details for shaft B, ropes S5 to S8 250
C.2.1 Torsion test constants for rope T8 253
C.3 Analysis details for shaft C, ropes S9 and S10 255
C.4 Analysis details for shaft D, ropes S11 and S12 257
C.5 Analysis details for shaft F, ropes S14 and S15 259
C.5.1 Torsion test constants for rope T10 260
C.6 Analysis details for shaft G, ropes S16 and S17 262
C.7 Analysis details for shaft H, ropes S18 and S19 264
C.8 Analysis details for shaft J, rope S20 266
C.9 Analysis details for shaft K, rope S21 268
C.9.1 Torsion test constants for rope T11 269
C.10 Analysis details for shaft L, rope S22 271
C.10.1 Torsion test constants for rope T12 272

D : GRAPHICAL METHOD FOR DETERMINING ROPE LAY LENGTHS AT INSTALLATION 274

D.1 Theory 275
D.2 Position at which the manufactured lay length occurs 276
D.3 Information required for the graphical solution 277
D.4 Procedure for determining estimates of the installation lay lengths 278
D.5 Curves for graphical lay length solution 279

REFERENCES 288

LIST OF FIGURES

Figure	Description	Page
1.1 -	Surface inclined and compound shafts	2
1.2 -	Configuration of a bi-cylindrical-conical drum winder	4
1.3 -	Distribution of drum winders serving vertical shafts deeper than 200 m	6
1.4 -	Future mine development options for the South African gold mining industry	8
1.5 -	Current and future shaft system elevations	9
1.6 -	Example of a circular shaft cross-section	11
1.7 -	Surface vertical shaft and rock winder elevation	12
1.8 -	Maximum amplitude of torsional oscillation during emergency braking	13
1.9 -	Ground and tower mounted Koepe friction winders	15
1.10 -	Project outline	20
2.1 -	Triangular strand rope cross-section	27
2.2 -	Suspension method for determining torsional rigidity and rope rotation	29
2.3 -	Tension-torsion testing machine of Anglo Continental Ropes	30
2.4 -	Torsion testing equipment used in Poland	31
2.5 -	The application of torsion testing in the design of low rotation balance ropes	32
2.6 -	Typical measured torsional response of stranded wire rope	32
2.7 -	Apparatus for measuring the torque and twist angle of wire rope	33
2.8 -	Rig for testing of wire strand	34
2.9 -	"Extrometer" developed by Utting and Jones (1985)	34
2.10 -	Test equipment for static and dynamic torsion tests on spiral strands	35
2.11 -	Testing machine for investigations into the effect of fluctuating load and twist on rope endurance	36
2.12 -	Rope rotation along a test section	37
2.13 -	Six strand rope element	39
2.14 -	Rope rotation and twist in a vertically suspended rope	40
2.15 -	Basic equations for describing rope torsional response	47
2.16 -	Measured parameters of a double drum rock winder during a winding cycle	50
2.17 -	Main components of a "jig-back" rope way (a) and the torsional response of Lang's lay ropes compared to ordinary lay ropes (b)	51
2.18 -	Torque versus twist relationship for a 39 mm structural strand	53
2.19 -	The "chalk line" method of determining rope rotation	54
2.20 -	Lay length measuring device	55
3.1 -	Configuration of an universal wire rope fatigue testing machine	58
3.2 -	General arrangement of the steel wire rope torque-tension testing machine	61
3.3 -	View of the steel wire rope torque-tension testing machine	62
3.4 -	View of the scissor mechanism at the rear of the hydraulic cylinder	62
3.5 -	Basic configuration of the machine control system	63
3.6 -	View of the load cell	64
3.7 -	Arrangement of the rope elongation measurement system	65

3.8 -	Tension cylinder end, LVDT configuration	66
3.9 -	Rotation end, LVDT configuration	66
3.10 -	Optical shaft encoder for end rotation measurement	67
3.11 -	Configuration of the rope diameter measurement jig	68
3.12 -	View of the rope diameter measurement jig	68
3.13 -	Wide jaw vernier for manual rope diameter measurement	69
3.14 -	Operation of the parallel V-block lay length measurement gauge	70
3.15 -	Views of the lay length measurement gauge	70
3.16 -	Structure of the testing machine control software menu system	71
3.17 -	Relationship between the measured load and the control voltage for the hydraulic cylinder	72
3.18 -	Relationship between the measured rotation head speed and the control voltage for the hydraulic motor	73
3.19 -	Example of a load and rotation control algorithm	73
3.20 -	Example of constant end rotation test parameter input screen	74
3.21 -	Constant end rotation (twist) test, parameter variations with time	75
3.22 -	Constant load test, parameter variations with time	75
3.23 -	Constant torque test, parameter variations with time	76
3.24 -	Load cycle test at constant twist, parameter variations with time	76
3.25 -	Rotation (twist) cycle test at constant load, parameter variations with time	77

4.1 -	Distribution of six strand rope diameters used on vertical shaft drum winders	79
4.2 -	Distribution of six strand rope constructions (wires per strand) used on vertical shaft drum winders	80
4.3 -	Distribution of six strand rope tensile grades (of roping wires) used on vertical shaft drum winders	80
4.4 -	Rope diameters and shaft depths considered for investigation	81
4.5 -	In-service lay length measurement position	84
4.6 -	Rope rotation measurement method applied to a rock winder rope	86
4.7 -	Process of loading a locomotive into a man cage	87
4.8 -	Test specimen preparation dimensions	89
4.9 -	Detail of the cast white metal collar and end cone	90
4.10 -	A test specimen installed in the tension-torsion machine	91
4.11 -	Effect of bedding in cycles on the constant twist test results	93
4.12 -	Two methods of limiting the maximum rope torque during a constant twist test	95
4.13 -	Constant load test based on the load and twist ranges of the constant twist test	97
4.14 -	A series of constant load tests to determine the detailed hysteretic torsional response	99
4.15 -	Tangent torsional stiffness variations calculated from the data in figure 4.14	99

5.1 -	Positions where quality control lay lengths are measured during rope manufacture	101
5.2 -	Distribution of "on tension" lay lengths measured during the manufacture of triangular strand ropes	102
5.3 -	Variations in "on tension" lay lengths for different diameters	102
5.4 -	New rope test lay lengths (free) for different rope diameters	103
5.5 -	Example of rotation in a manufactured coil relative to a torsion test specimen	104
5.6 -	Rotation in the manufactured rope in relation to the hoisting system geometry	106

5.7 -	Installation of a new rope on a single drum winder	107
5.8 -	The doubling down arrangement to ensure adequate tension in the dead coils	108
5.9 -	General relationship between load, torque and twist for Lang's lay triangular strand ropes	109
5.10 -	General form of the twist distribution in a rope after installation	113
5.11 -	General form of the rope rotation distribution after installation	113
5.12 -	General form of the lay length variation in a rope after installation	114
5.13 -	General form of the equilibrium rotation distribution after installation	116
5.14 -	General form of the equilibrium lay length variation after installation	118
5.15 -	A method of determining the rotation lost from a rope when it is detached from the conveyance	120
5.16 -	Change in the rope rotation distribution as a result of a loss in rotation from the rope	123
5.17 -	Change in the rope lay length variation as a result of a loss in rope rotation	123
5.18 -	General form of the torque surface defined by equation [5.3]	125
5.19 -	Accurate and approximate methods of calculating the torsional stiffness from constant twist test data	126
5.20 -	Example of the variation in rope torque while twisting at constant load	128
5.21 -	Example of the variation in rope torsional stiffness for a change in twist, from a stationary position, at constant rope load	128
5.22 -	Examples of variations in rope torsional stiffness for different loads and directions of twisting	130
5.23 -	Examples of variations in the constants a_{cl} , b_{cl} and c_{cl} with rope load and state of twisting	132
5.24 -	Changes in rope torque as a result of conveyance loading	133
5.25 -	Relationship between change in torque and change in twist along the suspended rope length	135
5.26 -	Example of the torsional stiffness variation along the suspended rope length	135
5.27 -	Rope rotation distribution for a loaded conveyance in relation to the empty rotation distribution	136

6.1 -	Measured and calculated rope torque versus load for rope T9	139
6.2 -	Measured and calculated rope torque versus load for rope T9	139
6.3 -	Equilibrium rope torques for rope S13 in relation to torsion test data	140
6.4 -	Torsional response due to changes in twist along the suspended length of rope S13	142
6.5 -	Variation in torsional stiffness for changes in twist from a stationary position, rope S13	142
6.6 -	Measurement and analysis results for rope S13	145
6.7 -	Detail of calculated and measured lay lengths for rope S13	147
6.8 -	Measurement and analysis results for ropes S1, S2 and S3	150
6.9 -	Measurement and analysis results for rope S4	151
6.10 -	Measurement and analysis results for rope S5	153
6.11 -	Measurement and analysis results for ropes S6, S7 and S8	154
6.12 -	Measurement and analysis results for ropes S9 and S10	156
6.13 -	Measurement and analysis results for ropes S11 and S12	158
6.14 -	Calculated and measured lay lengths for rope S14	160
6.15 -	Measurement and analysis results for rope S15	161

6.16 - Calculated and measured lay lengths for rope S16 and S17, at installation and at discard 163
6.17 - Measurement and analysis results for rope S16 164
6.18 - Measurement and analysis results for ropes S18 and S19 166
6.19 - Measurement and analysis results for rope S20 168
6.20 - Measurement and analysis results for rope S21 170
6.21 - Measurement and analysis results for rope S22 172
6.22 - Differences between the calculated (LL_e) and measured lay lengths for ropes S1 to S22 173
6.23 - Differences between the calculated ($\Delta\Phi$) and measured rope rotations during conveyance loading for ropes S1 to S22 174
6.24 - Correlation between service period and the rotation lost per unit length of suspended rope, for ropes S1 to S22 175
6.25 - Distribution of torsion test lay length errors 176
6.26 - Distribution of torsion test lay length errors 178
6.27 - Measured torsional hysteresis at constant load for **ungalvanised**, 40 mm, triangular strand ropes 180
6.28 - Measured torsional hysteresis at constant load for **galvanised**, 40 mm, triangular strand ropes 180
6.29 - Ratio of measured torsional stiffness for a specimen with and without lubricating oil applied 181
6.30 - Illustration of the effect of maximum load during a constant twist test on the shape of the fitted torque curves 184
6.31 - Linear extrapolation of torque versus load data based on the upper 20 percent of the measured results, rope T9 184
6.32 - Accurate method of determining the torsional response constants at an intermediate constant load and starting twist 185
6.33 - Torsional stiffness errors resulting from interpolation within the matrices a_{cl}, b_{cl} and c_{cl} 187
6.34 - Accurate and approximate methods of determining the torsional response constants at intermediate loads and starting twist values 188
6.35 - Measured rope end load and rope torque during conveyance loading 189
6.36 - Rope rotation and twist during loading determined using the twisting up and untwisting rope stiffness characteristics 191
6.37 - Rope rotation and twist during loading determined using the twisting up and untwisting rope stiffness characteristics 192
6.38 - Calculated and measured rotation of the splice end during detachment from the conveyance 193
6.39 - Lay length distributions for an empty conveyance and for zero end load 194
6.40 - Schematic illustration of the mid-shaft rope rotation during winder emergency braking 196
6.41 - Calculated maximum rope rotation amplitude during winder emergency braking for an empty conveyance being hoisted up the shaft 197

7.1 - Comparison between torsional stiffness inferred from the constant twist test and the full slip stiffness (c_{cl}) determined from the constant load tests 200
7.2 - Effect of torsional hysteresis on the calculation of rope rotation during conveyance loading 201

7.3 - Comparison of the effect of rotation boundary conditions on the general rotation distribution in a suspended rope 202
7.4 - Effect of rotation boundary conditions on the calculated lay lengths at installation 203
7.5 - Calculated variation in splice and sheave end lay lengths for different rope diameters and shaft depths 208
7.6 - Calculated variation in the maximum rope rotation during conveyance loading for different rope diameters and shaft depths 210
7.7 - Calculated variation in rope torque for different rope diameters and shaft depths 210
7.8 - Calculated variation in the maximum allowable end load for different rope diameters and shaft depths 211
7.9 - Calculated variation in splice and sheave end lay lengths for changes in the rope weight per unit length at different depths 212
7.10 - Calculated variation in the maximum rope rotation during conveyance loading for changes in the rope weight per unit length at different depths 212
7.11 - Calculated variation in splice and sheave end lay lengths for changes in the conveyance weight to payload ratio at different depths 213
7.12 - Calculated variation in the maximum rope rotation during conveyance loading for changes in the conveyance weight to payload ratio at different depths 214
7.13 - Calculated variation in splice and sheave end lay lengths for changes in the manufactured lay length at different depths 215
7.14 - Calculated variation in the maximum rope rotation during conveyance loading for changes in the manufactured lay length at different depths 215
7.15 - Calculated variation in splice and sheave end lay lengths for changes in the length of rope between the sheave and drum connection point 216
7.16 - Calculated variation in the maximum rope rotation during conveyance loading for changes in the length of rope between the sheave and drum connection point 217
7.19 - Option for reducing the weight of triangular strand ropes while maintaining the breaking strength and diameter 221

A.1 - The use of a collar mounted torque clamp for altering rope lay length prior to tensile testing 229
A.2 - Detail of the collar mounted torque clamp 229
A.3 - Variation in breaking strength with lay length for a 25 mm diameter Lang's lay triangular strand rope 230
A.4 - The effect of lay length on energy absorption at failure for a 25 mm diameter Lang's lay triangular strand rope 231
A.5 - Total strain at failure for a 25 mm diameter Lang's lay triangular strand rope with different lay lengths 232
A.6 - Torque versus load response for rope T1 233
A.7 - Relationship between the applied twist and lay length for rope T1 234
A.8 - Estimated failure torque for a 25 mm diameter Lang's lay triangular strand rope with different lay lengths 235
A.9 - Strain versus stress for zero twist, rope T1 236
A.10 - Rope modulus variation with applied stress for different lay lengths, rope T1 237
A.11 - Modulus range for different lay lengths, rope T1 239
A.12 - Approximated and expected actual rotation and twist distribution for a torsion test specimen 240

B.1 - Twist variation along the length of a rope, with a linear change in twist from the sheave wheel to the drum connection point 242
B.2 - The effect of varying *Df* on the rotation distribution between the sheave and drum connection point 244

C.1 - Equilibrium rope torques for ropes S1, S2 and S3 in relation to the torsion test data 248
C.2 - Equilibrium rope torques for rope S4 in relation to torsion test data 249
C.3 - Equilibrium rope torques for rope S5 252
C.4 - Equilibrium rope torques for ropes S6, S7 and S8 252
C.5 - Measured and calculated rope torque versus load for rope T8 253
C.6 - Equilibrium rope torques for ropes S9 and S10 256
C.7 - Equilibrium rope torques for rope S11 and S12 258
C.8 - Equilibrium rope torques for rope S15 260
C.9 - Measured and calculated rope torque versus load for rope T10 260
C.10 - Equilibrium rope torques for rope S16 263
C.11 - Equilibrium rope torques for ropes S18 and S19 265
C.12 - Equilibrium rope torques for rope S20 267
C.13 - Equilibrium rope torques for rope S21 269
C.14 - Measured and calculated rope torque versus load for rope T11 269
C.15 - Equilibrium rope torques for rope S22 in relation to the torsion test data 272
C.16 - Measured and calculated rope torque versus load for rope T12 272

D.1 - A graphical method for determining the equilibrium lay length distribution 275
D.2 - Position along the suspended rope length at which the manufactured lay length occurs 276
D.3 - Position along the suspended rope length at which the manufactured lay length occurs 277
D.4 - Approximate values of r_{LLm} for graphical lay length solution method 280
D.5 - Data for graphical lay length solution method, rope T1 281
D.6 - Data for graphical lay length solution method, rope T4 282
D.7 - Data for graphical lay length solution method, rope T8 283
D.8 - Data for graphical lay length solution method, rope T9 284
D.9 - Data for graphical lay length solution method, rope T10 285
D.10 - Data for graphical lay length solution method, rope T11 286
D.11 - Data for graphical lay length solution method, rope T12 287

LIST OF TABLES

Table	Description	Page
1.1 -	Maximum and minimum values of test parameters for the investigation of the effect of lay length on tensile test results	18
3.1 -	Measurement specifications of the tension-torsion testing machine	60
4.1 -	Shaft and rope details for in-service measurements	83
4.2 -	Important shaft and rope data obtained from the shaft engineers	85
4.3 -	Ropes on which torsion tests were conducted	88
4.4 -	Initial measured parameters of the torsion test rope samples	93
4.5 -	Load and twist ranges used for the constant twist tests	94
4.6 -	Test loads and twists for the various torsional stiffness tests	98
5.1 -	Steps of the numerical scheme for solving for the constant torque, *M*	111
5.2 -	Steps of the numerical procedure for determining the torsional equilibrium conditions after installation	117
5.3 -	Example of the effect of varying Df on the rotation and lay length distribution in a rope	118
6.1 -	Analysis and torsion test data for rope S13	144
6.2 -	Constants of the lay length versus twist equation for the twelve torsion test ropes	177
6.3 -	Calculated variation in the maximum rotation during conveyance loading for increased lubrication of a torsion test specimen	182
6.4 -	Examples of variations in the calculate maximum rotation using accurate and approximate a_{cl} , b_{cl} and c_{cl} interpolation	186
7.1 -	Details of ropes considered in investigating the factors influencing torsional behaviour	207
A.1 -	Strain versus stress constants for equation [A.2], rope T1	238
C.1 -	Analysis data for ropes S1, S2 and S3	247
C.2 -	Analysis data for rope S4	249
C.3 -	Analysis data for rope S5	250
C.4 -	Analysis data for ropes S6, S7 and S8	251
C.5 -	Analysis data for ropes S9 and S10	255
C.6 -	Analysis data for ropes S11 and S12	257
C.7 -	Analysis data for ropes S14 and S15	259
C.8 -	Analysis data for rope S16	262
C.9 -	Analysis data for ropes S18 and S19	264
C.10 -	Analysis data for rope S20	266
C.11 -	Analysis data for rope S21	268
C.12 -	Analysis data for rope S22	271

LIST OF SYMBOLS

Symbol	Description	Units
$\Delta\Phi_{max}$	Maximum calculated rope rotation during conveyance loading	(turns or °)
$\Delta\Phi_{trip}$	Maximum dynamic rotation amplitude encountered during winder emergency braking	(turns or °)
δF_{cl}	Load error for a constant load test, relative to the constant load F_{cl}	(kN)
Δl	Change in gauge length, l_0 , of a torsion test specimen	(mm)
ΔM	Change in torque along the rope required for the loaded conveyance equilibrium state, $f(z) = M_f - M_{f,Re}$	(Nm)
δM_{cl}	Torque error determined from the load error, δF_{cl} , measured during a constant load test	(Nm)
ΔM_t	Change in torque determined for a change in twist at constant load, constant twist test data	(Nm)
ΔM_{twist}	Change in torque at constant load as a result of twisting up the rope	(Nm)
$\Delta M_{untwist}$	Change in torque at constant load as a result of untwisting the rope	(Nm)
ΔR	Change in twist required to achieve ΔM, $f(z)$	(°/m)
ΔR_t	Change in twist associated with ΔM_t	(°/m)
ε	Rope test specimen strain $= \Delta l / l_0$	(mm/mm)
σ	Nominal rope stress $= F / A_{met}$	(MPa)
ϕ	General angle of rotation	(°)
Φ	Rope rotation, can be $f(z)$	(turns or °)
Φ'	Twist between the sheave wheel and drum connection point With the conveyance at the lowest position in the shaft, $f(z_1)$	(°/m)

$\Phi(0)_{constrained}$	Rope rotation boundary condition at the splice end prior to detachment of the rope from the conveyance	(turns or °)
Φ_{coil}	Rotation distribution in a manufactured rope coil, $\Phi_{coil} = R_{coil}.z$	(turns or °)
Φ_e	Rotation distribution for an empty conveyance, *f(z)*	(turns or °)
Φ_{ei}	Rotation distribution for an empty conveyance at installation equilibrium, *f(z)*	(turns or °)
Φ_f	In-service rope rotation distribution for a loaded conveyance, *f(z)*	(turns or °)
Φ_{lost}	Rotation lost from a rope as a result of routine maintenance practices	(turns or °)
Φ_t	Torsion test specimen end rotation	(°)
a	Acceleration	(m/s²)
$a_\varepsilon, b_\varepsilon, c_\varepsilon, d_\varepsilon, f_\varepsilon$	Constants for strain versus stress equation [A.2]	
A_1, B_1, C_1 c_1, c_2, c_3	Constants for general equations relating rope torque to load and twist	
a_{cl}, b_{cl}, c_{cl}	Matrices of constants defining the hysteretic relationship between torque and twist at constant load, each rope has unique values	
A_{met}	Rope metallic cross-sectional area based on the number of wires and their diameters	(mm²)
a_t, b_t	Constants for describing rope rotation during emergency braking	
C	Torque factor, proportionality between load and torque at constant twist	(Nm/kN)
d	Rope diameter	(mm)
D	Winder drum diameter	(mm)
d_0	Rope diameter at zero twist for a torsion test specimen	(mm)

Df	At installation equilibrium, the ratio between the rope twist at the sheave and the rope twist at the drum connection point with the conveyance at the lowest position in the shaft	
d_{nom}	Nominal rope diameter	(mm)
E	Young's modulus	(GPa)
EBL	Estimated rope Breaking Load	(kN)
F	Rope load, can be $f(z)$	(kN)
F_{cl}	Constant load values associated with the columns of the a_{cl}, b_{cl}, c_{cl} matrices, values may be unique for each rope	(kN)
F_{max}	Maximum static load applied to a rope in service	(kN)
f_s	Ratio between conveyance weight and payload	
g	Acceleration due to gravity = 9,81 m/s²	(m/s²)
G	Modulus of rigidity or shear modulus	(GPa)
K	General constant of integration	
K_{LL}	Least squares lay length factor, from data of the constant twist test	(1/(°/m))
L	Maximum suspended rope length, measured from the conveyance upwards	(m)
l_0	Torsion test zero twist gauge length	(mm)
L_b	Elevation from the bank to the headgear sheave	(m)
L_{drum}	L, on the drum side of the headgear sheave wheel	(m)
LL	Rope lay length	(mm)
LL_0	Torsion test zero twist lay length	(mm)
LL_{drum}	Lay length at the drum connection point	(mm)
$LL_e(0)$	Calculated lay length at the splice for an empty conveyance	(mm or % change from LL_{nom})
$LL_e(L)$	Calculated lay length at the sheave for an empty conveyance	(mm or % change from LL_{nom})

$LL_{ei}(L)$	Calculated installation equilibrium lay length at the sheave for an empty conveyance	(mm or % change from LL_{nom})
$LL_{ei}(0)$	Calculated installation equilibrium lay length at the splice for an empty conveyance	(mm or % change from LL_{nom})
$LL_f(L)$	Calculated lay length at the sheave for a loaded conveyance	(mm or % change from LL_{nom})
$LL_f(0)$	Calculated lay length at the splice for a loaded conveyance	(mm or % change from LL_{nom})
LL_m	"On-tension" lay length measured during rope manufacture	(mm or % change) from LL_{nom})
LL_{nom}	Nominal rope lay length	(mm)
LL_{sheave}	Lay length at the headgear sheave	(mm)
$L_{vertical}$	L, on the vertical side of the headgear sheave wheel	(m)
M	Rope torque	(Nm)
M_0	At a constant load, the torque for zero twist, constant twist test data	(Nm)
M_{cl}	Torque measured during a constant load test	(Nm)
M_{cl0}	Starting value of torque, M_{cl}, at twist R_{cl0}	(Nm)
M_{cl1}	$M_{cl} - M_{cl0}$	(Nm)
M_{cl2}	$M_{cl1} - \delta M_{cl}$, corrected torque at constant load	(Nm)
m_e	Empty conveyance mass	(kg or tonnes)
M_e	Rope torque for an empty conveyance, constant for $z = 0$ to L	(Nm)
M_{ei}	Rope torque for an empty conveyance at installation equilibrium, constant for $z = 0$ to L	(Nm)
M_f	Rope torque for an loaded conveyance, constant for $z = 0$ to L	(Nm)
$M_{f,Re}$	Rope torque for a loaded conveyance, with the empty conveyance twist distribution, $f(z)$	(Nm)
M_i	For a certain constant load, the value of torque at the twist R_i, constant twist test data	(Nm)

M_k	For a certain constant load, the value of torque at the twist R_k , constant twist test data	(Nm)
m_r	Rope mass per unit length	(kg/m or tonnes/m)
N	Matrix of constants which relate torque to load and twist for constant twist tests	
N_{avg}	Matrix of constants which relate torque to load and twist for constant twist tests, the loading and unloading values of torque are taken into account, each rope has unique values	
N_{load}	Matrix of constants which relate torque to load and twist for constant twist tests, only the loading values of torque are taken into account, each rope has unique values	
P	Rope end load in service	(kN)
P_e	Empty conveyance, rope end load	(kN)
P_f	Loaded conveyance, rope end load	(kN)
P_f - P_e	Conveyance payload	(kN)
q	Rope weight per unit length	(kN/m)
R	Rope twist = $d\Phi / dz$ for a rope in service = Φ_t / l_0 for a torsion test specimen, figure A.12	(°/m)
R_0	Zero twist for the constant twist tests	(°/m)
R_1	Twist at the sheave wheel in the suspended rope section	(°/m)
R_2	Twist in the section of rope between the sheave wheel and the drum connection point, can be constant	(°/m)
R_{cl}	Twist applied to a rope specimen during a constant load test	(°/m)
R_{cl0}	Starting twist values associated with the rows of the a_{cl} , b_{cl} , c_{cl} matrices, values may be unique for each rope	(°/m)
R_{cl1}	R_{cl} - R_{cl0}	(°/m)

R_{coil}	Twist, relative to the torsion test zero twist, corresponding to the lay length at which a rope was manufactured (LL_m)	(°/m)
$R_{coil}.z_{max}$	Rotation boundary condition at the drum connection point, for installation equilibrium	(turns or °)
R_i	At constant load, the twist corresponding to M_i, constant twist test data	(°/m)
R_k	At constant load, the twist corresponding to M_k, constant twist test data	(°/m)
r_{LLm}	Same as z for R_{coil}, but expressed as a ratio	
RSF	Rope Selection Factor or design factor = EBL / F_{max}	
$R_{unconstrained}$	Twist to which the splice end of a rope would unwind if it were detached from the conveyance at the bank, relative to the zero twist lay length of the constant twist test	(°/m)
ß	General angle of rotation	(°)
$S_{u,wire}$	Tensile grade of the rope wires	(MPa)
SWbc	Rotation boundary condition at the sheave wheel calculated for installation equilibrium	(turns or °)
T	Torsional stiffness, inferred from the constant twist test data	(Nm/(°/m))
T_{cl}	Torsional stiffness under conditions of constant load	(Nm/(°/m))
T_{max}	Maximum torsional stiffness determined for a constant load test, equal to the no-slip stiffness	(Nm/(°/m))
z	Distance along the rope from the conveyance end or distance along the length of a torsion test specimen	(m or mm)
z for R_{coil} at installation	Point along the suspended length where the manufactured lay length occurs at installation equilibrium	(m or % of L)
z for $\Delta\Phi_{max}$	Point along the suspended length where the maximum rotation occurs during conveyance loading	(m or % of L)
z_1	Distance measured from the sheave wheel along the rope with the conveyance at the lowest position in the shaft	(m)
z_{max}	Length of manufactured rope coil	(m)

LIST OF TERMS AND ABBREVIATIONS

Term	Description
Bank	Area around the mouth of a mine shaft
BMR	Blair Multi-Rope (winder)
Construction	Strands in the rope and wires in the strands
Lay type	RHL - Right Hand Lang's LHL - Left Hand Lang's
LHL	Left Hand Lang's (lay)
LVDT	Linear Variable Differential Transformer
NTS	Not To Scale
Payload envelope	Deliberate percentage variation of payload for the rotation calculations
RHL	Right Hand Lang's (lay)
S#	In-service rope number, 1 to 22, table 4.1
SAG	Steel Anti-corrosive Guma (rubber in Polish)
T#	Laboratory torsion test rope number, 1 to 12 tables 4.3 and 4.4
TSR	Triangular Strand Rope

1 INTRODUCTION

Chapter summary : As an introduction, the development of shaft and hoisting systems for gold mining in South Africa is discussed. The continuing need for increased depth of hoisting is traced through the 111 year period of gold exploitation in the Witwatersrand basin. The historical perspective leads to one of the main technical challenges which the industry faces at present namely, the establishment of deep, single lift shafts, exceeding 2500 m. Modelling of the static torsional behaviour of Lang's lay triangular strand ropes, in shafts of different depths, is the main focus of this study. It is therefore of interest to examine the effect of increased hoisting depth on the performance of triangular strand ropes. As an example, it is shown that the amplitude of rope torsional oscillations during winder emergency braking increases substantially with an increase in suspended length. In addition, literature on deep level hoisting indicates that severe changes in triangular strand rope lay lengths could be expected in very deep shafts. To demonstrate the significance of these anticipated changes, test results are presented which indicate how rope mechanical properties, measured during destructive testing, vary with lay length. The scope and objectives of the investigation are stated and an overview of the thesis structure is given.

1.1 Shaft and hoisting systems for gold mining in South Africa

The discovery of gold bearing ore on the farm Langlaagte by George Harrison in 1886 led to an influx of fortune seekers to the Witwatersrand area. The rapid development of Johannesburg followed and by 1888 there were 688 stamp mills crushing 180 000 tonnes of ore to produce 5670 kg of gold for the year (31,5 g/tonne). Discussing the first ten years of Johannesburg's history, Beavon (1996) stated that mining and processing capacity increased substantially after the introduction of the MacArthur-Forrest cyanide process for separating gold from pyrite ores in 1890. By 1893 there were 2000 stamp mills in operation and gold production reached 42 525 kg (15,48 g/tonne).

The rate of production soon resulted in the depletion of the high yield, oxidised, surface ores and shaft systems became necessary to access the deeper lying reef. Surface inclined shafts were first used. These were sunk parallel to the ore body with horizontal access levels to the reef. Vertical shafts were required as the reef deepened or where one mine was on the dip side of another. For access below 300 m, a system of combining a vertical shaft with a sub-inclined shaft was used (compound shaft). Figure 1.1 shows the inclined and compound shaft arrangements.

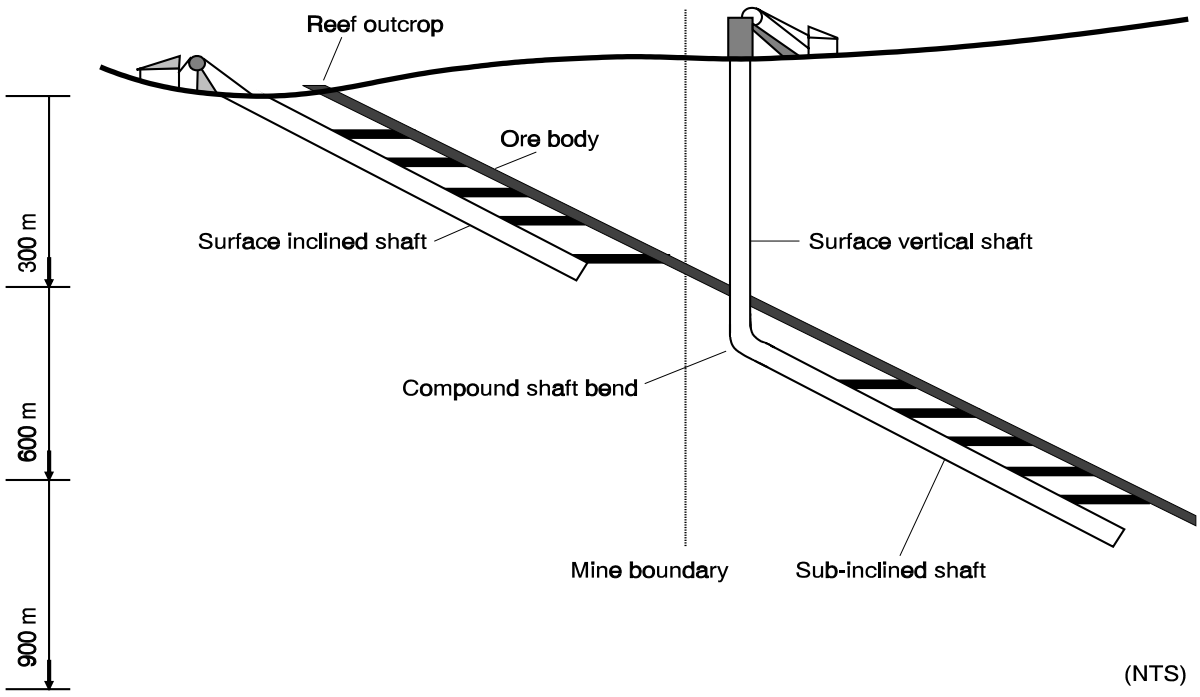

Figure 1.1 - Surface inclined and compound shafts used in the late 1800's for gold exploitation on the Witwatersrand, adapted from Campbell Pitt (1961).

From a hoisting point of view, the compound shafts were unsatisfactory as the capacity was limited by the reduced speed required for the conveyance to pass through the bend. It is also likely that the additional bending of the hoisting rope resulted in reduced service life. In many cases the compound shafts were converted to separate vertical and inclined shafts, requiring the construction of underground winder chambers for the inclined sections.

Probably the most visionary shaft hoisting publication of the early mining years was that of Behr (1902), "Winding Plants for Great Depths". Wayman (1973) reported

that Behr's paper stimulated world wide interest as it anticipated future hoisting depths of up to 8000 ft (2438 m). Particular attention was given to whether hoisting at this depth should be done in a single lift or in hoisting stages. It was realised that the main limitations would be the strength of steel wire ropes and the available drive power. Behr advocated the use of single layer winding using conical drums (to reduce torque requirements) and tapered ropes to increase the drum end rope factor of safety. Balance ropes, between conveyances, were also suggested to minimise the out of balance mass in winding. From 1902 the gold mining industry was to embark on deep level mining and Behr forecast that 81 shafts ranging from 900 m to 1200 m would be required in the then foreseeable future.

With regard to tapered ropes, Wainwright (1990) stated that these were used on parallel drum winders which resulted in coiling problems and consequently short rope life. To reduce starting power requirements, many drum winders were equipped with balance ropes. These were advantageous but, after 36 persons were killed as a result of a balance rope failure due to corrosion, their popularity dwindled. Additionally, the use of balance ropes prevented clutching of double drums to serve different levels in the shafts.

Initially, steam was the source of power for hoisting and, later, electric drives were employed. Analysing safety in winding operations, Vaughan (1918) stated that by the end of 1916, there were 443 main winding plants on the Witwatersrand with a collective power of 129 MW. Of these, 59 percent were powered by steam and the remaining 41 percent by electric motor. At that time, 200 000 persons were working underground on the gold fields. In addition to the main winding plants, there were also approximately 1000 small auxiliary hoists and winches with average installed powers of 12 kW for steam and electric, 49 kW.

According to Wayman (1973), the largest hoists installed in the pre-first World War period (1912-1914) were the three bi-cylindrical-conical winders at the Crown Mines No. 5 shaft in southern Johannesburg. The drums were 3,66 m in diameter at the start of the conical section and had a cylindrical section diameter of 6,3 m. By 1925 these three winders were considered the busiest in the world and were the key to the Crown Mines fame. For many years, no less than 315 000 tonnes of ore per month were hoisted and the peak tonnage, including waste rock, often exceeded 360 000 tonnes per month. By the 1920's systems of sub-vertical and

tertiary inclined and vertical shafts were being established and Wayman (1973) quoted a paper published in 1921 entitled "Schemes for Working City Deep Mine at a Depth of 7000 ft" (2133 m).

After the depression of the early 1930's, the boom which followed saw the era of "deep" deep shafts in the central Witwatersrand. Three 3,96 to 10,67 m diameter bi-cylindrical-conical winders were installed at the South Deep Simmer and Jack shaft where the maximum depth of wind was 1957 m. These winders were commissioned in the period 1935 to 1936 and were the most notable installations on the Rand next to Crown Mines No. 5 shaft. In the case of the deep level bi–cylindrical–conical winders, the ropes were coiled in two layers over most of the width of the cylindrical section, figure 1.2.

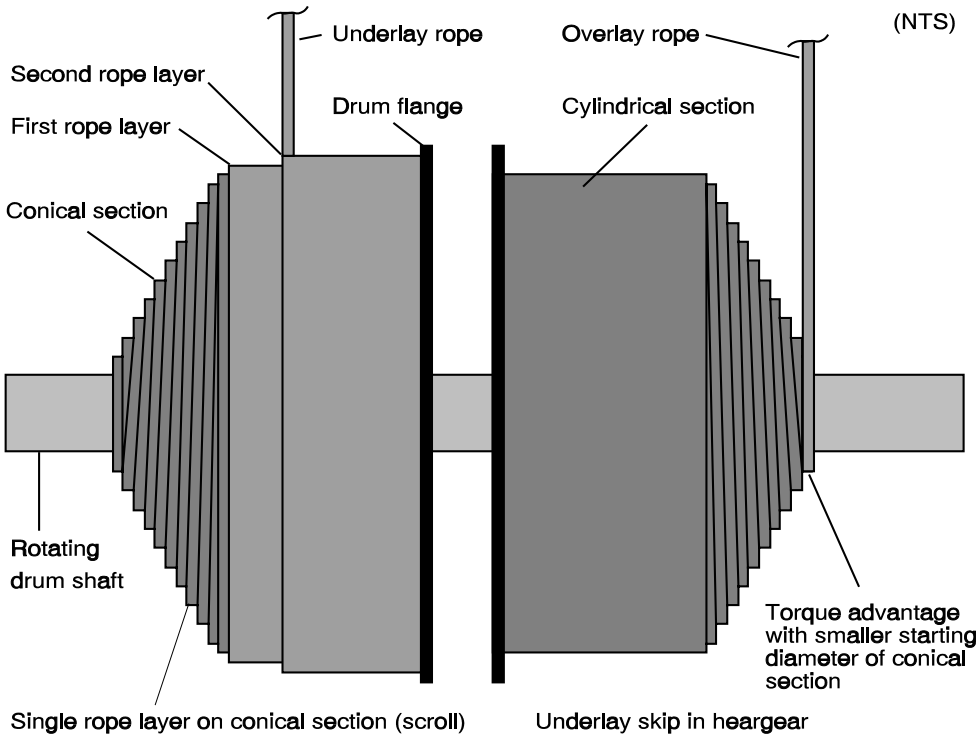

Figure 1.2 - Configuration of a bi-cylindrical-conical drum winder, top view.

The high initial costs (drum size) of the bi-cylindrical-conical winders and the doubtful overall power savings resulted in no new drums of this kind being ordered after the second World War. It was also realised that the torque advantage of the conical system was only applicable when winding from a single level. The transition to parallel, double drum, multi-layer hoisting soon followed and this became the most common system. Three layers of rope are frequently encountered but can

increase up to five in deeper installations. The increased number of rope layers on the drum are a result of having to maintain sheave wheel and drum fleeting angles (drum width dependant) within limits (maximum 1,5° to 2°) and the need to avoid excessive drum diameters (costs).

According to Wainwright (1990), six strand ropes and more specifically those of the triangular strand construction became the most favoured for drum winding applications. These proved to be cost effective and gave consistently acceptable service lives. The use of rope guides were avoided due to the sloping nature of the ore bodies and necessity to hoist from multiple levels. Fixed guide systems were established as standard practice and non-spinning properties were therefore not required of the hoisting ropes.

Gyngell (1967) pointed out that as the ore reserves deepened, the trend in containing operation costs, up to about 1957, was to increase the hoisting capacity and speed. This was achieved by scaling up the conventional double drum winder. At that stage the largest double drum machine was 4,88 m in diameter and was powered by a 4,9 MW direct current motor. A 10 tonne payload was hoisted at 15,2 m/s from a depth of 2300 m and 54 mm diameter ropes were used.

It was reported by Craib (1965) that the demand for increased payloads, beyond the capacity of single rope drum winding, resulted in South African engineers examining the use of multi-rope Koepe hoisting for the gold fields. Severe problems where however encountered with Lang's lay triangular strand head ropes on Koepe installations deeper than 1100 m. The main reason for the problems was the rapid fatigue of the ropes due to spinning during each winding cycle. It was realised that due to rope performance limitations the Koepe system would not be the best solution for hoisting of high payloads from great depths (> 2000 m). Craib (1965) listed the twenty main Koepe installations in South Africa at the time with the maximum winding depth being 1928 m (which is still the case).

Gyngell (1967) stated that at the same time as the introduction of four rope Koepe winders came the development of the Blair Multi-Rope (BMR) double drum winder. In this configuration, two ropes are used on either side of an otherwise conventional double drum machine. The drums are divided into two sections so that each rope is coiled on one half of a drum. Rope tension compensation is provided by means

of a conveyance mounted compensating sheave to which both ropes in a compartment are connected. Alternatively, the headgear sheaves can be mounted on interconnected hydraulic cylinders to achieve the same. Maintaining equal pressure in the cylinders results in automatic adjustment for differences in rope lengths, thereby ensuring equal rope tensions.

A parallel development to high capacity hoisting systems for deep shafts was ultra high tensile steel wire ropes. In an article entitled "Ultra High Tensile Wire Ropes for Hoisting From Depth", it was explained how the relatively high factor of safety requirement limited the depth of single lift shafts (Anon, 1972). It was stated that in spite of the limitations, improvements in available ropes had made shafts to 2500 m possible. At that time (1972) a shaft was being sunk to 2427 m from surface, then the deepest in the country. It was planned that 2000 MPa steel ropes would be used on the 4,92 m double drum winder. Another new shaft had also just been completed, reaching 2366 m from surface. All the ropes on the three double drum and one BMR winder, servicing the 2366 m shaft, had a minimum tensile grade of 2050 MPa. After the 2427 m deep shaft one reaching 2490 m from surface was completed in the same mining area. McKenzie (1993) stated that this is the deepest hoisting shaft in the world (deeper ventilation shafts do exist).

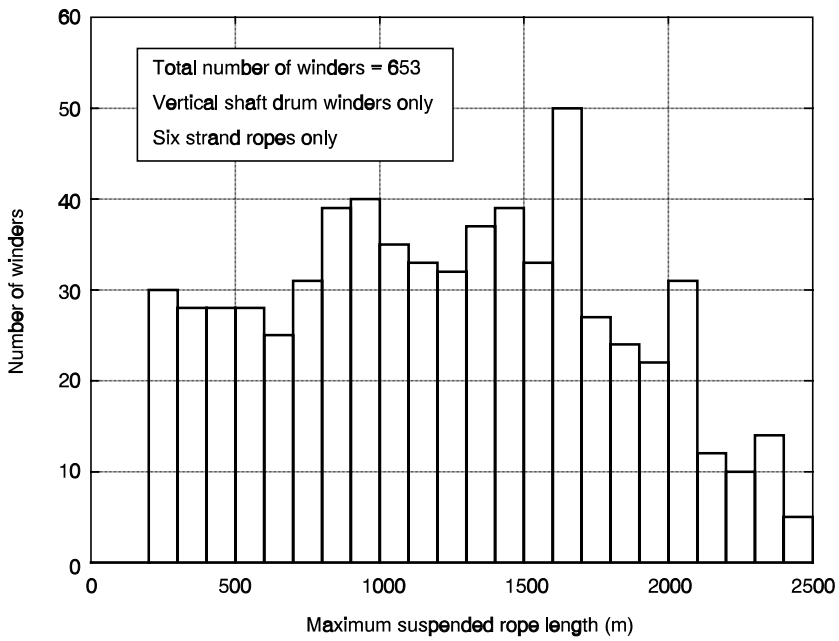

Figure 1.3 - Distribution of drum winders serving vertical shafts deeper than 200 m. Extracted from the CSIR Mine Hoisting Technology winder data base, December 1996.

The current depth based distribution of drum winders in South Africa is shown in figure 1.3. There are still many shallower shafts indicated but some of these may by now be out of commission. The mineral being mined is not taken into account in the data base so the winder distribution is not exclusive to gold mining.

It is clear that throughout the history of mining of the Witwatersrand basin, the need for increased depth as shallower ores were depleted has been a common factor. Discussing deep level mining geology, Viljoen (1996) stated that the average mining depth is currently 1800 m below surface and the deepest exploration borehole has reached 5500 m, which is an indication of where the industry is heading. Essentially the main problems have not changed over the last century but the level of technology required in the solutions has increased significantly. Pickering (1996) said that mining, by definition, is a process which depletes a natural resource. It starts with the recovery of the easy resources and progresses to the more difficult. As the difficulty of recovery increases so the planning and technology employed must be improved if the cost of recovery is to be contained.

Gold production peaked in 1970 with 1266 tonnes being produced. Since then there has been a steady decrease in production with 517,2 tonnes produced in 1994 and 491,9 tonnes in 1995 (≈ 5,8 g/tonne of ore mined). Even though the output of gold is decreasing, it still contributes close to 50 percent of South Africa's mineral revenue.

Figure 1.4 outlines the mine development options, particularly in the area of shaft systems, which the industry is considering at present. Examining the financial risks associated with deep level mining, Davis (1996) predicted that new green field projects are unlikely in the near future. With the gold price fluctuating around US$ 350 per ounce and funding estimates of US$ 500-600 million required to bring a new, single shaft, mine into operation, Davis suggested that possibly the best option for the industry would be brown fields expansion.

As far as reserve availability is concerned, it has been estimated that only 40 percent of gold in the Witwatersrand basin has been mined. Large scope for continued mining therefore exists, with the single most important parameter being increased depth.

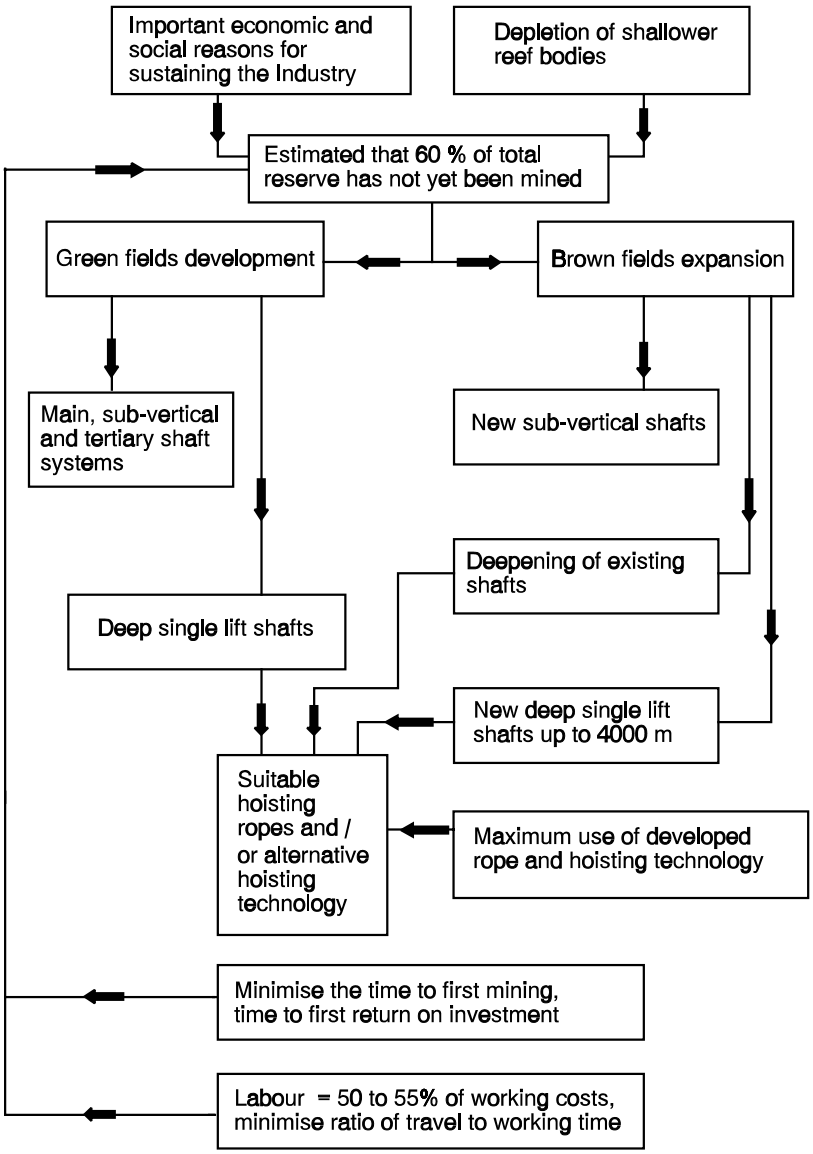

Figure 1.4 - Future mine development options for the South African gold mining industry as regards vertical shaft systems.

Pickering (1996) stated that approximately 10 percent of the present South African gold production originates from depths greater than 2500 m. It is estimated that by 2015, the figure will change to 50 percent. This estimate is based on the assumption that the technology will be available to mine the deeper deposits.

The costs involved in starting a new mine are very large and it may take between 10 to 14 years from start up before the mine reaches positive cash flow. The main costs involved in starting a mine are those required to access the ore body. For example, the time and costs associated with a vertical and sub-vertical shaft system are far more than a single deep shaft. Figure 1.5 shows the two layouts.

Pickering (1996) suggested that technologies permitting deeper single lift shafts could play a major role in the economics of opening up new ore bodies. Greenway (1990) stated that the time to develop cross over levels between main and sub-vertical shafts and the development of the underground winder chambers can take up to one year.

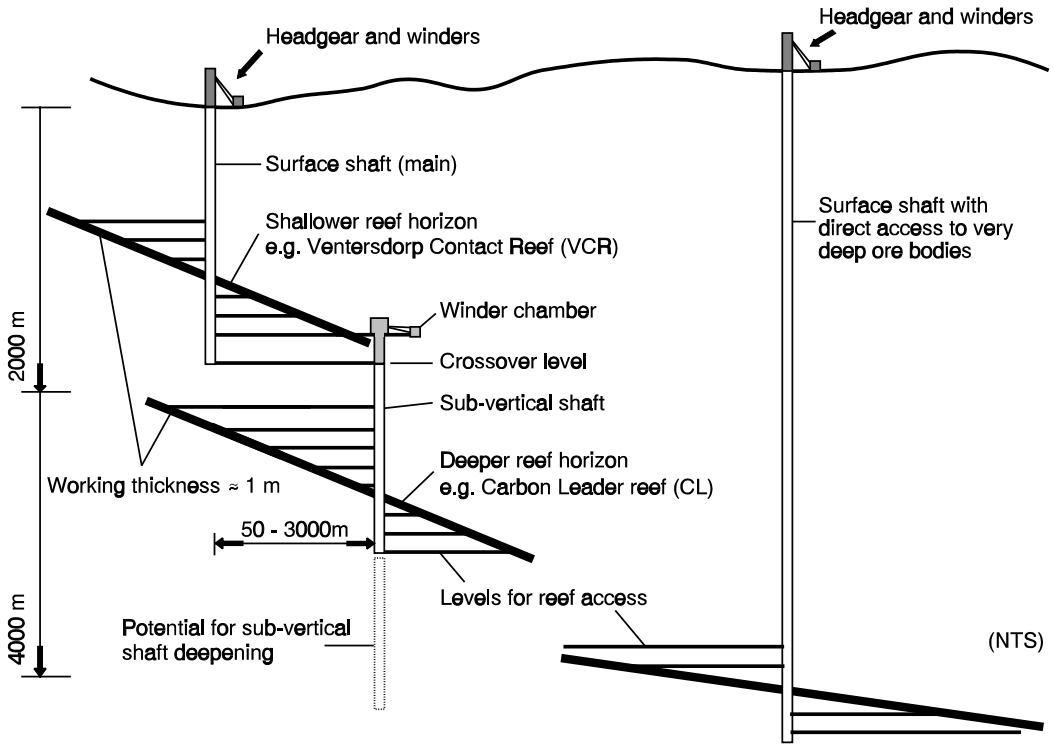

Figure 1.5 - Current and future shaft system elevations, adapted from Lane (1990).

Once the mine is established, the productivity of the workforce plays a critical role in the profitability of the operation. Analysis of operating expenses shows that 50 to 55 percent can be attributed to labour costs. Travelling times (surface to surface) of up to two hours in an eight hour shift are not uncommon with the current multi–shaft systems. Significant savings in this regard could be achieved with the use of deep single lift shafts.

Judging from two similar papers, Sparg (1993), Girodo and Sparg (1995) it is evident that winders for ultra deep shafts (4000 m) are feasible and well within the design and manufacturing capabilities of heavy engineering companies. The primary concern is the suitability of current Lang's lay triangular strand ropes for winding

from such depth. It is generally accepted that the torsional response of these ropes, under the influence of the differential loading associated with deep winds (rope weight), will affect their performance below a certain depth.

Multi-layer non-spin ropes are regarded as an option if conventional rope hoisting is used. However, Chaplin (1993) pointed out that the rather different fatigue properties of multi-strand ropes may lead to other problems in deep level applications. One of the main concerns is the predominant failure of internal rope wires and the ability to accurately detect these (Schrems, 1994; Kuun, 1993).

Triangular strand ropes have to date served the needs of drum winding extremely well, although below a shaft depth of 2500 m there has been no experience with these. It would be advantageous to be able to utilise the construction for as long as possible considering the extensive research and development that has been conducted into the design, operation and maintenance of such ropes. Initially the main concern with very deep level hoisting was the limitation which rope factors of safety had on the load carrying capacity at depth. This problem has essentially been overcome by investigating and defining new design factors for wire ropes (drum winders). Extensive research, described in part by Hecker (1990) and Sykes and Widlake (1990), has been carried out on the effects of increasing rope loads in vertical shafts. As a result of the research findings, changes in the South African regulations governing the design factors for ropes operating in deep shafts will soon come into effect. Laubscher (1995) discussed the implications and potential benefits of the proposed amendments to the regulations. In conclusion, Laubscher emphasised the benefits which the new factors could have for both shallower and deep shafts. However, concern was expressed about the suitability of the current drum winder ropes due to their torsional response at depth.

1.2 Typical shaft and winder layout

According to Glenday (1989), early shafts in South Africa were predominantly rectangular and were equipped with timber guides and buntons. This configuration gradually gave way to rectangular shafts with steel replacing the timber. The increased demand for greater hoisting capacity and more ventilation air in the deep mines led to the use of concrete lined circular shafts, figure 1.6.

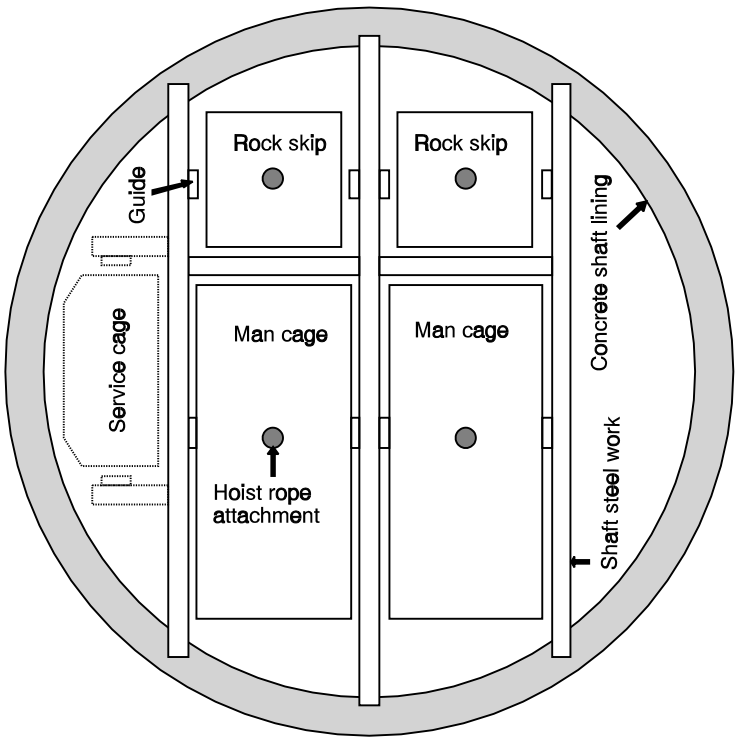

Figure 1.6 - Example of a circular shaft cross-section showing the hoisting compartments.

Typically, modern shafts are served by at least two double drum winders, one for rock and one for men and materials. Cages for men and materials have two or three decks with a capacity of 45 to 65 persons per deck. Rock skips payloads vary considerably depending on the winder power, shaft depth and the rope(s) used. The average for the industry is around 10 tonnes. Shaft diameters normally range from 7 to 11 m. In some cases a third winder hoists a small service cage in the shaft. This could be a single drum winder or double drum in which case a cage and counterweight or two service cages would be connected. Higher capacity shafts have up to five winders, two for rock, two for men and materials and a service winder. In these cases, the rock winders are often of the BMR type. Alternative configurations include the use of multi-rope Koepe winders (tower mounted) for rock hoisting and single rope units for men and material.

A shaft elevation is shown in figure 1.7. Due to the inclination and depth of the ore bodies, most modern surface shafts do not have levels in their upper half. An exception to this could be a water pumping chamber. Sub-vertical shafts, in contrast, usually have evenly spaced levels over their lengths (figure 1.5).

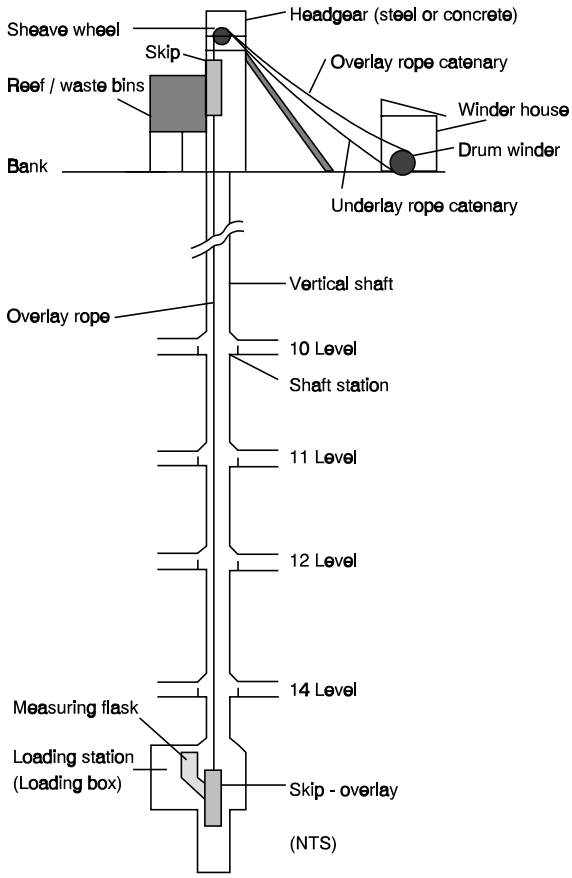

Figure 1.7 - Surface vertical shaft and rock winder elevation.

For surface shafts, double drum winders are always ground mounted and the hoisting ropes are routed over grooved sheave wheels fitted near the top of a steel or concrete headgear. Adjacent to the headgear are ore storage bins for the reef and waste rock which is hoisted from the underground loading station. The loading station is almost always located in close proximity to the shaft bottom. Ore from the various levels in the mine is gravity fed through an ore pass system to the loading station.

1.3 The significance of hoisting depth as regards torsional behaviour

Although a detailed investigation of the dynamic torsional behaviour of drum winder ropes was not within the scope of this study, an experiment was conducted to determine the effect which depth has on torsional oscillations during rock winder emergency braking. Two shafts were considered, one 760 m deep and the other 2000 m with all other parameters being nominally similar. In each case, an empty

rock skip was hoisted from the underground loading station and the winder was tripped by the driver at a predetermined point (≈ 10 m/s hoisting speed). Once the system had come to rest a yellow line was painted on one side of the rope from a station at the mid-shaft position. The line stretched over a length of approximately 30 m. The skip was returned to the loading station and the winder trip was repeated, with the same trip initiation point, while video filming the rope.

From the video image the number of rope rotations were determined. In the 760 m deep shaft, the rope rotated twice to the left and then twice to the right. In the 2000 m case the rope rotated 26 times to the left and the 26 times to the right. These results are shown in figure 1.8.

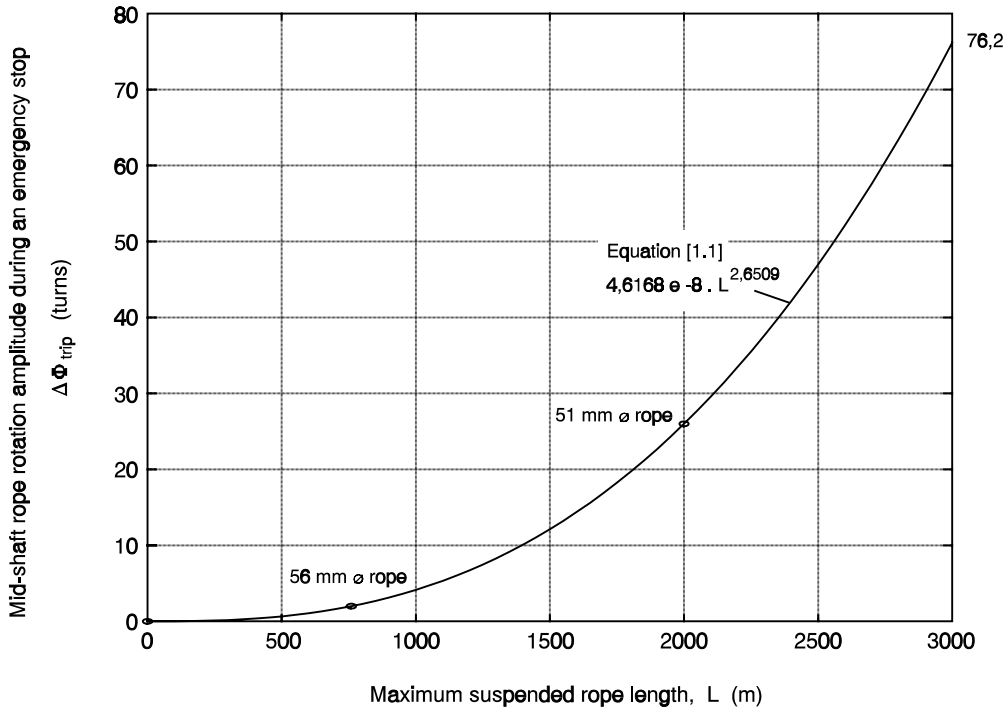

Figure 1.8 - Maximum amplitude of torsional oscillation during emergency braking with an empty conveyance hoisted from the loading station, Lang's lay triangular strand ropes.

Yiassoumis (1992) found that rope rotation on Koepe friction winders is a function of the square of the hoisting depth and for the purposes of this experiment it was assumed that a rope would exhibit a similar relationship on drum winders. It was also assumed that the rope rotation tends to zero as the maximum suspended length tends to zero. An equation of the form ($constant.L^2$) could however not adequately describe the observed data in figure 1.8 and so equation 1.1 was used.

$$\Delta\Phi_{trip} = a_t . L^{bt} \qquad [1.1]$$

where : L = maximum suspended length (m)

a_t , b_t = constants solved for numerically using the observed data

It is evident that the rope torsional response during emergency braking increases substantially with depth. Equation [1.1] was used to extrapolate the response to a 3000 m deep shaft. At this depth the rope is expected to rotate 76,2 times in one direction and then in the other under the same circumstances. It was mentioned earlier that the current limit of experience with triangular strand ropes is 2500 m suspended length. Increasing the suspended length by 500 m could result in a 62 percent increase in the amplitude of torsional oscillations associated with dynamic events. If this proves to be true then there may exist a transition depth where the coupled axial-torsional dynamics of the rope becomes severely detrimental to rope life (torsional fatigue).

As an analogy, it is interesting to note that on Koepe hoisting systems there is a transition depth where Lang's lay triangular strand head ropes are no longer suitable. Craib (1965) gave a detailed description of the operating experiences with Koepe winding ropes : In 1956 the first Koepe hoist was installed on a sub-vertical shaft (1067 m) using a single, 48 mm, triangular strand head rope and a 49 mm, 18 strand, non-spin balance rope. After a service period of four years and five months the ropes were removed. Careful examination of the ropes showed that their deterioration was not significant and they were kept as spare ropes for the same winder. The next two installations (4 rope Koepe machines) of 1958 and 1959 had depths of 1353 m and 1634 m respectively. Based on the experience with the first Koepe winder, it was decided that the triangular strand construction was the most suitable for head ropes. Unfortunately on both of the deeper installations, after six weeks of operation broken wires started to appear and after six months the ropes had to be discarded because of severe strand distortion due to spinning. It was only after a second set of ropes behaved in a similar manner that engineers realised that the cause was the system geometry. Figure 1.9 shows typical arrangements of the Koepe winding system.

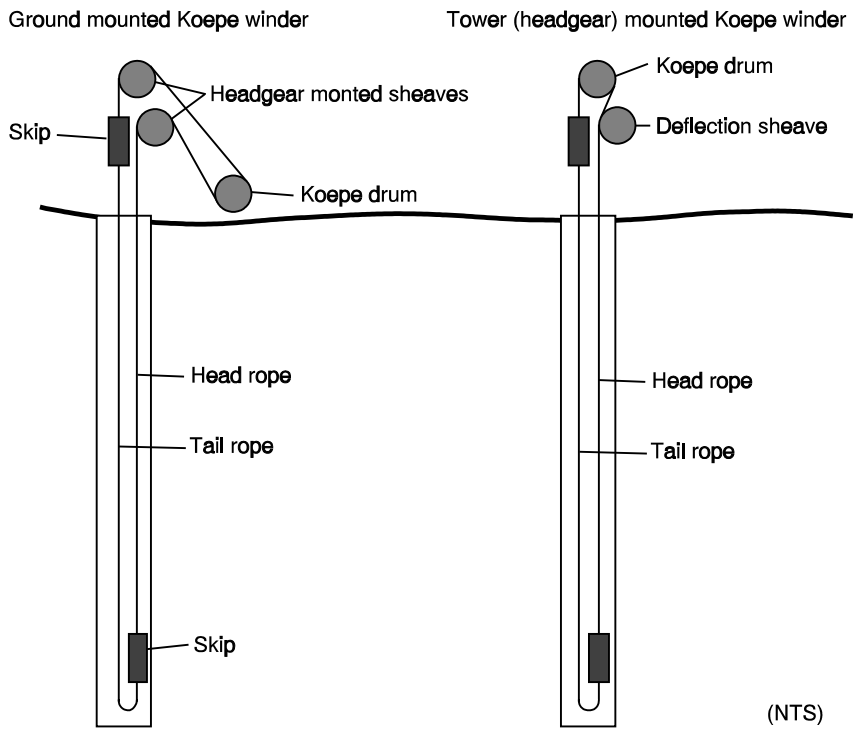

Figure 1.9 - Ground and tower mounted Koepe friction winders, adapted from Campbell Pitt (1961).

The reason for the spinning of the ropes during a winding cycle is that they are essentially end for ended every trip (bottom section to the top and visa versa). At the start of the winding cycle, the short length of head rope above the down going conveyance has a short lay length. This is abruptly altered by the long lay length from the upcoming head rope feeding into it. The change in lay length is accompanied by spinning of the rope about its axis. This spinning commences just before the rope leaves the Koepe drum treads. The rope rotation during each winding cycle was found to cause severe wear of the Koepe drum tread linings.

Although it is realised that the Koepe system, from a rope point of view, is significantly different to drum winding, the salient point in this example is that ropes which perform satisfactorily at a given depth may not do so if the depth is increased by even a relatively small amount. It should therefore be anticipated that the critical depth for triangular strand ropes on drum winders is being approached. It is important that the understanding of rope torsional behaviour is improved since insight into the mechanics which result in hoisting rope instability will undoubtedly enhance the engineer's ability to find effective solutions.

1.4 The effect of lay length on rope mechanical properties

McKenzie (1990) reported that in deeper shafts up to 2500 m, lay length changes of 80 percent longer than the manufactured lay length have been observed at the sheave end. At the splice end the lay lengths are known to have shortened by up to 30 percent. Figures of 40 percent shortening and 50 percent lengthening or more were quoted by Wainwright (1988). Greenway (1990) stated that there is some evidence of problems associated with lay length changes in shafts with depths of about 2400 m. It was proposed by Greenway (1990) that torsional deformation is proportional to rope length and therefore large changes in lay length are expected for very deep winds. MacDonald and Pienaar (1994) confirmed that the in-shaft torque differentials can cause lay length variations of 100 percent over the length of a rope. In addition it was not known what lay length variations may occur in a 3500 m deep shaft.

To date much emphasis has been placed on the results of tensile tests in assessing the condition of hoisting ropes. Three papers; Van Zyl (1956), Archer (1971) and Fritz (1982) deal in detail with history of statutory rope testing in South Africa, the preparation of test specimens, methods of testing (equipment) and the interpretation of the tests results. It has always been the practice to test Lang's lay triangular strand ropes at the free lay lengths which the sections have on arrival at the testing laboratory. Free lay length meaning the lay length in a torsionally unrestrained state.

A large amount of tensile testing has also been conducted in South Africa to establish an accurate drum winder rope condition assessment code of practice and discard criteria specifications. The code of practice relates specifically to Lang's lay triangular strand ropes. Contract investigations conducted by a local rope research organisation have included :

- Destructive testing of sections cut from discarded ropes.
- Investigations into the effect of cut wires on rope strength.
- Determination of spliced rope termination efficiencies.
- BMR compensating sheave tangent point degradation studies.

The purpose of testing sections from discarded ropes is to evaluate the accuracy of the rope condition assessment process. The statutory limit for degradation of a hoisting rope in South Africa is 10 percent decrease in breaking strength based on a test conducted on the rope when it was new. It would enhance safety and be economically ideal if all ropes could be discarded exactly at the point where the weakest section in service reaches the statutory limit.

Ropes on drum winders generally operate with considerably different lay lengths compared to those at which they are tested. It is therefore important to determine whether changes in lay length have any significant influence on the tensile test results. Discussing condition assessment of winding ropes and the drafting of the code of practice for this, Kuun et al. (1993) questioned whether the strength of a short sample removed from a discarded rope is truly representative of that section of rope under operating conditions. It was further stated that due to factors, of which shaft depth and maintenance practices are most important, the lay length of a free sample of rope can vary from its actual in-service lay length by up to 30 percent. The effect of this variation on the strength of discarded rope was not known.

To clarify some of the uncertainty, a series of 28 tests on a 25 mm, 6x27(9/12/6 + 3Δ)/F, compound triangular strand rope with different lay lengths was conducted using a 15 MN tensile testing machine. The rope samples were all cut from the same new coil supplied by a local rope manufacturer. Specimen lay lengths were changed manually prior to testing using a torque clamp attached to one of the white metal collars (two 800 mm moment arms) . Both end cones were locked in the grips by placing a preload on the rope. The torque clamp end was then loosened prior to inducing or removing rotations, while the other end remained fixed. Details of the test equipment and results are given in appendix A.

Table 1.1 lists the extent to which the various test parameters varied as a result of the lay length changes. Note that the values in the table are not necessarily associate, they only indicate the ranges encountered.

Table 1.1 - Maximum and minimum values of test parameters for the investigation of the effect of lay length on tensile test results. Note that the results are not necessarily associated.

	Change in lay length (%)	Change in breaking strength, figure A.3 (%)	Change in strain energy to failure, figure A.4 (%)	Change in strain at failure, figure A.5 (%)	Torque at failure, figure A.8 (Nm)	Maximum modulus, figure A.11 (GPa)
Maximum	80,0	5,1	20,2	43,2	1772,0	141,4
Minimum	-32,7	-11,0	-52,5	-42,9	714,3	90,8

These tests indicated that lay length changes can result in significant variations in the measured mechanical properties of triangular strand ropes. Based on the results, future research relating to condition assessment of triangular strand ropes for deep shaft winding systems should take into account the in-service lay length changes. It is possible that the sensitivity of the rope construction to damage (corrosion, abrasion, plastic deformation or broken wires) may be a function of lay length. It would therefore be of benefit to the future projects if an accurate method of quantifying in-service lay length variations is available.

1.5 Study objectives, scope and motivation

The primary objective of this research project was to investigate and develop a modelling approach which can be used to predict the static torsional behaviour of Lang's lay triangular strand ropes operating on drum winders in vertical shafts of different depths. The main parameters of interest were :

- The lay length changes at installation taking into account rope manufacturing details, installation geometry and applied loads.
- Variations in lay length with service period as a result of maintenance practices.
- Rotation of vertically suspended ropes during conveyance loading.
- Equilibrium rope torques for empty and loaded conveyances.

As far as could be established, this thesis forms the first comprehensive study on the static torsional behaviour of triangular strand ropes for drum winders. Analyses, which take full account of friction (hysteresis behaviour) in the rope rotation calculations have not been published. The inclusion of rotation boundary conditions which are dependant on the manufactured rope lay length, the torsion test section lay length and service period has also not been reported.

The first stage of the study involved the development of a laboratory rope tension–torsion testing machine. The main requirement was that the machine should perform torsion tests at constant rope load, twist and torque by means of computer control. In its previous form, the machine was capable of measuring rope torque for manually set constant end rotations (twists) and varying values of load. It was anticipated that the results of tests conducted at constant load and torque would indicate rope characteristics different from those explored by the constant twist method.

The development of the testing machine was followed by a series of in-service measurements. Lay length and rope rotation data of 22 ropes were collected from eleven shafts. The rope diameters varied from 41 mm to 54 mm and the shaft depths were in the range 1000 m to 2500 m. Men-material and rock winders were considered.

Laboratory torsion tests were subsequently conducted on samples matching the construction and diameter of the in-service ropes. The experimentally determined torsional properties, combined with the necessary analysis and assumptions, were used to calculate the in-service behaviour. Predictions from the modelling were then verified by comparison with the measured in-shaft data. Figure 1.10 shows an outline of the project structure.

The completion of the investigation has resulted in a generally better understanding of rope torsional behaviour on drum winders. Primarily, the improved knowledge will be applied to prediction of rope behaviour in future, very deep level winding applications. From the outset, it was realised that the findings may also be applicable to existing installations in improving rope utilisation and safety.

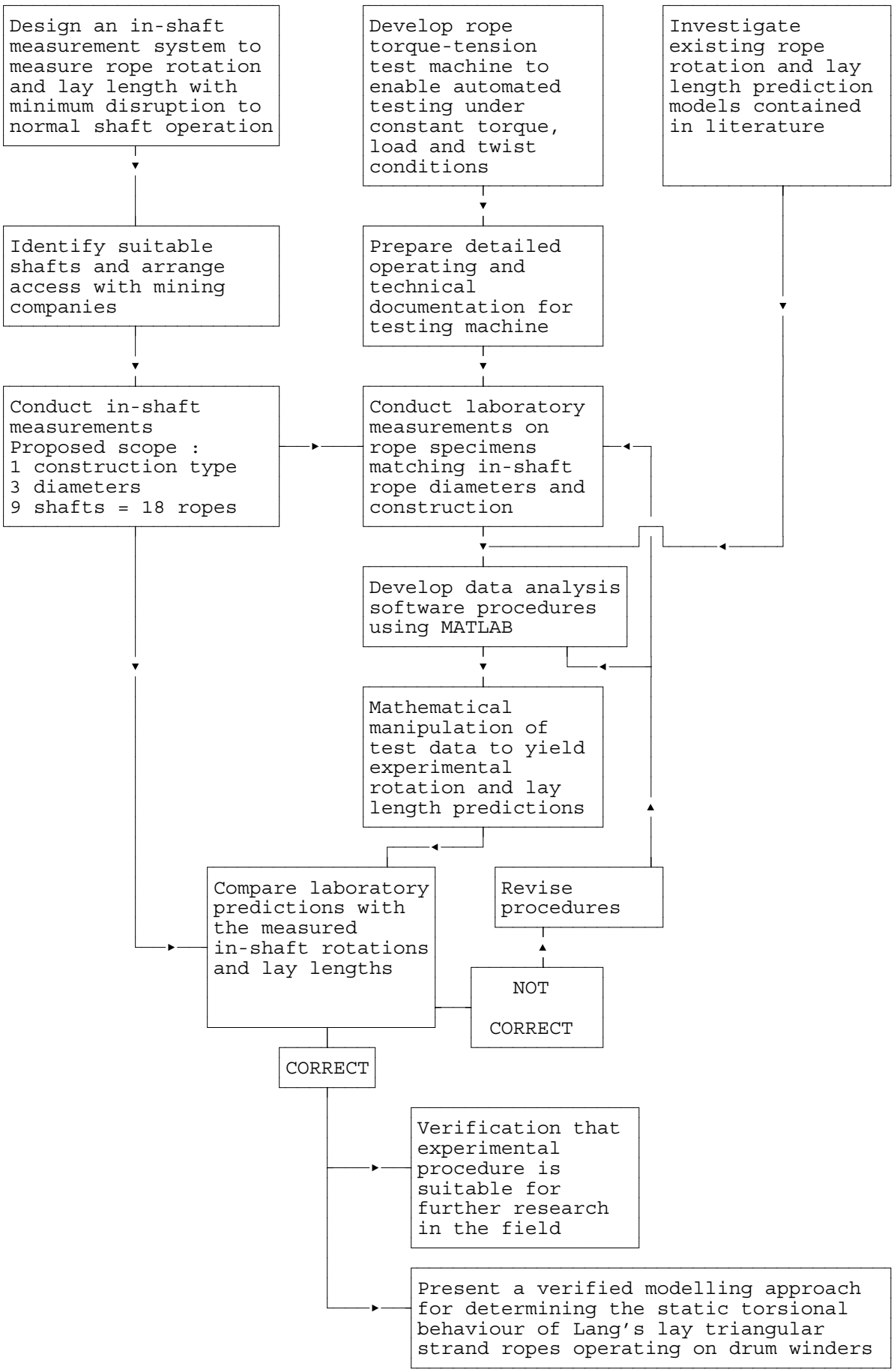

Figure 1.10 - Project outline.

The possible existence of a transition depth, for a particular rope construction and diameter, where a rope may no longer be suitable due to its torsional response has been suggested in section 1.3. The results of the investigation could be used to determine a likely estimate of such a depth. In addition, attempts at determining the effects of lay length changes on rope endurance world require quantification of the expected in-service variations.

With the ability to predict in-service rope rotation behaviour, a better understanding of the wear and fatigue modes of rope degradation could be gained. Triangular strand ropes show an even wear pattern around their circumference which is a result of rotation due to variations in applied loads as well as dynamic effects. Each time a section of rope passes over the sheave wheel and onto the winding drum it does so with different contact points. If the rope rotation is quantified then it may be possible to analyse the rope wear due to rotation on the sheave wheel and winding drum more precisely. In this regard, Chaplin (1993) stated that the overall process of triangular strand rope degradation results primarily from the interaction of plastic wear and subsequent fatigue of the outer wires. It is further complicated by the effects of torsional deformations which are inevitable in any application involving long ropes with fluctuating loads.

The results of the laboratory tension-torsion and tensile tests, conducted as part of this research, may also be used in future to calibrate finite element based rope models. This would be required since the complexity of inter-wire friction and other nonlinear relationships are not easily determined using a purely analytical approach.

1.6 Thesis structure

Relevant literature is reviewed in chapter two. The origin and features of the triangular strand construction are discussed and thereafter descriptions of machines for tension-torsion testing of wire ropes are given. Existing methods of calculating in-service rope rotation and torsional deformations are examined as is the general torsional behaviour of wire ropes suspended at great length. Methods of in-service rope rotation and lay length measurement are considered and the most important information gained from the literature review is summarised at the end of chapter two.

The development of the laboratory based wire rope tension-torsion testing machine is detailed in chapter three. A brief history of the testing facility is given and the various rope parameter measurement systems are described. The structure and features of the machine control software are also explained. Examples of the load, twist and torque variations with time, for the constant twist, load and torque type tests are presented. The constant load and twist tests were used extensively in qualifying the torsional properties of triangular strand ropes in this study.

Chapter four contains a discussion of the techniques used in obtaining the in–service and laboratory experimental data. The choices of rope diameters and shaft depths for the investigation are motivated. For simplicity all the ropes observed in service are numbered from S1 to S22. The torsion test specimens are numbered from T1 to T12. Specific details of the in-service ropes are given in table 4.1 and information relating to the torsion test ropes in tables 4.3 and 4.4.

The modelling approach used to calculate the in-service lay length changes, rope rotation during conveyance loading and the associated equilibrium rope torques is presented in chapter five. It is shown how lay length information from rope manufacture is taken into account in determining the rotation boundary conditions at installation in a mine shaft. The method of rotation calculation takes full account of torsional hysteresis in the determining rope rotation during conveyance loading. The removal of rotation from suspended ropes (which affects the lay length distributions) can also be accommodated in the analysis.

The results of the in-service lay length and rope rotation measurements are compared to the calculate values in chapter six. The deepest shaft considered in the study is examined in detail and for the other shafts, graphical comparisons of the values are included with additional detail contained in appendix C. Histograms describing the distribution of errors between the measured and calculated rope rotation and lay length results are presented. Factors which may have an influence on the accuracy of the in-service predictions are considered. Results which are of general interest to the torsional behaviour of triangular strand ropes are also presented.

A discussion of the most important findings of the investigation is contained in chapter seven. The significance of including accurate in-service rotation boundary

conditions and torsional hysteresis in the modelling of rope torsional behaviour is demonstrated. Through a parametric study, the factors which are most important as regards the torsional behaviour of triangular strand ropes are identified. This is followed by a discussion on possible options for extending the depth limit of application for triangular strand ropes.

Conclusions drawn from the investigations are listed in chapter eight as are recommendations relating to further work. Conclusions relate to the torsional properties of triangular strand ropes, modelling of rope torsional response and the in–service torsional behaviour of the ropes on drum winders. Recommendations are made regarding the modelling approach, the operation of triangular strand ropes in deep shafts and on the design and manufacture of these ropes for deep shaft drum winders.

Details of the investigation on the effect of lay length on rope tensile properties are presented in appendix A. Supplementary information on an approach for varying the lay length between the headgear sheave and drum connection point is given in appendix B. Appendix D contains a discussion and figures relating to a graphical method of determining rope lay lengths and the empty conveyance rope torque at installation in a mine shaft.

2 LITERATURE REVIEW

Chapter summary : Literature relevant to the study is reviewed. The origin and features of the triangular strand construction are discussed and thereafter a description of machines used for tension-torsion testing of wire strands and ropes is given. Existing methods of calculating in–service rope rotation and torsional deformations are examined as is the general torsional behaviour of wire ropes suspended at great length. Methods of in-service rope rotation and lay length measurement are considered. The most important information gained from the literature review is summarised at the end of the chapter.

2.1 Introduction

The complex construction of steel wire ropes and their behaviour under various loading conditions have formed the topics of many research efforts over the last 160 years. Published papers detail the findings in areas such as :

- Pure analytical investigations of rope geometry.
- Rope endurance predictions and measurements in tension, torsion and bending.
- Metallurgy and production of rope wires.
- Rope design, manufacture and inspection techniques.
- Rope termination methods and efficiencies thereof.
- Experimental measurements of rope parameters under laboratory and in-service conditions.
- Dynamic behaviour and loading of ropes as engineering systems components.

Wire rope literature reviews include Utting and Jones (1984), Utting (1994a, 1994b, 1995) and Ridge (1996). As regards analytical analyses, Costello (1978) considered some of the earlier contributions and more recently Raoof and Kraincanic (1994) critically reviewed the range of validity of various approaches for analysing helical strands. Analysis of wire rope has generally been confined to ropes with round strands where the wires form double helices (Karamchetty, 1980;

Lee et al., 1987). If a stranded rope is wrapped around a drum then the resulting wire geometry extends to a tipple helix (Lee, 1991).

The case of unequal lay strands of non-circular cross-section increases the complexity of the analytical analysis significantly. Mckenzie (1989) pointed out that the complication in modelling triangular strands arises from the non-uniform path of a wire about the strand axis. Conceptually, as a wire is followed, the radial distance between the wire and the strand axis changes from a maximum at the apices of the triangle to a minimum along the flattened sides. From the outset of this investigation it was decided that the determination of rope material properties through laboratory testing would produce the best results for input data into rope behaviour models. From a literature point of view, topics relating to methods of testing of ropes in tension and torsion, the response of ropes to applied loads and twisting and approaches to in-service modelling were therefore of most interest.

Inevitably, research efforts are associated with industrial problems encountered with the application of engineering products. It was mentioned in section 1.3 that the torsional behaviour of Lang's lay ropes on the earliest deeper level Koepe winding installations resulted in significant performance limitations. The immediate concern was then the development of suitable non-spin ropes with the correct torsional properties. Most investigations relating to wire rope torsion have been in connection with ropes of a non-spin or low-rotation design since these have to exhibit specific features relating to their torsional response (Costello and Miller, 1980; Gibson at al., 1969). Generally it is accepted that if a rope is operated with both ends prevented from rotating, then the torsional properties of the rope are not as important. This is true for shorter ropes but, as the rope length is increased, the effects of rope weight can result in undesirable torsional deformations in spite of the ends being restrained (Gibson, 1980). The South African Koepe winder rope problems of the 1950's showed that the torsional behaviour of wire ropes cannot be ignored at increased depth (Craib, 1965). Often the occurrence of the problems has not been well understood because of the generally limited understanding of rope tension-torsion interactions.

Another example of unexpected torsional behaviour was described by McGrath (1994a, 1994b) : In oceanographic research projects very long wire ropes are used at depths ranging from 3000 m to 6000 m. In these applications, the

weight of the rope is generally equal to or greater than the attached load. During the 1960's much equipment was lost as a result of rope failures which, after considerable investigation, were attributed to kinking of the ropes. The ropes used at the time were not torque balanced. During deployment, one end of the rope was attached to a buoy and the other to a seabed anchor. The weight of the anchor resulted in the rope unlaying while is was sinking. The sudden load release when the anchor reached the sea bed caused the rope to kink when attempting to return to its original lay length. The development details of the three strand (3x19), ordinary lay, torque balanced ropes which were employed to solve this problem were given by Lucht and Donecker (1981).

The understanding of wire rope torsional behaviour is reaching a level where possible problems in future rope applications can be anticipated. This is particularly true for the use of Lang's lay triangular strand ropes in deep, single lift, mine shafts (Rebel et al., 1996a). Serious problems have not been encountered in existing shafts and therefore research into the torsional behaviour of these ropes on drum winders has been limited to a few investigations (Yiassoumis, 1992 ; Hecker and van Zyl, 1993; Rebel et al., 1996b)

2.2 Triangular strand rope construction

The ropes considered in this project are all of the Lang's lay triangular strand construction with a sisal rope core as shown in figure 2.1a. According to McKenzie (1990) the triangular strands are characterised by one or two wire layers, laid in an unequal configuration around a triangular core.

The most common core in use is the "Plaited" core which is generally found in larger diameter, high strength ropes in South Africa. Figure 2.1b shows the detail of the core. The core is essentially a three strand rope of two wires per strand with three filler wires placed in the strand interstices. In the case where the triangular strand has two wire layers over the core, it is termed "compound" and the single layer strands are known as "simple". Typically, the outer wire diameters would be in the range 3,10 mm to 3,40 mm for compound triangular strand ropes with diameters from 38 mm to 56 mm (Haggie Rand, 1987).

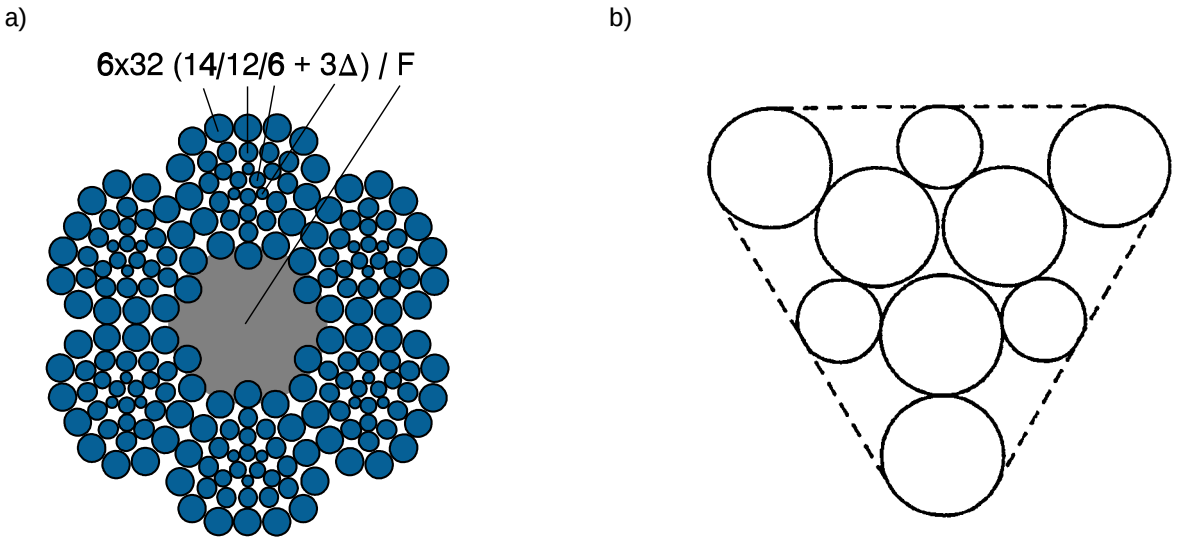

Figure 2.1 - Triangular strand rope cross-section (Haggie Rand, 1987), construction nomenclature and detail of the "Plaited" core (McKenzie, 1989).

McKenzie (1990) and Wainwright (1990) listed the features of Lang's lay triangular strand ropes which make them particularly suited to application on drum winders :

- Relatively easy to manufacture (single rope closing operation).
- Robust, stable (six strand, single layer) and resistant to abrasion.
- High strength to mass ratio and good efficiency of construction.
- Resistant to crushing due to compactness.
- Good wear properties due to increased outer wire surface area.
- Acceptable fatigue performance (compared with six strand ordinary lay ropes).
- High reserve strength of compound construction. (theoretical rope strength with the outer wires of the strands removed).

Ridge (1993) reported that the term "Lang's lay" originated from the name of its inventor John Lang. Lang realised that by laying the wires in the strands and the strands in the rope in the same direction, the wear properties of a rope could be improved. The length of exposed wire on the outer surface of the rope is greater than in the case of ordinary lay. In 1879, Lang obtained a patent for his lay design entitled "Improvements in the Construction of Wire Ropes" (Lang, 1879). Lang's lay wire ropes were first introduced in the round strand configuration.

Further attempts at improving the wear properties focused on making the rope cross-section more cylindrical. Verreet (1989) described how Arthur Latch and Telford Batchelor first developed locked coil ropes and then later the flattened strand rope. The 1888 patent drawings of Latch and Batchelor (Verreet, 1989) show six strand rope cross-sections both with flattened, oval and triangular strands. According to Ridge (1993), the first flattened strand ropes were manufactured by Latch and Batchelor in 1894.

Verreet (1986) pointed out that ropes which are of Lang's lay design can also be termed "long lay" or "Albert's lay". One of the first stranded wire ropes produced was that of Wihelm A.J. Albert. The "Albert rope", as it is commonly known, was tested for the first time on the 23 July 1834 in 484 m deep mine shaft near Clausthal in Germany. The rope consisted of three strands, each with four wires. Both the strands and the rope were laid right hand.

2.3 Tension-torsion testing of wire ropes and strands

A considerable portion of this project was devoted to the development of the wire rope tension-torsion testing machine (Rebel and Chandler, 1996) which is discussed in more detail in chapter three. It is therefore of interest to briefly consider similar machines or arrangements which have been used for torsion tests on wire ropes and strands.

Discussing the torsional properties of wire ropes, McKenzie (1987) identified various methods by which tension-torsion tests could be conducted. The first, and most elementary, involves vertical suspension of a rope section with a load applied at the free end by means of dead weights. The loaded end can be allowed to rotate as the rope unlays to maintain zero torque. Alternatively, a reaction torque can be provided by spring balances or pulley-weight systems applying tangential forces to the loading platform. This approach was used by Layland et al. (1951) in an investigation of the torsional properties of Lang's lay ropes for mine hoisting at Mysore Gold Mining Company in India. Figure 2.2 shows the equipment used by Layland and his co-workers.

McKenzie (1987) stated further that the suspension method resulted in considerable alignment problems at the free end with care having to be taken to ensure that the restraining forces (if used) were applied equally and tangentially to the loading platform. The limitations of the suspension method were overcome by using a low friction bearing at the rotating end of the rope to ensure axial and radial alignment during testing. Such an arrangement was used by McKenzie (1987) at Anglo Continental Ropes in Belgium. The main feature of the machine was the application of a hydrostatic thrust bearing originally developed for British Ropes Limited. The configuration of the machine is shown in figure 2.3 and a detailed description of the bearing operation was given by Pennycuick (1963). According to Pennycuick, coefficients of friction as low as 0,00001 were attainable with such a hydrostatic bearing.

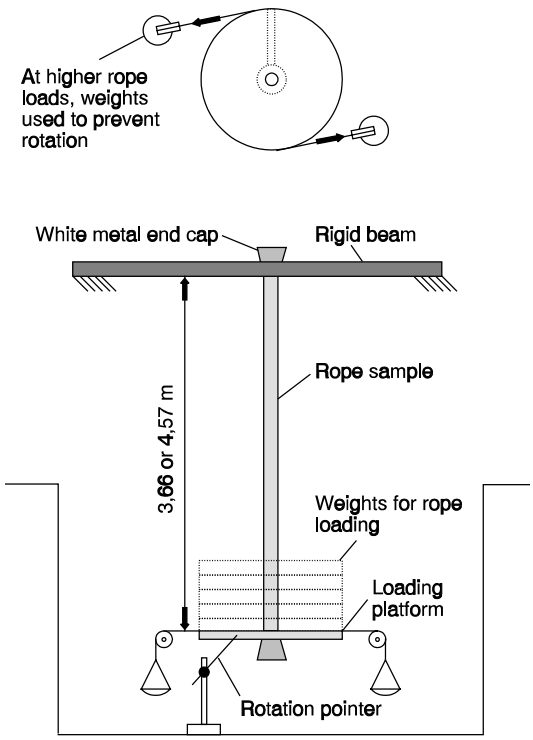

Figure 2.2 - Suspension method for determining torsional rigidity and rope rotation due to applied loading (Layland et al., 1951).

The primary importance of achieving very low friction coefficients in the bearing under axial loading was to simulate the response of a rope with one end loaded and free to rotate. This was particularly important when investigating the mechanical properties of non-spin ropes applied in lifting and hoisting applications where the loaded end was unrestrained. Examples of such ropes are those used on cranes and

for mine shaft sinking operations. According to Lucht and Donecker (1981) the fatigue and strength properties of ropes can also be significantly affected by conducting the investigative tests with a torsionally unrestrained end. Tensile tests conducted on five 18 and 19 strand non-spin ropes, showed an average decrease in strength of 22 percent with one end free to rotate. The results were compared to identical tests conducted with both ends fixed. Further investigation showed that the bending fatigue life could be reduced by up to 50 percent in the case of a free end.

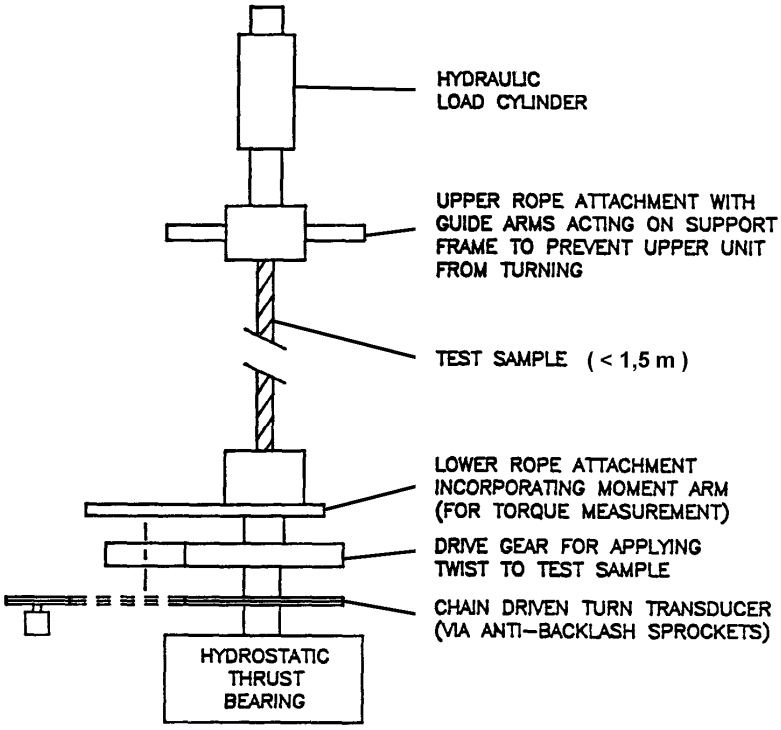

Figure 2.3 - Tension-torsion testing machine of Anglo Continental Ropes described by McKenzie (1987) and based on the British Ropes bearing designed by Pennycuick (1963).

McGrath (1994a) reported that during the development of three strand ropes for oceanographic research, tests were conducted to evaluate the tendency for kinking of various constructions. This was done by lifting a heavy load (25 percent of rope breaking force) with a 30,5 m length of rope and allowing the load to rotate until a torsional equilibrium in the rope was reached. The load was then lowered to ground level. Ropes of inadequate torsional design would immediately loop and kink and in some cases even break wires. During lifting, ropes with good torque balance would turn once or twice at the loaded end while others of poorer design showed up to 500 turns under the same conditions (≈ -5900 °/m applied twist).

Generally, tensile testing of wire ropes is accomplished in horizontal machines. Numerous papers describe methods of investigating rope torsional properties by the addition of torque measuring and twist application devices to the standard tensile testing machine. Carbogno and Czaja (1982) presented the results of laboratory tests on non-spin hoisting ropes (Koepe winding head ropes), conducted in Poland, using the equipment shown in figure 2.4. Removal of the dynamometer moment arm arrangement also allowed for free end testing. More recently the same equipment was also reported by Carbogno (1995) where the untwisting torque of flat steel wire rubber balance ropes, of the SAG type, required investigation. Hankus (1996) reported tests to determine the torque generated by large diameter lang's and ordinary lay ropes (> 50 mm) using a 5000 kN machine also with a dynamometer arrangement for the torque measurement.

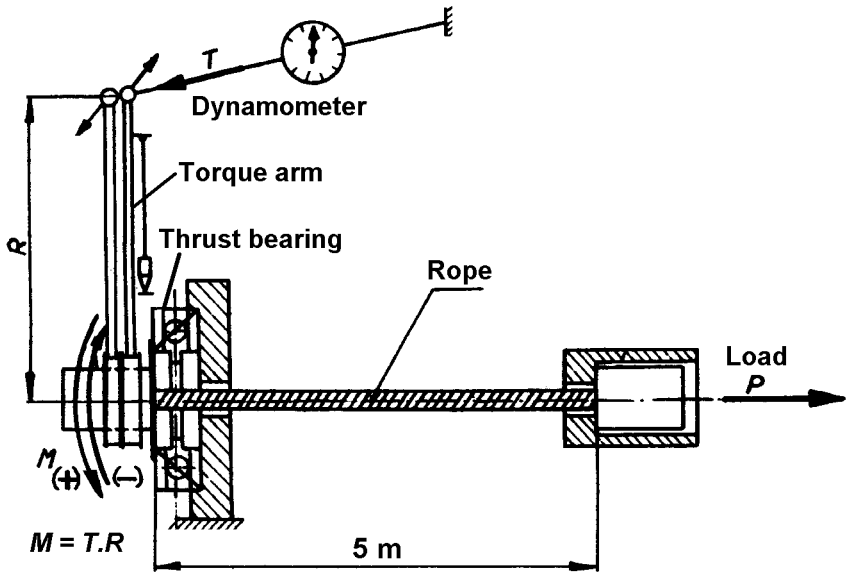

Figure 2.4 - Torsion testing equipment used in Poland by Carbogno and Czaja (1982).

Typical torsion test results achieved with the machine in figure 2.4 were presented by Lesnak (1983). Figure 2.5 shows the response of six low rotation rope designs. In figure 2.5, ropes F, G and H are of the same construction but with different outer strand lay lengths which are indicated in brackets adjacent to the letters. It is evident form the test results that, in terms of non-spinning properties, the outer strand lay length of 390 mm is the most suitable. In the case of these tests the torsional response was determined for zero applied twist. This example demonstrates the usefulness of torsion testing in optimising the response of complex rope constructions.

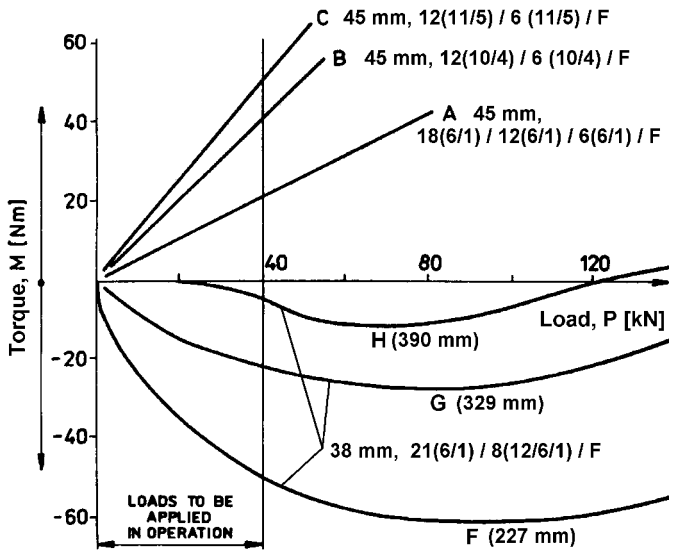

Figure 2.5 - The application of torsion testing in the design of low rotation balance ropes for Koepe winders (Lesnak, 1983).

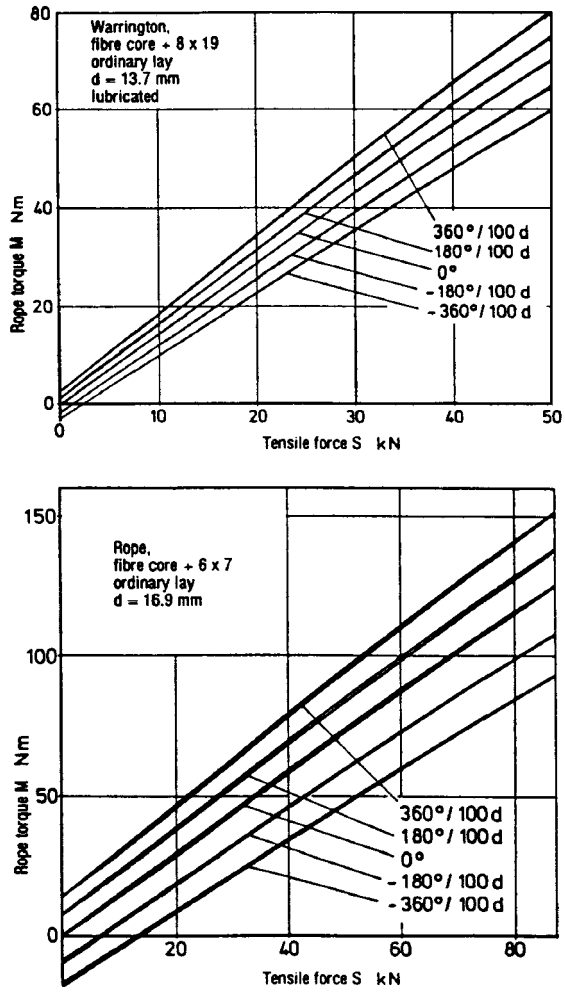

Figure 2.6 - Typical measured torsional response of stranded wire rope (single layer), Feyrer and Schiffner (1987).

Kollros (1976) investigated the effect of load and twisting on the resulting torque of two ordinary lay and two Lang's lay ropes using a machine similar to that in figure 2.4. Following on from the work of Kollros and others, Feyrer and Schiffner (1986,1987) generated typical tension-torsion curves, figure 2.6, using the equipment shown in figure 2.7. The measured results were compared with theoretical predictions based on modelling of the rope helix geometry.

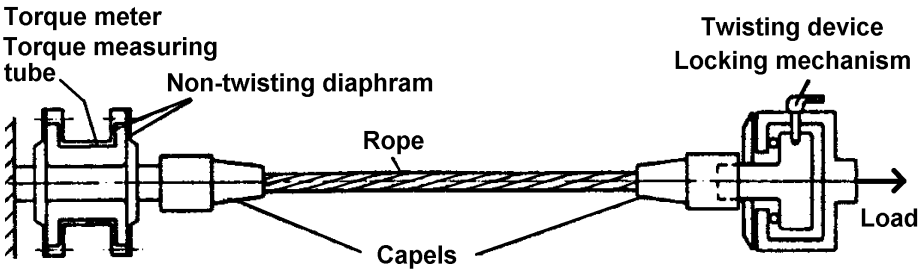

Figure 2.7 - Apparatus for measuring the torque and twist angle of wire rope, Feyrer and Schiffner (1987)

Utting and Jones (1985) conducted experiments in which wire rope strands were subjected to static axial loads. The strands were held in conical end grips which allowed full end fixity, partial restraint, or zero torsional resistance (free end). The layout of the testing rig used is shown in figure 2.8. Strain gauge load cells monitored the tensile load and the associated torque developed in strands when restrained at both ends. An instrument, figure 2.9, was designed to simultaneously record the extension and rotation over a predetermined gauge length. This device was termed an "extrometer".

Preliminary tests on seven wire strands demonstrated that the "extrometer" instrument was capable of providing reliable results. The extension and rotation characteristics recorded on a seven wire strand under tensile load agreed reasonably well with the corresponding predictions based on the theory presented by Machida and Durelli (1973). In their theory development, Machida and Durelli conducted physical tests on an oversized epoxy model of a seven wire strand. The strand extension versus axial load was measured for both torsionally free and fixed ends and the torque versus angle of applied twist was recorded for different constant loads.

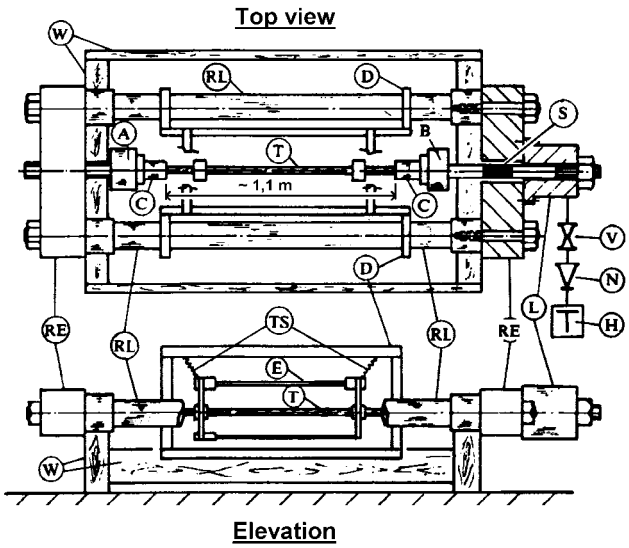

Figure 2.8 - Rig for testing of wire strand, from Utting and Jones (1985)

A - Adapter	D - Dexion support	N - Non-return valve
B - Boss	E - Extrometer, figure 2.9	V - Valve
C - Conical strand grip	TS - Tension springs	RL - Rig longitudinal bar
L - Load ram	RE - Rig end member	S - Strain gauged load cells
H - Hand pump	T - Test strand	W - Wooden support

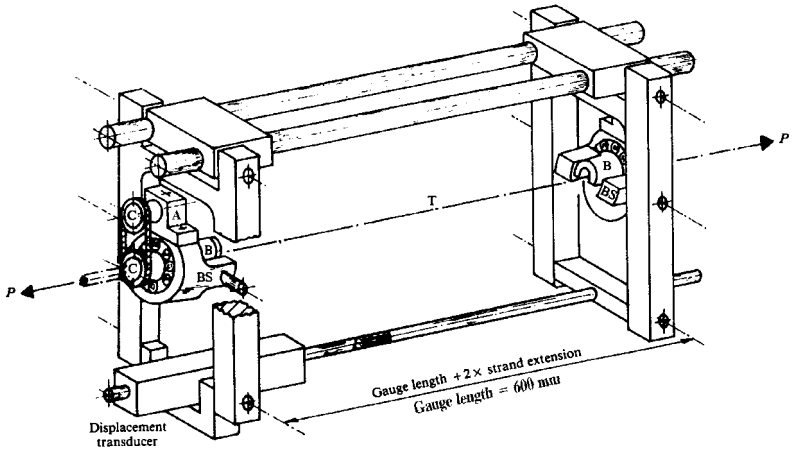

Figure 2.9 - "Extrometer" developed by Utting and Jones (1985)

A - Rotary potentiometer	C - Sprocket	B - Ball bearing
P - Load on strand	BS - Pivoted boss	T - Strand axis

Utting and Jones (1987) later applied the equipment (figures 2.8 and 2.9) to further investigations on seven wire strands and then to a nineteen wire strand. The focus of the investigations was comparison of the calculated strand responses, based on mathematical modelling from first principles, with the measured behaviour. Utting

and Jones (1988) concluded that the overall response to axial loads for the nineteen wire strand (12/6/1) could not be predicted as accurately as was the case with the seven wire strand previously investigated. This suggests an increased need for physical testing as the complexity of the strand or rope construction increases.

Raoof and Hobbs (1988a) conducted experimental studies on the static and dynamic torsional stiffness and hysteresis properties of a used 39 mm and new 41 mm structural strand using the equipment shown in figure 2.10. The 1000 kN capacity dynamic tensile testing machine (figure 2.10a) was complemented by a purpose designed torque application system, capable of applying a pure external torque at any desired position along the length of the strand, figure 2.10b. For the specific tests reported, the torsion frame was located at the mid–point of the specimen. The torque was generated by placing weights on the load hanger. The applied twist was measured by clamping a bar to the strand (near to the torque arm) and measuring its tip deflection with a displacement transducer. Dynamic tests were all of the free decay type and the soldered lap joint allowed sudden release of the initial constant torque (heating with a naked flame). It is evident that the method of torque application, shown in figure 2.10, results in one half of the strand being twisted up and the other half untwisted.

a)

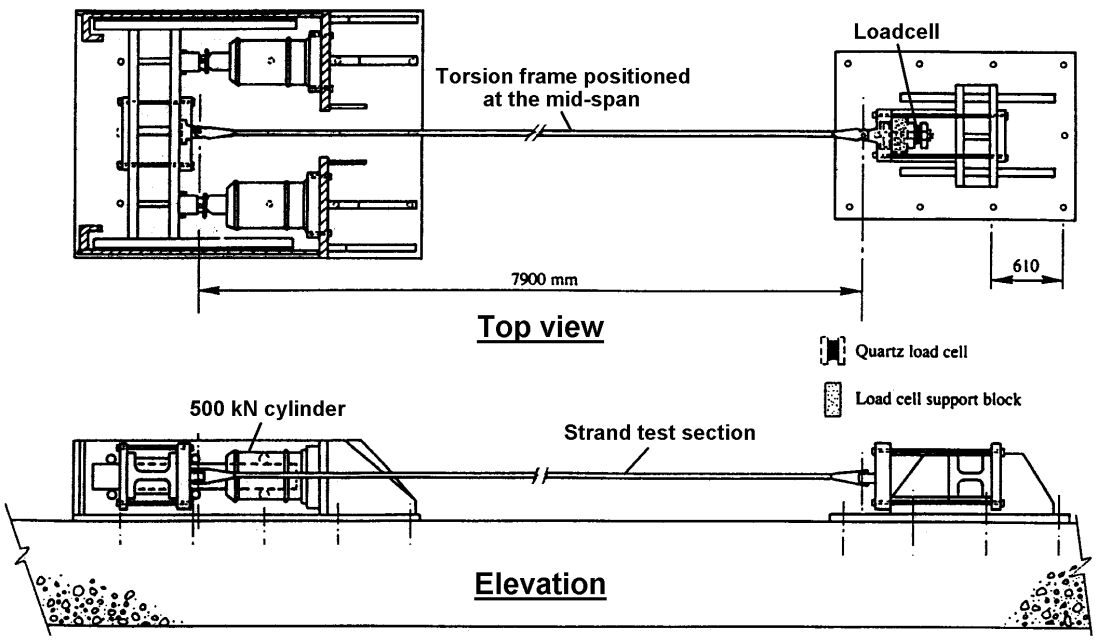

Figure 2.10 - Test equipment for static and dynamic torsion tests on spiral strands ....

b)

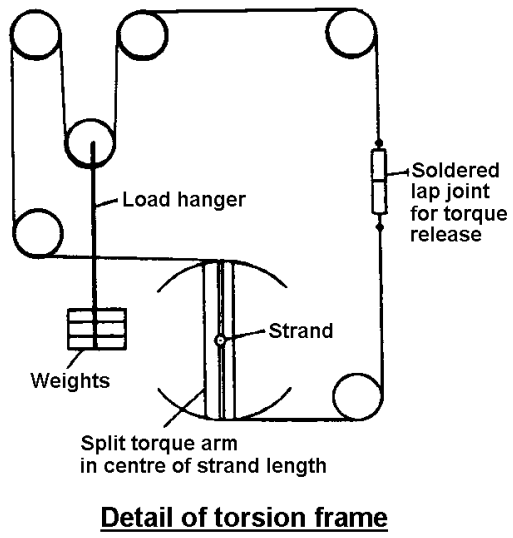

Figure 2.10 - Test equipment for static and dynamic torsion tests on spiral strands, Raoof and Hobbs (1988a). The soldered lap joint (b) allows for sudden torque release by heating the joint with a torch.

Oplatka and Roth (1996) recently presented findings on the effect of fluctuating tension and twist on the endurance of Lang's and ordinary lay haulage ropes for "jig-back" rope ways (cable car systems). The focus of the investigations was to determine which of the two lay types is the most suitable (from an endurance point of view) for application in installations with relatively large changes in height. The machine shown in figure 2.11 ensures a constant torque in the rope section under conditions of fluctuating load. This is approximately equivalent to the loading conditions which are experienced in service. Fluctuating bending of the rope in close proximity to the socket is also catered for. It can be seen that the method of torque application is very similar to that used by Raoof and Hobbs (1988) although in this case the torque is applied to one end of the rope.

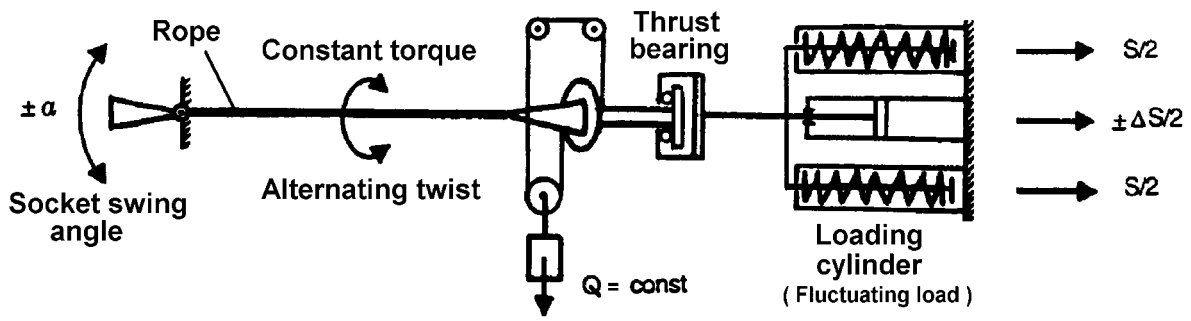

Figure 2.11 - Testing machine for investigations into the effect of fluctuating load and twist on rope endurance (Oplatka, 1996).

In France, Cantin et al. (1993) conducted tension-torsion studies on a 40,5 mm 6x17 Seale, Lang's lay rope with a solid polypropylene core (described by Durat, 1993). The machine used was capable of applying load and torque up to 500 kN and 5000 Nm respectively. Measurements included load and torque (strain gauge bridges) as well as extension, diameter and lay length. Of most interest was the placing of rotation measurement transducers at ten positions along the 7,0 m test length. In theory the rope cross-section should not rotate when subjected to axial loading only. The rotation transducers indicated that different sections exhibit relative rotations depending on the mean axial load (i.e. varying torsional stiffness along sample). Figure 2.12 shows the results of the intermediate rotation measurements for loads in the range, 20 kN to 300 kN. The rotations were measured before and after bedding in cycles (20 kN to 360 kN) the number of which was not given. Tests were also conducted to determine typical torque–tension curves shown earlier in figure 2.6.

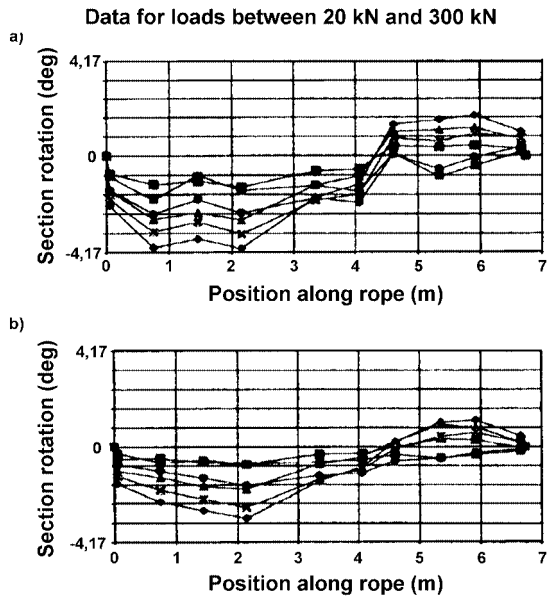

Figure 2.12 - Rope rotation along a test section as a result of axial loading, a) before bedding in cycles, b) after bedding in cycles, Cantin et al. (1993).

A considerable amount of rope tension-torsion research has been conducted in South Africa primarily for the development of non-spin or low-rotation ropes for Koepe winders (head and tail ropes). Most of the research results are contained in unpublished propriety reports commissioned by a local rope manufacturer. In most instances, the investigations were conducted by the CSIR Mine Hoisting Technology

Division (formerly, the Mine Equipment Research Unit of the National Mechanical Engineering Research Institute). Fritz (1982), McKenzie (1987), McKenzie (1989) and Yiassoumis (1992) have previously reviewed and referenced the majority of the relevant unpublished reports.

Shelly (1974) referred to the use of a universal wire rope fatigue testing machine (figure 3.1) for determining the variation of torque with load for different applied twists. Shelly also stated that a new testing rig of simpler design than the universal testing machine was under construction. The new rig was the original version of the testing facility described in chapter three. Since approximately 1975, all tension–torsion testing in South Africa has been conducted on the newer CSIR machine, primarily by Fritz, McKenzie, Yiassoumis and their assistants.

In most of the later versions of tension-torsion testing facilities, strain gauge load cells are used for the measurement of rope load and torque. The earlier machines utilised dynamometer type arrangements (torque arm combined with compression load cell or spring balance). A detailed account of the various methods of torque measurement and the history thereof is given by Gindy (1985). The information in Gindy's paper was applied to torque measurement for wire rope by Cisko and Phillips (1986). Earlier Milburn and Rendler (1972) had applied similar principles to their investigation on the response of axially loaded wire ropes. Another notable publication on the topic of torque measurement is that of Hottinger Baldwin Messtechnik GMBH (1990). In this book, the principles of strain gauge transducers for measuring torque are well documented.

2.4 Wire rope torsional behaviour

Wire ropes generate a torque when they are subjected to a tensile load. The magnitude of the torque is a function of the helix geometry of the rope construction, figure 2.13. If the helix geometry of a section of rope with length, *dz*, is altered by an applied rotation, $d\Phi$, then it follows that the torque would also change. Using this reasoning, Hermes and Bruens (1957) proposed the following equations relating rope torque, *M*, to the applied load, *F* and twist, $d\Phi/dz$:

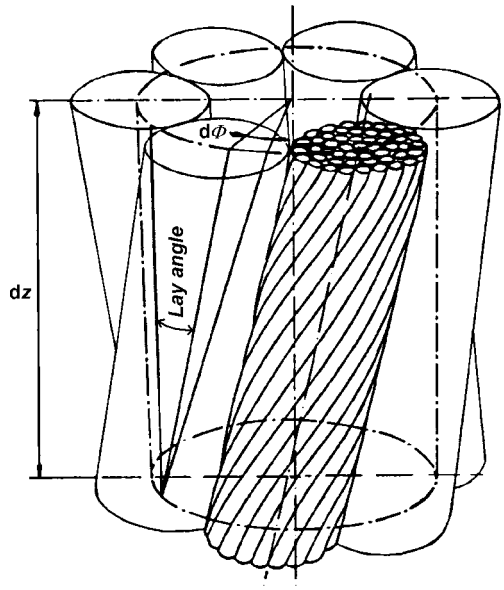

Figure 2.13 - Six strand rope element, RHL, from Hermes and Bruens (1957)

$$M = C.F$$
$$M = T.\frac{d\Phi}{dz} \qquad [2.1]$$

Under the action of simultaneous load and twist, the equations [2.1] can be combined :

$$M = C.F + T.\frac{d\Phi}{dz} \qquad [2.2]$$

where :

M	=	rope torque (Nm)
$d\Phi/dz$	=	rope twist relative to an initial lay angle (°/m)
F	=	rope load (kN)
C	=	constant of proportionality between load and torque (Nm/kN)
T	=	torsional stiffness constant (Nm/(°/m))

Immediately after presenting equations [2.1], Hermes and Bruens, without any derivation, stated that equation [2.3] describes the rotation in a vertically suspended rope of weight per unit length, *q*. Figure 2.14 was described in reference to equation [2.3].

$$\Phi = \frac{C.q}{2.T} (L.z - z^2) \qquad [2.3]$$

$$\frac{d\Phi}{dz} = \frac{C.q}{2.T} (L - 2.z) \qquad [2.4]$$

It turns out that equation [2.3] was determined by writing equation [2.2] in the form, $d\Phi/dz = f(M,F,C,T)$ with $F = P + q.z$, and then integrating with respect to z, applying the boundary conditions, $\Phi = 0$ at $z = 0$ and $z = L$. Two boundary conditions are required to solve for the constant of integration and the unknown constant torque, M. Note that neither equation [2.3], or its derivative [2.4] are functions of the rope end load, P. This implies that the state of rope rotation (and twist) does not change with changes in end load, although the torque, M, does.

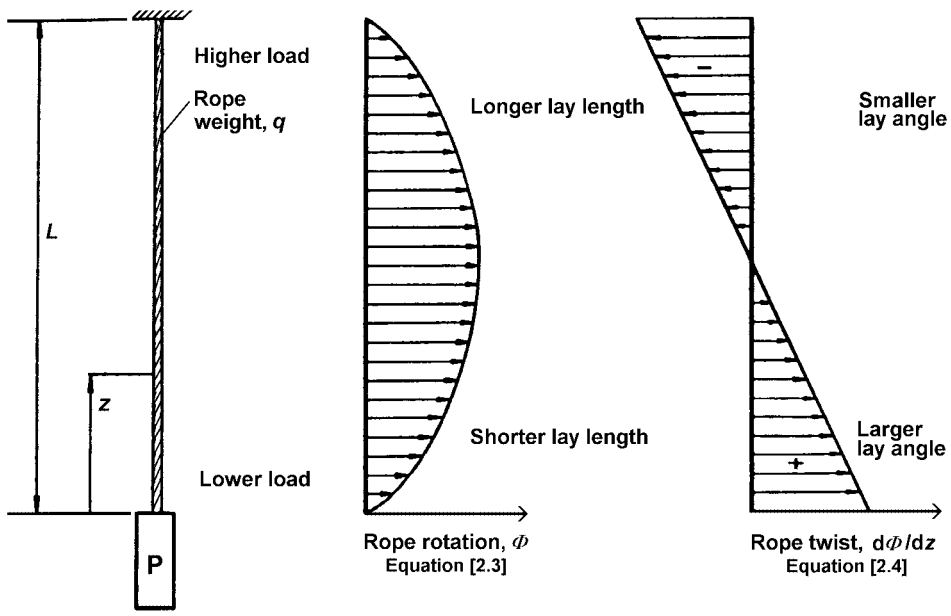

Figure 2.14 - Rope rotation and twist in a vertically suspended rope, according to Hermes and Bruens (1957)

Hermes and Bruens (1957) assumed that the torsional stiffness of a rope was constant for all loads and twists and that ropes have equal torsional stiffnesses for twisting up and untwisting. The paper dealt primarily with the determination of rope rotation on Koepe installations but the following statement was made regarding drum winders :

Spin in a Lang's lay wire rope causes the angle of lay of the strands to adopt various values along the rope. Starting from a linear theory for the

spin phenomenon the variations from the mean angle of lay can be calculated. In the case of a drum winder it has been found that the angle of lay in the various rope parts decreases linearly with the distance from the cages but does not vary during the wind. The variations increase with the depth of the winding installation

The analysis of Hermes and Bruens (1957) seems to be the earliest reference to methods of calculating rope rotation and lay length changes on drum winders (lower end fixed against rotation) and it formed the basis for further work. It will become evident in this section that refinements to the basic model (equation [2.2]) were primarily in the form of more accurate descriptions of the rope torsional properties with less attention being given to detailed understanding of the in-service rotation boundary conditions.

A contribution, often referenced in relation to rope torsion, is that of Hruska (1953). Hruska presented an analysis for determining the torque generated by stranded ropes as a result of axial loading. The changes in wire stresses caused by rope rotation were also considered. Components of the work presented were based on the investigations of Dreher (1934). Dreher's study was mainly devoted to determining the angle through which a loaded rope would rotate in the absence of torsional restraint. The determination of free end rope rotation appears to have been the preoccupation of initial researchers in the field. As an introduction to the determination of stresses in rope wires, Haid (1983) discussed some of the early papers relating particularly to the rotation behaviour of ropes. Haid quoted experiments conducted in Berlin and Munich during 1929 and 1930 in which rope rotation was determined as a function of load.

Another significant example of early rope tension-torsion research is the investigation of Layland et al. (1951). The response of Lang's lay ropes to loading and twisting was examined experimentally. Both the free suspension method (torsion pendulum) and a torsion machine (modified lathe) were used to determine the torsional stiffness properties and relationship between load and torque. The ropes considered were of the Lang's lay type (6x7 and 6x19) in the diameter range 12,7 mm to 22,2 mm. Torsion of ropes had been observed in cargo handling installations and it was proposed that mine hoisting ropes should be subject to similar behaviour. It was stated that "if the spin of the rope, or its effects, were in

any way proportional to the length of rope which was unreeled, there would be a case for investigation". A limited range of experiments was conducted which the authors intended should form the basis for more detailed research into the problem of hoisting rope torsion. Some of the most important findings and conclusions of the investigations relating to the torsional properties of Lang's lay ropes were :

- Ropes with a greater number of wires (6x19) show a lower torsional stiffness than ropes with few wires (6x7).
- The resistance of a stranded rope structure to torsional deformation is of a very low order when compared to solid steel bars.
- The torsional behaviour of very long ropes of large diameter (i.e. greater than 22,2 mm) needs investigation, particularly for application on drum winders.
- Torsional stiffness is greater for twisting in the laying up direction than for the unlaying.
- In the case of a torsion pendulum, damping is greater in the laying up direction of rotation than in the unlaying direction.
- Lubrication can affect the rope's torsional stiffness properties and torsional hysteresis is reduced by increased lubrication.
- Ordinary lay ropes have a higher torsional stiffness than the Lang's lay ropes.
- The need for torque-rotation analysis begins to appear when the diameter to length ratio (*d/L*) is in the order of 1/12000 and there are more than 60 wires. It is known to be absolutely essential at *d/L* = 1/42000 with 168 wires (6x28).
- The relationship between torsional stiffness and the helix angle (90° – lay angle) is nonlinear.

Layland et al. (1951) stated that it was well known that a rope with one fixed end and the other free to rotate will do so in the unlaying direction until a condition of torsional equilibrium is established. In the case where the lower end is not able to rotate, a torque of a certain magnitude would result in the rope. Layland and his associates were aware of two methods of dealing with induced torque in mining practice :

- The South African and European approach involved fixing the vehicle end of the rope against rotation upon installation and never thereafter releasing turns except at the top of its run (bank), when re-shackling (re-terminating). This

action resulted in the minimum overall extension of the whole rope and a shortening of the lay length at the conveyance end.

- In other countries all or most of the rope torque was removed at installation. This was invariably prescribed where keps* were used and the conveyance was connected to the rope by chains with the rope being slacked at every landing. If torque was present, intolerable twisting of the chains would result. The removal of torque was accomplished by the insertion of a temporary swivel between the rope and the chains with only the empty conveyance suspended. Slow descent was then made to the maximum depth, where torsional equilibrium for the given suspended weight was supposedly reached. This was followed by slow ascent and finally by the removal of the swivel. In these circumstances, the rope was allowed to unlay until rotation had ceased with the result that the extension of the whole rope was considerable and the lay length at the conveyance end remained at or exceeded the manufactured lay length. A rope which had been deliberately unlaid by this means was often observed to later rotate in the laying up direction when detached from the conveyance at the bank.

It was unfortunately not stated which countries employed the second practice. In the conclusions it was suggested that the practice of preventing unlaying of the rope was favoured from a rope endurance point of view. The paper of Layland et al. (1951) indicated that mine rope operators at that time had a basic understanding of rope torsion and were aware that the removal of rotation from a rope in service (or not) could have a significant influence on the subsequent lay length variations. It was also realised that there could be a correlation between the state of unlaying of a Lang's lay rope and its endurance.

* The word "kep" originates from keep and is used in the northern British dialect, the meaning, "to catch".

In three papers dealing with various aspects of the extension and torsional behaviour of wire ropes on Koepe winders, Hankus (1993a, 1993b, 1995) reported that Glushko (1966) proposed a two degree of freedom elastic system of the form :

$$A_1.\frac{du}{dz} + C_1.\frac{d\Phi}{dz} = F(z) = P + q.z$$
$$C_1.\frac{du}{dz} + B_1.\frac{d\Phi}{dz} = M(z) = constant \qquad [2.5]$$

where A_1 , B_1 and C_1 are constants

Considering only the rope twist, and applying the same boundary conditions as Hermes and Bruens (1957), the resulting equation for in-service rope rotation is identical to equation [2.3] :

$$\Phi = \frac{C_1.q}{2.(A_1.B_1 - C_1^2)} (L.z - z^2) \qquad [2.6]$$

and

$$C = \frac{C_1}{A_1} \quad and \quad T = \frac{A_1.B_1 - C_1^2}{A_1} \qquad [2.6a]$$

Gibson (1980) gave approximate equations for the torque generated by Lang's lay ropes under load, as a function of their nominal diameter (d_{nom}) and lay length (LL). Although equation [2.7] was presented in 1980, it was developed in the work of Gibson et al. (1970).

$$M = f(d_{nom}^2).\frac{F}{LL} \qquad [2.7]$$

In addition to presenting simplified equations for rope torque, Gibson (1980) also gave a concise description of the reasons for the in-service lay length changes observed on deeper shaft drum winders. The contents of three paragraphs from Gibson's paper are included below as they deal directly with the rope behaviour pattern with which this thesis is concerned :

A number of applications require that a wire rope be suspended vertically in great lengths. Because of the large tension gradient associated with the weight of the rope, it would appear from equation [2.7] that the rope torque at the top of the shaft would be greater than the torque at the bottom of the shaft. However, in practice, under static conditions, there can be no torque gradient in the hoist rope between the head sheave and the attachment to the skip since no externally applied torsional forces exist anywhere along the length of the suspended rope.

In order to seek a condition of uniform torque in the presence of a significant tension gradient, certain geometric changes occur within the rope structure which alter the torque characteristics. Measurements of such a hoist rope will reveal that the lay length of the rope near the head sheave is longer than that of the as-manufactured rope, while the lay length of the rope adjacent to the skip is shorter. The increase in lay length near the top of the shaft reduces the torque, while the decrease in lay length at the bottom of the shaft increases the torque. The extent to which these lay length changes occur, as the rope seeks a uniform torque condition, is dependent upon the length of the rope suspended in the shaft. The rope achieves these changes in lay length through a rotation of the suspended section even though rotation is prevented at each end. The maximum rotation occurs approximately at the mid-span between the head sheave and the conveyance

As the skip is hoisted from the loading station, the rope having the increased lay length at the top of the shaft passes over the head sheave and onto the drum. As the hoisting cycle is repeated, the hoist rope eventually achieves a relatively stable rotation condition. In practice, it is frequently observed that the twisting of the rope extends even to the dead wraps (coils) on the drum. It is also common practice for the rope to be periodically detached from the conveyance and allowed to rotate so as to relieve some of the "built-up" twist. This spin release further changes the geometry of the hoist rope, and additional rope twisting then occurs as the hoisting cycle is repeated.

Shelly (1974) used theoretical relationships derived from experimental tension–torsion results to predict the in-service behaviour of multi-strand non-spin Koepe balance ropes. Shelly named the constant *C*, of equation [2.2], the "torque factor" and *T*, the "torsional stiffness". After examining typical torque versus load curves for varying twists, Shelly realised that neither *C* or *T*, as constants, could describe the general response of a rope over a range of loads and applied twists. An approach was subsequently adopted in which a computer algorithm calculated values of *C* and *T* at fixed increments of load and applied twist. The measured test data formed the input to the algorithm. Similar approaches have since been applied by Yiassoumis (1992) and Rebel (1993).

Kollros (1976) presented a revised equation for torque which included a product between load and twist :

$$M = f(d).F + f(d,LL_0).F.\frac{d\Phi}{dz} + f(d^4,G).\frac{d\Phi}{dz} \qquad [2.8]$$

where : d is the rope diameter, LL_0 is the lay length at zero applied twist and G is the shear modulus of the rope cross-section.

Kollros stated that the values for the constants preceding the load, twist and load–twist product terms could obtained analytically by considering the helix geometry of a rope construction. It was however suggested that the constants should rather be determined by means of a tension-torsion test. The work of Feyrer and Schiffner (1986) was based on the general equation for torque, [2.9]. The difference in their approach was that the constant preceding the load-twist product term was altered to be a function of the diameter squared.

$$M = f(d).F + f(d^2).F.\frac{d\Phi}{dz} + f(d^4,G).\frac{d\Phi}{dz} \qquad [2.9]$$

The objective of the works of Kollros (1976) and Feyrer and Schiffner (1986) was the calculation of the rope torsional response constants from first principles and the comparison of these to measured laboratory results. Neither of the papers make any significance reference to the in-service torsional behaviour of ropes.

When plotted in the torque versus load plane, the equations of the form [2.2], [2.7] and [2.9] give different general shapes of tension-torsion curves. Figure 2.15 shows comparative representations of the three equations.

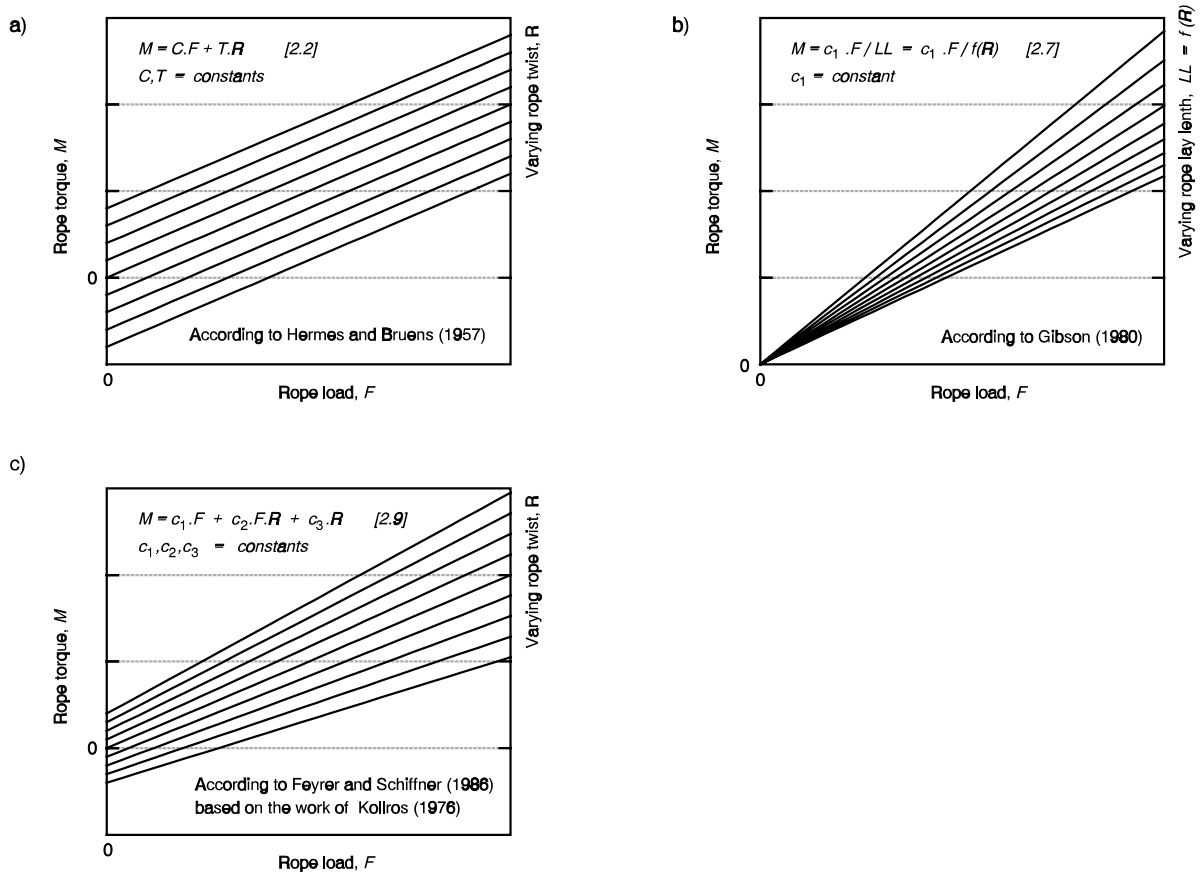

Figure 2.15 - Basic equations for describing rope torsional response to axial loading for different values of applied rope twist.

Equation [2.2], shown in figure 2.15a, suggests that the proportionality between load and torque is independent of the applied twist (lay length). It would be expected that for a certain construction, the change in torque for given change in load would be greater for a shorter lay length than for a longer lay length. In the cases of figure 2.15b and 2.15c, variations in the proportionality between load and torque are taken into account. Equation [2.7] has the limitation that it is not suited for describing the response of a single rope specimen for varying angles of twist since the application of twist to the specimen would require a torque at zero load. The equation is however suited to approximating the torque in a variety of specimens of the same construction but with different initial lay lengths (zero applied twist).

Yiassoumis (1992) also investigated the torsional behaviour of steel wire ropes for Koepe winders. Experimental tension-torsion testing was combined with in-situ measurements on a 1800 m deep shaft and used to determine a theoretical model of the head and tail (balance) rope behaviour during a winding cycle. Yiassoumis found that the measured rotation in the head rope during a cycle was significantly lower than the calculated value. It was realised that the large error could be due to the fact that torsional hysteresis effects had been neglected in the modelling.

As regards further research, Yiassoumis (1992) recommended that efforts should be aimed at improving the quantitative accuracy of predictions of rope torsional behaviour. In particular, modelling of the torsional behaviour of the ropes should take into account hysteresis effects. It was anticipated that this would lead to a significantly more complex algorithm since the condition of each rope element will depend not only on the torque and tension in the element but also on the torque and tension history. Further investigation into the torsional properties of wire ropes were recommended. These included aspects such as the variation of the torsional properties of ropes along their length and the effective torsional stiffness of wire ropes in service.

Hecker and van Zyl (1993), discussed torque-tension rotation behaviour of Lang's lay ropes on drum winders. The explanation of the behaviour phenomenon was similar to that of Gibson (1980) and the equation used to relate rope torque to load and twist was of the same form as the equation proposed by Feyrer and Schiffner (1986). The boundary conditions used in calculating the in-service rotation and lay length variations (48 mm Lang's lay rope) were based on the same assumptions as Hermes and Bruens (1957). The limitation of their analysis was that it neglected torsional hysteresis behaviour in calculating rope rotation during conveyance loading. A certain position along a suspended rope was observed to have rotated 12,5 times during conveyance loading. Their analysis predicted 28 turns at the same point. With regards to the lay length calculations, the rotation boundary conditions were assumed to be zero at the head sheave and at the conveyance. This assumption led to errors when calculating the in-service lay lengths. Using an analysis similar to that of Hecker and van Zyl (1993), Rebel et al. (1996a) presented calculated results of in-service lay length and rotation for a 54 mm Lang's lay triangular strand rope. These results were subject to the same assumptions and therefore the same limitations as those of Hecker and van Zyl (1993).

Hecker and Van Zyl (1993) also measured rope torque and load during the operation of a rock winder. Figure 2.16 shows an example of the measured parameters of the winder over a full cycle. Skip position, rope load at the skip and rope torque are plotted against time for a 2200 m length of wind. The rope used on the double drum rock winder had a diameter of 48 mm and was of the triangular strand construction. The skip mass was 9820 kg with a rock payload of 14 070 kg. The load and torque measurements were achieved by strain gauging and calibrating the skip draw bar (connection between skip and rope).

The cycle commenced with the rock skip at the loading station where it was loaded. Since the equilibrium torque in the rope is related to the rope load, an initial step change in torque occurred (≈1200 Nm) and the rope would have immediately rotated about its axis to establish the new torsional equilibrium. The subsequent rope tension fluctuations, which resulted from the dynamics of drum acceleration, layer crossovers and deceleration of the system would have caused the rope to rotate accordingly throughout the trip. It can be seen in figure 2.16 that the torque in the rope increases slightly during the up going and down going trips. Since no two winding cycles are ever exactly the same, drum winder ropes in general pass over the sheave wheel and onto the winding drum with varying contact points, (as a result of load induced rotation) thereby uniformly distributing the wear and plastic deformation of the outer wires.

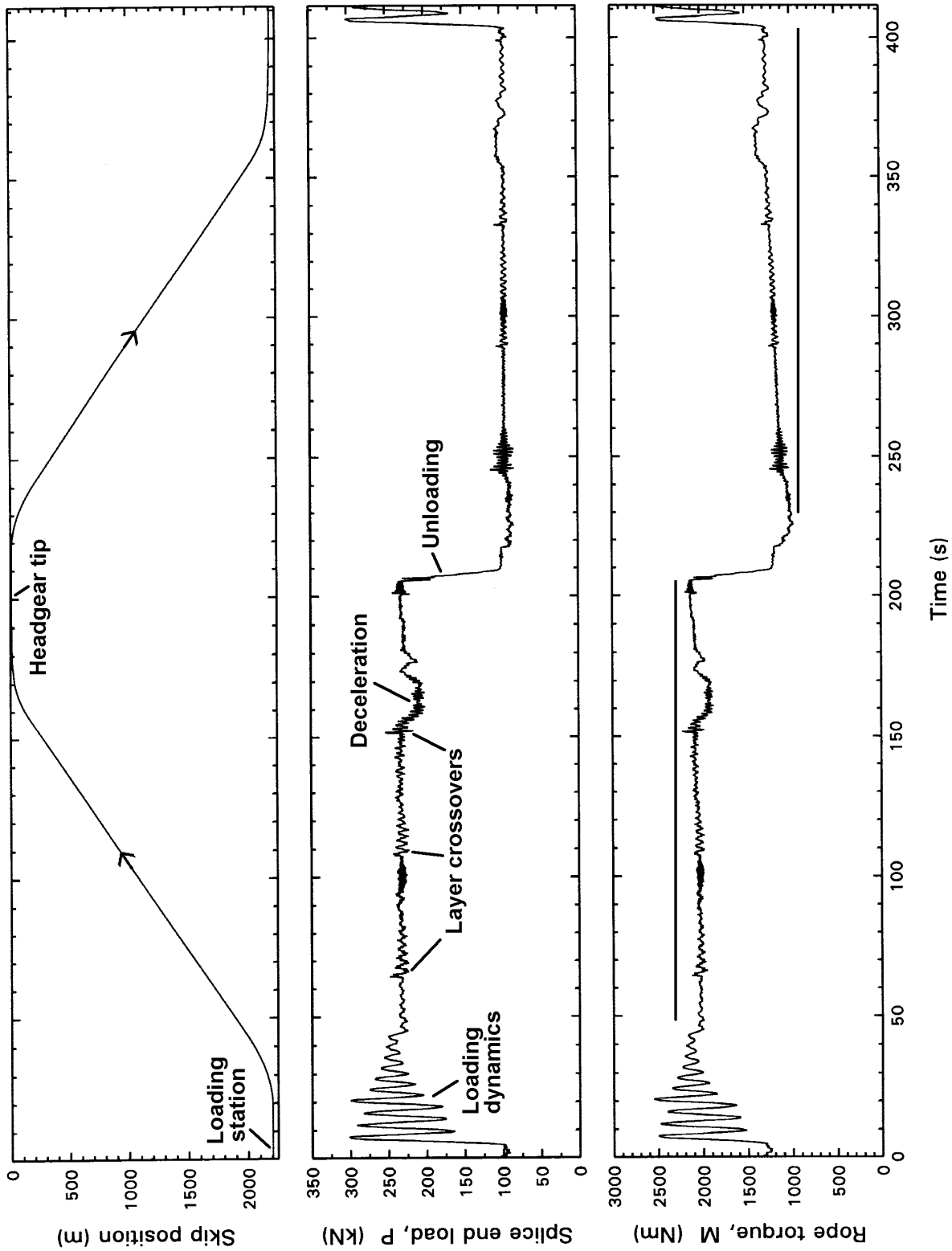

Figure 2.16 - Measured parameters of a double drum rock winder during a winding cycle, adapted from Hecker and van Zyl (1993).

Oplatka (1996) reported that Lang's lay haulage ropes operating on "jig-back" rope ways (figure 2.17a) are subject to increased lay length variations as the vertical height between the upper and lower stations is increased, Δh. It has been observed that, in the vicinity of the terminations, the rope is subjected to alternating bending, tensile and torsional loading. The alternating twist is greater in the case of Lang's lay ropes compared to regular (ordinary) lay ropes. Oplatka suggests that the same loading patterns and therefore similar problems (relating to rope endurance) may occur with ropes used in mine shaft installations with long suspended rope lengths.

a)

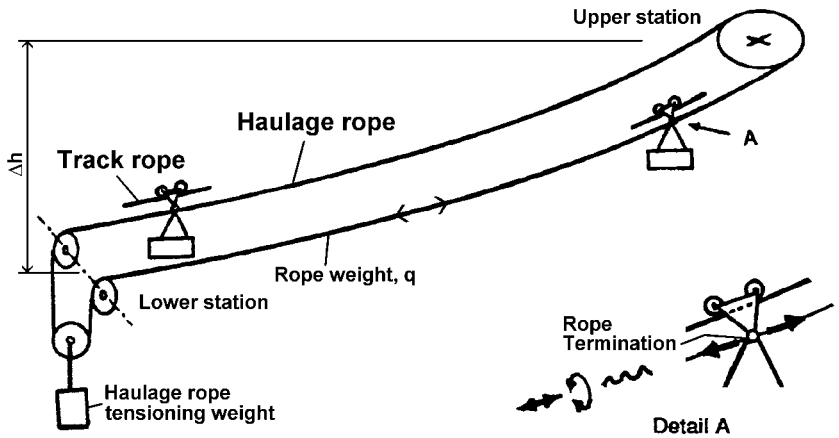

b)

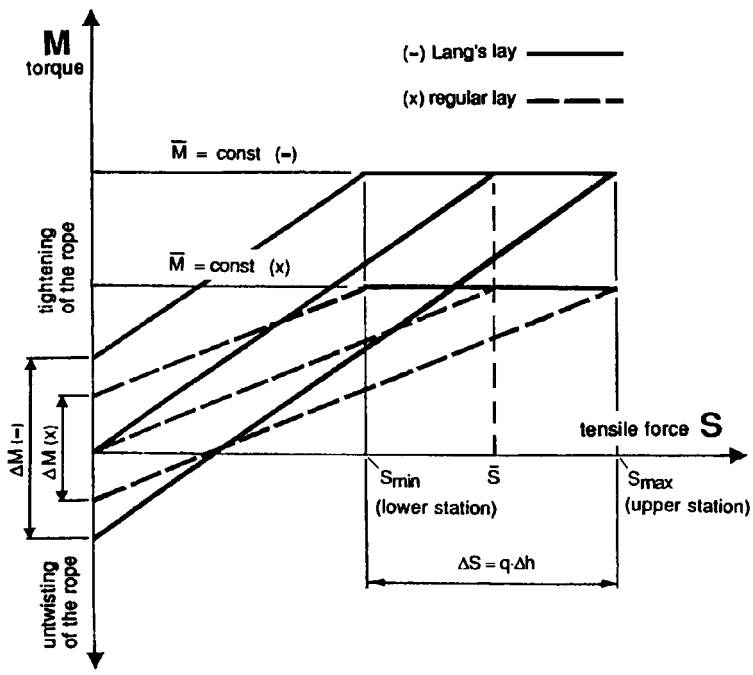

Figure 2.17 - Main components of a "jig-back" rope way (a) and the torsional response of Lang's lay ropes compared to ordinary lay ropes (b), from Oplatka (1996).

In figure 2.17b, Oplatka (1996) showed how the torsional response of ordinary lay ropes (x) compared to that of Lang's lay ropes (**–**). For a fixed change in height of an installation, the constant rope torque for a Lang's lay rope would be greater than if an ordinary lay rope was used. The variations in the helix geometry (lay angle) would also be expected to be greater in the case of Lang's lay ropes. In both cases it was assumed that zero twist occurs at the mid-span position. Judging from the position where the values $\Delta M(-)$ are read off (zero load), it appears as if Oplatka used a tension-torsion-twist relationship in the form of equation [2.2]. After having conducted investigations into the endurance of the two lay types (machine in figure 2.11) Oplatka suggested that the Lang's lay construction should be considered in future for haulage ropes of installations with large differences in height. This statement does not appear to be consistent with the experiences reported with the use of Lang's lay ropes on deeper level Koepe winding installations (Δh > 1300 m, section 1.3) .

Raoof and Hobbs (1989) showed that taking into account inter-wire friction in multi–layered structural strands can have a significant effect on the calculated response of the strands to externally applied torques. The analysis conducted was based on the well established orthotropic sheet theory (Raoof and Hobbs, 1988b) which is capable of modelling the detailed contact patch behaviour between wires within a layer and between wires in different layers of the strand. Raoof and Hobbs demonstrated that a spiral strand exhibits a nonlinear relationship between applied torque and twist, figure 2.18.

It follows from figure 2.18 that the torsional stiffness of the strand is both a function of the applied twist (or torque) and mean load. The authors ascribed this behaviour to a transition from a state of no-slip between the wires for very small perturbations to full slippage at larger deformations. In figure 2.18, a line indicates the points at which the torsional stiffness (1/slope) tends to a constant. The onset of full-slip is delayed as a result of increased inter-wire contact forces associated with higher axial loads. Even though triangular strand ropes have considerably different geometric properties to spiral strands, it would be expected that on a qualitative basis they would exhibit similar behaviour. However, quantitatively, the results may vary significantly.

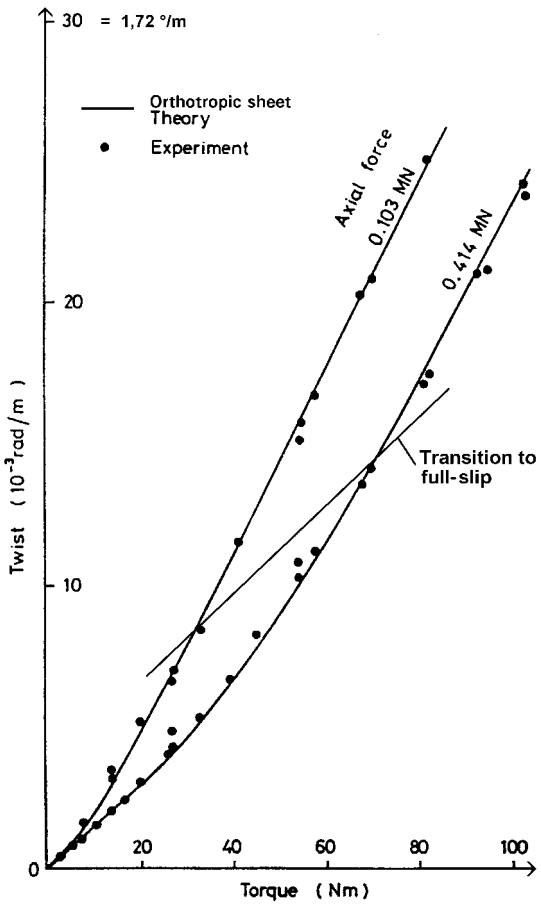

Figure 2.18 - Torque versus twist relationship for a 39 mm structural strand, from Raoof and Hobbs (1989). Experimental data generated with equipment in figure 2.10.

2.5 In-service rope rotation measurement

Hermes and Bruens (1957), Carbogno (1991), Yiassoumis (1992) and Hankus (1993) describe the measurement of rope rotation on Koepe winders using the "chalk line" method. The basic principle is that a continuous line is drawn (or painted) onto the rope as it travels in one direction of the hoisting cycle. Rotation of the rope cross-section (for whatever reason) causes the line to form a spiral along the length of the rope. Providing that the rope does not rotate when the direction of travel is reversed, it is possible to count the rope rotations by counting the number of spiral line crossings (or parts thereof) viewed from one side of the rope (similar to counting the number of thread turns on a screw). In order to obtain a rotation distribution, $\Delta\Phi(z)$, counting of the turns has to be combined with distance measurement along the rope, z. Figure 2.19 schematically illustrates the "chalk line" method.

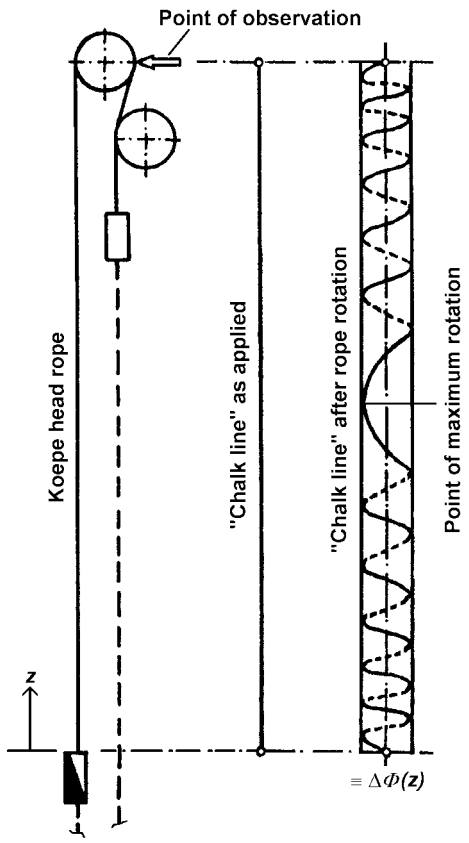

Figure 2.19 - The "chalk line" method of determining rope rotation, adapted from Carbogno (1991)

It is known that Hecker and van Zyl (1993) attached a piece of string to a drum winder rope to measure the rotation at a single point along the rope during loading of a skip. The amount of string wound up by the rotating cross-section, divided by the circumference, yielded the number of turns. Access to the rope was achieved by placing wooden planks over the shaft steel work at the measurement position (this was not at the bank).

2.6 Rope lay length measurement

Rope lay lengths are generally measured manually either by means of a tape or form of lay length gauge which can ensure that the measurement is taken parallel to the rope axis (Kuun, 1995). There are very few examples of continuous lay length measurement systems. Harvey and Kruger (1959) reported on the development of a lay length measuring device shown diagrammatically in figure 2.20.

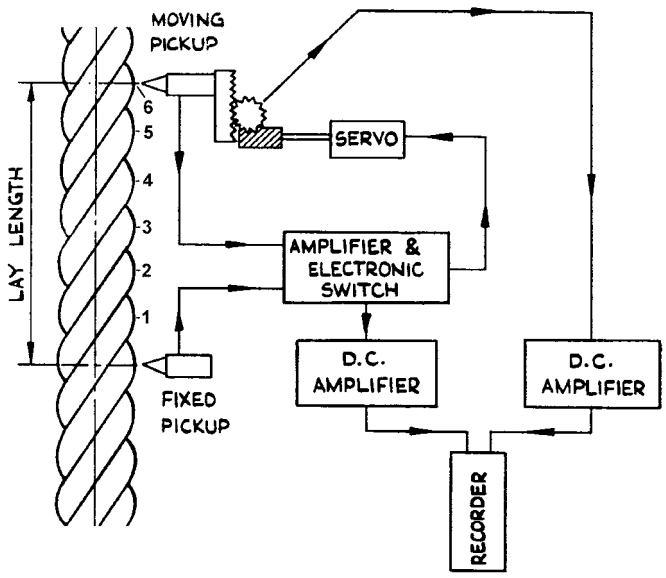

Figure 2.20 - Lay length measuring device, from Harvey and Kruger (1959).

The instrument was based on the use of magnetic vibration pick-ups, of the type used to measure the vibration of ferrous bodies. Such pick-ups were sensitive to the distance of a body from their probes. By placing them close to the rope surface alternating signals were generated. If the two probe were mounted exactly one lay length apart then the output signals would be in phase. Should the lay length differ from the distance between the probes, then the two signals would no longer be in phase. The position of one of the probes was adjusted automatically in such a manner that the phase angle between the probe signals remained as near to zero as possible. The distance which the probe was moved, from the initial setting, gave the measure of the change in lay length. The lay length measuring device was developed to be used in conjunction with magnetic non-destructive testing instruments. Harvey and Kruger proposed that rope lay length would shorten locally at a point where the rope had weakened. Continuous lay length measurement would indicate such areas providing additional information for rope condition assessment.

Haller (1989) discussed experiences with untwisted cable way haulage ropes in Switzerland. These ropes would be of the round strand, Lang's lay, Seale construction as described by Oplatka (1994). It was found that untwisting of the ropes could lead to reduced operating life. Haller stated that since 1982 rope lay lengths were measured (manually) at each inspection and that a "sensor" was being

developed to monitor the lay length along the rope. The purpose of the sensor was to assist in quantifying the twist distribution in the ropes. Details of the sensor were not given.

2.7 Summary

1. A wire rope tension-torsion testing machine with the capability of automatic control and recording of rope load, torque and twist would satisfy all combinations of loading and torsional deformation that may be required to fully quantify the torsional response of a specific rope construction. Such a machine was not previously available and it was therefore necessary for the laboratory facilities to be development as part of this investigation

2. Most rope tension-torsion research to date has concentrated on constant twist tests, with varying load. Constant load tests, with varying twist, are equally important and in some cases they can highlight rope properties which would otherwise not have been apparent hence the importance of item 1 above.

3. The general form of an equation for relating rope torque to load and twist should describe the measured test data in the most accurate manner. This equation should also allow for nonlinear relationships between the three parameters.

4. Anticipating that ropes generally have a nonlinear relationship between torque and twist at constant load, all torsional stiffness measurements should be conducted under constant load conditions (varying twist). Similarly, the proportionality between load and torque should be determined from constant twist tests, as has been the case in the past. The detailed torsional stiffness properties of a rope construction cannot necessarily be inferred from a test where the rope twist is kept constant.

5. When twisting ropes at constant load, inter-wire friction can have a significant effect on the torsional stiffness. Even if the twist deflection is relatively small, large changes in stiffness can result from the transition from no-slip between the rope wires to full-slip. Thus, torsional hysteresis effects in wire ropes should not be ignored.

6. The rotation boundary conditions of ropes in service (drum winders) can significantly affect the lay length distributions. It is therefore important to consider that the rotation boundary condition at the drum end may be different from the boundary condition at the conveyance at installation. Boundary conditions and hence lay lengths can be altered by rope maintenance practices and are therefore not necessarily constant over the service period.

7. There have been examples of in-service lay length calculations for drum winder ropes but these have not been verified with in-service measurements. There are a considerable number of references which suggest that severe lay length changes may be expected in shafts deeper than 2500 m but none were able to quantify these. It was therefore of interest to rope manufacturers and mining companies to be able to accurately predict the lay lengths at future depths, hence a major reason for this study.

8. Very few attempts have been made at the calculation of rope rotation due to changes in the loading of vertically suspended ropes. The available examples were not able to accurately calculate rope rotation during conveyance loading. The reason for this was that the torsional stiffness properties used in the modelling approaches were based on tests which only determined measures of the full-slip stiffnesses (i.e. torsional stiffnesses inferred from constant twist tests). In such cases torsional hysteresis (friction) was not considered with the resulting rotation predictions being considerably larger than those occurring in operating ropes. In anticipation that load induced rotation of triangular strand rope in deep shafts may be important as regards rope performance, it is desirable to be able to model such rotational behaviour.

3 DEVELOPMENT OF THE LABORATORY TESTING FACILITY

Chapter summary : The development of the steel wire rope tension torsion testing machine used in the investigation is discussed in this chapter. A brief history of the testing facility is given and the rope parameter measurement systems are described. The structure and features of the machine control software are also explained. Examples of the load, twist and torque variations with time, for the main test categories, are presented.

3.1 Torsion testing machine history and requirements

The basic concept of the testing machine used in this project originated in the design of an universal wire rope fatigue testing machine, figure 3.1, which was built in the 1960's by the Mine Equipment Research Unit of the National Mechanical Engineering Research Institute (Shelly, 1974). The purpose of the fatigue machine was to assist in the study of hoisting rope deterioration due to a combination of fluctuating tensile, bending and torsional loads. Rope specimen lengths of 4,8 m could be accommodated. During the preliminary design phase of the fatigue machine, Kuun (1962) identified torsional strain as a service condition having a direct bearing on service life. This feature was therefore included in final the design to allow for accurate simulation of in-shaft conditions.

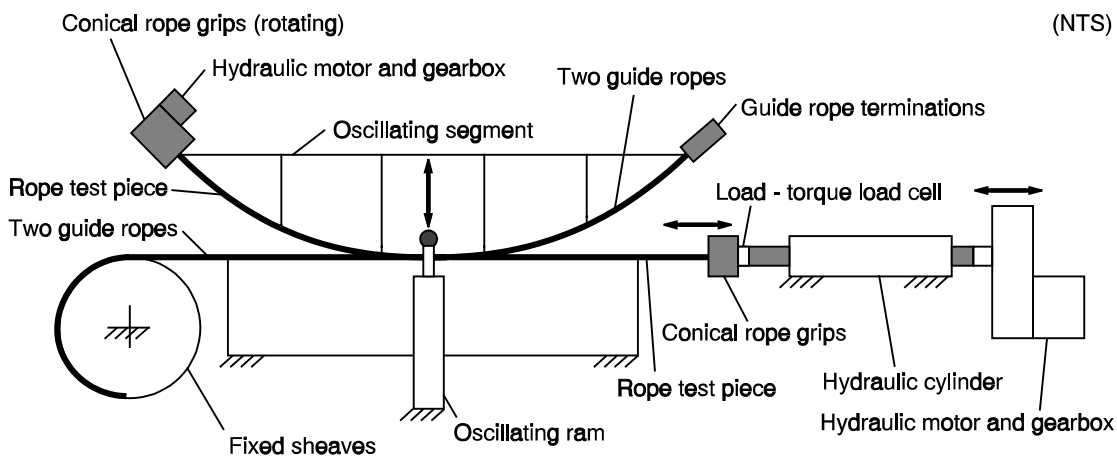

Figure 3.1 - Configuration of an universal wire rope fatigue testing machine of the Mine Equipment Research Unit, National Mechanical Engineering Research Institute. Adapted from Kuun (1962). The machine is no longer in existence.

The fatigue machine used an oscillating segment for rope bending, with a hydraulic motor connected to the one end of the rope and another motor and tensioning cylinder attached at the other end. The machine was also used to conduct tension–torsion tests as it had the capability of loading and twisting a rope sample while measuring the load and torque. This proved to be cumbersome and as a result the current tension-torsion machine was purpose built between 1972 and 1974. Since then a number of modifications have been made to the mechanical, electrical and control systems although the desired level of sophistication was never achieved.

During 1993 a final year engineering research project was conducted using the tension-torsion machine in its original form (Rebel, 1993). The data acquisition system was based on Hewlett Packard (HP) digital volt meters interfaced to a HP 86® computer. The slow rate of data acquisition resulted in extended periods of time for conducting relatively simple tests. Yiassoumis (1992) reported a loading rate of 40 kN per minute using the same equipment. Data analysis relied on custom written HP Basic programs since the data files were not compatible with MS-DOS® type computational packages. The machine was poorly documented and unreliable with breakdowns in both the electrical and mechanical systems being common.

The need for more accurate and detailed research into the torsional behaviour of Lang's lay triangular strand ropes resulted in a decision to completely re-develop the existing torque-tension machine as part of this project. The main requirement of the modified machine was that it should, through computer control, perform torsion tests at constant rope load, twist and torque to allow more realistic simulation of in-service rope tension-torsion interactions. In the original form, it was capable of measuring rope torque for manually set constant end rotations (twists) and varying values of load. Based on the literature reviewed in chapter two, it was anticipated that conducting tests at constant load and torque would indicate unexpected rope phenomena.

The machine upgrading process incorporated :

- Re-design, replacement or overhaul of problematic mechanical components.
- A complete new design and replacement of the electrical control and instrumentation systems.

- Modifications to the hydraulic systems including speed and position control for the hydraulic motor.
- Development of customised, personal computer (PC) based, control and data acquisition software.
- Detailed documentation of all mechanical, hydraulic, electrical, electronic and software components of the machine (Rebel, 1996).

The objective of the machine development project was to establish a wire rope testing facility which would not only fulfil the needs of the study described in this thesis but also be of benefit to future projects. Most of the contents of this chapter has been extracted from a published paper outlining the machine's current features and capabilities (Rebel and Chandler, 1996).

3.2 Torque-tension machine description

3.2.1 General layout

Figures 3.2 and 3.3 show the layout of the main components of the torque-tension machine. The hydraulic cylinder provides the axial load and the motor, with a reduction drive, can twist up or untwist the specimen as required. The scissor mechanism at the rear of the hydraulic cylinder, figure 3.4, allows axial movement but prevents rotation of the cylinder shaft. The measurement specifications of the machine are listed in table 3.1. The overall accuracies of the measurement systems were determined during the development project and represent the worst cases. They include nonlinearity, hysteresis, temperature effects and the data acquisition system resolution.

Table 3.1 - Measurement specifications of the tension-torsion testing machine.

Measurement parameter	Allowable range	Overall accuracy
Load	0 → 500 kN	± 1.8 kN full scale
Torque	-3200 → +3200 Nm	± 4.9 Nm full scale
Elongation	-130 → +130 mm	± 1.3 mm full scale
Diameter change	-5 → +5 mm	± 0.03 mm full scale
End rotation	-700 → +700 turns	± 1.0° (backlash in the reduction drive)

Rope diameters up to 64 mm can be accommodated. Depending on the construction, the maximum load may need to be limited so as not to exceed the torque limits of the loadcell.

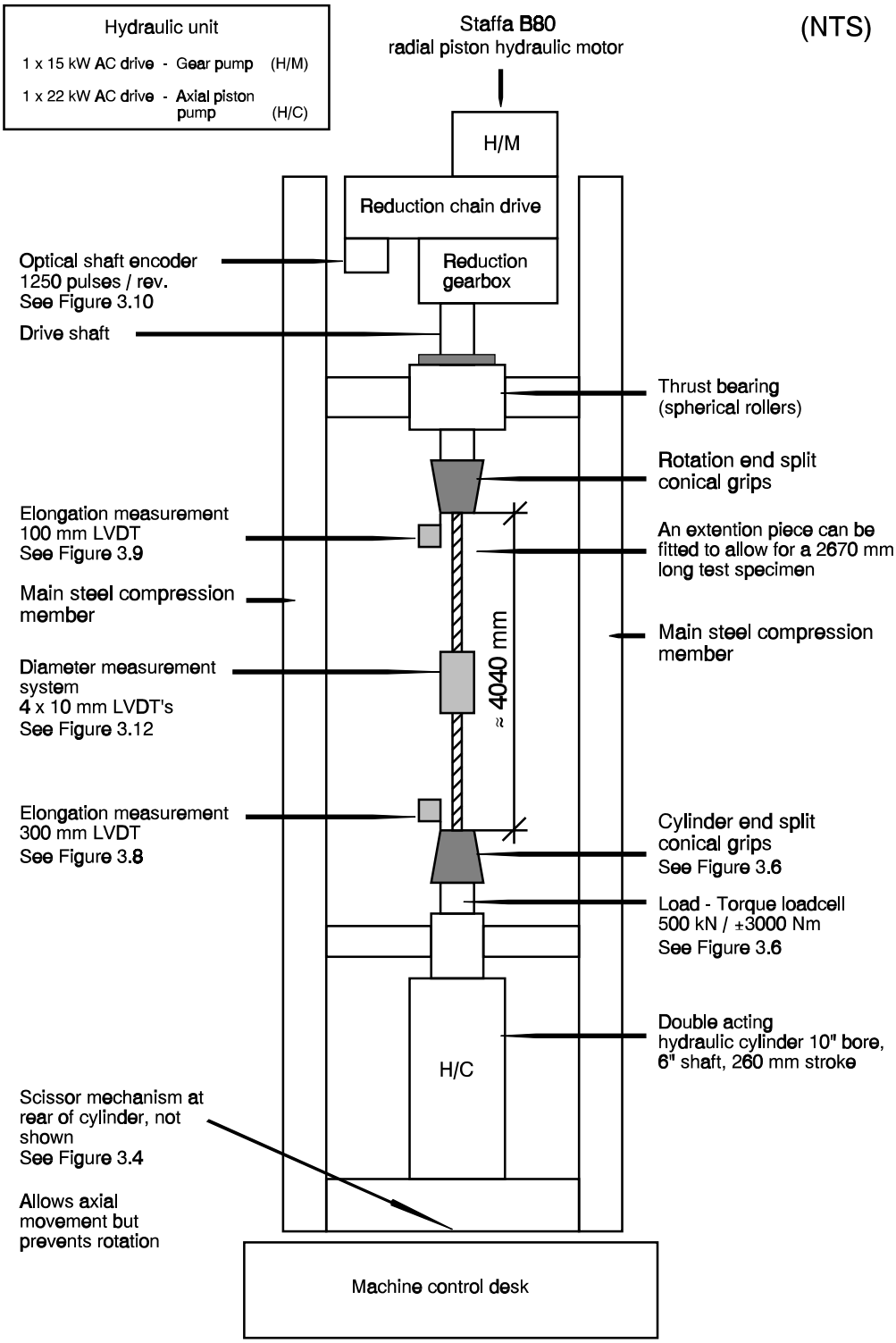

Figure 3.2 - General arrangement of the steel wire rope torque-tension testing machine.

Figure 3.3 - View of the steel wire rope torque-tension testing machine. The entire machine operation is controlled by the PC in the foreground.

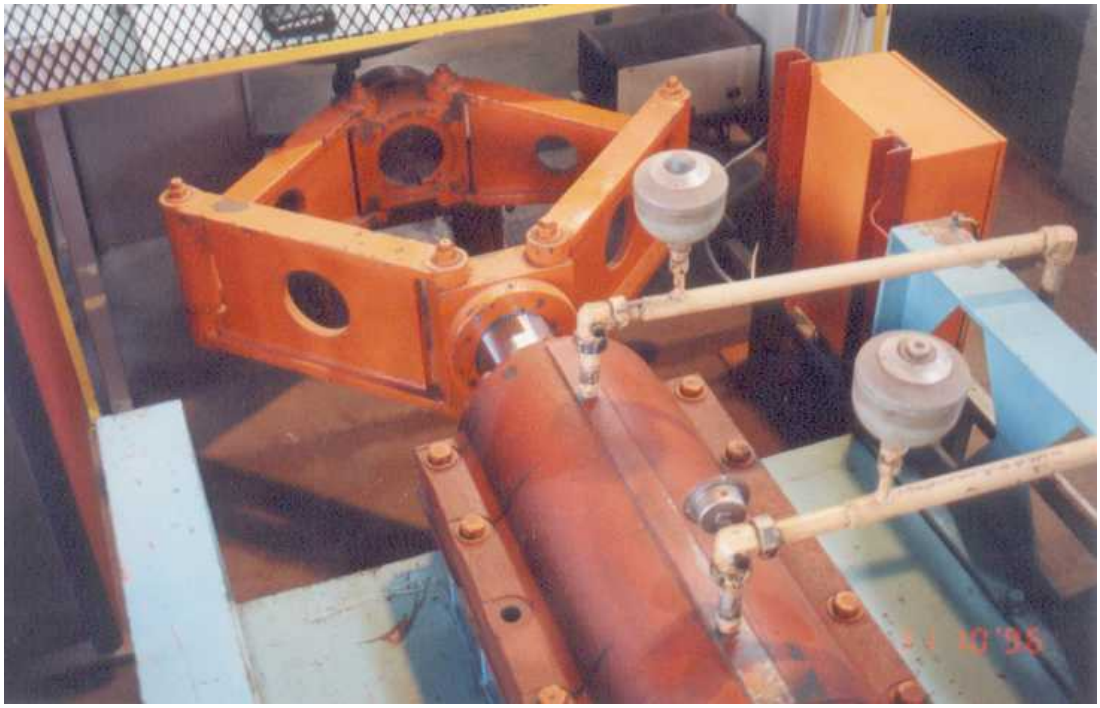

Figure 3.4 - View of the scissor mechanism at the rear of the hydraulic cylinder (orange linkage arrangement). Rotation of the cylinder shaft is prevented while allowing axial movement

3.2.2 Electrical and hydraulic control system

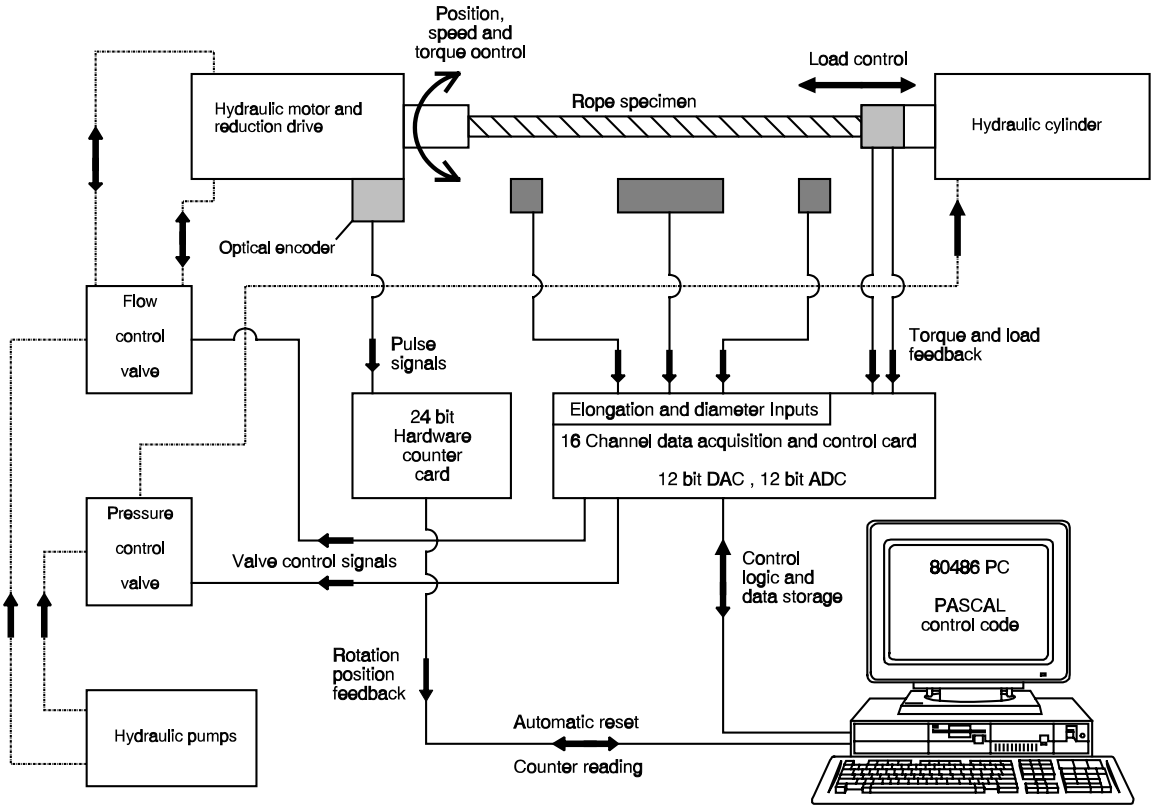

Figure 3.5 - Basic configuration of the machine control system.

Closed loop control of rope load, torque and end rotation is achieved with the system shown in figure 3.5. PASCAL control and data acquisition software provides the machine - operator interface. Proportional pressure relief and flow control valves are used to vary the rope load and end rotation respectively. It was originally anticipated that an electromechanical brake may be required to hold the rotation end drive shaft (figure 3.2) in a fixed position during testing. This was however not necessary as the software control of the five cylinder radial piston motor resulted in an angular position error of less than 1°.

3.2.3 Load and torque measurement

A combination load-torque load cell is used to measure the rope load and torque simultaneously. Two strain gauge bridges (full) are applied to a heat treated En30B circular shaft with end fittings which connect to the hydraulic cylinder and the split

conical grips. Mounting of the load cell directly behind the grips on the cylinder end, figure 3.6, eliminates measurement errors due to the shaft bearing friction. During the dead weight calibration of the load cell, the cross load and cross torque outputs of the bridges are taken into account in determining the overall accuracy. The bridges are fitted with shunt resistances for in-situ calibration of the load and torque outputs. The mechanical equivalence of the shunt induced imbalance was determined during the dead weight calibration procedures.

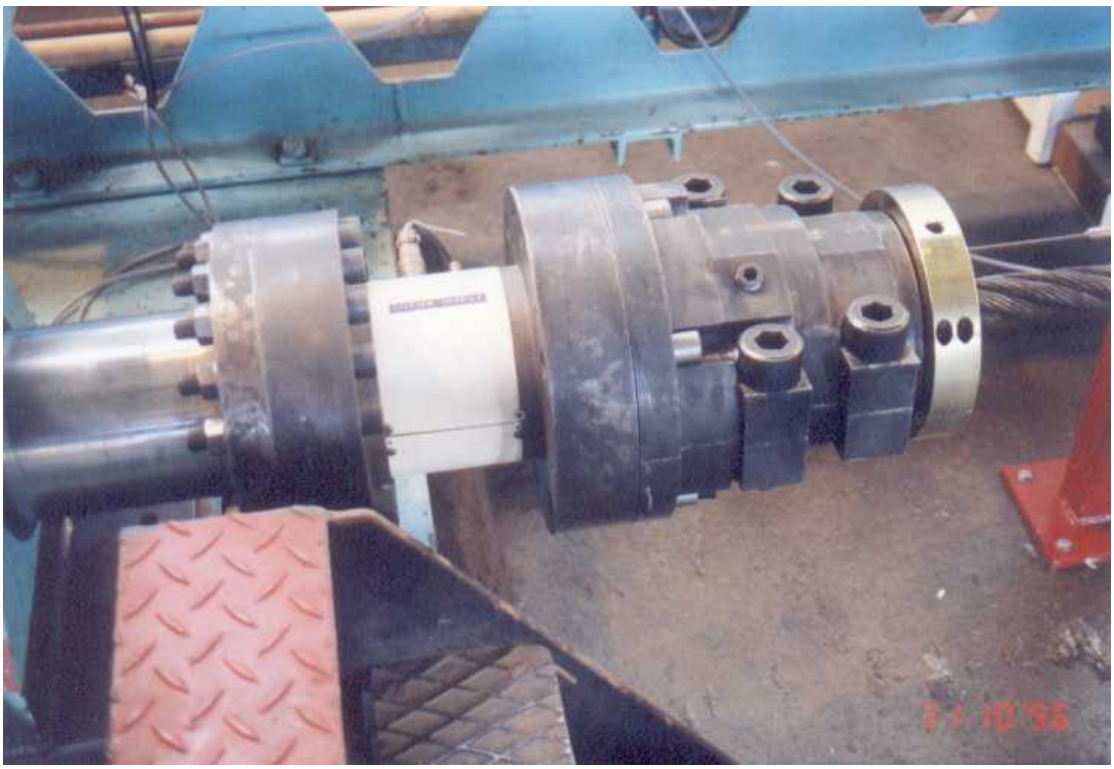

Figure 3.6 - View of the load cell (white cylindrical section) installed between the cylinder shaft and the conical rope grips. The rope specimen is to the right and the shaft bearing arrangement is on the extreme left.

3.2.4 Elongation measurement

Rope specimen elongation, as a result of loading and changes in the state of twisting, is measured by two Linear Variable Differential Transformers (LVDT) mounted on support pedestals bolted to the laboratory floor. The general arrangement of the LVDT's is shown in figure 3.7 with detail of the cylinder and rotation ends contained in figures 3.8 and 3.9. When the system was first installed elongation was determined using equation [3.1].

$$\Delta l = \Delta \text{ LVDT}_{\text{Cylinder End}} + \Delta \text{ LVDT}_{\text{Rotation End}} \qquad [3.1]$$

However, it was discovered that there was an error in the elongation value depending on the position of the rotation head, figure 3.9. The rotation end split collar clamp is attached to the cast white metal collar of the rope and is therefore unlikely to be perfectly perpendicular to the axis of rotation. The result is a sinusoidal oscillation of the rotation end LVDT plunger which gives rise to the error in the reading. To overcome the problem the software executes a check, at constant load, to determine the magnitude of the sinusoidal displacement for angles between -180° to +180°. During testing, equation [3.2] is used to accurately determine the rope elongation.

$$\Delta l = \Delta \text{ LVDT}_{\text{Cylinder End}} + \Delta \text{ LVDT}_{\text{Rotation End}} - \text{skewness factor} \qquad [3.2]$$

The skewness factor is interpolated from a look up table created during the skewness check and is a function of the current angle of rotation. The look up table is valid for all angles since any angle ϕ can be converted to an angle $ß$ between -180° and +180° using equation [3.3]. The gauge length (l_0) of the specimen is determined by measuring the distances x and y and adding these to the fixed length between the measurement pedestals, figure 3.7.

$$ß = (\phi/360 - \text{round}(\phi/360 - 1) - 1).360 \qquad [3.3]$$

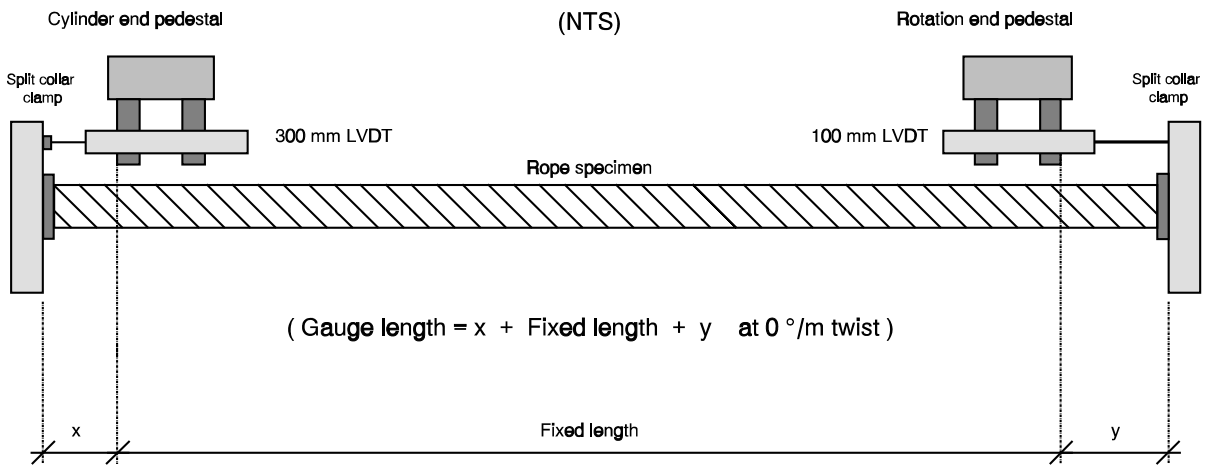

Figure 3.7 - Arrangement of the rope elongation measurement system hardware.

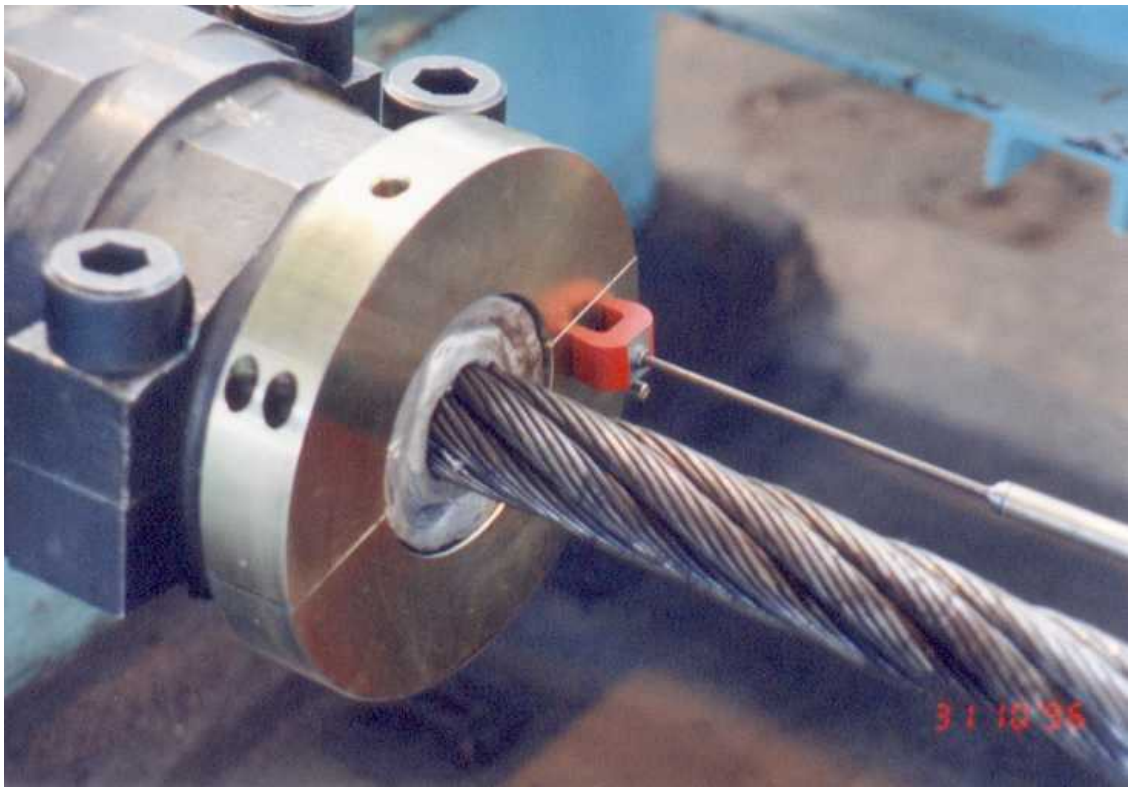

Figure 3.8 - Tension cylinder end, LVDT configuration. The magnet ensures that the LVDT plunger follows the split collar clamp movement and allows for simple connection during the rope installation. Sprung LVDT's of 300 mm stroke are not readily available.

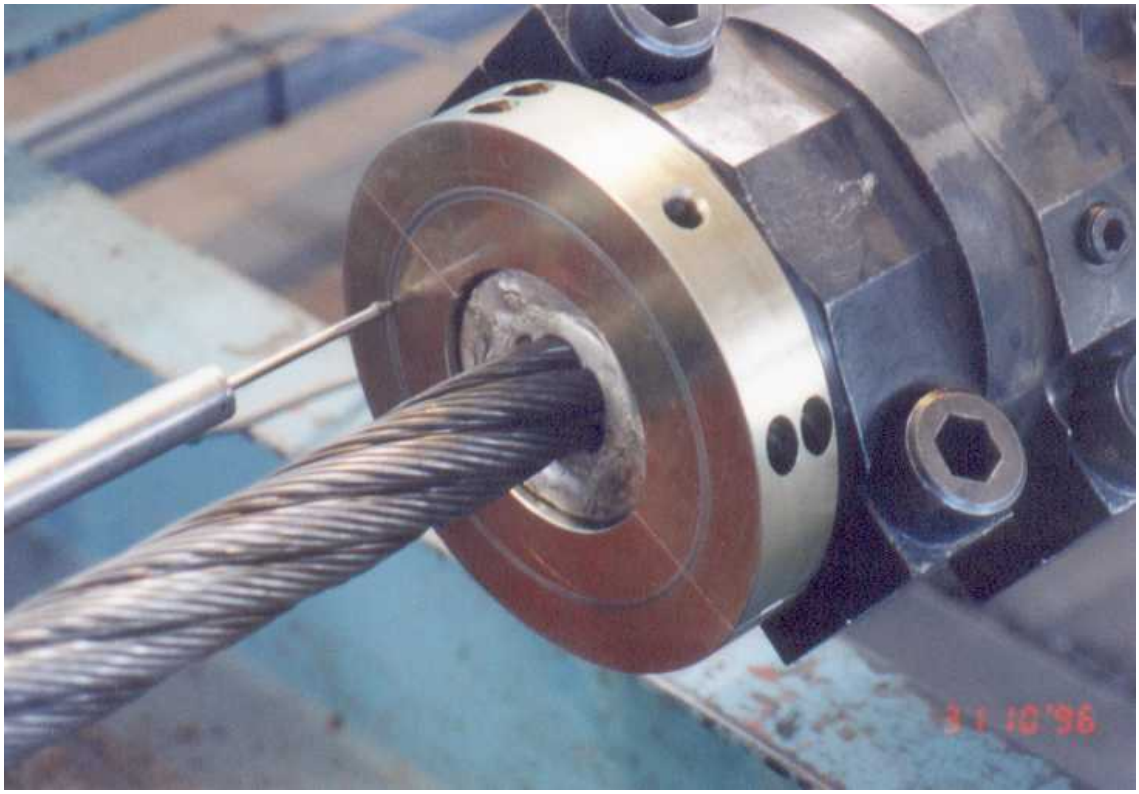

Figure 3.9 - Rotation end, LVDT configuration. The LVDT plunger is sprung to follow the rotating split collar clamp surface (galvanised annular assembly in the centre).

For constant end rotations, the elongation measurement is used to determine rope modulus. The LVDT on the rotation end is sprung and the nib follows the movement of the split collar clamp, figure 3.9. On the cylinder end a magnet is used to connect the LVDT plunger to the clamp. Accurate measurement of the rope end rotation is achieved with an optical shaft encoder fitted to the first stage (shaft) of the reduction chain drive as shown in figure 3.10.

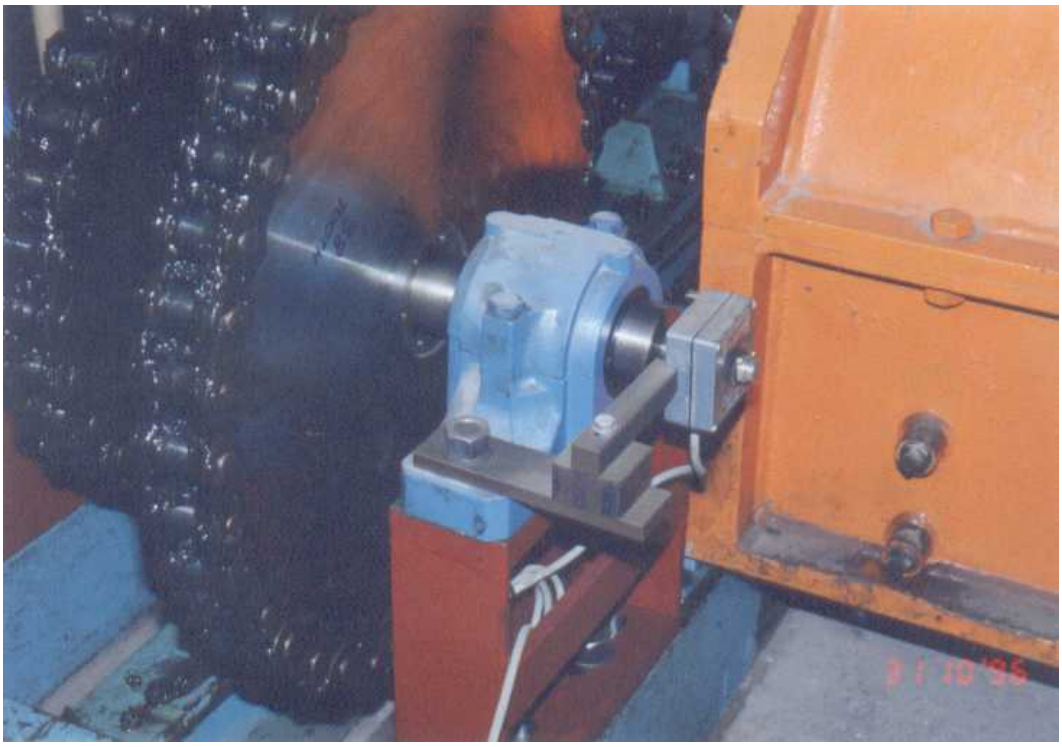

Figure 3.10 - Optical shaft encoder for end rotation measurement. The reduction chain drive is to the left and the gearbox to the right.

3.2.5 Diameter and lay length measurement

Two sets of sprung parallel plates, each with two LVDT's, measure the change in rope diameter. The plate sets are mounted perpendicular to one another as shown in figure 3.11. The change in diameter in calculated from the average of the four displacements measured by the LVDT's. The spring force on the plates results in the jig rotating with the rope when the end rotation is varied. For clarity the springs and steel slides, which keep the plate surfaces parallel, are not shown in figure 3.11 but are indicted in figure 3.12. Torsional strains in winding installations result in the alteration of rope strand orientations and therefore rope diameter. Similarly axial loading is accompanied by reductions in rope diameter. The

relationship between the sheave grove radius and rope diameter can affect the in–service endurance of a rope and it is therefore of interest to be able to determine the variation in diameter under the influence of twisting and load.

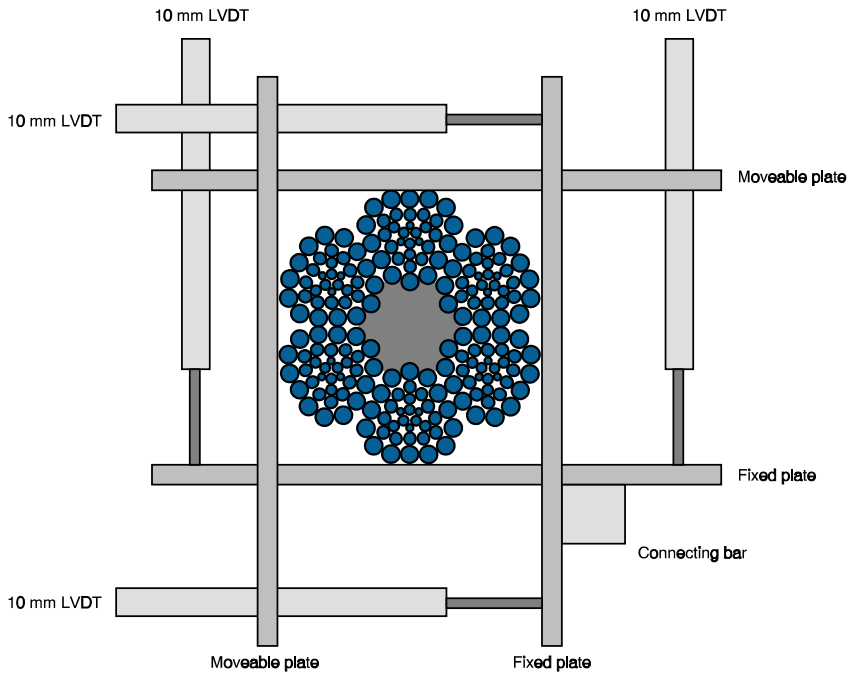

Figure 3.11 - Configuration of the rope diameter measurement jig.

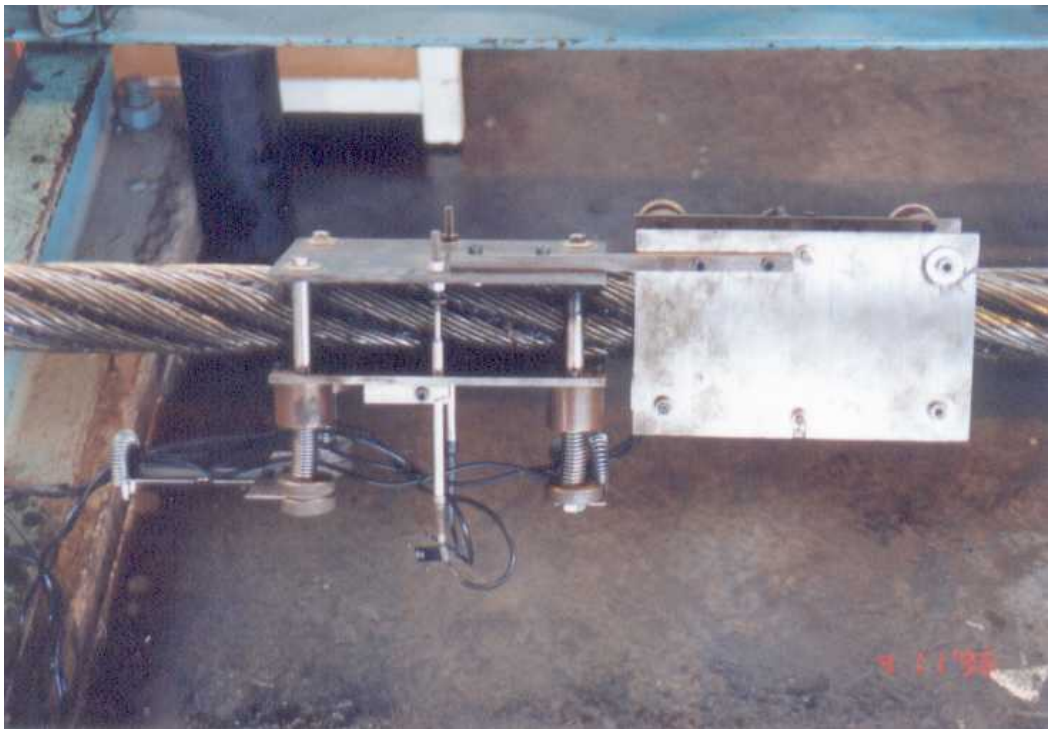

Figure 3.12 - View of the rope diameter measurement jig fitted to a triangular strand rope.

Prior to testing, the rope's zero twist diameter (d_0) is measured with a wide jaw vernier, shown in figure 3.13.

Figure 3.13 - Wide jaw vernier for manual rope diameter measurement.

The strand lay length of a rope specimen is measured manually with a lay length gauge, shown in figures 3.14 and 3.15. The double slide mechanism with the two V-blocks ensures that the lay length is measured parallel to the longitudinal axis of the rope. The pointed screws, through each block, can be adjusted for depth depending on the rope diameter. Once the blocks and screws have been correctly positioned, the lay length is measured across the centre lines of the screws. The use of this type of gauge results in very accurate and repeatable readings for rope lay length. The gauge was designed and manufactured specifically for this study. On a six strand rope it is advisable to measure the lay length over twelve or eighteen strands and divide the result by two or three respectively to further reduce the measurement errors.

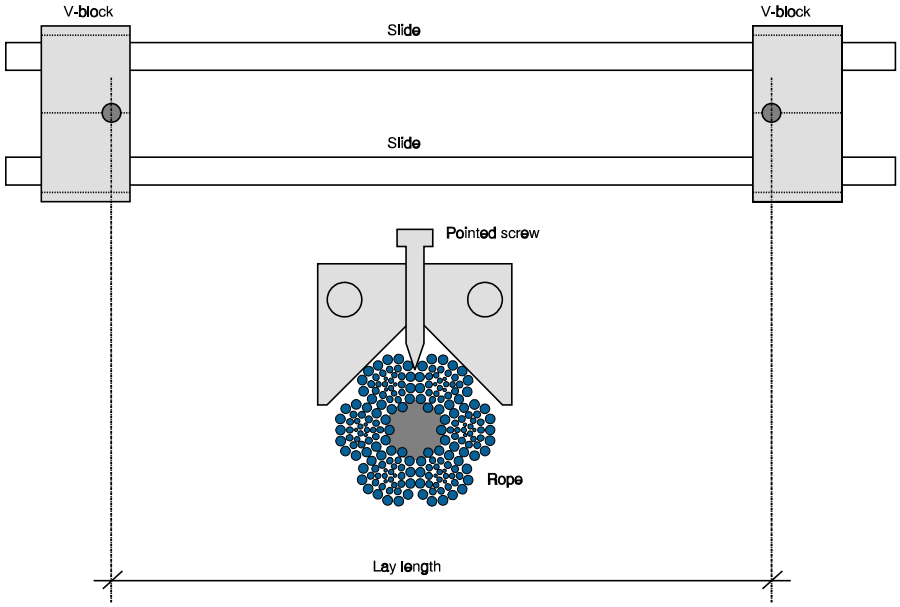

Figure 3.14 - Operation of the parallel V-block lay length measurement gauge.

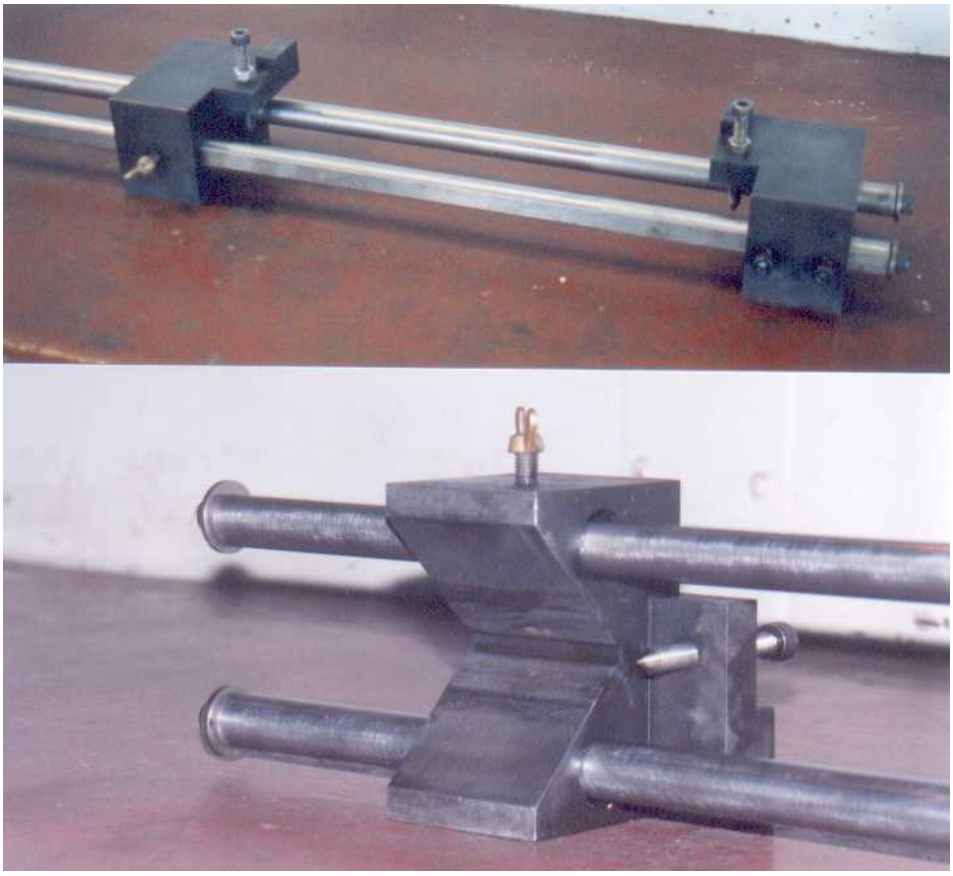

Figure 3.15 - Views of the lay length measurement gauge. A machined, rectangular protrusion on each V-block allows for simple location of the pointed screw centre line.

3.3 Control software

The code for the software is written in Turbo Pascal for MS-DOS®. Figure 3.16 shows the structure of the menu system.

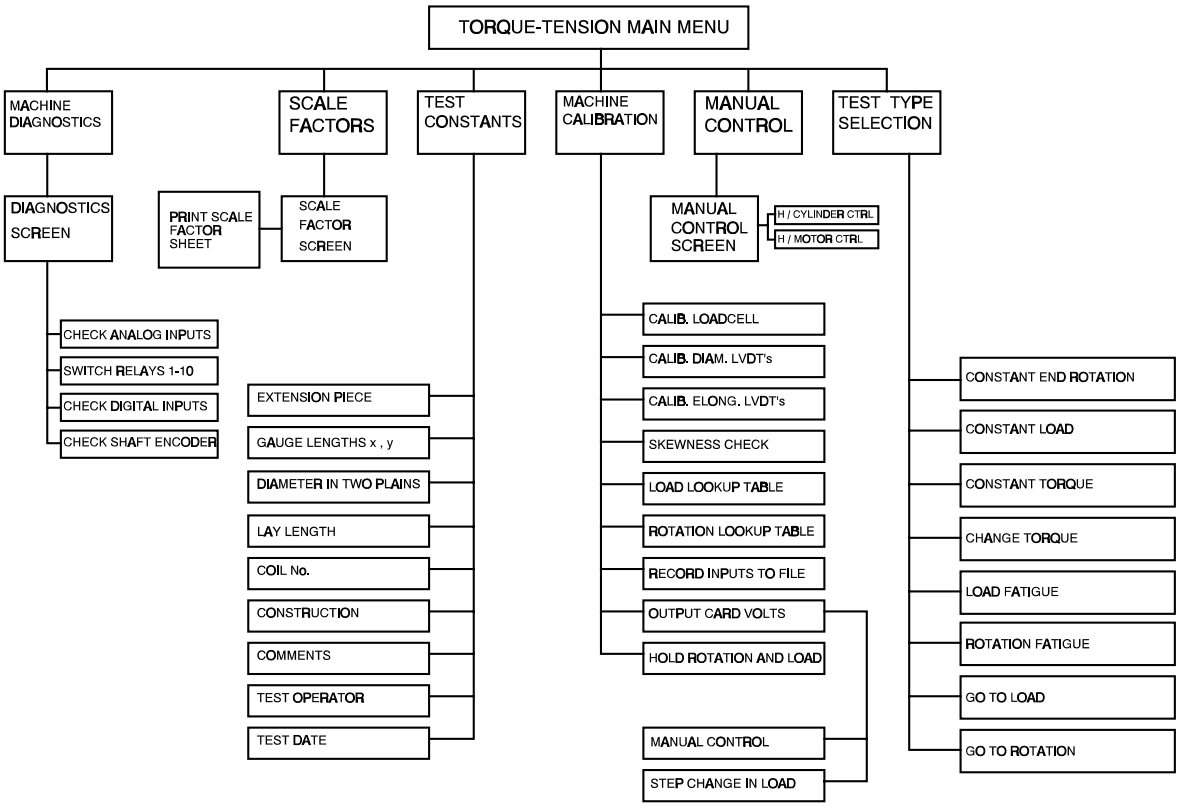

Figure 3.16 - Structure of the testing machine control software menu system.

Diagnostics allows the user to view the input voltages and manually switch the ten PC controlled relays. The digital inputs from the hydraulic cylinder limit switches and the shaft encoder reading can also be monitored from the diagnostics screen.

The scale factors (mechanical units per volt) are determined through automatic calibration procedures and can be printed from the scale factor screen. The values are also saved to an information file for every test data file (*.DAT and *.INF). For each new rope tested, the test constants are entered and are saved to the test information files. If the extension piece is fitted to allow for a shorter rope specimen (2670 mm as opposed to 4040 mm) the software adjusts the fixed length value between the elongation measurement pedestals used to determining the gauge length, figure 3.7.

The calibration menus include automated procedures for in-situ calibration of the measurement instruments. The LVDT's are calibrated using steel blocks and plates of known thicknesses to induce displacements. The motor end split collar clamp skewness factors for the elongation correction (equation [3.2]) can also be determined. The relationship between input voltages to the hydraulic cylinder and motor control cards and the resulting load and rotation speed can be measured and saved as look up tables to data files. As part of diagnostics and fault finding, the input channels can be saved to files without automatic control of the machine taking place. The output control voltages can be varied manually from the keyboard for setting up the hydraulic control cards and determining the load system response to step changes in control voltage. User defined load and rotation values can be maintained by the control PC. Figures 3.17 and 3.18 show how the rope load and rotation head speed vary with changes in the control voltage output from the PC.

Friction in the hydraulic cylinder is considered to be the primary cause of the large hysteresis area associated with the load control. The response shown in figure 3.17 complicates the control since there is a range of voltages associated with a specific load. For example, a 200 kN load could have a control voltage between 6,51 and 7,28 volts. In spite of this limitation it was found that a combination of proportional and integral components in the algorithm ensures adequate levels of control (within ± 3 kN of the control value).

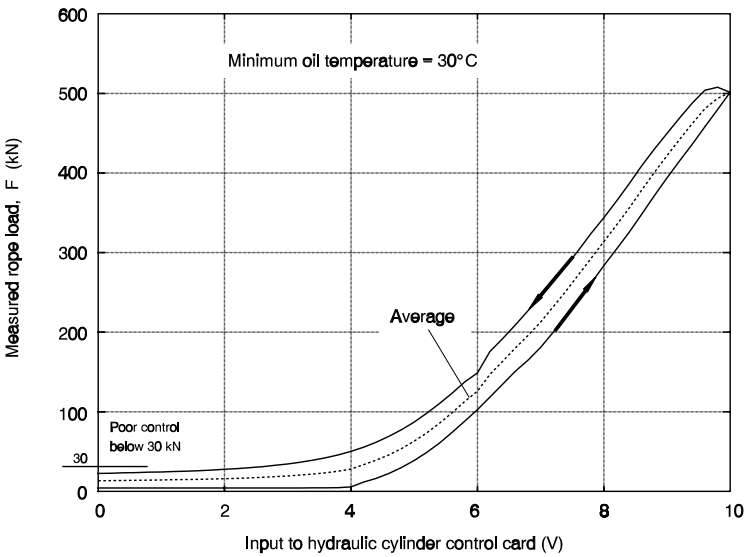

Figure 3.17 - Relationship between the measured load and the control voltage for the hydraulic cylinder. Data for load control look up table.

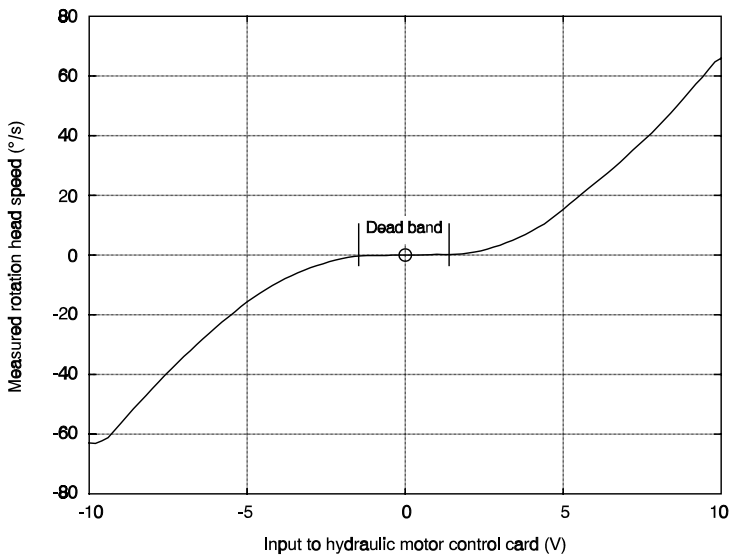

Figure 3.18 - Relationship between the measured rotation head speed and the control voltage for the hydraulic motor. Data for rotation control look up table.

The hydraulic motor is considerably more responsive than the hydraulic cylinder so only a proportional control component is required. For illustration, a procedure which increases the load while maintaining the end rotation constant is listed in figure 3.19. The arctan function for the rotation control reduces the dead band region around the zero output point and limits the maximum output voltage to a predetermined value irrespective of the magnitude of the error. This reduces the likelihood of system instability.

```
Procedure Go_To_Load_Hold_Rot( Rate, Terminal_Load, Rot_Value : real );

repeat
   Check_Time    :=  Read_Time - Start_Time;       { Time since start       }
   Load_Actual   :=  Read_Load;
   Load_Required :=  Start_Load + Rate * Check_Time;
   Load_Error    :=  Load_Actual - Load_Required ;
   I_Part        :=  I_Part + Ic * Load_Error;     { Integral part          }
   Load_Volts    :=  Start_Load_Volts              { Starting CTRL voltage  }
                     + Cc * Check_Time * Rate      { Forcing function       }
                     - Load_Error * Pc             { Proportional CTRL      }
                     - I_Part;                     { Integral CTRL          }
   Pull(Load_Volts);                               { Voltage output         }
                                                   { Ic, Cc, Pc = constants }
   Rot_Actual    :=  Read_Rotation;
   Rot_Error     :=  Rot_Actual - Rot_Value;
   Rot_Volts     :=  -2*arctan(5*Rot_Error);       { Proportional CTRL      }
   Rotate(Rot_Volts);                              { Voltage output         }
until Load_Actual >= Terminal_Load;                { Termination condition  }
```

Figure 3.19 - Example of a load and rotation control algorithm. CTRL = control.

Constant end rotation (≈ constant twist), load and torque tests are conducted from the tests selection screen (figure 3.16). Test parameters are entered by the user in a tabular form as shown in figure 3.20. The software interprets the input parameters and manipulates the machine hardware to achieve the desired results.

```
CONSTANT ROPE END ROTATION TEST

Start Rotation          (°)     : -1000.00
Number of Increments            :    10.00
Rotation Increment      (°)     :   200.00
Load End Point          (kN)    :   450.00
Rate of Load            (kN/s)  :    10.00
Rate of Data Capture    (Hz)    :     0.80
No of Bedding In Cycles         :     2.00
Measure Lay Lengths     (Y/N)   : N
File Name for Results           : C:\TESTS\CR_TEST.DAT

Press ESC when finished ....

Press ESC    to return to the TEST MENU.
Press ENTER  to start the test.
Press SPACE  to change the values.
```

Figure 3.20 - Example of constant end rotation test parameter input screen.

In addition to the constant load, torque and twist tests, it is possible to alter the rope torque at constant loads and conduct rotation and load cycles (sinusoidal) at constant load and end rotations respectively. Tests where changes in load and rotation are made without controlling the other parameters can also be conducted.

3.4 Examples of test variable control

Figures 3.21 to 3.23 depict the time based variations in load, twist and torque for the constant twist, load and torque tests. Similar data for load and rotation cycle tests are shown in figures 3.24 and 3.25. The rope used for the tests was a 40 mm, 6x28(10/12/6 + 3Δ), right Lang's lay, of triangular strand construction with 1900 MPa tensile grade wires. The zero twist gauge length was 2676 mm. The first example is for a constant end rotation test, the parameters of which correspond to the operator inputs in figure 3.20. In the case where bedding in cycles are requested, they are executed in between the main loading cycles but are not recorded in the data files. The purpose of the bedding in cycles is to improve repeatability of the test results, allowing the construction to settle down after the change in twist. Note that in all of the five figures which follow, the values shown are those actually measured during the tests.

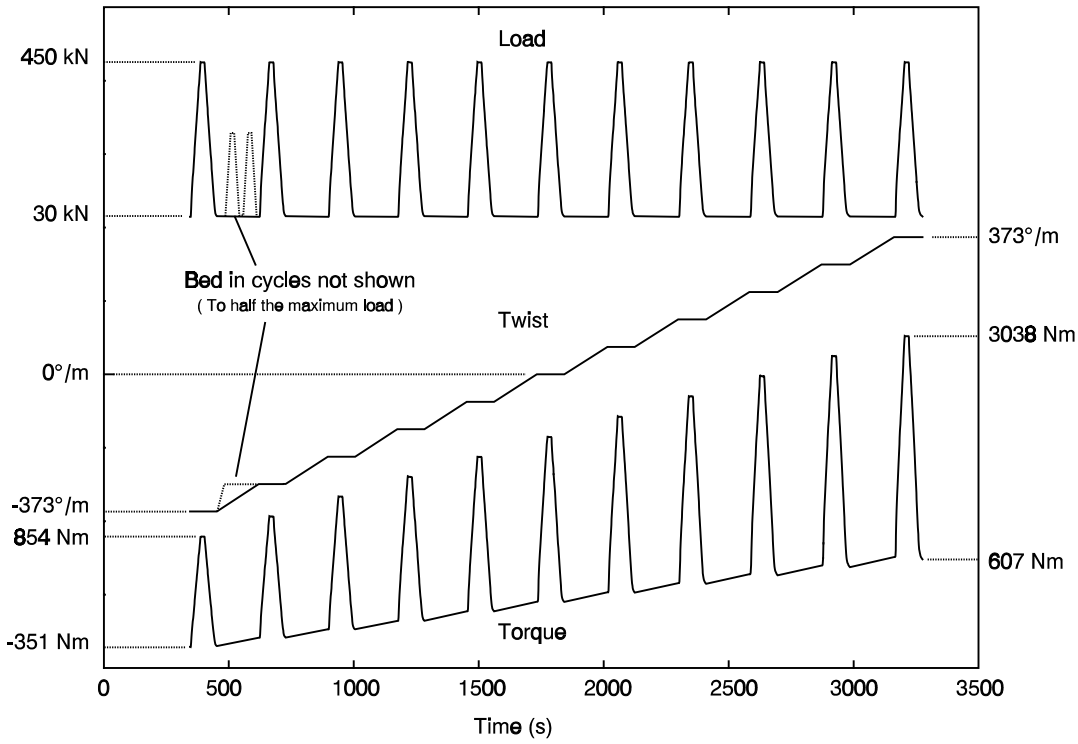

Figure 3.21 - Constant end rotation (twist) test, parameter variations with time.

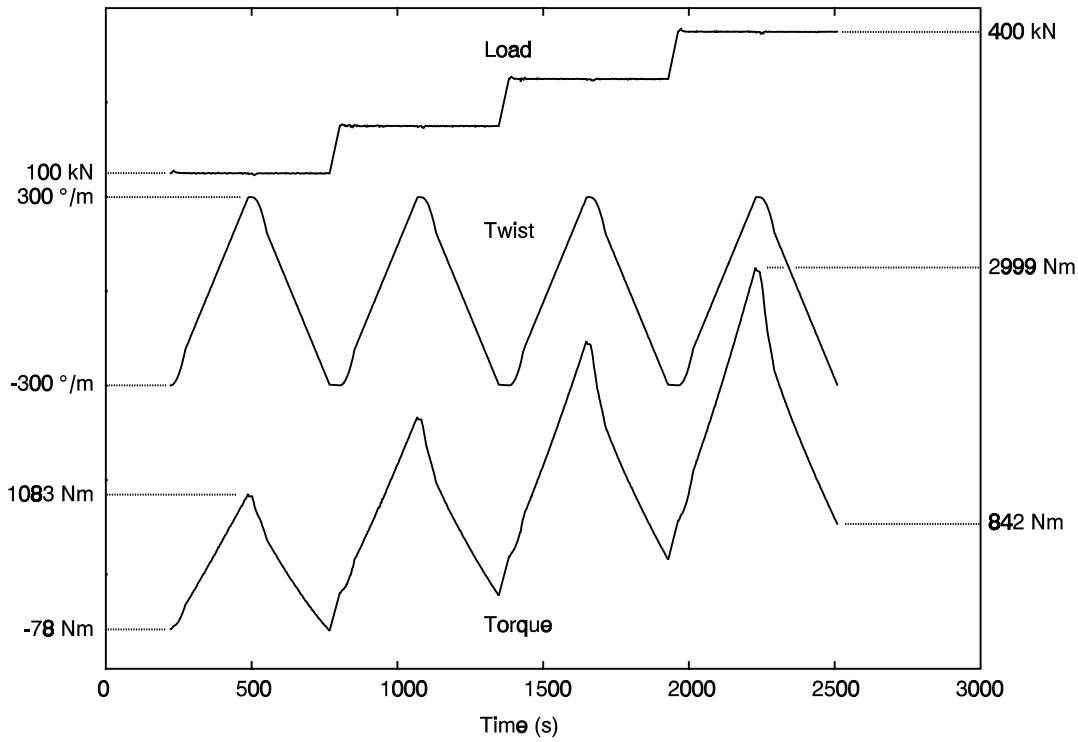

Figure 3.22 - Constant load test, parameter variations with time.

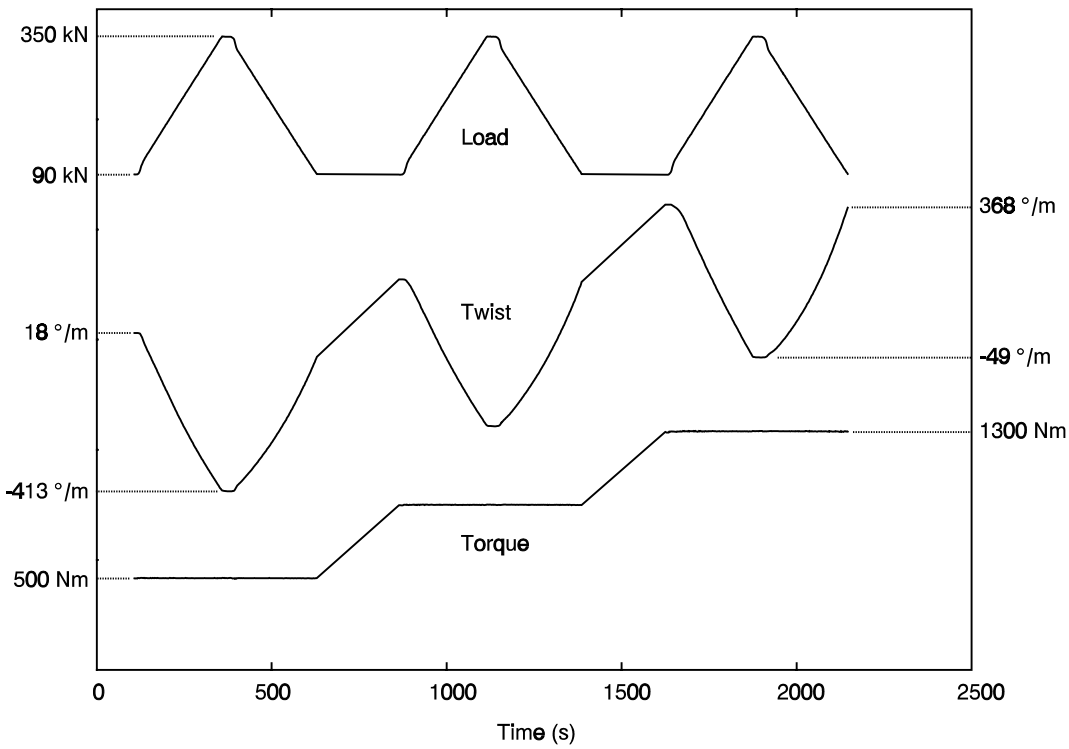

Figure 3.23 - Constant torque test, parameter variations with time.

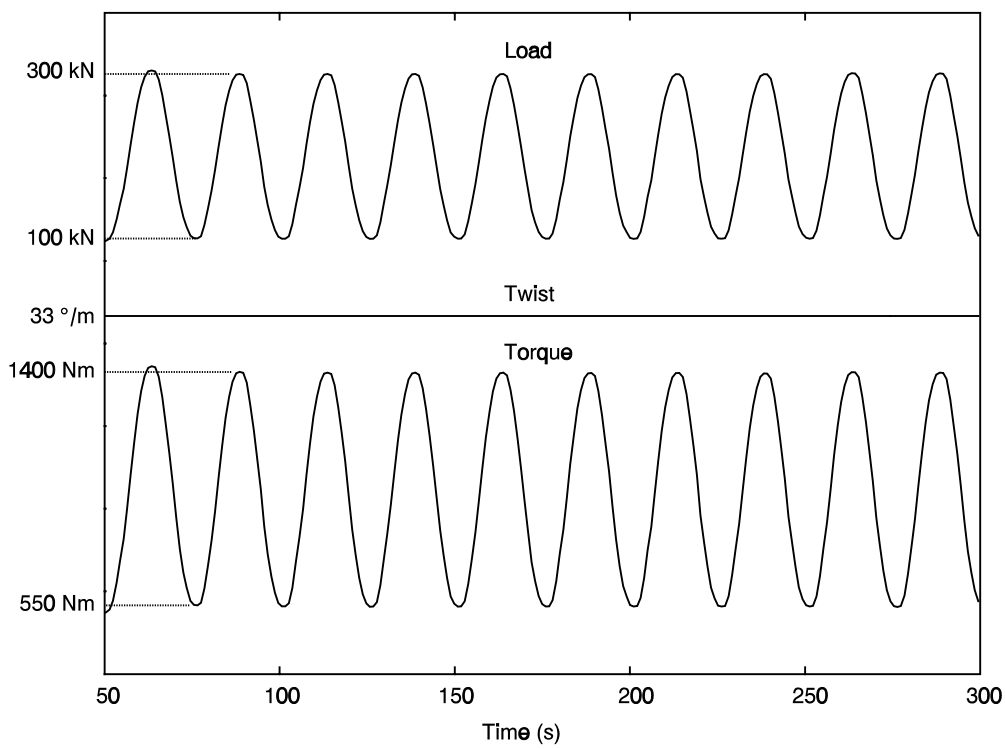

Figure 3.24 - Load cycle test at constant twist, parameter variations with time. Used for bedding in of a new rope sample. The maximum practical frequency is 0,1 Hz.

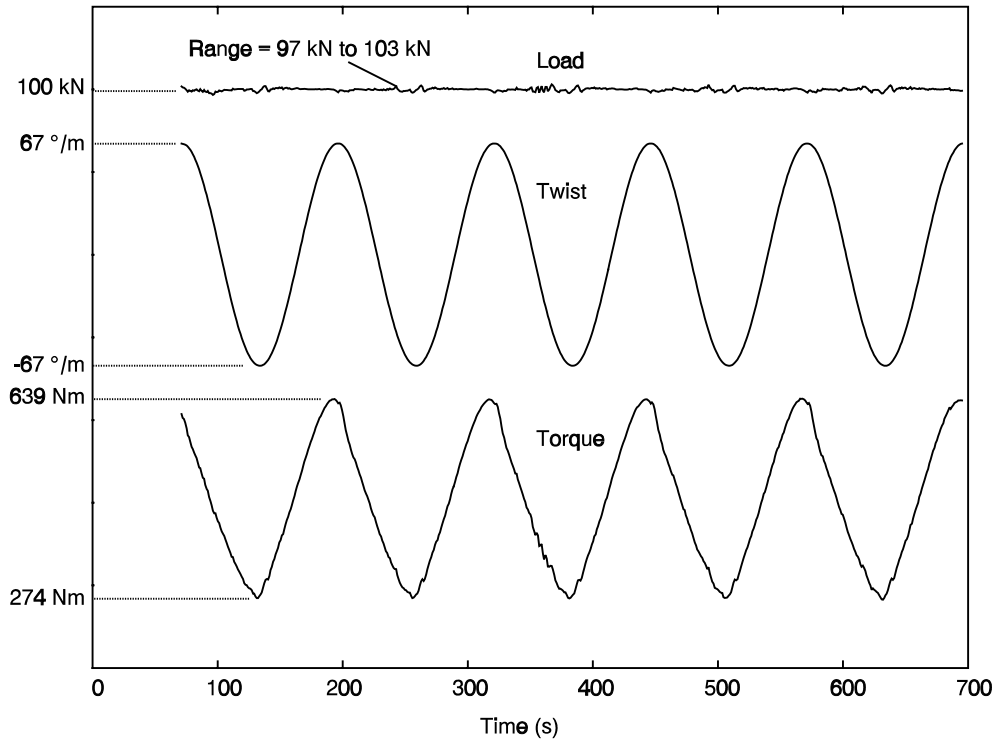

Figure 3.25 - Rotation (twist) cycle test at constant load, parameter variations with time. Used for bedding in of a new rope sample. The maximum practical frequency is 0,08 Hz.

4 EXPERIMENTAL APPROACH

Chapter summary : The rope diameters and shaft depths selected for investigation are motivated in this chapter. A description of the techniques used in obtaining the experimental data is given. Data gathering consisted of in-service rope lay length and rotation measurements and laboratory tension-torsion testing. The torsion tests were conducted on samples of rope matching the diameters and constructions of the in-shaft ropes. In the case of the mine shaft measurements the equipment used is briefly described. For the laboratory torsion tests, details of the test procedures are discussed.

4.1 Mine shaft measurements

4.1.1 Shaft measurement scope

Investigation of actual rope torsional behaviour in existing vertical shafts formed an important part of the research. For the compound triangular strand construction, shaft depth and rope diameter ($\propto$ rope weight per unit length, equation [4.1]) were considered to be the main factors influencing the static torsional behaviour. The first stage of the measurement program was to identify the most appropriate depth and diameter ranges in which to conduct measurements.

$$q \approx 4{,}31935e{-}5 . d_{nom}^{1{,}99136} \qquad [4.1]$$

(Determined from data of the most commonly used triangular strand ropes (Haggie Rand, 1987))

Information gathered during the literature review indicated that for shaft depths of less than 1000 m, the torsional behaviour would probably not be significant enough to warrant investigation. This depth was therefore chosen as the lower limit. For the upper, the deepest available shafts needed to be considered. From the data of figure 1.3 (depth based distribution of winders), the maximum depth is in the region of 2500 m. To identify suitable shafts, a local winder database search was conducted. Only vertical shaft drum winders using six strand ropes were

considered. A data set of 653 winders resulted and the information in figures 1.3 and 4.1 to 4.4 all relate to this set.

Figure 4.1 shows the distribution of six strand rope diameters for vertical shaft drum winders. The most used rope diameters are in the range 40 mm to 50 mm. All diameters greater than 32 mm are of the compound triangular strand construction (figure 2.1). From figure 4.2 it is apparent that this construction is by far the most common. It is employed on 86,2 percent of all the winders considered. Of secondary interest is the tensile grade of the rope wires. Figure 4.3 indicates that 1800 MPa, at 53,6 percent of the total, is the most used.

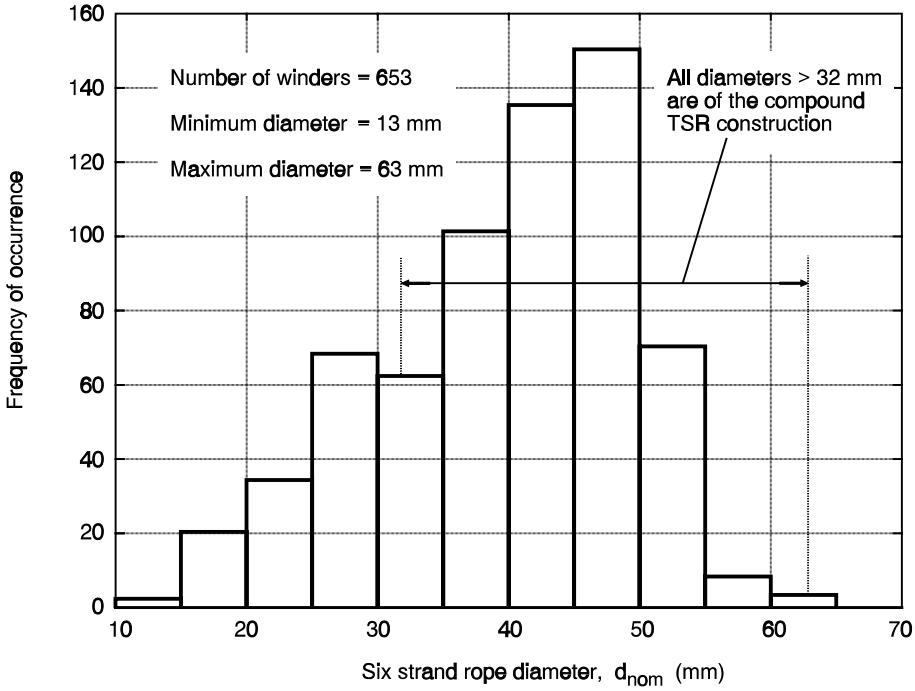

Figure 4.1 - Distribution of six strand rope diameters used on vertical shaft drum winders in South Africa. Extracted from the CSIR Mine Hoisting Technology winder data base, December 1996.

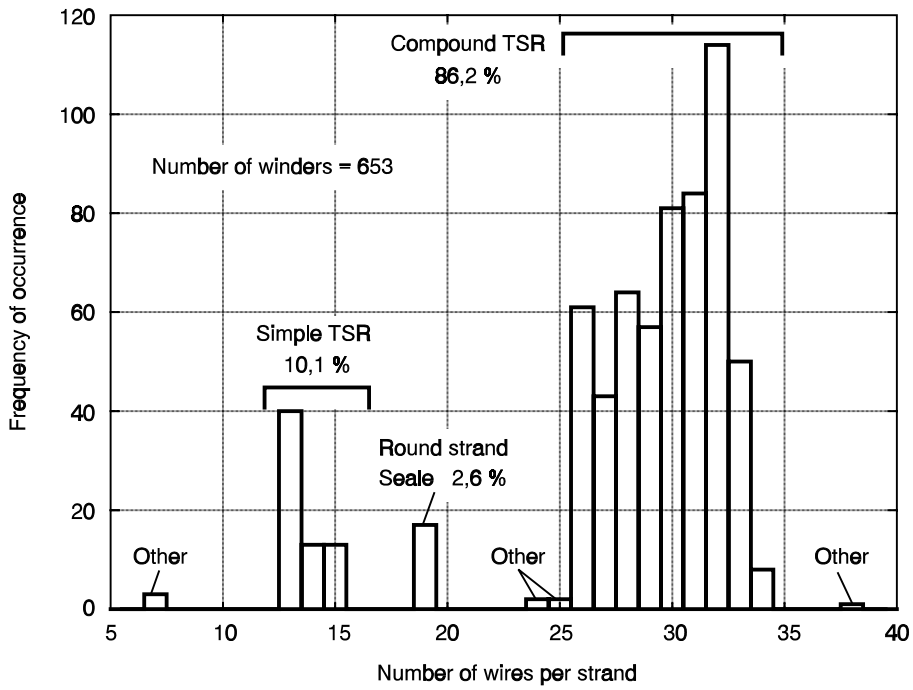

Figure 4.2 - Distribution of six strand rope constructions (wires per strand) used on vertical shaft drum winders in South Africa. TSR = triangular strand rope. Extracted from the CSIR Mine Hoisting Technology winder data base, December 1996.

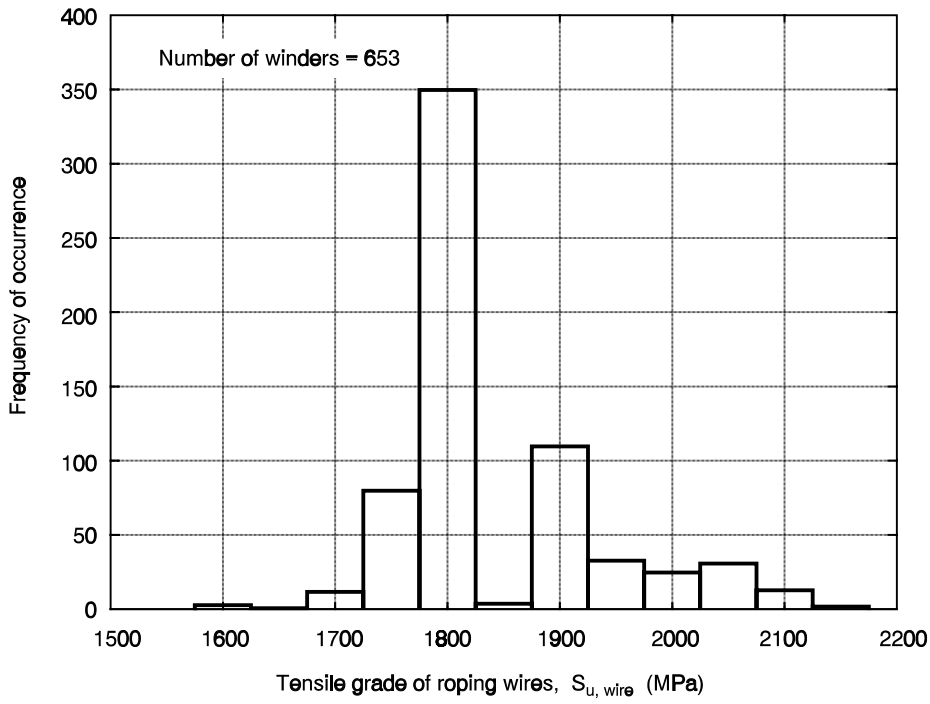

Figure 4.3 - Distribution of six strand rope tensile grades (of roping wires) used on vertical shaft drum winders in South Africa. Extracted from the CSIR Mine Hoisting Technology winder data base, December 1996.

Having decided on a maximum suspended rope length (≈ shaft depth) range of 1000 m to 2500 m, figure 4.4 was used to identify the appropriate diameter range. The investigations were not limited to ropes for rock winders. However, these are of greater interest from a research point as they generally accumulate damage more rapidly than man-material winding ropes. For depths greater than 1000 m, most rock winders are fitted with ropes in the diameter range 38 mm to 56 mm. Smaller ropes lack load carrying capacity and larger ropes require excessively large drum and sheave diameters to satisfy a satisfactory drum to rope diameter ratio (D/d_{nom}) between 100 and 120 (Haggie Rand, 1987). Above depths of 2000 m the diameter range tends to converge as the rope strength to weight ratio becomes critical. Based on the information available from the database a diameter range of 38 mm to 56 mm was regarded as acceptable. The resulting depth-diameter envelope is indicated in figure 4.4. All the ropes in the diameter range were also capable of being tested in the laboratory tension-torsion machine.

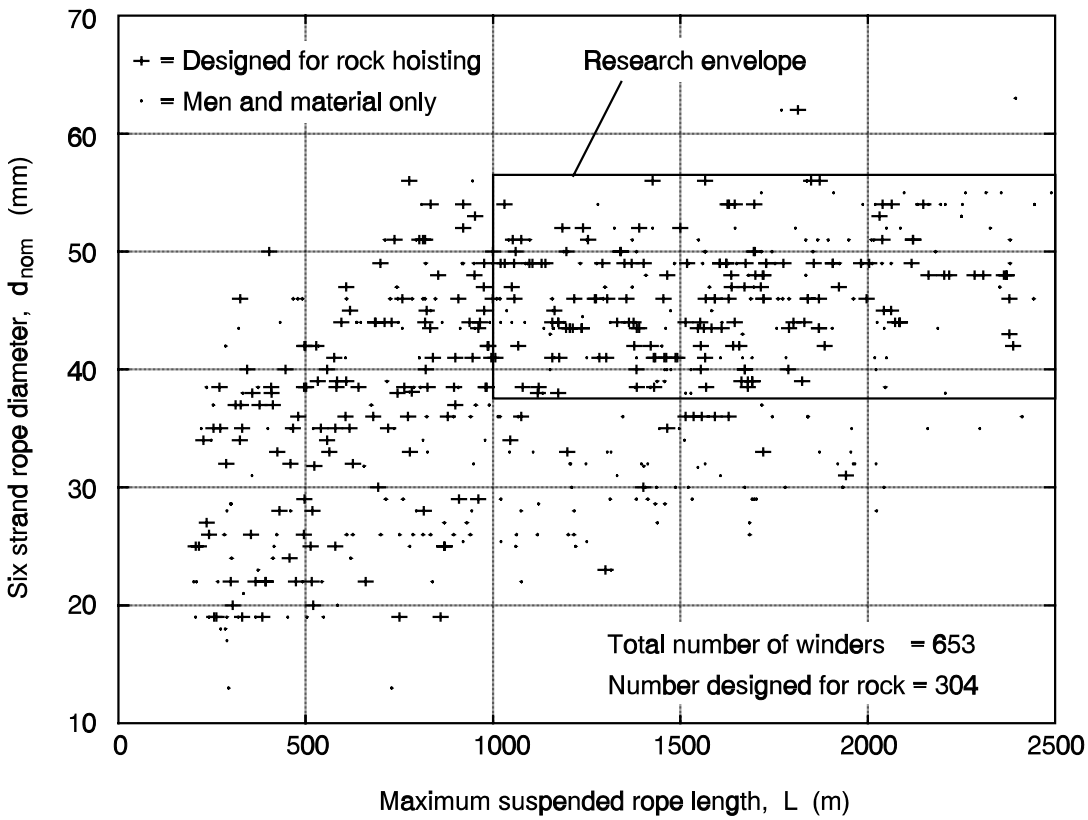

Figure 4.4 - Rope diameters and shaft depths considered for investigation in relation to all the vertical shaft drum winders identified. Extracted from the CSIR Mine Hoisting Technology winder data base, December 1996.

With the depth and diameter ranges determined, actual shafts were listed which suited the depth and diameter criteria. Discussions were held with local mining companies and shafts were select which could accommodate the measurements. Probably the most complex part of the shaft investigations was the protocol and arrangements required before they could be conducted. On average, an equal amount time was spent in preparation and on site work. The two main concerns of the shaft engineering personnel were that the work should be carried out safely and with the minimum disruption to the operation of the shaft. Visits to the shafts prior to the day of measurements were in all cases required so that the persons involved could be briefed on the exact order of events. On busy production shafts, time is critical and any activity that involves use of the shaft demands careful organisation.

In planning the project, it was proposed that at least nine shafts and three rope diameters of the compound triangular strand construction should be considered, figure 1.10. This objective was achieved. Table 4.1 lists the shaft and rope details for which in-service data was obtained. Shaft **F** (48 mm ropes at 2196 m) did not form part of the measurements, the data was extracted from available literature (Hecker and van Zyl, 1993 ; Borello, 1991). Shafts **C** and **D** (46 mm ropes at 1426 m) are the same shaft but are separated because measurements were taken on two sets of ropes. The first set was old ropes (62,2 months service) and the second had been on the winder for two weeks.

Table 4.1 - Shaft and rope details for in-service measurements. **Note :** Shaft name "I" is purposefully omitted.

For documentation purposes, the ropes are numbered S1 to S22.

Shaft description		Rope number	Coil number	Nominal diameter (mm)	Rope lay type	Construction	Wire tensile grade (MPa)	Mass per unit length (kg/m)	Maximum suspended length (m)
A	Sub-vertical shaft BMR rock winder	S1	020712	41	LHL	6x29(11/12/6 + 3Δ)	1800	7,19	1071,3
		S2	020957	41	RHL	6x29(11/12/6 + 3Δ)	1800	7,19	1071,3
		S3	020646	41	RHL	6x29(11/12/6 + 3Δ)	1800	7,19	1071,3
		S4	020648	41	LHL	6x29(11/12/6 + 3Δ)	1800	7,19	1071,3
B	Sub-vertical shaft BMR rock winder	S5	135575/001	41	RHL	6x29(11/12/6 + 3Δ)	1900	7,19	1528,6
		S6	135576/001	41	LHL	6x29(11/12/6 + 3Δ)	1900	7,19	1528,6
		S7	135575/002	41	RHL	6x29(11/12/6 + 3Δ)	1900	7,19	1528,6
		S8	134826/001	41	LHL	6x29(11/12/6 + 3Δ)	1900	7,19	1528,6
C	Surface shaft double drum rock winder (old ropes)	S9	121047/001	46	RHL	6x31(13/12/6 + 3Δ)	1800	9,04	1425,5
		S10	121047/002	46	RHL	6x31(13/12/6 + 3Δ)	1800	9,04	1425,5
D	Surface shaft double drum rock winder (new ropes)	S11	122312/001	46	RHL	6x31(13/12/6 + 3Δ)	1800	9,04	1425,5
		S12	122312/002	46	RHL	6x31(13/12/6 + 3Δ)	1800	9,04	1425,5
E	Surface shaft double drum man winder	S13	016289	46	RHL	6x31(13/12/6 + 3Δ)	2150	9,12	2403,0
F	Surface shaft double drum rock winder	S14	124930/001	48	RHL	6x32(14/12/6 + 3Δ)	1800	9,81	2196,0
		S15	124930/002	48	RHL	6x32(14/12/6 + 3Δ)	1800	9,81	2196,0
G	Surface shaft double drum rock winder	S16	131275/001	49	RHL	6x32(14/12/6 + 3Δ)	1900	10,14	1126,0
		S17	131275/002	49	RHL	6x32(14/12/6 + 3Δ)	1900	10,14	1126,0
H	Sub-vertical shaft double drum rock winder	S18	021079	49	RHL	6x32(14/12/6 + 3Δ)	1800	10,14	1068,1
		S19	021183	49	RHL	6x32(14/12/6 + 3Δ)	1800	10,14	1068,1
J	Surface shaft double drum man winder	S20	018434	49	RHL	6x32(14/12/6 + 3Δ)	1800	10,14	1598,6
K	Surface shaft double drum man winder	S21	116724/002	49	RHL	6x32(14/12/6 + 3Δ)	1800	10,14	1935,4
L	Surface shaft double drum man winder	S22	129020/001	54	RHL	6x32(14/12/6 + 3Δ)	1950	12,53	1886,9

4.1.2 Rope lay length measurements

Strand lay lengths were measured for both empty and loaded conveyances. The measurements were conducted at the bank (i.e. on surface or at sub-vertical crossover level, figure 1.5) with the conveyances moving up the shaft. It was assumed that, for a given state of loading, the rope does not rotate when the conveyance is hoisted upwards. This assumption was based on rope rotation theory discussed by Hankus (1993a). In-shaft observations of rope rotation behaviour later confirmed this. Figure 4.5 illustrates the position from which the lay lengths were measured.

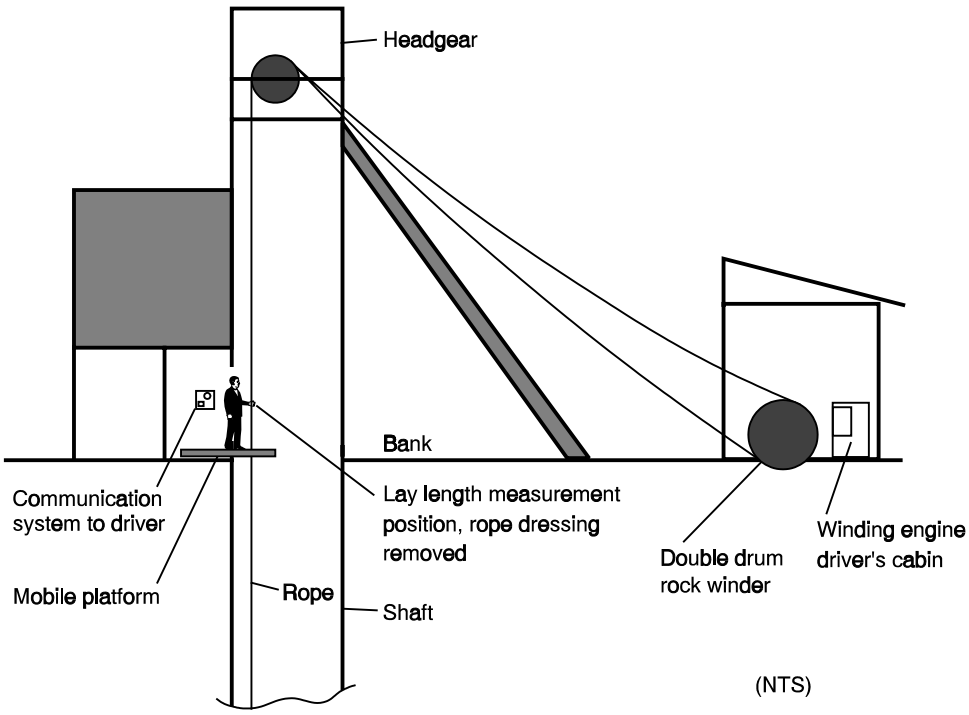

Figure 4.5 - In-service lay length measurement position.

The significance of the rope not rotating, while being hoisted up the shaft, is that it allows the lay length at any point along the suspended length to be measured from the bank. Equipment is always available at the bank to safely access the rope. This is usually in the form of a moving platform placed over the shaft. Further down the shaft the only positions where the rope could be accessed are at the shaft stations (figure 1.7). There are however no facilities at the stations to safely reach the rope which may be located between 1,5 m and 2,0 m from the edge of the shaft (figure 1.6).

Before the measurements were conducted, stopping positions for the conveyances were decided on. These were either at known repeatable locations in the shaft, or after a certain number of drum revolutions. In both cases the positions had to be such that the suspended rope length, relative to the maximum suspended length, could be calculated. The first lay length was always measured with the conveyance at the lowest position in the shaft. The last measurement was always taken just above (2 m to 4 m) the rope splice (connection point to the conveyance).
In shafts **C** (46 mm ropes at 1426 m) and **G** (49 mm ropes at 1126 m), the lay lengths were measured over six strands with a steel rule and tape respectively. Repeatability and accuracy of the measurements was found to be poor (large scatter). In the other shafts, a tape was used to measure over 18 strands which reduced the measurement error. In addition to the lay length measurements, details of the shaft and winding system, listed in table 4.2, were obtained from the engineer responsible for the shaft.

Table 4.2 - Important shaft and rope data obtained from the shaft engineers.

1. Shaft station and headgear elevation details (figure 1.7) measured from the bank (m).
2. Mass of rock or locomotive used for loading of the skip or cage (kg).
3. Maximum skip or cage design payload (kg).
4. Mass of empty skip or cage with all the attachments (kg).
5. Date of rope installation.
6. Number of times the splice end had been cut for statutory testing at the measurement date (termed "front ends").
7. Whether any rotation was returned to the splice end after cutting for test, prior to reattachment.
8. Number of times drum end connection point had been pulled in at the measurement date (termed "back ends").
9. Splice end lay length after installation (mm)
10. Drum end lay length after installation, measured at the bank with the conveyance at the lowest position in the shaft (mm).
11. Rope coil number with which the rope details could be extracted from a rope tests database.
12. Shaft compartment names and drum coiling details, underlay or overlay.
13. Winder permit number with which the winder details could be extracted from a winder database.

4.1.3 Rope rotation measurements

Rope rotation during conveyance loading was measured at different positions along the suspended rope length. The procedure involved video filming paint marks on the rope from different levels in the shaft while the conveyance was being loaded. The paint marks were applied to the rope using a 1,9 m long extension pole with a brush and yellow road marking paint. This method was preferred to the traditional "chalk line" approach (section 2.5, figure 2.19) as it resulted in the minimum disruption to the normal shaft operation. Figure 4.6 shows the application of the video filming method for rope rotation measurement.

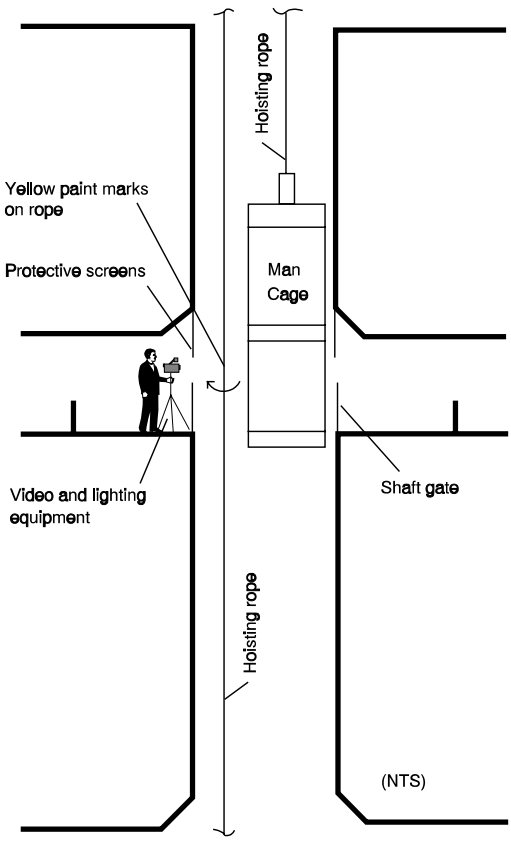

Figure 4.6 - Rope rotation measurement method applied to a rock winder rope.

The first measurement position was always at the bank. In the case of man cages, diesel locomotives were used as the load. In contrast to loading of rock into skips, the process of loading a locomotive into a cage is discontinuous. Figure 4.7 shows the three loading stages. Some shafts are fitted with equipment which allows the cage to be held in position while the locomotive is loaded. None of the man-material winders considered in the investigation were fitted with such devices.

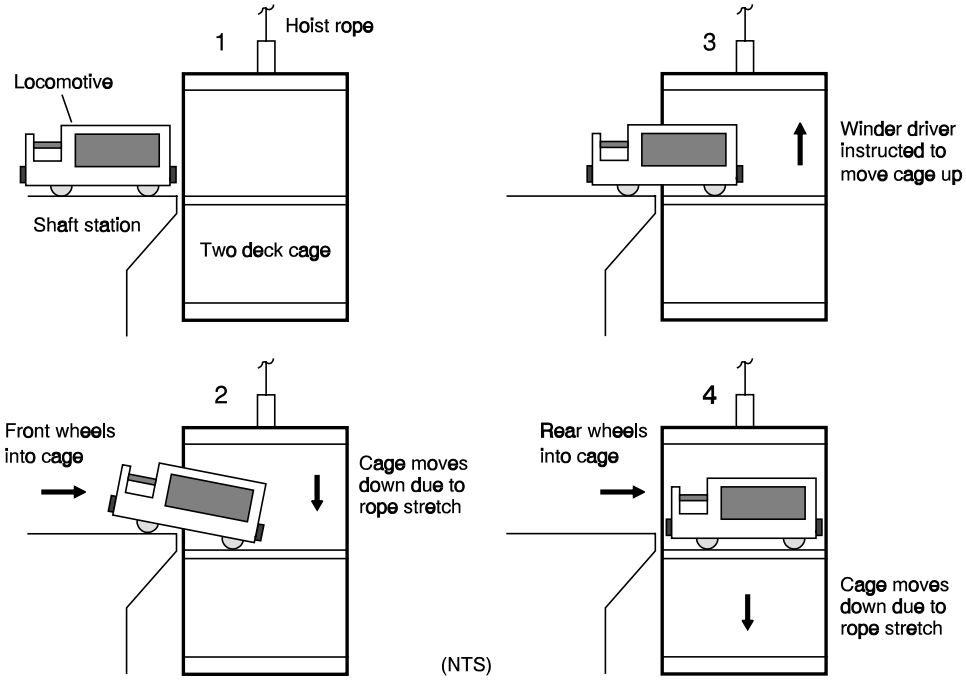

Figure 4.7 - Process of loading a locomotive into a man cage with no cage holding devices employed.

The measurement procedure for both man and rock winders was the same. With the conveyance at the loading position (lowest in the shaft) lines were painted on the rope from a shaft station. Once the video camera was in position, an instruction was given (via shaft telephones) to load the conveyance. The rotation of the rope during loading was filmed. It turned out that the rotations could have been counted manually from the shaft stations. However, if there was any doubt over a rotation value, it would not have been possible to repeat the measurement due to time constraints. Three paint marks were applied to the rope, each 90° apart (in a plane perpendicular to the rope axis). It was found that this resulted in a rotation resolution of 45°.

4.2 Laboratory based rope tension-torsion tests

4.2.1 Scope of laboratory testing

For all the rope diameters and constructions for which shaft measurements were completed, laboratory torsion tests were conducted to determine the torsional properties. For the torsion tests, the main parameters of interest were :

- Proportionality between load and torque for various states of twisting (lay length), derived from the constant twist test.
- Torsional stiffness of the rope for different loads and applied twists, calculated from the constant twist and load tests.
- Changes in torsional stiffness associated with the extent of twist displacements from a stationary point, determined from constant load tests.
- The relationship between applied twist and lay length.

Table 4.3 lists the rope diameters, constructions and tensile grades on which laboratory torsion tests were conducted. The purpose of tests conducted on each set of ropes is also included.

Table 4.3 - Ropes on which torsion tests were conducted. For documentation purposes, the torsion test ropes are numbered T1 to T12.

Nominal diameter (mm)	Construction and coil number (rope number)	Tensile grade	Purpose of tests and relevant thesis section
25	6x27(9/12/6 + 3Δ)/F 303851/001 (**T1**)	1800	Lay length versus breaking strength torque calculation, section 1.4 and appendix A. Investigation of factors influencing in–service torsional behaviour, section 7.3.
40	6x28(10/12/6 + 3T)/F 137931/001 (**T2**) 134226/001 (**T3**)	1900	Effect of lubrication of the degreased ends on torsional stiffness, section 6.5.2. Effect of wire galvanising on torsional hysteresis, section 6.5.1.
40	6x29(11/12/6 + 3T)/F 137517/001 (**T4**) 129880/001 (**T5**)	1800	Rope torsional properties for investigation of factors influencing in–service torsional behaviour, section 7.3. Effect of wire galvanising on torsional hysteresis, section 6.5.1.
40	6x30(12/12/6 + 3T)/F Drawn galvanised 2 x 129543/001 (**T6, T7**)	1800	Effect of wire galvanising on torsional hysteresis, section 6.5.1.
41	6x29(11/12/6 + 3T)/F 136053/001 (**T8**)	1800	Torsional properties for the ropes of shafts **A** and **B**, section 6.3, appendix C.
46	6x31(13/12/6 + 3T)/F 137944/001 (**T9**)	1800	Torsional properties for the ropes of shafts **C**, **D** and **E**, sections 6.2 and 6.3, appendix C.
48	6x32(14/12/6 + 3T)/F 140156/001 (**T10**)	1800	Torsional properties for the ropes of shaft **F**, section 6.3, appendix C.
49	6x32(14/12/6 + 3T)/F 135197/001 (**T11**)	1800	Torsional properties for the ropes of shafts **G**, **H**, **J** and **K**, section 6.3, appendix C.
54	6x32(14/12/6 + 3T)/F 139666/001 (**T12**)	1950	Torsional properties for the rope of Shaft **L**, section 6.3, appendix C.

4.2.2 Rope specimen preparation and installation

New rope specimens for laboratory testing were obtained from a local rope manufacturer. The sections were supplied in 3,5 m lengths and figure 4.8 gives the dimensions to which the test pieces were prepared.

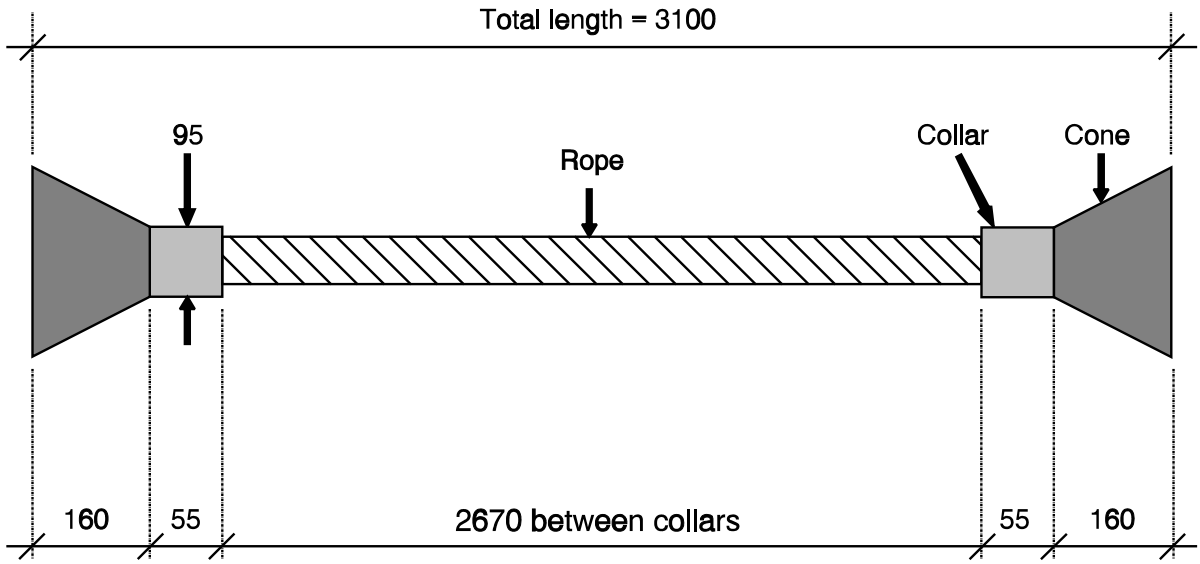

Figure 4.8 - Test specimen preparation dimensions (in millimetres).

Examples of the rope sections as received and a rope with a cast end fitting are shown in figure 4.9. Once a specimen was prepared, it was installed in the testing machine with the split collar clamps attached to the collars and the diameter measurement jig positioned at the mid-point, figure 4.10. The rotation end extension piece was used to accommodate the 2670 mm test gauge lengths (figure 3.2). No rotation was applied to the ends of the specimens during the installation procedure.

Figure 4.9 - Detail of the cast white metal collar and end cone. The specimens as received from the rope manufacturer are shown in the background. Note that all the free specimens were prevented from distortion by three portions of serving wire. These were later removed once the collars and end cones had been cast. The split collar clamps (figures 3.8 and 3.9) are attached to the cylindrical white metal collars.

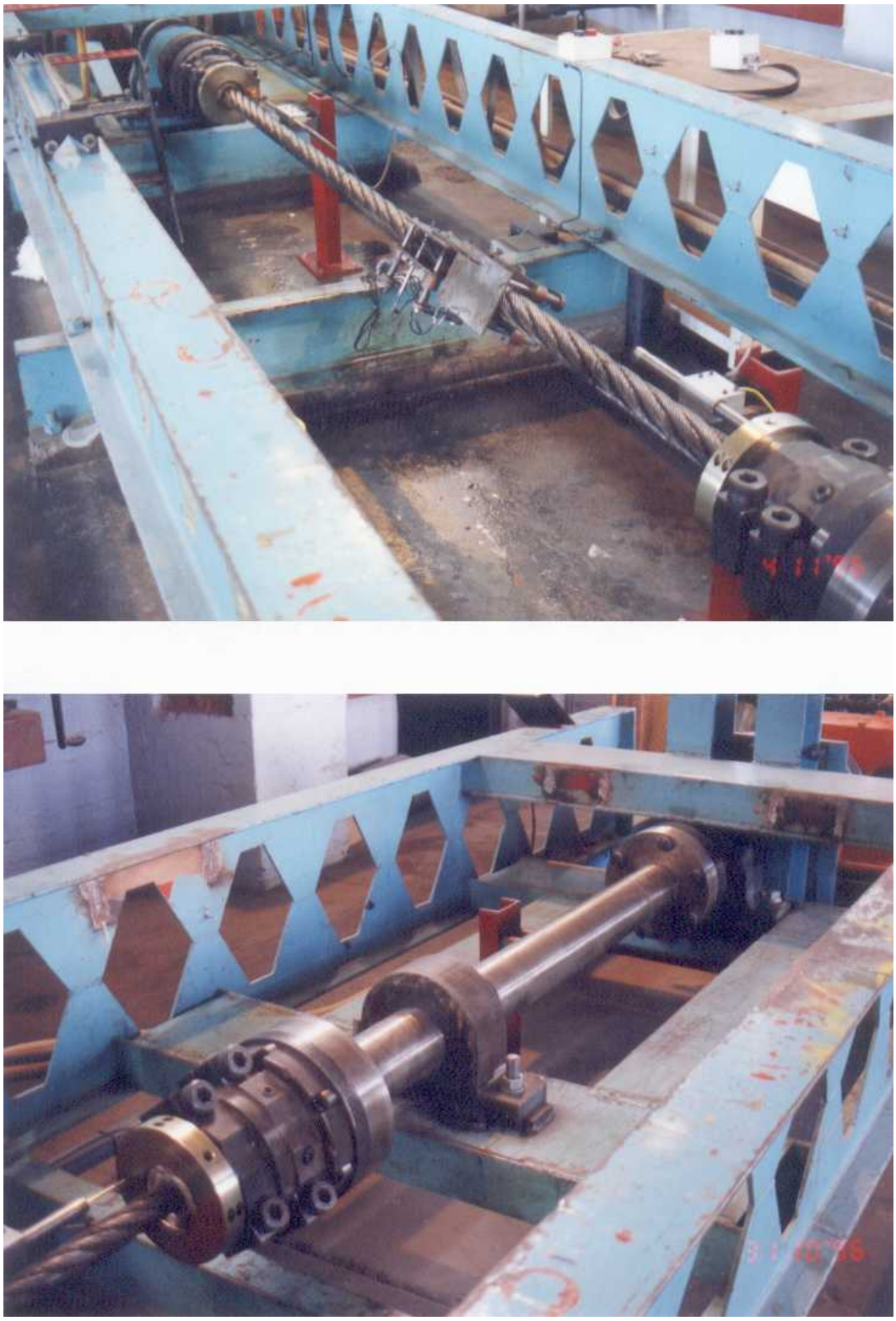

Figure 4.10 - A test specimen installed in the tension-torsion machine using the rotation end extension piece. The gauge length ≈ 2670 mm.

4.2.3 Transducer zero values and torque - rotation convention

At the start of each test the torque and load readings were zeroed with the rope in the slack position and the lay length as it was at installation. For the diameter and elongation measurement systems, zero points were taken with the rope load set at 10 kN. Zero end rotation (0°/m twist) corresponded to the installation lay length. Since all the ropes tested were of the RHL construction, a convention was adopted that they generate positive torques when tensioned. Positive end rotation or twist was associated with shortening and negative twist with lengthening of the strand lay length.

4.2.4 Bedding in cycles

After the specimens had been installed in the machine a series of load and rotation bedding in cycles were run to allow the construction to settle down. In all cases, except for the 25 mm diameter rope (T1) 300 load cycles between 150 kN and 450 kN at zero twist were completed. These were followed by 150 rotation cycles between -180° and +180° (≈ ± 67,4 °/m) at 300 kN load. The cycling was important since the subsequent test results were used for prediction of in-service behaviour of ropes that had been in operation for at least two weeks. Under operating conditions, a rope experiences both axial and torsional displacements which needed to be simulated in the laboratory bedding in cycles.

With one of the 40 mm ropes, T2, the load bedding in cycles (figure 3.24) were conducted fifty cycles at a time. Figure 4.11 indicates how the repeatability of the constant twist test results improved after 150 cycles. A fourth set of fifty load cycles was also run with no further improvement in repeatability evident. After the 200 load cycles, 50 rotation cycles (–180° to 180° at 300 kN, figure 3.25) were completed. A further set of 50 load cycles were run after the rotation cycles in which there was negligible variation in data compared to the third and forth sets.

The end rotation was then altered to various positions and it was found that after the first two cycles, the repeatability was comparable to that at zero twist. In all the constant twist test conducted, two bedding in cycles were therefore run to half the maximum test load after a change in twist and prior to the actual measurement cycle (figure 3.21).

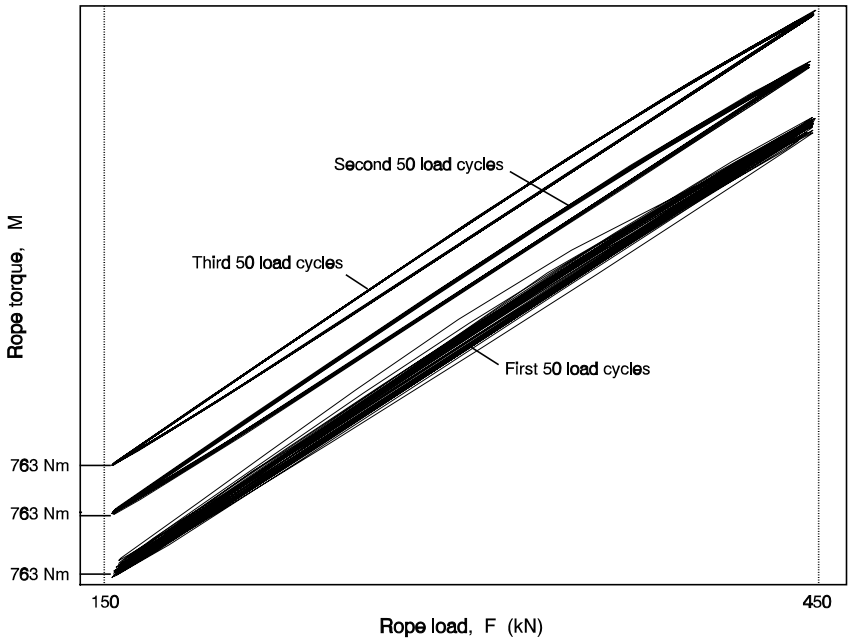

Figure 4.11 - Effect of bedding in cycles on the constant twist test results. Rope T2, 40 mm, 6x28(10/12/6 + 3Δ)/F, 1900 MPa.

While the bedding cycles were conducted the ends of the rope, which had been degreased during preparation, were oiled. This restored the lost lubrication and probably reduced the effects of the end constraints on the test results. After the bedding in cycles, the zero twist gauge length, lay length and diameter were measured, table 4.4.

Table 4.4 - Initial measured parameters of the torsion test rope samples. Nominal values for the particular diameters are also included.

Rope number	Nominal diameter d_{nom} (mm)	Zero twist gauge length l_0 (mm)	Zero twist diameter d_0 (mm)	Zero twist lay length LL_0 (mm)	Nominal lay length LL_{nom} (mm)	Metallic area A_{met} (mm²)
T1	25	2670	24,90	203,8	188	280,6
T2	40	2676	40,95	353,0	302	732.9
T3	40	2649	41,15	342,0	302	732,9
T4	40	2651	41,40	331,7	300	728,5
T5	40	2650	40,85	339,0	300	728,5
T6	40	2663	40,65	334,0	299	722,5
T7	40	2655	40,60	332,4	299	722,5
T8	41	2670	42,60	325,0	309	773,2
T9	46	2661	47,00	392,4	348	970,3
T10	48	2670	49,55	402,8	361	1051,3
T11	49	2669	50,40	421,5	368	1088,2
T12	54	2666	55,95	485,0	409	1344,0

4.2.5 Constant twist tests

In conducting the constant twists tests, the objective was to measure the torsional response over as large a twist and load range as possible. Two factors limited the amount of load and twist that could be applied to a specimen :

- The stroke of the hydraulic cylinder, especially in the twisting up direction where the rope shortens more rapidly than for untwisting.
- The maximum torque capacity of the loadcell (3200 Nm).

The maximum value of positive twist applied was such that it resulted in the cylinder approaching the limit of its travel. The maximum value of untwisting was normally taken as the equivalent negative number or one increment larger. The number of intermediate constant twist positions was chosen such that 10 or 11 load cycles were achieved (figure 3.21). In the case of the 25 mm diameter rope the applied twists were similar to those of the destructive tests (figures A.6 and A.7).

Table 4.5 - Load and twist ranges used for the constant twist tests. Note that the effect of twisting on lay length is a function of the zero twist lay length and the rope diameter, equation [5.2].

Nominal diameter, d_{nom} (mm)	Minimum load (kN)	Maximum load (kN)	Minimum twist (°/m)	Maximum twist (°/m)	Number of load cycles
25 (**T1**)	30	244[1]	-734	734	11
40 (**T2** → **T7**)	30	453[2]	-376	376	11
41 (**T8**)	30	503[3]	-337	270	10
46 (**T9**)	30	364[2]	-338	338	11
48 (**T10**)	30	366[2]	-337	270	10
49 (**T11**)	30	503[3]	-337	270	10
54 (**T12**)	30	503[3]	-337	270	10

1 - Load ≈ 50 percent of rope breaking strength.
2 - Tests conducted as per figure 4.12a.
3- Tests conducted as per figure 4.12b.

Initially, the maximum load was chosen so that, in the most twisted state, the rope torque did not exceed the loadcell's limit. The system was later changed to allow the software to monitor the torque during loading and stop the load increase once the torque limit was reached. This approach allowed the maximum amount of data

to be measured. Figure 4.12 shows the torque versus load curves for the two options. The minimum test load was in all cases 30 kN. Below 30 kN, poor load control was achieved, figure 3.17 (cylinder load control). Table 4.5 lists the maximum loads and twists that were applied to the rope samples tested.

a)

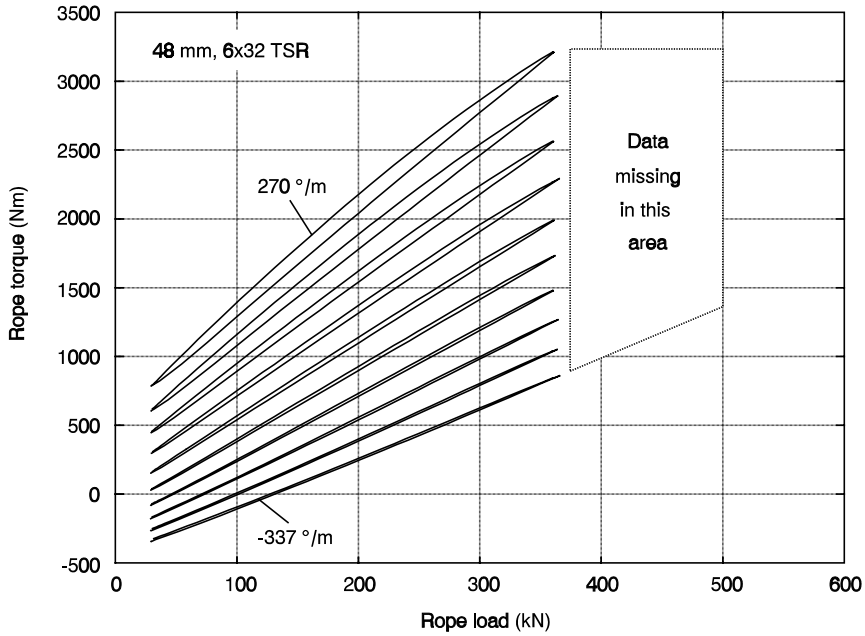

b)

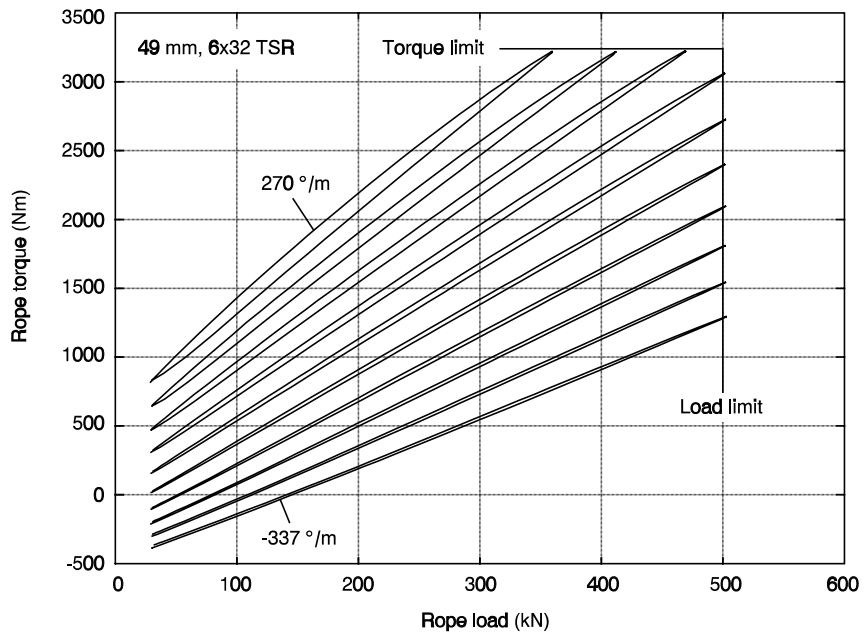

Figure 4.12 - Two methods of limiting the maximum rope torque during a constant twist test. In the second case (b) considerably more data is captured. TSR = triangular strand rope.

4.2.6 Constant load tests

At first, constant load tests were conducted for three or four load values and within the twist range of the constant twist tests. An example of the relationship between the two tests is shown in figure 4.13. In figure 4.13a the torque versus load variation for the constant load test is superimposed on the results for the constant twist test. Figure 4.13b shows the variation of torque with twist for four constant load values.

It was observed that when a rope was twisted from a stationary position, a significant change in torque occurred for a relatively small change in twist. Differentiating torque with respect to twist (slope of constant load curves) gives the torsional stiffness. After experimenting with these tests, it was found that the variation in torsional stiffness is a function of the constant load at which twisting takes place. This is apparent in figure 4.12b. It was also discovered that the value of twist, from which twisting is initiated, affects the response. Notice in figure 4.13b that there is only a small variation in slope at the start of the cycles (–300 °/m). At the same constant load, but at + 300 °/m, the variation in slope is far more pronounced. It was concluded from these observations that torsional stiffness is firstly function of change in twist from a stationary position and secondly, a function of the load at which twisting occurs and the starting value of twist (congruent with the observations of Raoof and Hobbs (1989)).

In order to quantify the torsional stiffness function was necessary to conduct a series of individual torsion test for different constant loads and starting twist values. Figure 4.14 illustrates forty such tests plotted on the same set of axes. The twist starting values and constant loads are indicated. It is not shown in figure 4.14 that the rope responds differently when it is twisted up from a certain starting twist value than when it is untwisted. The curves are the averages of the twisting up and untwisting responses. Table 4.6 lists the constant loads and starting twist values for the seven ropes on which such tests were conducted. Figure 4.15 contains the torsional stiffnesses calculated from the data in figure 4.14. It is possible for there to be an order of magnitude difference between the no–slip and full–slip stiffnesses particularly for positive starting twist values (short lay length). From the stiffness curves in figure 4.15, it is evident that changes in rope lay length affect the torsional stiffness more significantly than changes in load.

a) constant twist test :

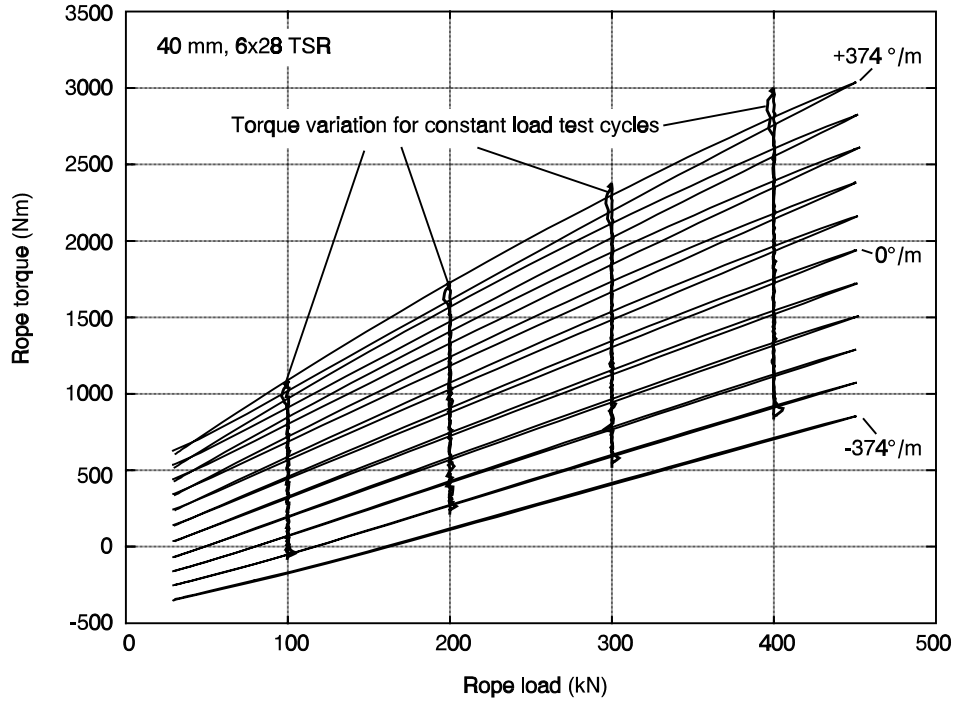

b) constant load test :

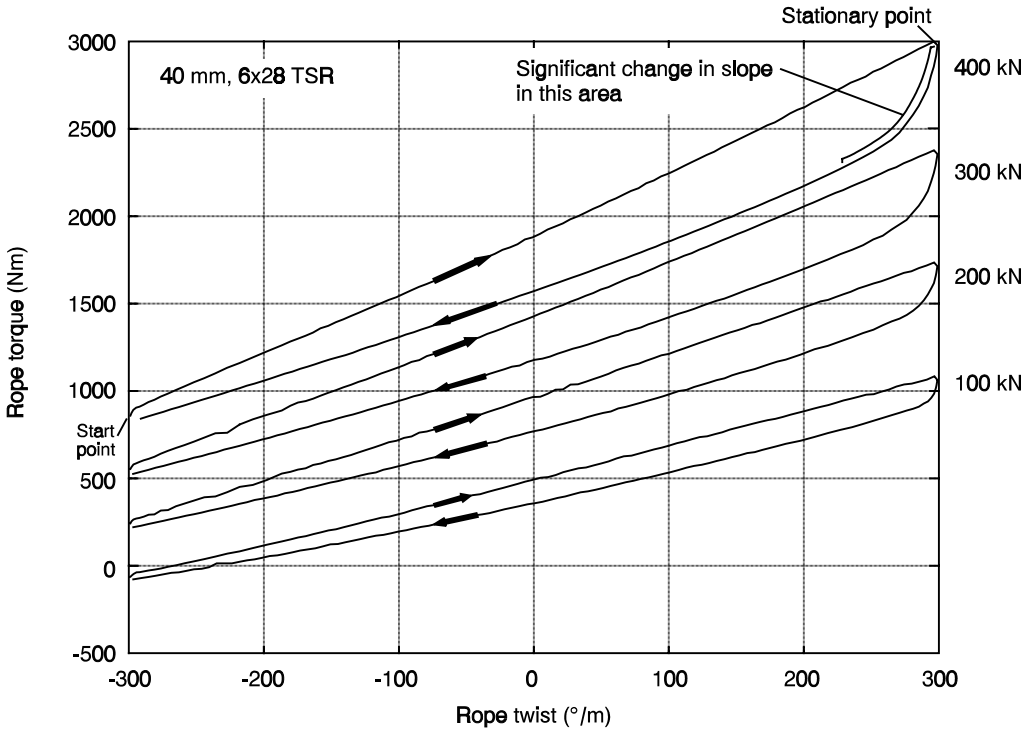

Figure 4.13 - Constant load test based on the load and twist ranges of the constant twist test.

Table 4.6 - Test loads and twists for the various torsional stiffness tests.

Nominal diameter, d_{nom} (mm)	Starting values of twist, R_{cl0} (°/m)	Change in twist, winding up (°/m)	Change in twist, unwinding (°/m)	Rate of twisting ((°/m)/s)	Constant load values, F_{cl} (kN)
40 (**T2**)	269	+45	-45	0,375	100
	0	+45	-45		200
	-269	+45	-45		300
40 (**T7**)	271	+45	-45	0,375	100
	0	+45	-45		200
Galvanised	-271	+45	-45		300
41 (**T8**)	270	+45	-45	0,375	60
	67	+45	-45		170
	-135	+45	-45		280
	-337	+45	-45		390
46 (**T9**)	271	+45	-45	0,376	60
	68	+45	-45		170
	-135	+45	-45		280
	-338	+45	-45		390
48 (**T10**)	-270	+34	-34	0,375	90
	-135	+34	-34		170
	0	+34	-34		250
	135	+34	-45		330
	243	+45	-45		
49 (**T11**)	270	+45	-45	0,375	60
	67	+45	-45		160
	-135	+45	-45		260
	-337	+45	-45		360
54 (**T12**)	67	+45	-45	0,375	60
	-67	+45	-45		160
	-202	+45	-45		260
					360

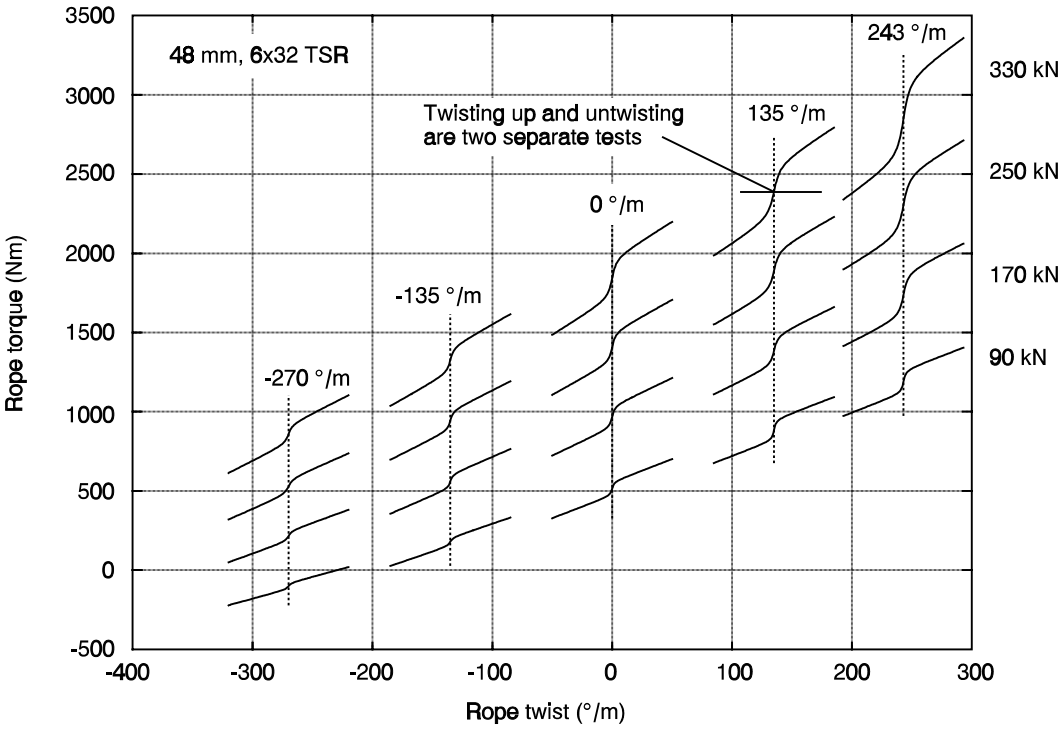

Figure 4.14 - A series of constant load tests to determine the detailed hysteretic torsional response of a triangular strand rope.

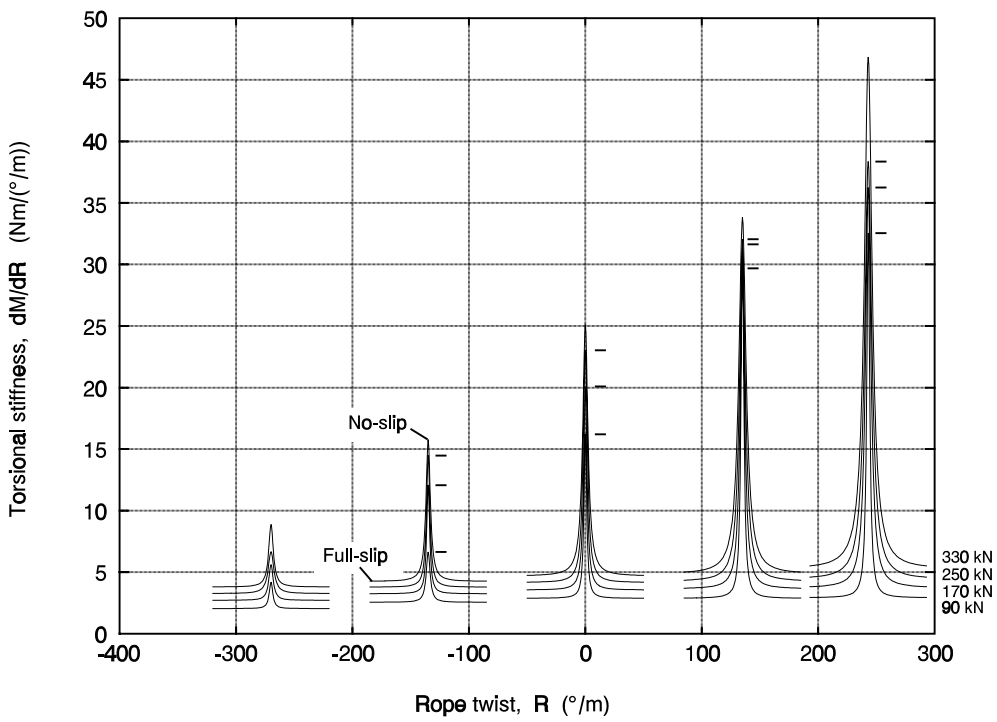

Figure 4.15 - Tangent torsional stiffness variations calculated from the data in figure 4.14.

5 MODELLING OF ROPE TORSIONAL RESPONSE

Chapter summary : The modelling approach used for calculating the in–service lay length changes and rope rotation during conveyance loading is detailed in this chapter. It is shown how lay length data from rope manufacture is used to determine the rotation boundary conditions at installation in a mine shaft. With the assumption that the torque along the suspended length is constant, the lay length distribution at installation can be calculated. Maintenance practices result in the gradual unlaying of ropes in service. The effect of removal of rotation on the lay length distribution is shown. Accurate rope load and lay length values are required to determine the torsional stiffness characteristic at each position along the rope length. It is possible to split the loading process into two components, an increase in load at constant twist and a subsequent change in twist at constant load. The change in twist is required to establish a torque equilibrium in the rope for the increased end load. The magnitude of the change in twist is dependant on the hysteretic torsional properties of the rope. Integration of the change in twist during loading results in the rope rotation which can be compared to site measurements. A method of taking into account the variation of torsional stiffness, as twisting progresses, is presented. The analysis described in this chapter differs from previous approaches discussed in the literature review since it is not assumed that the rotation boundary conditions at either end of the rope are zero. Further, the rotation analysis takes full account of torsional hysteresis effects which have been found to significantly influence the magnitude of calculated rope rotation.

5.1 Rope lay lengths in design and manufacture

Lang's lay triangular strand ropes are designed with an optimum lay length which is a function of the number of wires in the rope cross-section and the diameter of the rope. Implementation of the exact design lay length during manufacture is however not possible and a closing specification range is normally given, figure 5.1. It was found that the nominal lay length of a rope, as reported on the tensile test

certificates, corresponds to the minimum lay length in the closing specification range. The maximum lay length value for closing is equal to the nominal lay length plus five percent. For the ropes considered, equation [5.1] relates nominal lay length to nominal diameter :

$$LL_{nom} \quad = \quad (7{,}48 \rightarrow 7{,}64) \, . \, d_{nom} \qquad [5.1]$$

(Determined from the manufacturing data for the particular triangular strand ropes)

Figure 5.1 shows the positions where the rope lay length is examined during manufacture. The "on tension" lay length is measured between the lay block and the capstan. The rope tension at this position is estimated to be between five and ten percent of the rope breaking strength. The lay length taken between the capstan and the take-up drum is termed "off tension". The quality control system requires that the on tension lay length must lie in the closing specification range.

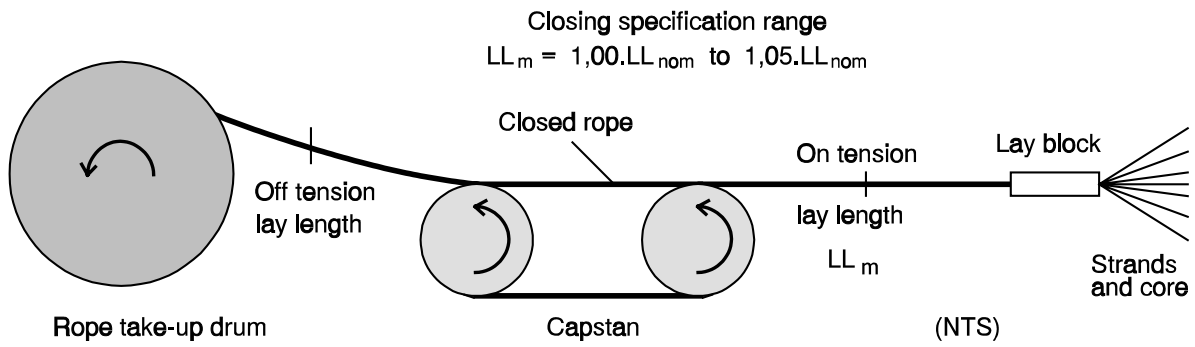

Figure 5.1 - Positions where quality control lay lengths are measured during rope manufacture. "Closing" is the term used to describe the process of laying the strands around the core to form the completed rope.

"On tension" lay lengths values were extracted from the manufacturer's quality control documentation for the ropes on which in-service measurements and laboratory torsion tests were conducted and for additional ropes for which lay length data was obtained from various mines. Figure 5.2 shows the distribution of the "on tension" lay lengths recorded. It was understood from the rope manufacturer that the "on tension" lay length is dependant on the gearing arrangement of the rope closing machine. Figure 5.3 indicates that there can be variability in the lay lengths recorded at manufacture, even for a single diameter.

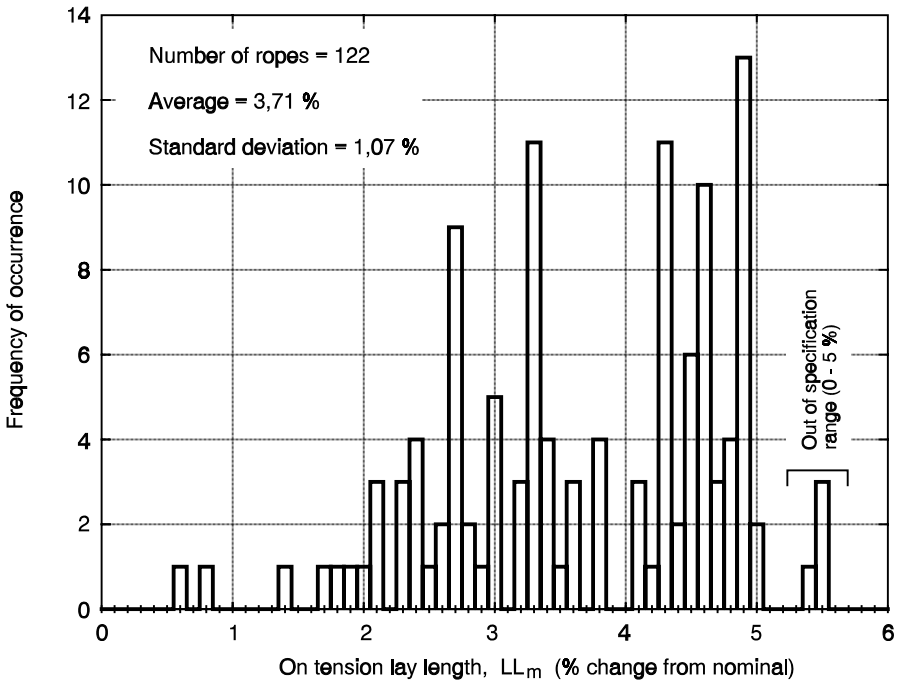

Figure 5.2 - Distribution of "on tension" lay lengths measured during the manufacture of triangular strand ropes.

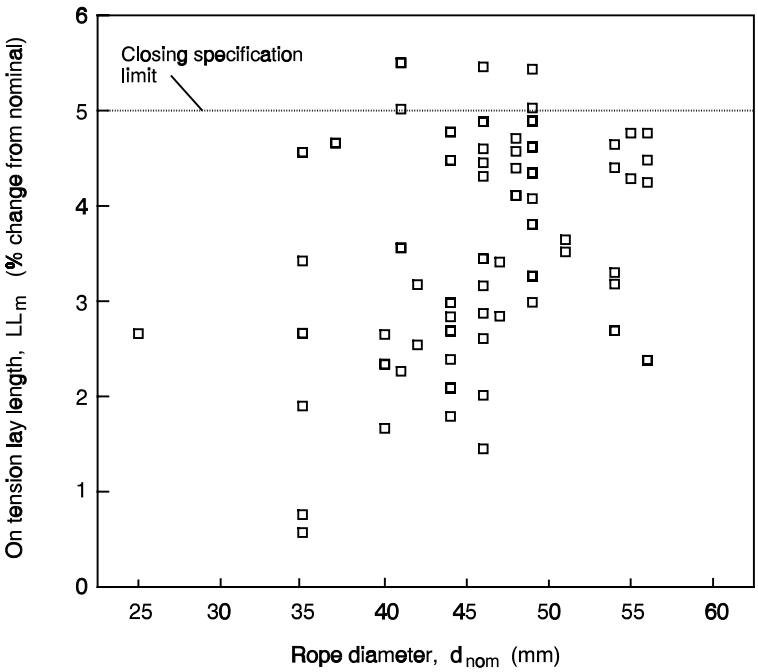

Figure 5.3 - Variations in "on tension" lay lengths for different diameters. Same ropes as in figure 5.2. Percentage change from nominal determined by : $(LL_m / LL_{nom} - 1).100$.

When a section of triangular strand rope is cut from a manufactured coil, the free lay length of the cut section normally increases to a value different from the manufactured lay length (LL_m). A section of every new hoisting rope is subjected to a tensile test before which the lay length is measured. From the tensile test certificates, the free lay lengths of the ropes considered in figures 5.2 and 5.3 were established and are shown in figure 5.4. There is considerable variability even for a specific diameter. The free lay length of a sample is largely dependant on the effectiveness of the preformation process (plastic deformation into a helical form) which the strands undergo during manufacture. Quantification of the dependence is not within the scope of this project. What is pertinent is that each rope, even though it may be of a common construction and diameter, can have unique lay length properties.

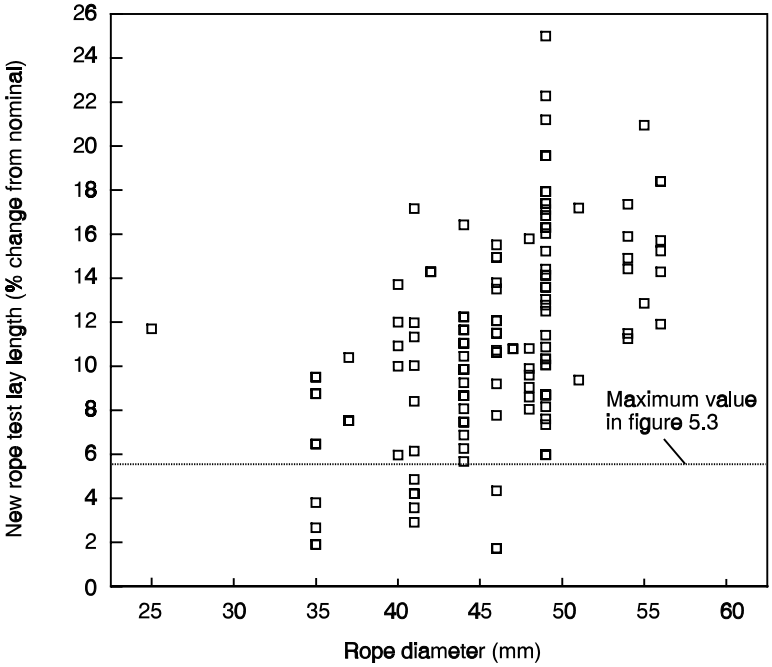

Figure 5.4 - New rope test lay lengths (free) for different rope diameters. Same ropes as in figure 5.2. Percentage change from nominal determined by : (LL_m / LL_{nom} - 1).100.

The existence of lay length variations, between different coils of the same construction and diameter, has to be considered in the torsional behaviour analysis. When a torsion test is conducted on a section of rope, the lay length which the sample has when it is installed in the machine is defined as the zero twist lay length (LL_0). For example, this lay length could be 15 percent greater than the nominal

value, as was the case with a number of the ropes shown in figure 5.4 (free lay lengths).

The coil of rope which arrives at the mine for installation on a drum winder has an approximately constant lay length over its length. This lay length corresponds to the value at which the rope was manufactured, figures 5.2 and 5.3 (LL_m). The rope wound onto the transportation reel or take-up drum is torsionally restrained as it was during manufacture. The lay length at manufacture could, for example, be three percent greater than the nominal lay length as was the case with a number of the ropes in figure 5.3.

The consequence of the lay length difference between the free tests piece and the manufactured coil is that the rope arriving at the mine has one end rotated with respect to the other, relative to the section on which the torsion test was conducted. Figure 5.5 illustrates this schematically.

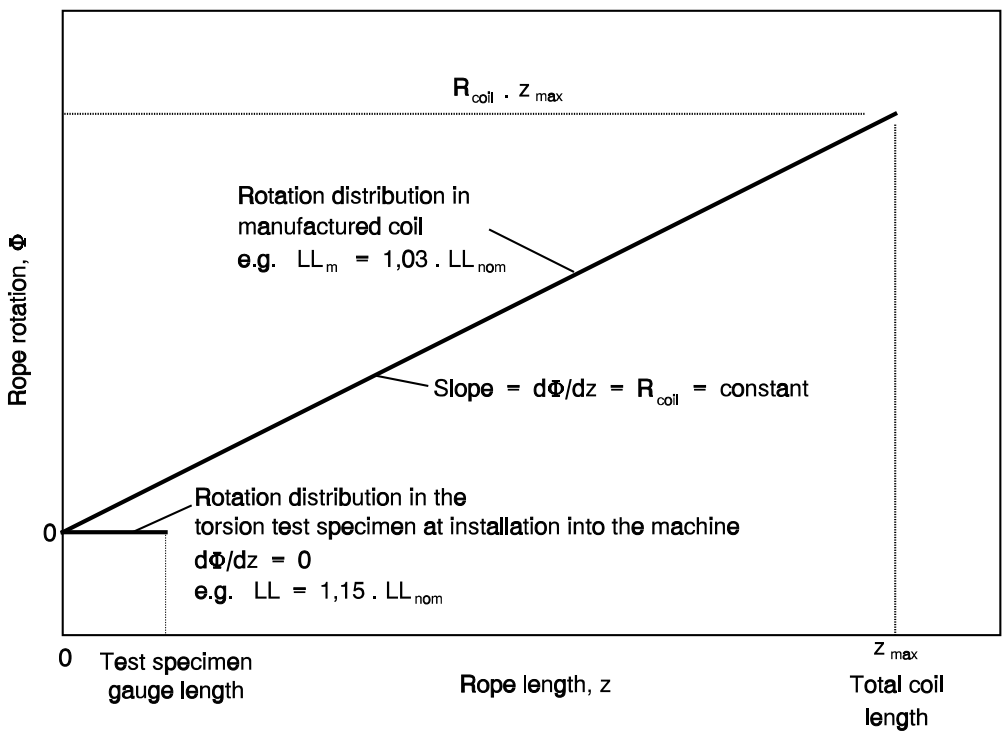

Figure 5.5 - Example of rotation in a manufactured coil relative to a torsion test specimen which is subject to zero rotation at installation into the testing machine. The values of $1{,}03.LL_{nom}$ and $1{,}15.LL_{nom}$ were selected from figures 5.3 and 5.4 for illustration purposes only.

Knowing the lay length at which the rope was manufactured, it is possible to determine the corresponding torsion test twist. During the torsion tests, the relationship between applied twist and lay length is determined (figure A.7). Zero twist, for the above example, would be associated with a lay length of $1{,}15.LL_{nom}$. A lay length of $1{,}03.LL_{nom}$ (which is shorter) would therefore require a positive twist, R_{coil}. The value of R_{coil} is determined from an equation of the form :

$$LL = \frac{\pi.d_0}{tan(\ atan(\frac{\pi.d_0}{LL_0}) + k_{LL}.R\ )} \qquad [5.2]$$

where :

d_0	=	test specimen diameter at zero twist (mm)
LL_0	=	test specimen lay length at zero twist (mm)
k_{LL}	=	least squares lay length factor (°/(°/m))
		(determined numerically from lay length and twist data)
R	=	rope twist (°/m)
	=	Φ_t / l_0
Φ_t	=	test specimen end rotation (°), figure A.12
l_0	=	test specimen gauge length at zero twist (m), figure 3.7

The relative rotation of one end of the manufactured coil with respect to the other is determined by multiplying the twist, R_{coil}, by the total length of the rope, z_{max}. For deep shaft hoisting ropes, small changes in R_{coil} can result in substantial changes in the relative end rotation value since z_{max} is large (2000 m - 4000 m). Note that z_{max} includes the suspended rope length, the catenary section and the remaining rope on the drum when the conveyance is at the lowest position in the shaft. Figure 5.5 can be redrawn to show the portions of the rope coil relative to the hoisting system geometry, figure 5.6.

From figure 5.6, it can be seen that if the rotation at the conveyance end is taken as zero then the rotation at the drum connection point would be (R_{coil} . z_{max}). This is assuming that the rope length is not changed in the process of connecting it to the drum and conveyance and that no rotation is added to or lost from the coil.

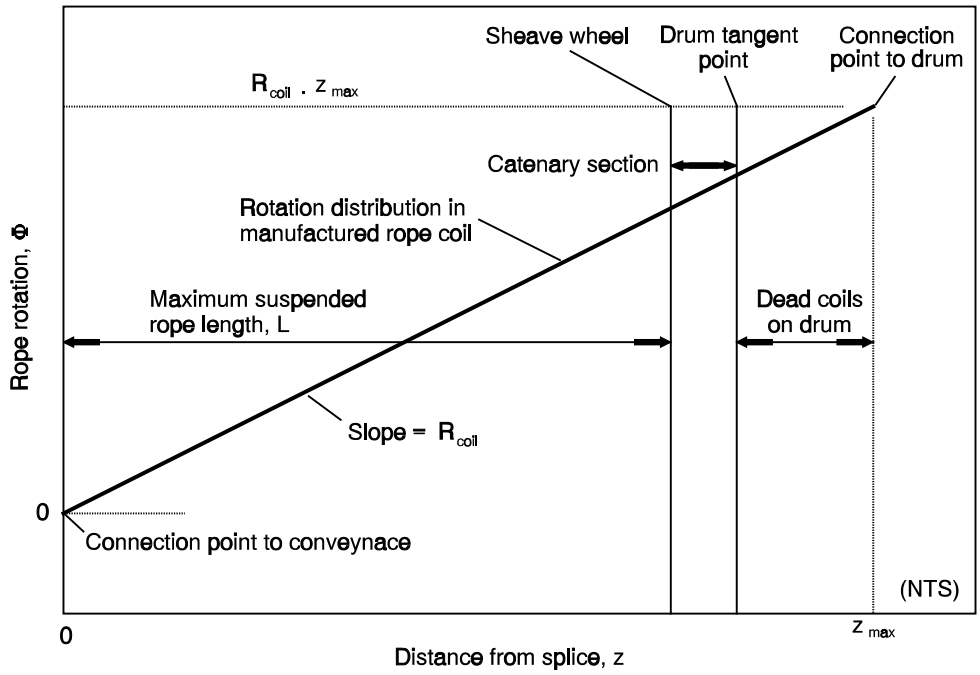

Figure 5.6 - Rotation in the manufactured rope in relation to the hoisting system geometry. The conveyance is assumed to be at the lowest position in the shaft and no rotation of the suspended section is taken into account.

5.2 Rope installation on a drum winder

In considering the transition from the manufactured lay length state (figure 5.6) to that of in-service torsional equilibrium, a brief description of the rope installation procedure is appropriate. To gain a better understanding of the installation process, the changing of the ropes on shaft **C** (46 mm ropes at 1426 m) was observed. The description given below is for a single drum winder but the principle is the same for a double drum machine.

The new rope coil is placed on a stand in which it can rotate. Some form of braking system is usually fitted to this stand to keep the rope taught during unreeling. Steel beams are used to support the conveyance at the bank level and the old rope is detached and connected to the drum end of the new rope. By winding in the old rope, the new rope is drawn up and over the head sheave. A deflection sheave can be used to alter the direction of the new rope at the conveyance point. Figure 5.7 shows the elevation of such an arrangement.

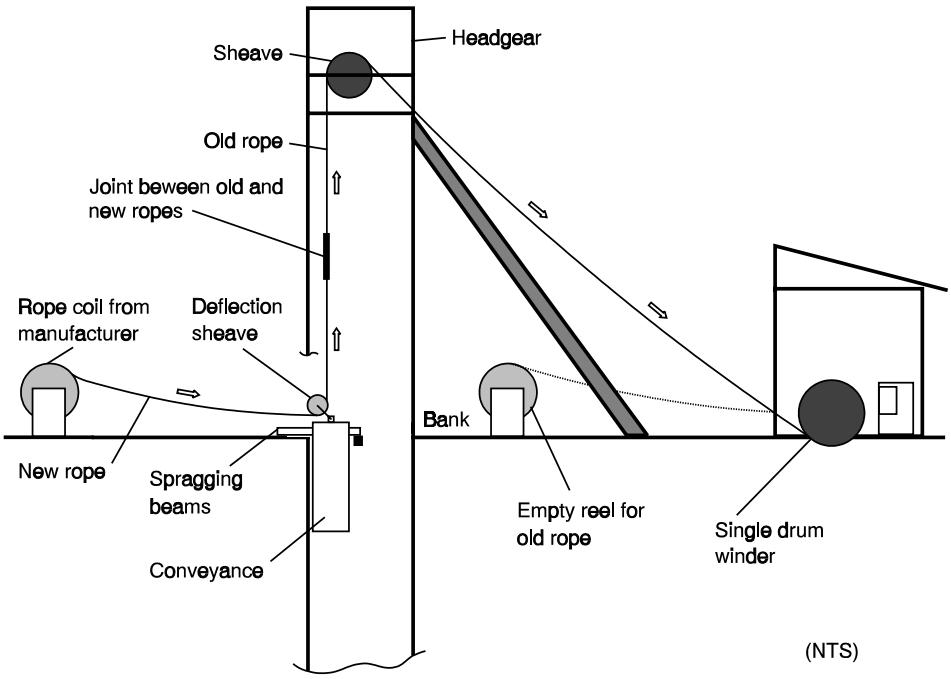

Figure 5.7 - Installation of a new rope on a single drum winder, also applicable to double drum winders.

A sufficient amount of new rope is pulled over the head sheave to allow for connection to the drum. It is then disconnected from the old rope which is subsequently unwound entirely from the drum onto an empty reel positioned in front of the winder. With the old rope removed, the new rope is connected to, and wound onto, the winder drum. At this stage the tension of the new rope on the drum is relatively low. To ensure accurate coiling and acceptable fatigue life of the rope it is important that it is unwound almost entirely and then rewound onto the drum under tension. The tension should preferably be equal to but not less than half of the operating tension (Haggie Rand, 1987). This is particularly relevant to the section of rope which does not leave the drum during normal operation (dead coils or dead turns).

A procedure termed "doubling down" is often used to achieve the required tension in the dead coils. It involves connecting the splice end if the rope to a point in the headgear which, with the use of a conveyance mounted sheave, results in two falls of rope in the shaft, figure 5.8. If the splice end is connected directly to the conveyance, it cannot descend far enough down the shaft to unwind all the rope on the drum. In the case of doubling down, the conveyance travel distance is halved.

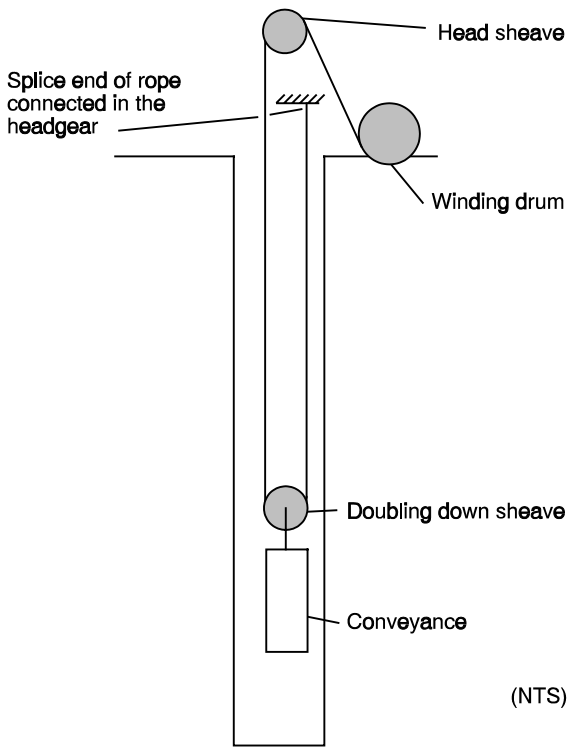

Figure 5.8 - The doubling down arrangement to ensure adequate tension in the dead coils on a single winder drum, also applicable to double drum machines.

5.3 Installation equilibrium conditions

The term "equilibrium" is widely used in this chapter and unless otherwise stated, it refers a condition of constant torque in the vertically suspended rope section. In figure 5.6, the twist (rotation per unit length) in the section of rope from the sheave wheel to the conveyance connection point was shown as constant which is the case at the start of the installation process. When fully suspended, the rope load in this section increases linearly towards the sheave wheel due to the rope weight per unit length, q. An example of the general relationship between load, torque and twist for a triangular strand rope is shown in figure 5.9. It is apparent from the data in figure 5.9 that if the load in the rope changes, at constant twist, then the torque will also change. The suspended section of rope has no externally applied torques, therefore the torque must be constant. This can only be achieved by a variation in twist along the length. The phenomena of vertically suspended ropes twisting to establish a torque equilibrium is well reported in the literature and was discussed earlier in section 2.4.

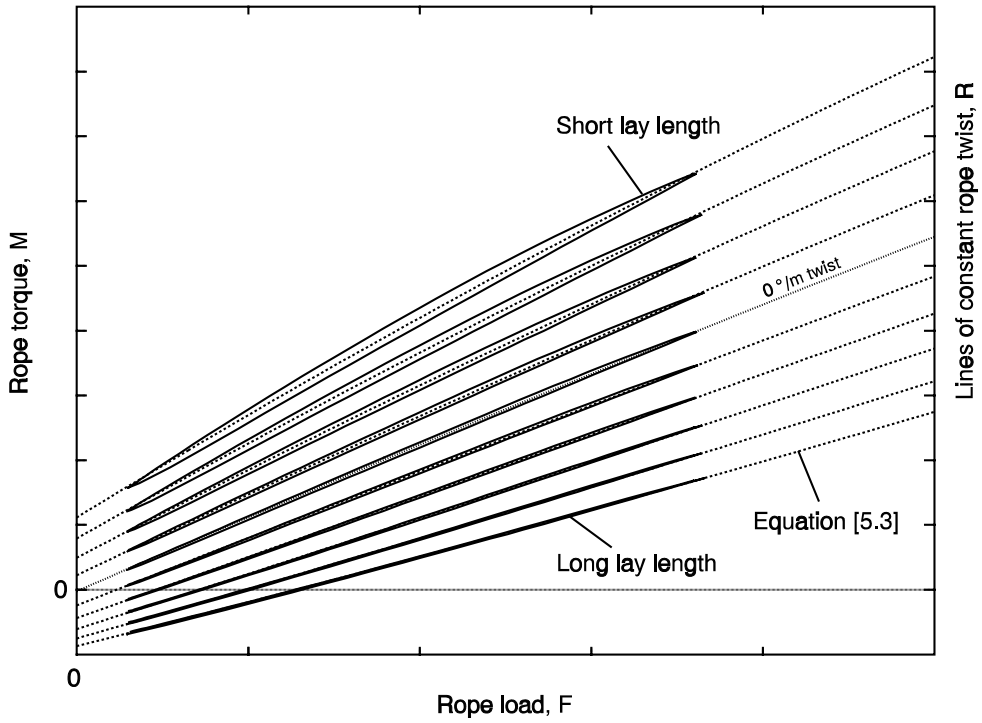

Figure 5.9 - General relationship between load, torque and twist for Lang's lay triangular strand ropes resulting from constant twist tests.

The relationship between load, torque and twist can be accurately described by equation [5.3] :

$$M = [R^2 \;\; R \;\; 1].\left[\begin{bmatrix} N_{11} & N_{12} & N_{13} \\ N_{21} & N_{22} & N_{23} \\ N_{31} & N_{32} & N_{33} \end{bmatrix}.\begin{bmatrix} F^2 \\ F \\ 1 \end{bmatrix}\right] \qquad [5.3]$$

where :	M	=	rope torque	(Nm)
	R	=	rope twist $d\Phi/dz$	(°/m)
	F	=	rope load	(kN)

Equation [5.3] was adopted specifically for describing the constant twist test data of triangular strand ropes. It was found that equation [2.9] of Feyrer and Schiffner (1986) could not adequately represent the nonlinearities in the response which become evident at larger twist deformations. The equation was arrived at by assuming that each constant twist curve can be represented by a second order polynomial in terms of load, *F*. Three sets of polynomial coefficients result (for F^2, *F, constant*) with each set then being described by second order

polynomials in terms of twist, *R*. In all cases the coefficients are determined according to the least squares criterion of fit.

For the in-shaft rope torsional analysis it is necessary to calculate the twist distribution which would result in a constant torque, *M*, for varying load, *F(z)*. For this purpose, equation [5.3] can be written as twist, *R*, in terms of *M* and *F*.

setting :

$$A_R = \left[N_{11} \;\; N_{12} \;\; N_{13} \right] . \begin{bmatrix} F^2 \\ F \\ 1 \end{bmatrix} \qquad [5.4]$$

$$B_R = \left[N_{21} \;\; N_{22} \;\; N_{23} \right] . \begin{bmatrix} F^2 \\ F \\ 1 \end{bmatrix} \qquad [5.5]$$

$$C_R = \left[N_{31} \;\; N_{32} \;\; N_{33} \right] . \begin{bmatrix} F^2 \\ F \\ 1 \end{bmatrix} - M \qquad [5.6]$$

then :

$$R = \frac{-B_R \pm \sqrt{B_R^2 - 4.A_R.C_R}}{2.A_R} \qquad [5.7]$$

For increasing positive torques associated with positive twists and increasing load, the positive root returns a meaningful solution.

The linear variation in rope load along its length is described by equation [5.8] :

$$F = P + q.z \qquad [5.8]$$

where : P = rope end load (kN)
q = rope weight per unit length (kN/m)
z = distance along the rope measured from the splice (m)

Combining equations [5.7] and [5.8] results in equation [5.7a] for twist (*R*) in terms of rope length (*z*), torque (*M*), end load (*P*) and rope weight per unit length (*q*). The unknown in equation [5.7a] is the equilibrium torque, *M*.

$$R = f(M,P,q,z) \qquad [5.7a]$$

([5.8] $\rightarrow$ [5.4], [5.5], [5.6] $\rightarrow$ [5.7] $\Rightarrow$ [5.7a])

The boundary conditions for rope twist are also unknown. However, for rope rotation, Φ, there are two known boundary conditions which were discussed in sections 5.1 and 5.2. If it is assumed that the doubling down procedure does not affect the initial rotation distribution in the rope, then, for the vertically suspended section only :

i. $\Phi = 0$ at $z = 0$

ii. $\Phi = R_{coil}.L$ at $z = L$

where : L = maximum suspended rope length (m), figure 5.6

By integrating rope twist (equation [5.7a]) with respect to rope length, z, the rotation, $\Phi(z)$ can be determined :

$$\Phi = \int R\, dz + constant \qquad [5.9]$$

A constant of integration will result but application of the first (i) boundary condition above returns a zero value for this constant. The second (ii) boundary condition will be satisfied if the constant torque, M, is chosen correctly. It is possible to solve for the torque and twist distribution with the numerical scheme described in table 5.1.

Table 5.1 - Steps of the numerical scheme for solving for the constant torque, M, in equation [5.7a] while satisfying the boundary conditions for equation [5.9].

1. Assume a value for M
2. Knowing $F = f(P,q,z)$ calculate $R = f(M,F)$, equation 5.7a
3. Integrate R with respect to z to determine rope rotation, $\Phi(z)$, equation [5.9]
4. Check whether $\Phi(L) = R_{coil}.L$
5. Adjust the value of M according to the error ($\Phi(L) - R_{coil}.L$)
6. Repeat steps 2 to 5 until the desired level of convergence is achieved i.e. until M is determined such that ($\Phi(L) = R_{coil}.L$)

A typical twist distribution, $R(z)$, in the suspended rope section resulting from this numerical method is shown in figure 5.10. Figure 5.11 shows the corresponding rotation values, $\Phi(z)$. The position were zero twist occurs is not necessarily at the midpoint of the suspended length as was suggested by Hermes and Bruens (1957). Depending on the system geometry, it may not even be close to the mid shaft position. It is important to restate that the change in twist (to reach torsional equilibrium in the suspended section) does not take place from zero twist but rather from the twist corresponding to the lay length at which the rope was manufactured, R_{coil}. The value of R_{coil} is dependant on the difference between the zero twist lay length (LL_0) for the torsion test and the lay length of manufacture, LL_m.

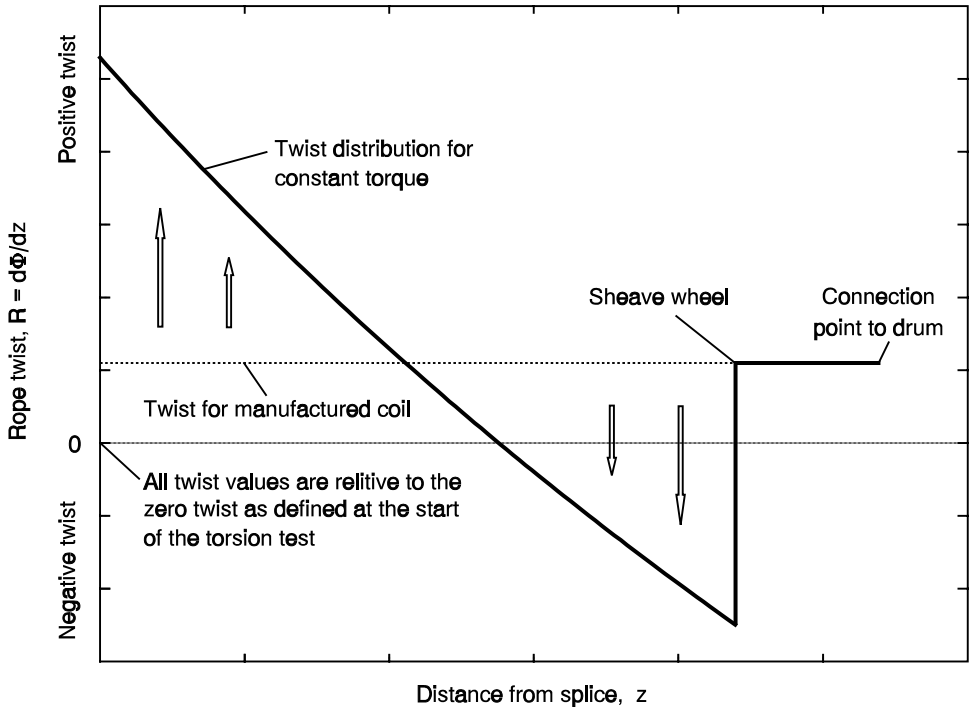

Figure 5.10 - General form of the twist distribution in a rope after installation. In this case it is assumed that there has been no torsional interaction between the vertically, catenary and dead coils sections of the rope.

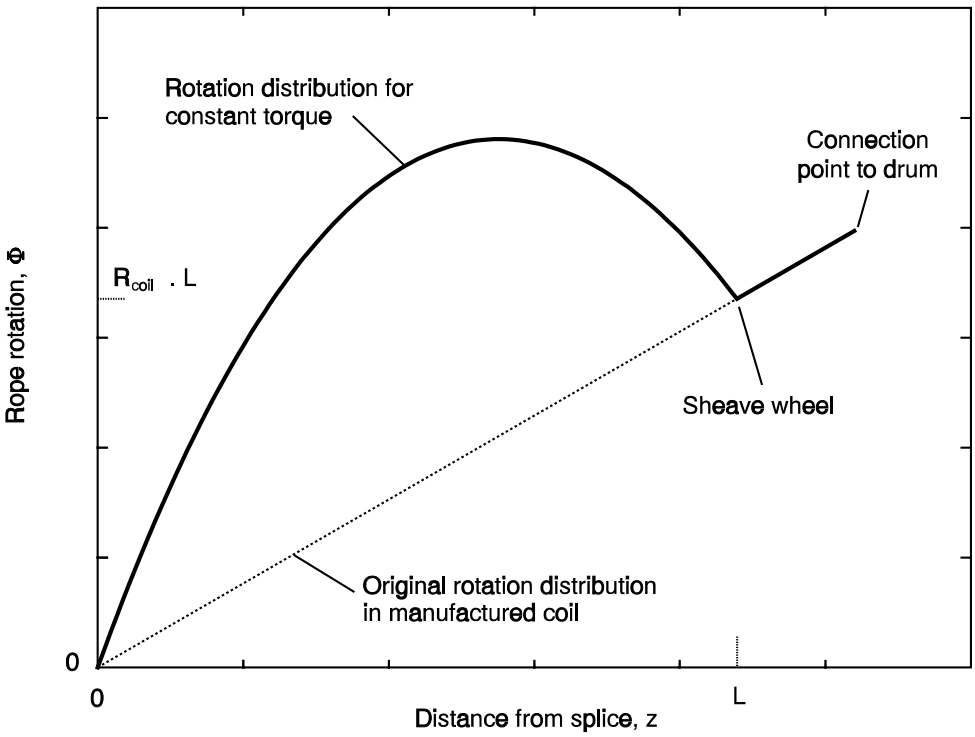

Figure 5.11 - General form of the rope rotation distribution after installation. Determined by integrating twist, *R*, with respect to rope length, *z*. Rotation between the sheave wheel and the drum connection point is unchanged

In the analysis it is assumed that the contact arc length between the headgear sheave and the rope is negligible compared to the total rope length. The contact arc is therefore taken as a single point on the rope which constitutes full torsional restraint only.

By substituting the solution for rope twist, $R(z)$, into equation [5.2] the lay length variation of the suspended section, $LL(z)$, can be determined, figure 5.12. The limitation of the analysis described thus far is that it does not take into account any changes in lay length from the head sheave to the drum connection point. Figure 5.12 shows that the lay length in this region is still equal to the lay length at which the rope was manufactured. Notice that there is a step change in lay length from one side of the sheave to the other.

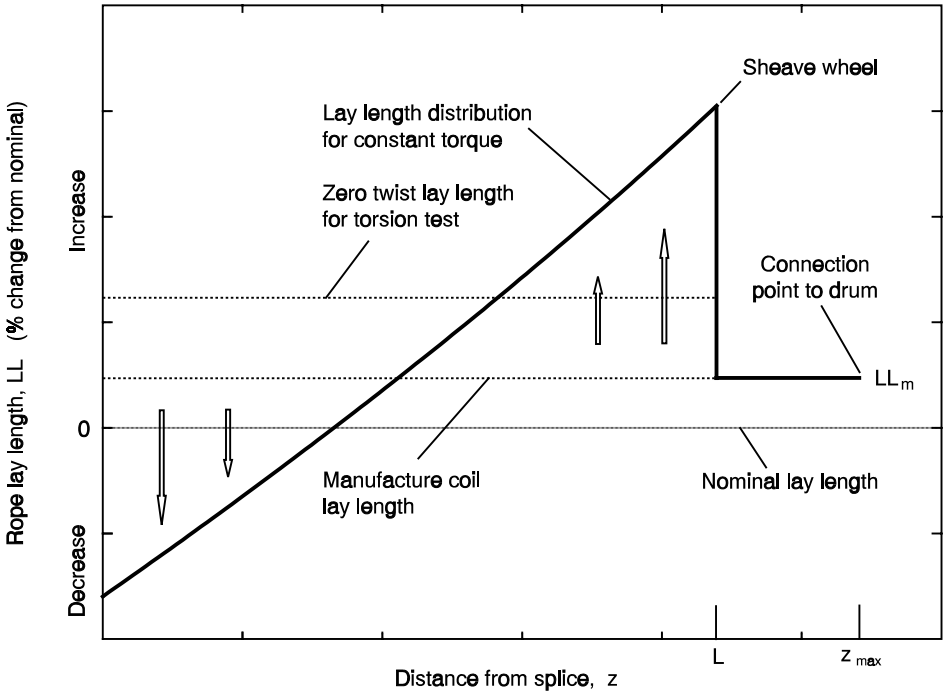

Figure 5.12 - General form of the lay length variation in a rope after installation. Torsional interaction between the vertical and drum side sections of the rope is not taken into account.

When a conveyance is hoisted and lowered in the shaft, it is equivalent to moving the sheave wheel from one end of the rope to the other. With reference to figures 5.11 and 5.12, all the rope on the right of the sheave interacts with drum (and catenary) and the portion on the left is vertically suspended. If the sheave

wheel is moved towards the left (equivalent to hoisting) then the portion of rope with a longer lay length will move over the sheave to the drum side and influence the twist, rotation and lay length distributions on the drum side. Eventually, after some hoisting and lowering cycles, a state of equilibrium would be reached where the lay length distribution on the drum side of the sheave is steady (Gibson, 1980).

Clearly, if this process occurs, the rotation boundary condition at the sheave (originally $R_{coil}.L$) would change to a new, unknown, value. With each hoisting cycle, during which the sheave boundary condition changes, the twist distribution in the vertical section and the equilibrium torque would also change. The doubling down procedure at installation (figure 5.8) would probably expedite the process of reaching such an equilibrium state.

It is realised that there is a process whereby the twist distribution in the vertically suspended and drum side sections of the rope reach an steady state some time after installation. The significance of this is that the rotation boundary condition at the sheave is influenced during the equalising process. A change in the sheave wheel boundary condition (*SWbc*) alters the twist distribution in the vertical section and the equilibrium torque. Previous attempts at modelling torsional deformations in the vertical rope section have not taken this fact into account. The cycle by cycle details of the equalising process and the exact time period over which it occurs are however not pertinent to this study. Of importance is quantification of the final equilibrium conditions.

A solution to determining the equilibrium conditions after installation is to assume that the twist in the catenary and dead coils section will eventually equal the twist in the vertical section at the sheave. The solution of the equilibrium state is then relatively simple considering that the rotation boundary condition at the connection point to the drum ($R_{coil}.z_{max}$) does not change while the sheave boundary condition changes. Figure 5.13 shows the rotation distribution from figure 5.11 and the equilibrium condition where the twist from the sheave to the drum connection point equals the twist at the sheave end of the suspended section ($R_1 = R_2$). This state is achieved by increasing the sheave rotation boundary condition and using the drum connection boundary condition as a pivot point for the drum side rotation distribution.

For the data in figure 5.13 :

$$R_2 = (R_{coil} . z_{max} - SWbc) / (z_{max} - L) \quad (°/m) \qquad [5.10]$$

$$R_1 = R(L_{vertical}) \quad (°/m) \qquad [5.11]$$

where : R = rope twist determined using *SWbc* and a numerical method similar to that described in table 5.1 (°/m)

$SWbc$ = sheave wheel rotation boundary condition (° or turns)

$L_{vertical}$ = at the sheave, on the vertical side (m)

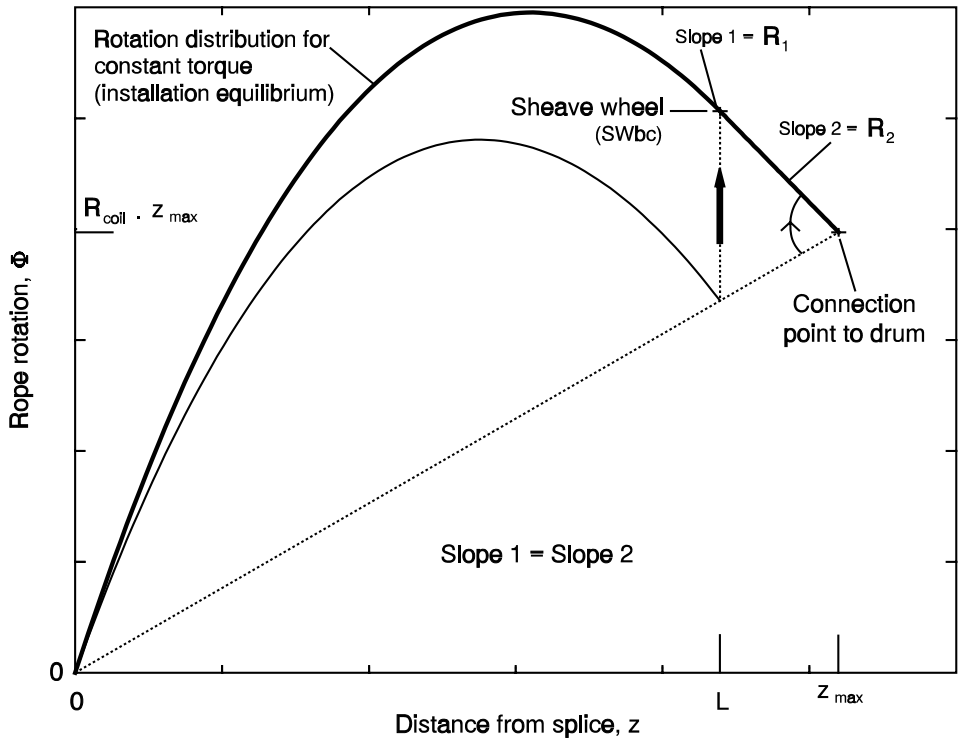

Figure 5.13 - General form of the equilibrium rotation distribution after installation. Torsional interaction between the vertical and drum side sections of the rope is taken into account.

The complete numerical scheme used to determine the equilibrium condition after installation is listed in table 5.2.

Table 5.2 - Steps of the numerical procedure for determining the torsional equilibrium conditions after installation.

1. Take M equal to the torque determined from the scheme listed in table 5.1
2. Take $SWbc = R_{coil}.L$

3. Knowing $F = f(P,q,z)$ calculate $R = f(M,F)$, equation [5.7a]
4. Integrate R with respect to z to get rope rotation, $\Phi(z)$, equation [5.9]
5. Check whether ($\Phi(L) = SWbc$)
6. Adjust the value of M according to the error ($\Phi(L) - SWbc$)
7. Repeat steps 3 to 6 until the desired level of convergence is achieved i.e. until M is determined such that ($\Phi(L) = SWbc$)

8. Calculate R_2 using equation [5.10]
9. Check whether ($R_1 = R_2$)
10. Adjust the value of $SWbc$ according to the error ($R_1 - R_2$)

11. Repeat steps 3 to 10 until the desired level of convergence is achieved i.e. until SWbc is determined such that ($R_1 = R_2$)

If the twist in the drum side section of the rope is equal to the twist at the sheave, in the suspended section, then the lay lengths must also be equal. Figure 5.14 shows the change from the initial lay lengths at installation (figure 5.12) to the final installation equilibrium condition. Note that taking into account the interaction between the vertical section and the drum side affects the lay length variation in the vertical section.

In reality the lay length at the sheave (with the conveyance at the lowest position) would be the maximum and it would decrease again towards the drum connection point (site observations). The cause of this would be friction between the rope and drum and a less significant load differential compared to the vertical section. An approach to accommodating such a variation would be to assume a linear change in twist between the sheave and the drum connection point. Details of the implementation of such an approach are contained in appendix B.

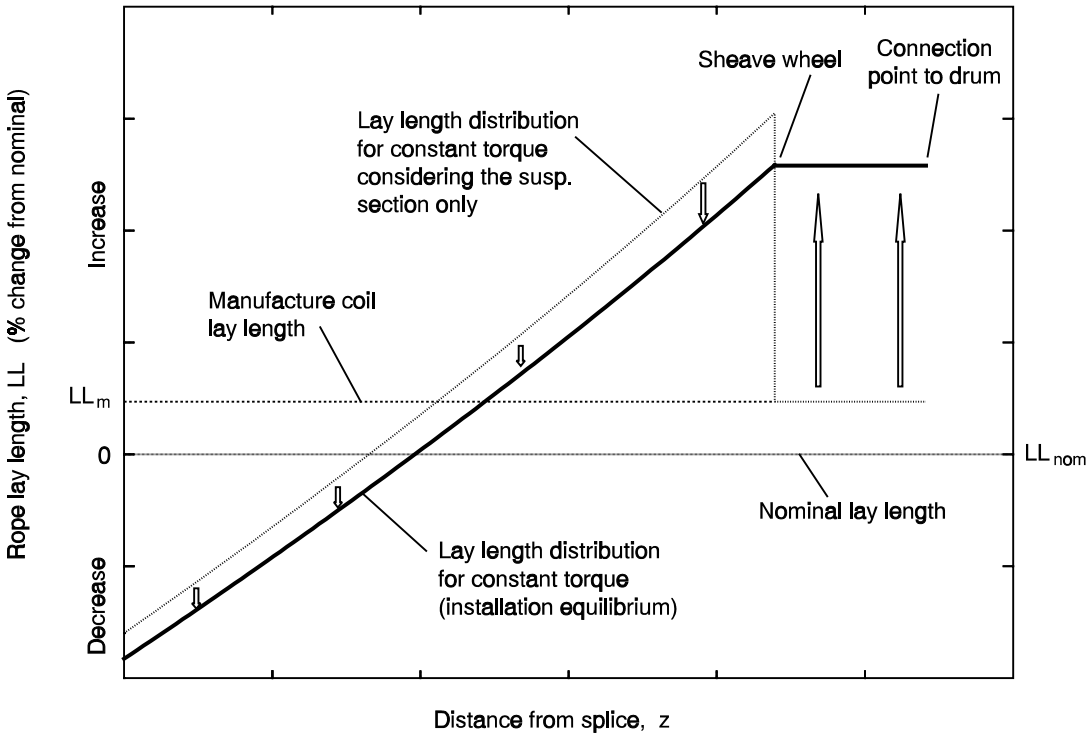

Figure 5.14 - General form of the equilibrium lay length variation after installation.

A factor *Df* is defined as the ratio of the twist at the drum connection point to the twist at the sheave. The factor therefore allows adjustment of the lay length ratio between these two points. It was however found that the effect of varying *Df* is not significant on the vertical section lay length distribution. The results of an example calculation for a 2200 m suspended rope length is given in table 5.3.

Table 5.3 - Example of the effect of varying *Df* on the rotation and lay length distribution in a rope. L = 2200 m and z_{max} = 2600 m, rope T10, 48 mm, 6x32(14/12/6 + 3Δ)/F, 1800 MPa. Further details in appendix B.

Df	**Lay length ratio** LL_{drum} / LL_{sheave} **(%)**	**Change in *SWbc* (%)**	**Vertical rope section**	
			Change in splice end lay length (% of nominal)	**Change in sheave end lay length (% of nominal)**
0,0	87,7	-10,0	0,6	1,4
1,0	100,0	0,0	0,0	0,0
1,2	102,5	1,8	-0,1	-0,3

Table 5.3 indicates small changes in the vertical section lay lengths for *Df* in the range 0 to 1,2. Of greater significance is the effect on the *SWbc* where the

associated changes are considerably larger. A similar set of calculations were completed for L = 1000 m and z_{max} = 1400 m with all other values remaining constant. The results indicated even smaller changes in lay length and in the *SWbc* value.

In section 5.4, which follows, it will be shown what effect standard rope maintenance practices have on the vertical section lay length distribution. The significance of the *SWbc* value is that it affects the number of turns which need to be removed from the rope in order to produce certain changes in lay length. For the purposes of the analysis for this study, *Df* is taken as 1.

It is possible that rotation could be lost from a rope during the installation procedure which can be accommodated in the analysis presented thus far. The rotation lost can be subtracted from the drum connection point rotation, $z_{max}.R_{coil}$, prior to the execution of the numerical schemes listed in tables 5.1 and 5.2. Calculation of the exact rotation lost during installation is not possible. It could however be quantified by counting the rotation of both ends of the rope during the installation procedure. For consistency, it is assumed that no rotation was lost during the installation of the ropes on which shaft measurements were conducted. It should be noted that the effect of a given number of turns lost from the rope on the equilibrium lay length distribution would be greater for a shorter rope than for a longer one.

5.4 The effect of rope maintenance on lay length variations

The South African regulations governing the use of wire ropes for mine hoisting require that a section of rope be cut from above the splice on a six monthly basis. This section is sent to an approved testing station where it is subjected to a destructive test. The cutting requirement also results in six monthly re-splicing which, from a termination degradation point of view, is advantageous. The position of the conveyance during cutting of the rope for test is identical to the configuration shown earlier in figure 5.7. The conveyance is spragged at the bank and the rope is disconnected. Care is normally taken in this operation because as the rope is detached from the conveyance it tends to spin. The general perception of rope maintenance staff is that the rope "builds up spin" after a period of operation which is released during detachment.

If the equilibrium rotation distribution is considered, then it can be seen why the end of the rope rotates when it is detached from the conveyance. With the conveyance at the bank (surface level), almost all the rope is wound onto the drum except the vertical portion between the conveyance and the sheave and the catenary section. For purposes of calculating the rotation released only the length of rope from the conveyance to the sheave needs to be considered. Figure 5.15 shows the general equilibrium rotation distribution in a rope with detail of the length between the conveyance and sheave with the conveyance at the bank.

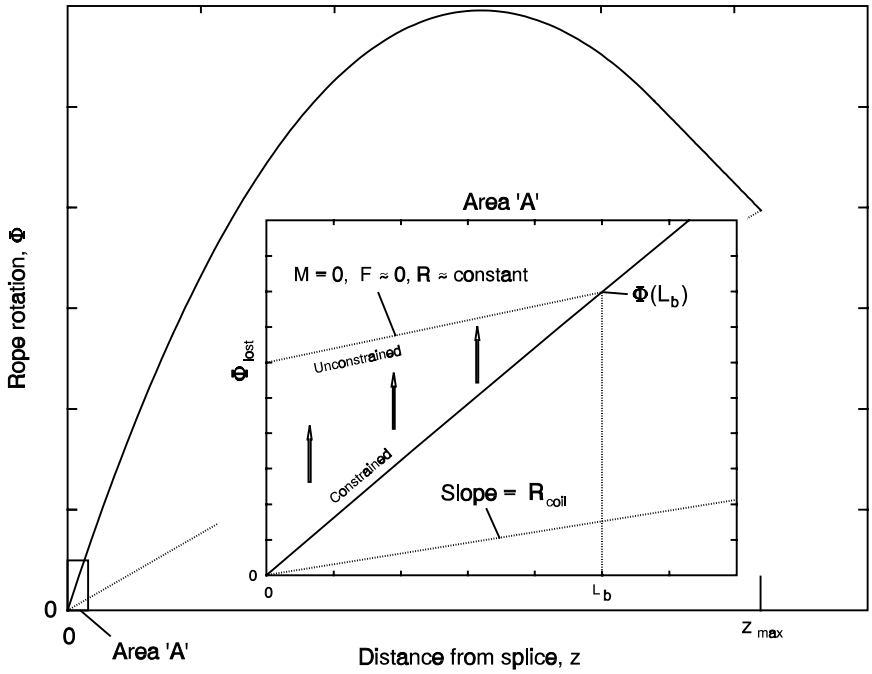

Figure 5.15 - A method of determining the rotation lost from a rope when it is detached from the conveyance.

The rotation distribution in the constrained state (prior to detachment) is determined from the equilibrium conditions discussed in section 5.3. It can be assumed that the rotation at the sheave ($z = L_b$) will remain constant during detachment because of friction between the rope and the sheave groove. The rotation distribution between L_b and z_{max} will also remain constant. By definition, when the rope is detached, the torque in the suspended section ($z = 0$ to L_b) must be zero. This can only be achieved by a change in twist with corresponding change in the rotation value at the splice. For surface shafts, the value of L_b is typically be between 40 m and 50 m. For sub-vertical shafts L_b could vary from 70 m to 110 m. As a first approximation the load in the section, $z = 0$ to L_b, could be taken as zero. The

resulting twist in the section would then be such that zero load and torque conditions are both satisfied. It would also be reasonable to assume that the unconstrained twist value would not vary between 0 and L_b. If the rope, in-service, was manufactured under identical conditions to the laboratory test section, then the twist corresponding to $M = 0$ and $F = 0$ would be $R = 0$. Alternatively stated, $\Phi(0)_{unconstrained} = \Phi(L_b)$. Judging from the variability in the data of figure 5.4, this is unlikely to be the case. The exact value of the unconstrained twist (or lay length) is therefore unknown. The twist corresponding to the new rope test lay length could however be used as a reasonable approximation since this lay length was measured at $M = 0$ and $F \approx 0$. This assumption would be ignoring the possibility of plastic lay length deformation as a result of continuous operation at a shortened lay length value which has been observed in practice (Rebel, 1993).

The general form of the equation to calculate the rotation lost at the splice during detachment is :

$$\Phi_{lost} = \Phi(L_b) - (R_{unconstained}.L_b) - \Phi(0)_{constrained} \qquad [5.12]$$

For the first detachment, $\Phi(0)_{constrained} = 0$.

$R_{unconstrained}$ could be taken as the torsion test twist which results in the lay length equal to the new rope test lay length of the in-service rope (equation [5.2]).

A more detailed approach to calculating the lost rotation would be to assume a linear load distribution between the splice and the sheave with an applied end load at the splice equal to the weight of the safety detaching hook and connecting shackles. Typically, safety detaching hooks vary in mass from 150 kg to 440 kg for a 120 kN to 240 kN safe working load range.

If the new splice is reattached to the conveyance without adding any of the lost rotation, the splice end boundary condition would be :

$$\Phi(0)_{constrained} = \Phi(L_b) - (R_{uncounstrained}.L_b) \qquad [5.13]$$

Ropes are also detached from the conveyance for other reasons which may not coincide with the cutting of test sections. These reasons include :

- Changing conveyances.
- Replacement of safety detaching gear.
- For doubling down only.
- For doubling down so that the drum connection point can be pulled in.

Each time the rope is detached from the conveyance rotation is lost. It is possible to count and record the lost rotation from a rope in-service since when the ends are free to rotate, they are also visible. This is however not a statutory requirement and is not commonly practised in the industry.

When the drum connection point is pulled in, or the splice end is cut for test the value of z_{max} is decreased. In both cases, the drum connection point is being moved closer (rope length wise) to the conveyance (*L* remains constant). The result of this is that the rotation boundary condition at the drum and z_{max} are maintenance practice dependant functions of service period. Most of the ropes on which shaft measurements were conducted had been in service for different time periods. On shaft **G** (49 mm ropes at 1126 m) it was reported that five turns were put back into the rope after cutting of a tensile test section. On the other shafts there was no procedure for restoring lost rotation. Each time rotation is lost from the rope, the rotation boundary conditions and therefore the lay length distribution are affected.

It was shown in section 5.3 that the sheave to drum rotation distribution does not significantly affect the vertical section lay lengths. For the purposes of calculating the effect of lost rotation on lay length, it was therefore assumed that the *SWbc* remains fixed at the installation equilibrium value and that all rotation is lost from the splice end of the rope.

For the analysis a change in the splice end rotation boundary condition can be included. Equation [5.9] resulted in a constant of integration which was calculated as zero since $\Phi(0) = 0$ at installation. To incorporate a varying boundary condition at the splice, equation [5.9] can be altered to :

$$\Phi = \int R \, dz + \Phi(0) \qquad [5.9a]$$

where : $\Phi(0) = \Phi_{lost} \neq 0$

The equilibrium twist distribution is still determined such that $\Phi(L) = SWbc$. Figures 5.16 and 5.17 show the general form of the rotation and twist distributions which result from a change in the splice end boundary condition.

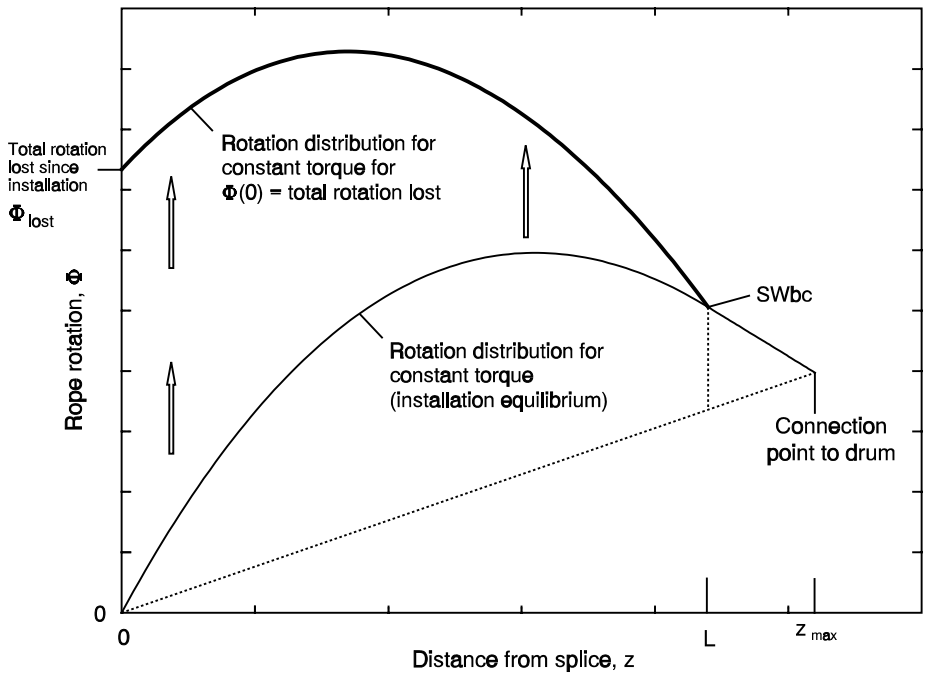

Figure 5.16 - Change in the rope rotation distribution as a result of a loss in rotation from the rope.

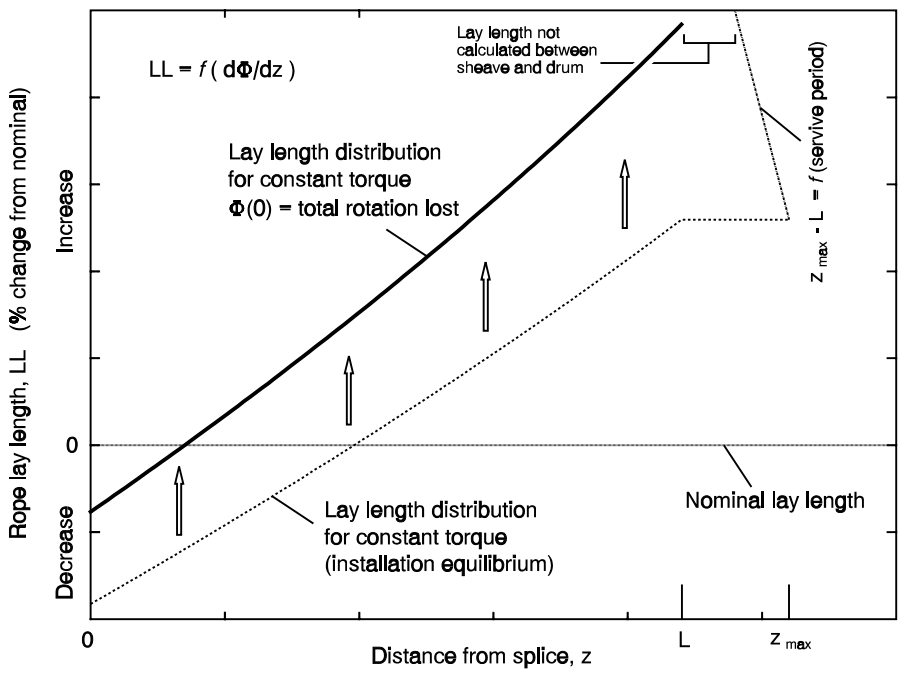

Figure 5.17 - Change in the rope lay length variation as a result of a loss in rope rotation. Notice that the sheave end lay length increases more rapidly than the splice end.

Because of the nonlinear relationship between twist and lay length, the sheave end lay length increases at a greater rate than the splice end. In theory, the rope will continue to unwind until the twist in the constrained state, between 0 and L_b, is approximately equal to the twist in the unconstrained state. It can be seen, considering figure 5.15 and 5.16, that if the boundary condition at the splice end is increased sufficiently, then the twist at the splice will eventually equal the twist corresponding to $M = 0$ and $F \approx 0$.

Unless a rope in service is carefully monitored from installation it is difficult to accurately quantify the total rotation that has been lost from the rope. For this investigation the rotations lost from the various in-service ropes were unknown. An approach was therefore adopted whereby it is shown that at some point of unlaying the predicted lay length distribution line passes through the measured lay lengths with acceptable accuracy. In doing this, the only variable in the analysis algorithm that is altered is Φ_{lost}, figure 5.16.

It is likely that for further investigations, the analysis presented in this section would be used to determine the effect which removing or adding rotation has on the lay length distribution and equilibrium rope torque. The rotation value, Φ_{lost}, would therefore be known.

5.5 Rope torsional stiffness properties

The typical surface described by equation [5.3] for a triangular strand rope is shown in figure 5.18. As discussed in section 2.4, literature on rope torsional response referred to a "Torque factor", *C*, which was defined as the proportionality between rope load and torque for constant twist.

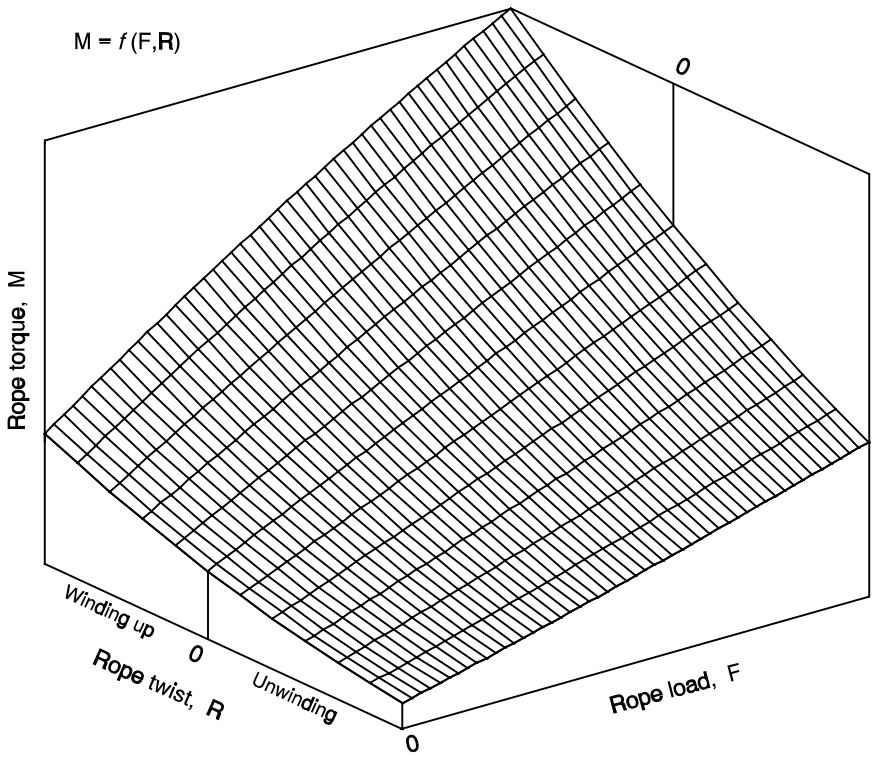

Figure 5.18 - General form of the torque surface defined by equation [5.3].

Considering the surface defined by equation [5.3], the torque factor is clearly the partial derivative, $\partial M/\partial F$:

$$C = \frac{\partial M}{\partial F} = [R^2 \;\; R \;\; 1].\left[\begin{bmatrix} N_{11} & N_{12} \\ N_{21} & N_{22} \\ N_{31} & N_{32} \end{bmatrix} . \begin{bmatrix} 2.F \\ 1 \end{bmatrix} \right] \qquad [5.14]$$

The literature also referred to the "Torsional stiffness", T, which similarly would be the partial derivative, $\partial M/\partial R$ (tangent stiffness), which can also be determined directly from equation [5.3] :

$$T = \frac{\partial M}{\partial R} = [2.R \;\; 1].\left[\begin{bmatrix} N_{11} & N_{12} & N_{13} \\ N_{21} & N_{22} & N_{23} \end{bmatrix} . \begin{bmatrix} F^2 \\ F \\ 1 \end{bmatrix} \right] \qquad [5.15]$$

Torsional stiffness was previously defined by Yiassoumis (1992) as :

$$T = \frac{\Delta M_t}{\Delta R_t}_{(R = Ri)} = \frac{M_i - M_0}{R_i - R_0} \qquad [5.16]$$

At $R_i = R_0$, this equation is undefined. Further, it can be seen in figure 5.19 that for larger twist displacements, the torsional stiffness calculated by equation [5.16] is not equal to the partial derivative, $\partial M/\partial R$. Only for small displacements ($R_0 \rightarrow R_k$) does equation [5.16] give an approximate value of the torsional stiffness inferred from the constant twist test.

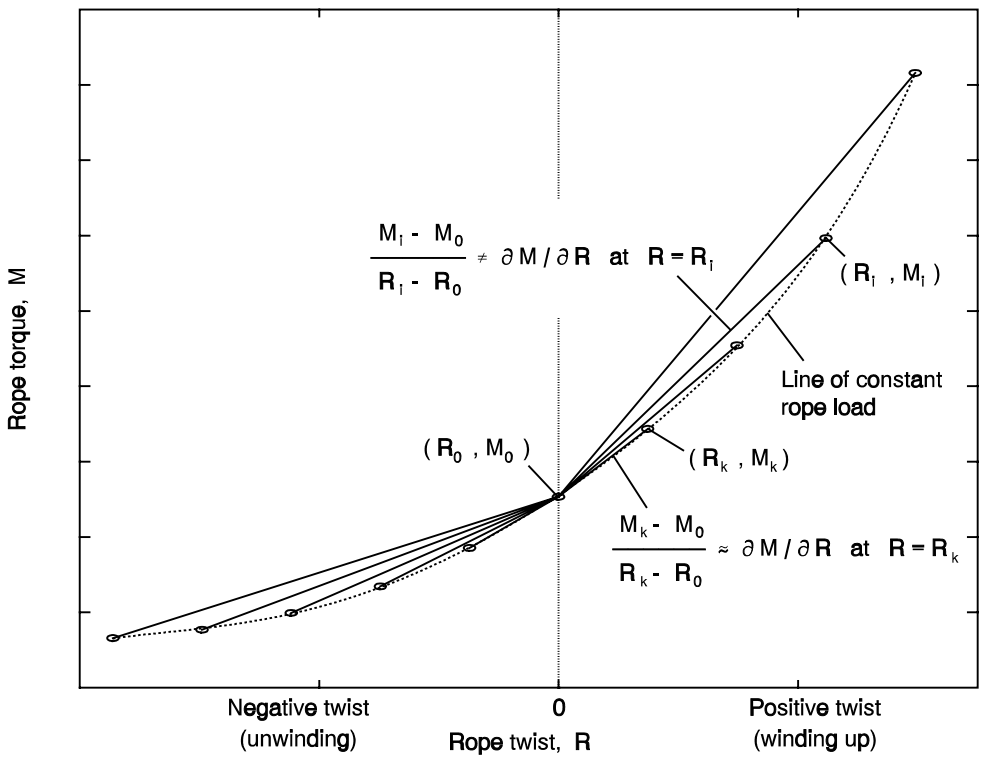

Figure 5.19 - Accurate and approximate methods of calculating the torsional stiffness from constant twist test data. $\partial M/\partial R$ is the tangent stiffness and is calculated for torque versus twist curves inferred from a constant twist test results.

Note that if C and T are not constant then torque cannot be defined by equation [2.2], as previously reported by Yiassoumis (1992) :

$$M \neq C.F + T.R \qquad [2.2]$$

since

$$M \neq \frac{\partial M}{\partial F}.F + \frac{\partial M}{\partial R}.R \qquad [5.17]$$

Further to this, it was found that the torsional stiffness calculated from the constant twist test (equation [5.15]) is not a true representation of the actual torsional stiffness characteristic of the rope. It was stated in section 4.2.6 that while conducting constant load tests it was observed that large changes in torque occurred for relatively small changes in twist from a stationary twist position. The typical torsional response of a triangular strand rope twisted at constant load, is shown in figure 5.20.

Perfect control of the rope load was not possible due to limitations of the testing machine. The corresponding load error, δF_{cl}, is also shown in figure 5.20. It was noticed that disturbances in the measured torque value occurred at exactly the same points as small fluctuations in the constant load. From this observation it was concluded that the measured torque is a superposition of changes due to twisting and changes due to load fluctuations. The changes in torque due to load fluctuations cause errors in the measurement (noise). The torque error for the constant load test must therefore be a function of the load error :

$$\delta M_{cl} = f(\delta F_{cl}) \qquad [5.18]$$

If the changes in F are small and R is constant then :

$$\delta M_{cl} = \frac{\partial M}{\partial F} . \delta F_{cl} \qquad [5.18a]$$

where $\partial M/\partial F$ is defined by equation [5.14].

Knowing the load error and the proportionality between load and torque at constant twist, it is possible to calculate the torque error and correct the measured torque values for small fluctuations in the constant load. The partial derivative, $\partial M/\partial F$, is a function of the correct constant load (F_{cl}) and the value of twist (R_{cl}) at which the correction calculation is being performed (equation [5.14]).

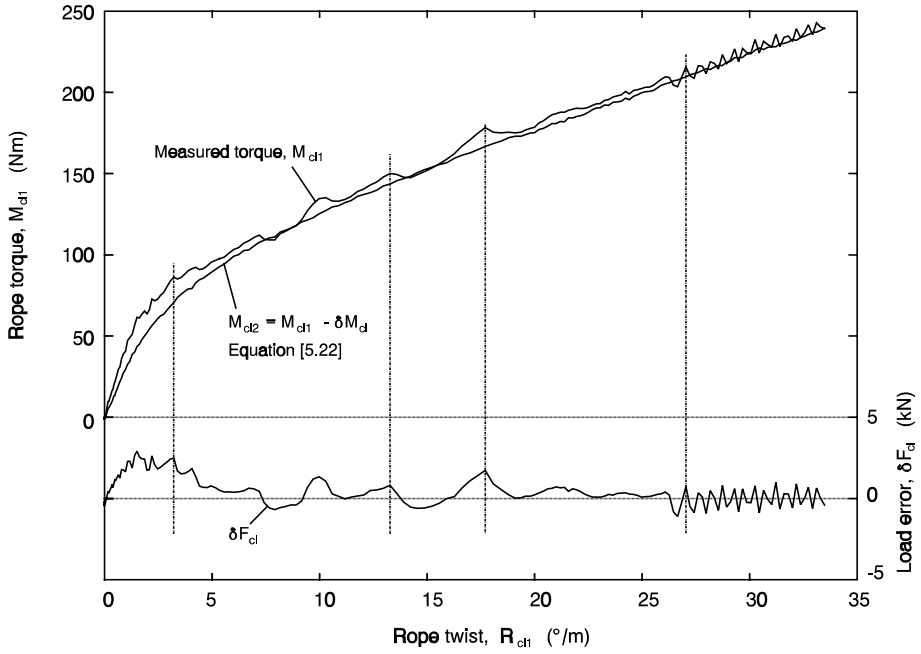

Figure 5.20 - Example of the variation in rope torque while twisting at constant load. The load error is also indicated. The measured torque is corrected using the load error and the proportionality between load and torque at each twist value, R_{cl}.

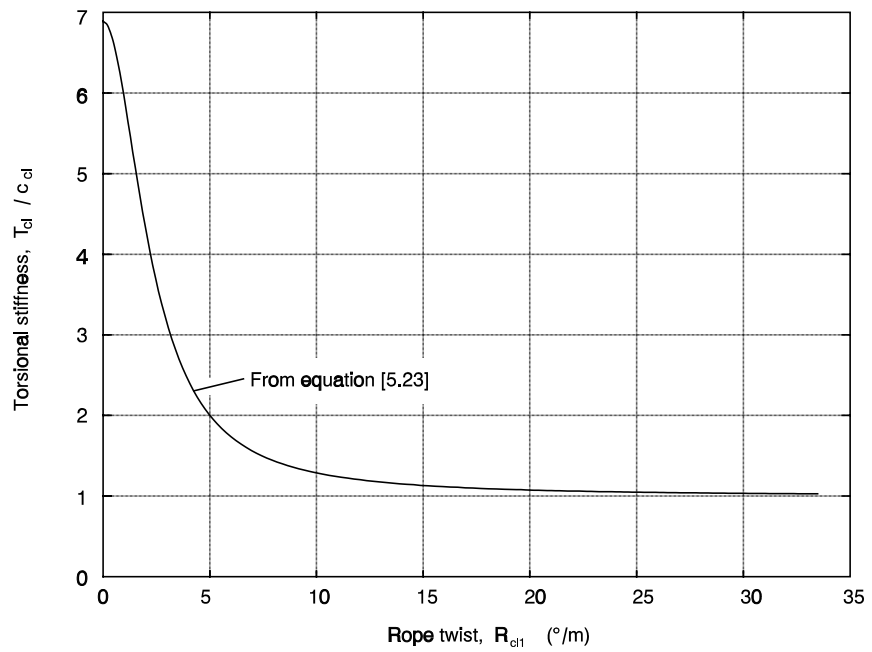

Figure 5.21 - Example of the variation in rope torsional stiffness for a change in twist, from a stationary position, at constant rope load. Determined from the derivative of the data (M_{cl2}) in figure 5.20.

For figures 5.20 and 5.21 :

$$M_{cl1} = M_{cl} - M_{cl0} \qquad [5.19]$$

$$M_{cl2} = M_{cl1} - \delta M_{cl} \qquad [5.20]$$

$$R_{cl1} = R_{cl} - R_{cl0} \qquad [5.21]$$

where : M_{cl} = torque measured during the constant load test
M_{cl0} = initial value of torque for the constant load test
R_{cl} = applied twist for the constant load test
R_{cl0} = initial value of applied twist for the constant load test

The corrected torque curve can be accurately described by an equation of the form :

$$M_{cl2} = a_{cl}.\arctan(b_{cl}.R_{cl1}) + c_{cl}.R_{cl1} \qquad [5.22]$$

where : a_{cl} , b_{cl} , c_{cl} are constants solved for numerically using the modified test data M_{cl2} and R_{cl1}.

The torsional stiffness can be obtained by differentiating torque with respect to twist :

$$T_{cl} = \frac{dM_{cl2}}{dR_{cl1}} = \frac{a_{cl}.b_{cl}}{1 + (b_{cl}.R_{cl1})^2} + c_{cl} \qquad [5.23]$$

From equation [5.23] it is evident that the torsional stiffness tends to a constant value, c_{cl} , after some angle of twist. Figure 5.21 shows the ratio between the torsional stiffness and the constant torsional stiffness, c_{cl} . It is common for there to be an order of magnitude difference between the initial stiffness and the value of c_{cl} . As was discussed in section 2.4, this marked variation in stiffness is attributable to a transition from no-slip to full-slip between the rope wires as twisting progresses.

The stiffness characteristic is dependant on the initial value of twist, R_{cl0}, and the constant load at which twisting occurs (F_{cl}). Different results are obtained for twisting up and untwisting from the same starting point. Figure 5.22 illustrates examples of results for twisting up and untwisting, at two different constant loads, from the same twist starting value. It follows that the constants a_{cl}, b_{cl} and c_{cl} are dependant on the constant load (F_{cl}) and initial value of twist, R_{cl0} (refer to figure 4.15).

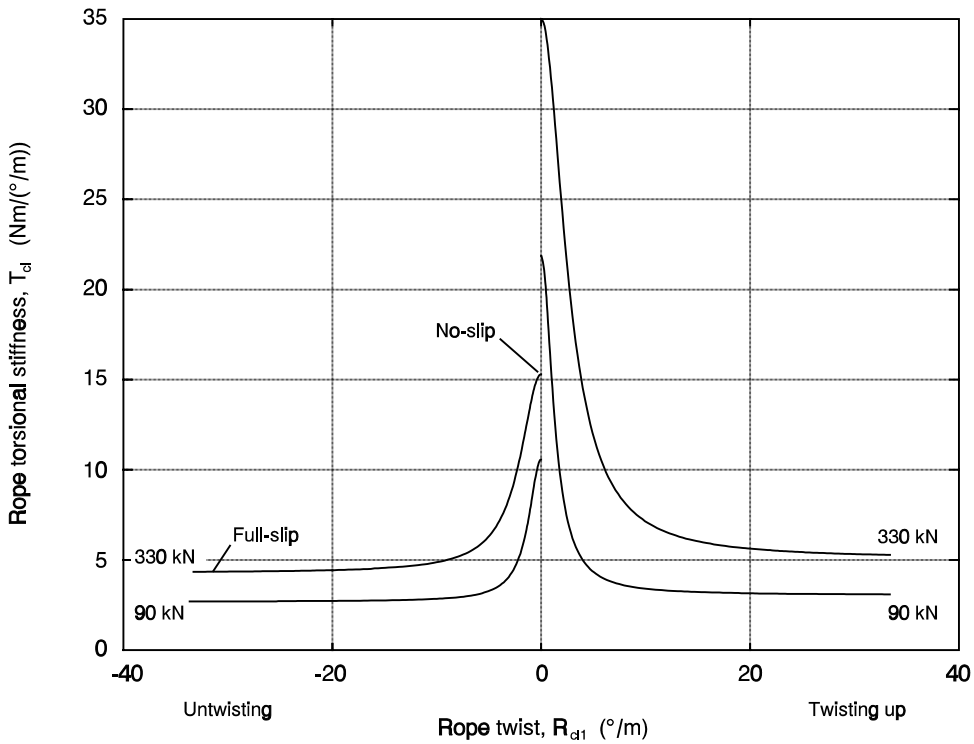

Figure 5.22 - Examples of variations in rope torsional stiffness for different loads and directions of twisting. The twisting commenced from R_{cl1} = 0.

Values of a_{cl}, b_{cl} and c_{cl} can be calculated for a specific rope by conducting a series of constant load tests as described in section 4.2.6. Six matrices will result containing the values for a_{cl}, b_{cl} and c_{cl} for different loads and starting twists for twisting up and untwisting. It is possible to combine the values of a_{cl}, b_{cl} and c_{cl} for twisting up and untwisting. This is achieved by calculating the torsional response for each and then solving for the combined values of a_{cl}, b_{cl} and c_{cl} using the average of the two torsional responses. It is expected that this would return similar stiffness values to those which would be measured if the twist was applied to the centre of the rope specimen as was the case in the investigation of Raoof and Hobbs (1988a), figure 2.10.

Using equation [5.22] :

$$\Delta M_{untwist} = f(a_{cl}, b_{cl}, c_{cl})_{untwist} \quad [5.24]$$

$$\Delta M_{twist} = f(a_{cl}, b_{cl}, c_{cl})_{twist} \quad [5.25]$$

$$(a_{cl} .\arctan(b_{cl} .R) + c_{cl} .R)_{average} = (\Delta M_{untwist} + \Delta M_{twist}) / 2 \quad [5.26]$$

Typical resulting values of a_{cl} , b_{cl} and c_{cl} are plotted against load and twist in figure 5.23. The data is for the 48 mm rope, T10. The general shapes of the curves, were found to be consistent for all the ropes tested (table 4.6) :

- a_{cl} varies linearly with load and quadratically with twist
- b_{cl} does not display a specific pattern of variation with load and twist although in general, the values tend to become more stable at higher loads and positive twists (shorter lay lengths)
- c_{cl} varies linearly with load and quadratically with twist

In order to calculate the rope rotation during conveyance loading, it is necessary to determine the values of a_{cl} , b_{cl} and c_{cl} along the length of the suspended rope. Double linear interpolation in the a_{cl} , b_{cl} and c_{cl} matrices is used rather than expressing the variations as functions of load and twist.

The limitation of a double linear interpolation approach is that values of a_{cl} , b_{cl} and c_{cl} can only be determined within the load and twist range for which matrix entries exist. This is also a safe guard as it prevents application of the equation outside of the test measurement range. The maximum torque limitation of the testing machine (3200 Nm) only allows constant load tests to be conducted up to certain loads and twists. For the interpolation, data may however be required outside of these ranges. It was found acceptable to extrapolate the values of a_{cl} and c_{cl} for larger twists and loads using quadratic and linear equations respectively.

Determination of extended values of b_{cl} is more complex because there is a less clear pattern in the variation of b_{cl} with load and twist. It was however noted that the maximum torsional stiffness for each load - twist coordinate increased approximately linearly with twist and load. The maximum (initial, no-slip) torsional

stiffness is defined by :

$$T_{max(i,j)} = a_{cl(i,j)} . b_{cl(i,j)} + c_{cl(i,j)} \qquad [5.27]$$

Knowing this relationship, and the extrapolated values of a_{cl} and c_{cl}, the most likely corresponding value of b_{cl} can be determined :

$$b_{cl(i,j)} = \frac{T_{max(i,j)} - c_{cl(i,j)}}{a_{cl(i,j)}} \qquad [5.27a]$$

Where $T_{max(i,j)}$ is determined from $T_{max(1..i-1,j)}$ or from $T_{max(i,1..j-1)}$ with i and j denoting the row and column numbers of the matrix respectively.

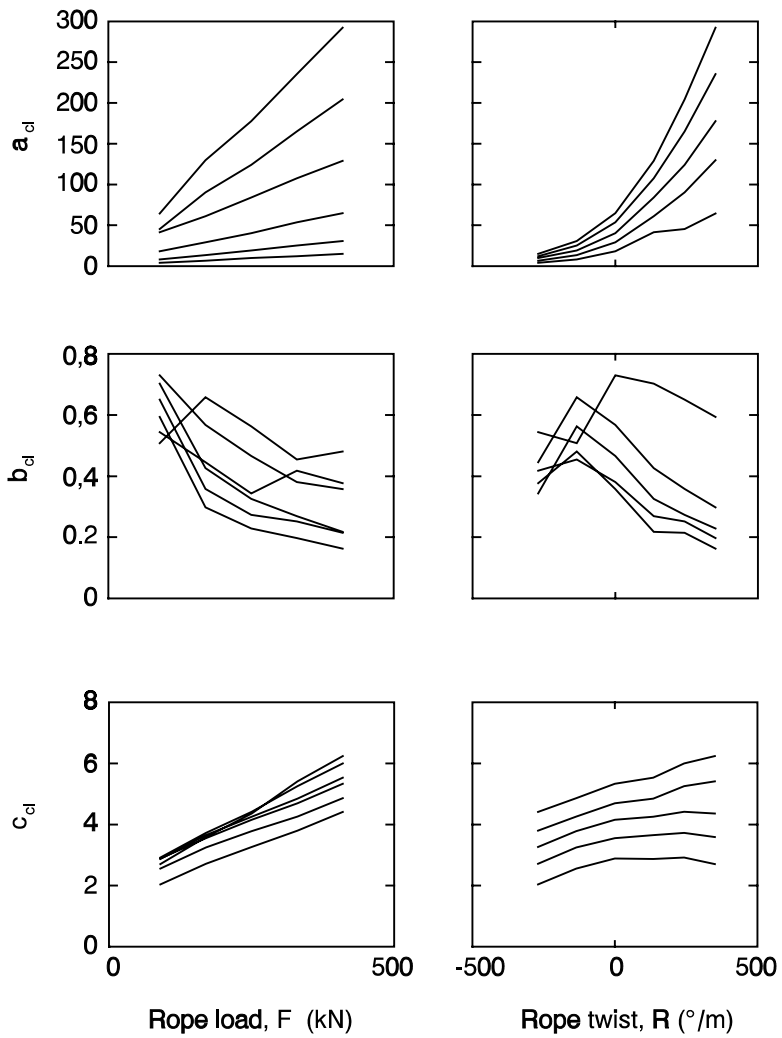

Figure 5.23 - Examples of variations in the constants a_{cl}, b_{cl} and c_{cl} with rope load and state of twisting, 48 mm rope, T10. Where axes values are not given, they are the same as those for the axes to the left or below.

5.6 Response of a rope to changes in conveyance load

When a conveyance is loaded there is an equal increase in load at every point along the suspended rope length (ignoring dynamic effects). If the general relationship between load, torque and twist is considered then it is apparent that the increase in load must be accompanied by an increase in torque, figure 5.24. If the increase in load is not accompanied by any changes in twist, then the torque in the suspended rope ($M_{f,Re}$) will not be constant as it should be. The rope adjusts for the torque imbalance by twisting and the value of the equilibrium torque for the loaded conveyance (M_f) will be such that the rotation boundary conditions at the conveyance and sheave remain constant during loading. This is assuming that friction at the sheave is sufficient to prevent the rope from rotating there.

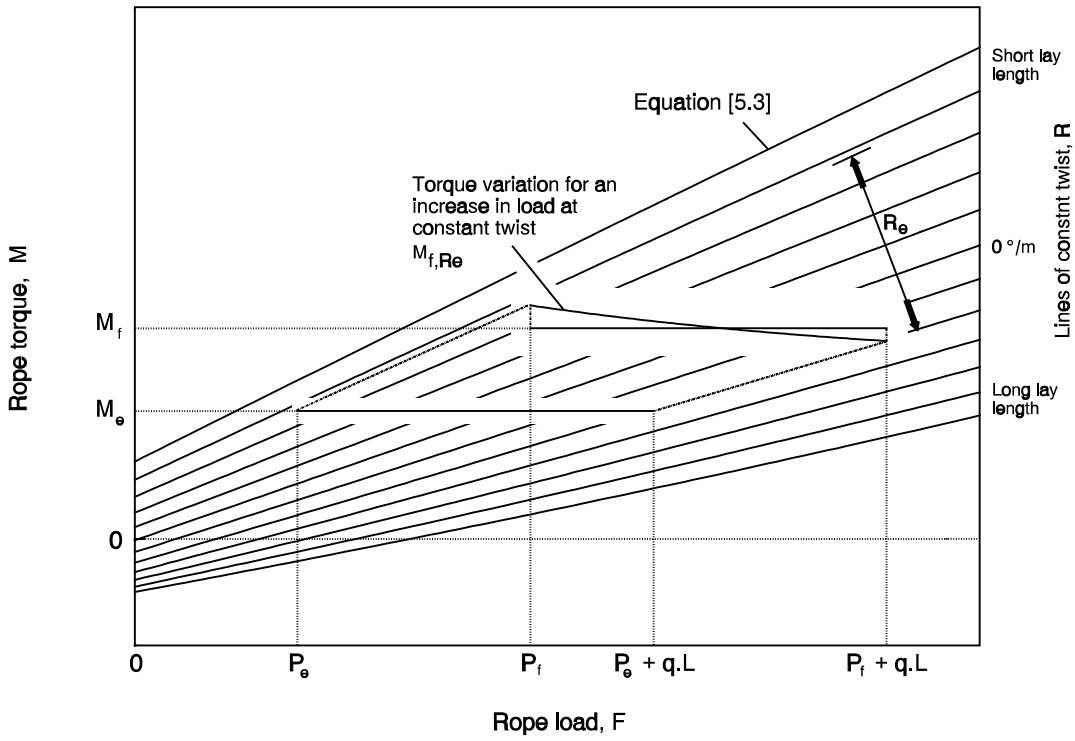

Figure 5.24 - Changes in rope torque as a result of conveyance loading.

P_e	=	empty conveyance rope end load (kN)
P_f	=	loaded conveyance rope end load (kN)
M_e	=	equilibrium rope torque for the empty conveyance (Nm)
M_f	=	equilibrium rope torque for the loaded conveyance (Nm)
L	=	suspended rope length (m)
q	=	rope weight per unit length (kN/m)
R_e	=	twist distribution for the empty conveyance (°/m)

From a torsional behaviour point of view, the loading process can be divided into two parts :

1. An increase in load at constant twist, R_e .
2. A change in twist (ΔR) at constant load to establish a torque equilibrium for the loaded conveyance, M_f .

5.7 Calculation of rope rotation during conveyance loading

During the loading of a conveyance the rope will achieve the change in twist, required for a new torque equilibrium, by rotating about it's longitudinal axis. The change in twist will be dependant on the torsional stiffness of the rope and the required change in torque. Since the twisting takes place from a stationary position, the torsional stiffness characteristics would be similar to that shown in figures 5.21 and 5.22. From the values of a_{cl} , b_{cl} , c_{cl} , the load variation due to rope weight (P_f + $q.z$) and the empty twist distribution (R_e), it is possible to determine the relationship between twist and torque at each position along the rope length. An example is shown in figure 5.25 and the corresponding torsional stiffness in figure 5.26. It is important to note that the surfaces shown in the two figures are only valid for specific rope load and twist distributions. If either of these are changed then new values of a_{cl} , b_{cl} and c_{cl} need to be calculated along the length of the rope.

Assuming a value of equilibrium torque, M_f, the change in torque, ΔM, is calculated from the data in figure 5.24 ($\Delta M = M_f - M_{f,Re}$). The change in twist, required to achieve the change in torque, is then determined numerically from the data of figure 5.25. Note how the line defining the torque change (ΔM) is projected onto the z - R plane to determine the change in twist. In the numerical scheme, ΔR is determined at finite points along the length of the rope using the equation :

$$\Delta M(z_i) = a_{cl}(z_i).\arctan[\, b_{cl}(z_i).\Delta R(z_i)\,] + c_{cl}(z_i).\Delta R(z_i) \qquad [5.28]$$

Integration of the change in twist, will give the change in rotation. The constant of integration will be equal to the empty (conveyance) rotation at $z = 0$. The value of M_f has to be determined such that the rotation value at $z = L$ equals the empty rotation value at that point ($SWbc$) :

$\Phi_e(0) = \Phi_f(0)$ gives the constant of integration

$\Phi_e(L) = \Phi_f(L)$ gives the constant torque M_f

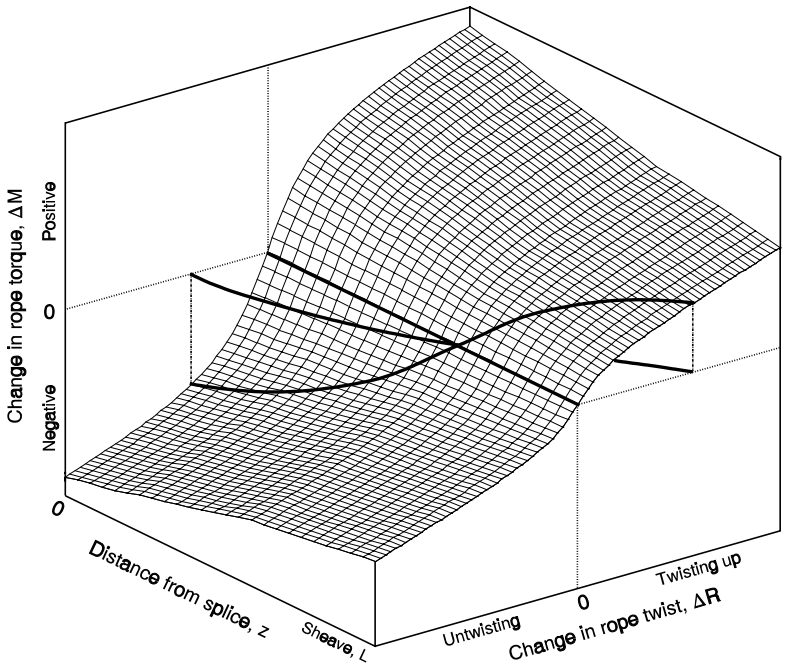

Figure 5.25 - Relationship between change in torque and change in twist along the suspended rope length. $\Delta M = M_f - M_{f,Re}$. Data represents the average of the twisting up and untwisting responses measured during the constant load tests.

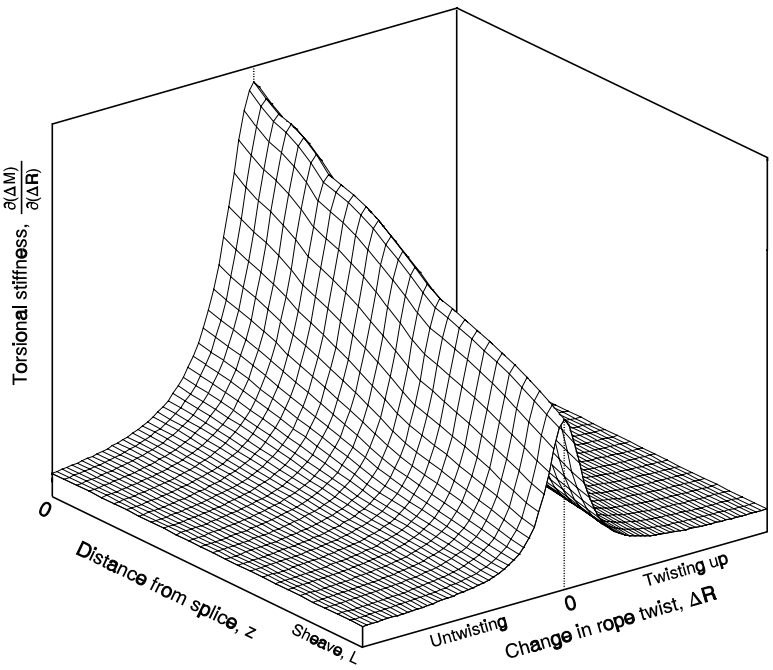

Figure 5.26 - Example of the torsional stiffness variation along the suspended rope length. Determined from the derivative of the data in figure 5.25.

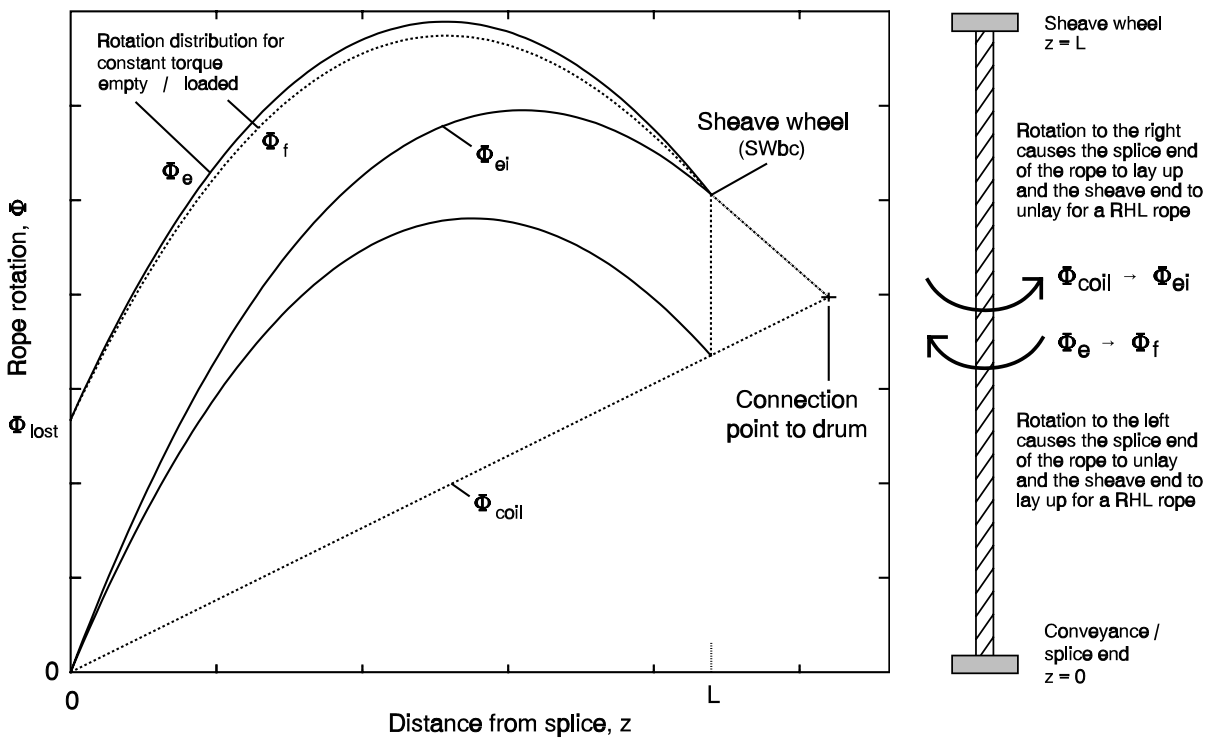

Figure 5.27 - Rope rotation distribution for a loaded conveyance in relation to the empty rotation distribution. The effect or rope rotation direction is also described for a RHL rope.

It was shown in figure 5.24 that the splice end of the rope has to untwist ($M_{f,Re}(0) > M_f(0)$) and the sheave end has to twist up ($M_{f,Re}(L) < M_f(L)$) in order to establish a torque equilibrium for the loaded conveyance. In terms of lay lengths, the splice end lay length increases during conveyance loading and the sheave end lay length decreases. In this process, the rope rotates in the opposite direction to which it rotated for the empty conveyance equilibrium condition (i.e. $\Phi_f < \Phi_e$). The empty and loaded rotation distributions are shown in figure 5.27. The calculated difference in rotation between the empty and loaded state is readily compared to the in-service rotation observations. Viewing a RHL rope in-service, the initial rotation from the manufactured state to that of installation equilibrium will be to the right ($\Phi_{coil} \rightarrow \Phi_{ei}$). Subsequent rotation during conveyance loading is to the left ($\Phi_e \rightarrow \Phi_f$).

6 MEASURED AND CALCULATED RESULTS

Chapter summary : In this chapter, the lay length and rotation values calculated using the modelling approach presented in chapter five are compared to the mine shaft measurements. The detailed results of the rope operating at the greatest suspended length, 2403 m, are presented followed by summaries of the results for the other 21 ropes. Distributions of the errors determined by subtracting the measured values from those calculated are also shown. It was found that for the 195 lay length observations, 86,1 percent of the errors lie in a range of plus and minus two percent of the nominal lay lengths. In the case of the rotation errors, 80,5 percent of the 113 measurements are in the range, plus and minus one turn. The maximum lay length error was 5,41 percent of the particular nominal lay length and the maximum rotation error, –3,17 turns. The accuracy of the lay lengths measured during the torsion tests are also examined and an empirical equation for calculating the effect of torsion test end rotation on lay length is presented. Factors which may have an influence on the calculated results are subsequently discussed and additional results regarding rope torsional behaviour in general are included.

6.1 Presentation of results

It is necessary to show that the analysis approach presented in chapter five predicts the measured in-service lay length changes and rope rotations during conveyance loading with reasonable accuracy. The results for the rope with the longest suspended length, S13 (46 mm at 2403 m), are presented in detail. For the remainder of the 22 ropes listed in table 4.1, only graphical comparisons between the measured and calculated rotation and lay length values and the associated twist and rotation distributions are shown. Further details relating to the remaining ropes are contained in appendix C. All in-service ropes are numbered "S#" and torsion test ropes, "T#". Table 4.1 contains information on the in-service ropes and tables 4.3 and 4.4 list details of the torsion test ropes.

6.2 Detailed results for shaft E, 46 mm rope at 2403 m

The information in this section serves two purposes. The first is the presentation of the lay length and rotation results of the 46 mm rope, S13, operating at 2403 m suspended length on a surface shaft, double drum man winder. Secondly, in presenting the results, the analysis method of chapter five is summarised.

From the data of the constant twist test conducted on the 46 mm rope, T9, the matrix N for equation [5.3] was determined. Since data was available for loading and unloading values of torque the least squares algorithm for calculating the matrix entries could take either into account. Figures 6.1 and 6.2 show the calculated and measured constant twist test results for rope T9. In figure 6.1 both the loading and unloading values of torque were considered in the calculation of the matrix entries, N_{avg}. In figure 6.2, only the loading values of torque were used for the fit, N_{load}. For all the calculations presented in this chapter, the matrix N_{load} (unique for each torsion test rope) was used. It was found that the fits to the loading values of torque proved to be more stable in extrapolation of the torsional properties to loads outside those of the test range.

From the constant twist test data of rope T9, 46 mm, 6x31(13/12/6 + 3Δ)/F, 1800 MPa :

$$N_{avg} = \begin{bmatrix} -1.2530e-009 & 1.4125e-006 & 1.2260e-003 \\ -3.4234e-006 & 6.8187e-003 & 1.5320e+000 \\ -4.2778e-004 & 5.2493e+000 & -7.1036e+000 \end{bmatrix} \qquad [6.1]$$

$$N_{load} = \begin{bmatrix} 1.5829e-009 & 4.2655e-007 & 1.1605e-003 \\ -1.0236e-006 & 5.8743e-003 & 1.5374e+000 \\ 8.4110e-005 & 5.0628e+000 & -1.0342e+001 \end{bmatrix} \qquad [6.2]$$

The relationship between load, torque and twist defined by the matrix N_{avg} or N_{load} is not only applicable to the calculations for rope S13 but to all 46 mm diameter ropes of the same construction. The matrix N_{load}, equation [6.2], was also used in the calculations for the 46 mm ropes S9, S10, S11 and S12 (table 4.1).

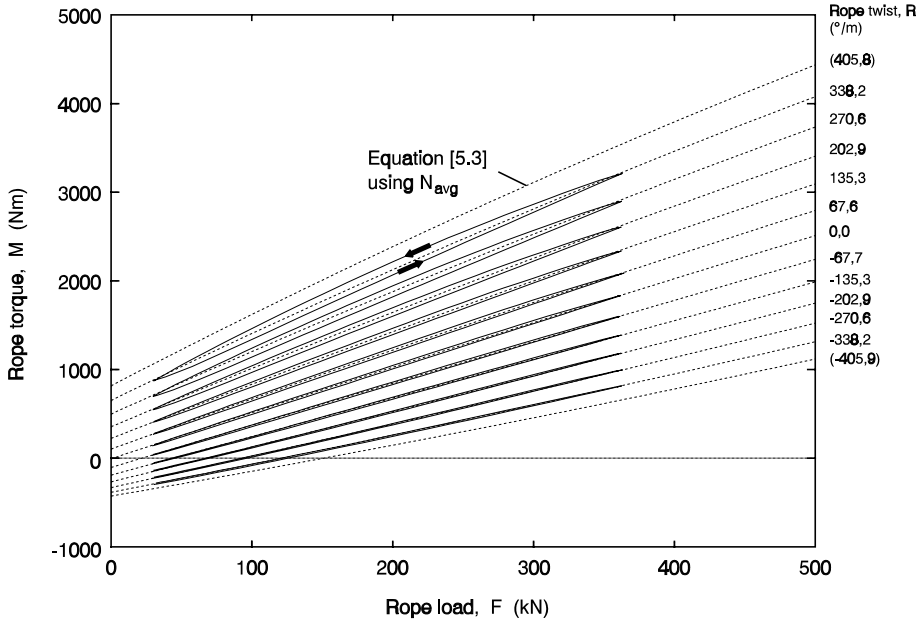

Figure 6.1 - Measured and calculated rope torque versus load for rope T9, 46 mm, 6x31(13/12/6 + 3Δ)/F, 1800 MPa. Loading and unloading values of torque are taken into account. The bracketed values of twist represent extrapolated data.

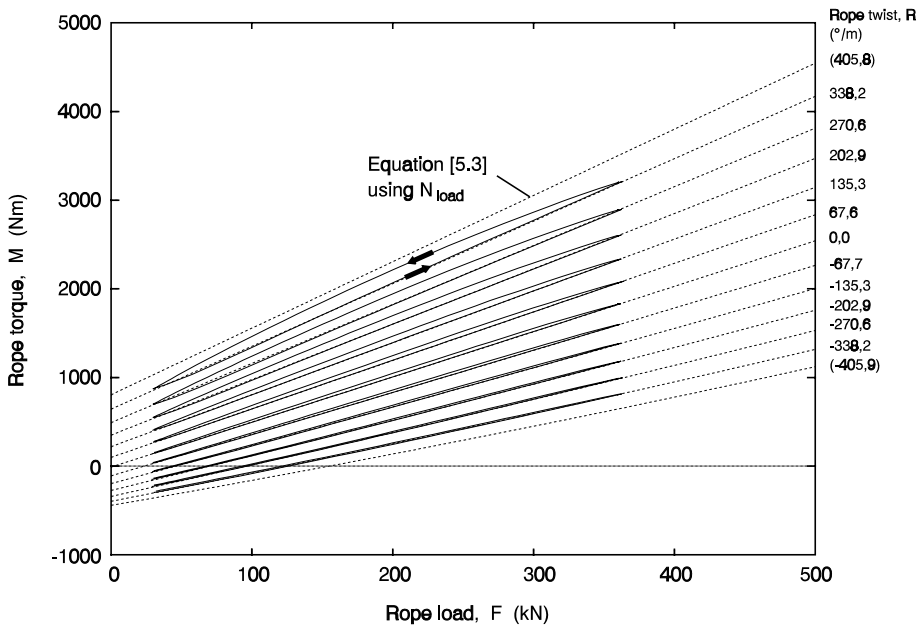

Figure 6.2 - Measured and calculated rope torque versus load for rope T9, 46 mm, 6x31(13/12/6 + 3Δ)/F, 1800 MPa. Only loading values of torque are taken into account. The bracketed values of twist represent extrapolated data.

Figure 6.3 shows the analysis results for rope S13, displayed in the load – torque plane. At installation the equilibrium state is associated with the constant torque, M_{ei}, which is for the empty conveyance. The torque M_{ei} was determined using the numerical scheme listed in table 5.2. The twist distribution in the rope is represented by the intersection of the constant torque line (M_{ei}) with the lines of constant twist. As the service period progressed rotation was lost from the rope (Φ_{lost}) and the equilibrium torque reduced to M_e which corresponds to the state in which the shaft measurements were conducted (76,5 months of operation). As the conveyance was loaded, the torque in the rope, for no change in twist from the empty state (R_e) increased to the values defined by the dashed line $M_{f,Re}$.

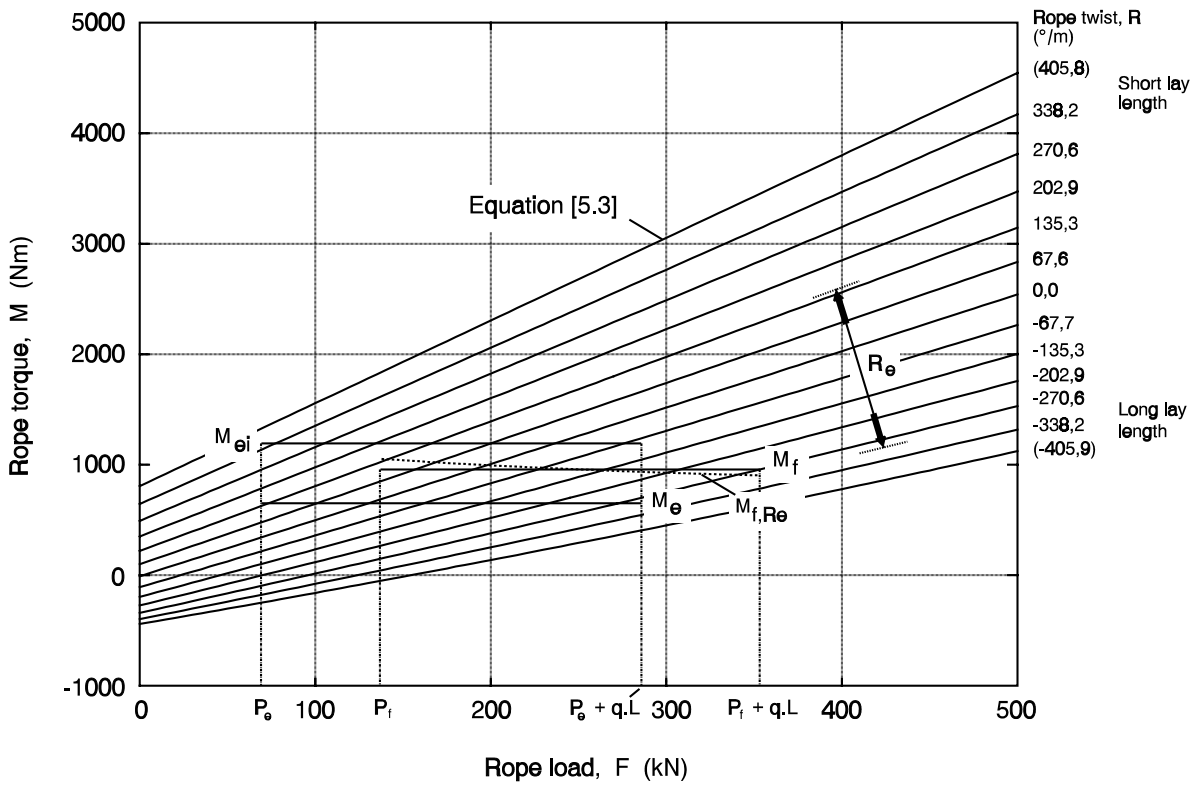

Figure 6.3 - Equilibrium rope torques for rope S13 in relation to torsion test data. Torsion test data from rope T9, 46 mm, 6x31(13/12/6 + 3Δ)/F, 1800 MPa.

The equilibrium torque for the loaded conveyance, M_f, was determine numerically such that no change in rotation occurred at the splice and sheave during loading. The change in torque at each position along the rope, required to reach the loaded equilibrium state, was calculated using equation [6.3].

$$\Delta M = M_f - M_{f,Re} \qquad [6.3]$$

With the load distribution (P_f + $q.z$) and the empty twist distribution, R_e, it was possible to calculate the torsional response to twisting along the rope using the matrices a_{cl}, b_{cl} and c_{cl} i.e. double linear interpolation within the matrices defined by equations [6.4] to [6.8]. The values of a_{cl}, b_{cl} and c_{cl} were determined from the constant load tests conducted on rope T9 (section 4.2.6). Figures 6.4 and 6.5 show the change in torque and associated torsional stiffness for rope S13 at the time of the measurements. The variation in the torsional stiffness along the rope is considerable. At the splice end (z = 0) the no-slip torsional stiffness is almost seven times greater than the full-slip stiffness. The values shown in figures 6.4 and 6.5 are the averages of the twisting up and untwisting responses measured during the constant load tests.

From the constant load test data of rope T9, 46 mm, 6x31(13/12/6 + 3Δ)/F, 1800 MPa :

$$a_{cl} = \begin{bmatrix} 87.0047 & 164.6146 & 238.5415 & 319.9984 & 395.7668 \\ 48.6630 & 92.4894 & 135.6286 & 181.8018 & 225.2846 \\ 20.9082 & 40.9722 & 61.5393 & 81.2507 & 101.5663 \\ 7.9326 & 14.4817 & 22.0945 & 30.4368 & 37.5177 \\ 4.1465 & 7.1265 & 9.5328 & 13.2380 & 15.9312 \end{bmatrix} \quad \text{(Nm)} \qquad [6.4]$$

$$b_{cl} = \begin{bmatrix} 0.2948 & 0.2040 & 0.1635 & 0.1422 & 0.1318 \\ 0.4119 & 0.2801 & 0.2224 & 0.1995 & 0.1834 \\ 0.5342 & 0.3830 & 0.3271 & 0.2751 & 0.2642 \\ 0.2463 & 0.3968 & 0.3508 & 0.3543 & 0.3647 \\ 0.1342 & 0.1979 & 0.2947 & 0.2971 & 0.3176 \end{bmatrix} \quad \text{(1/(°/m))} \qquad [6.5]$$

$$c_{cl} = \begin{bmatrix} 2.3836 & 3.4414 & 4.8430 & 6.0734 & 7.3031 \\ 2.3350 & 3.4417 & 4.4508 & 5.4243 & 6.4822 \\ 2.3257 & 3.2771 & 4.0933 & 4.8563 & 5.7401 \\ 1.8762 & 2.8066 & 3.4577 & 4.0976 & 4.8884 \\ 1.6260 & 2.2181 & 2.9611 & 3.5108 & 4.1784 \end{bmatrix} \quad \text{(Nm/(°/m))} \qquad [6.6]$$

Constant loads corresponding to the columns of a_{cl}, b_{cl} and c_{cl} :

$$F_{cl} = [\ 60 \quad 170 \quad 280 \quad 390 \quad (500)\ ] \qquad \text{(kN)} \qquad [6.7]$$

For equations [6.7] and [6.8], the values for which a_{cl}, b_{cl} and c_{cl} were extrapolated are bracketed.

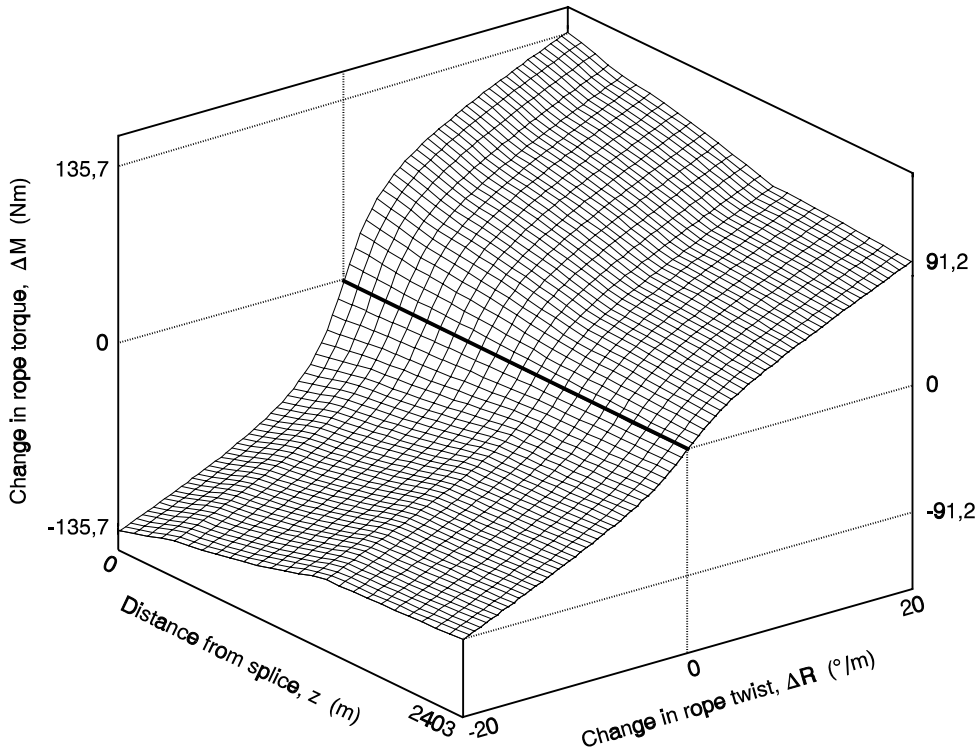

Figure 6.4 - Torsional response due to changes in twist along the suspended length of rope S13. Note that the depicted response is only valid for the specific values of load (P_f + $q.z$) and twist R_e corresponding to the equilibrium torque, M_e of figure 6.3.

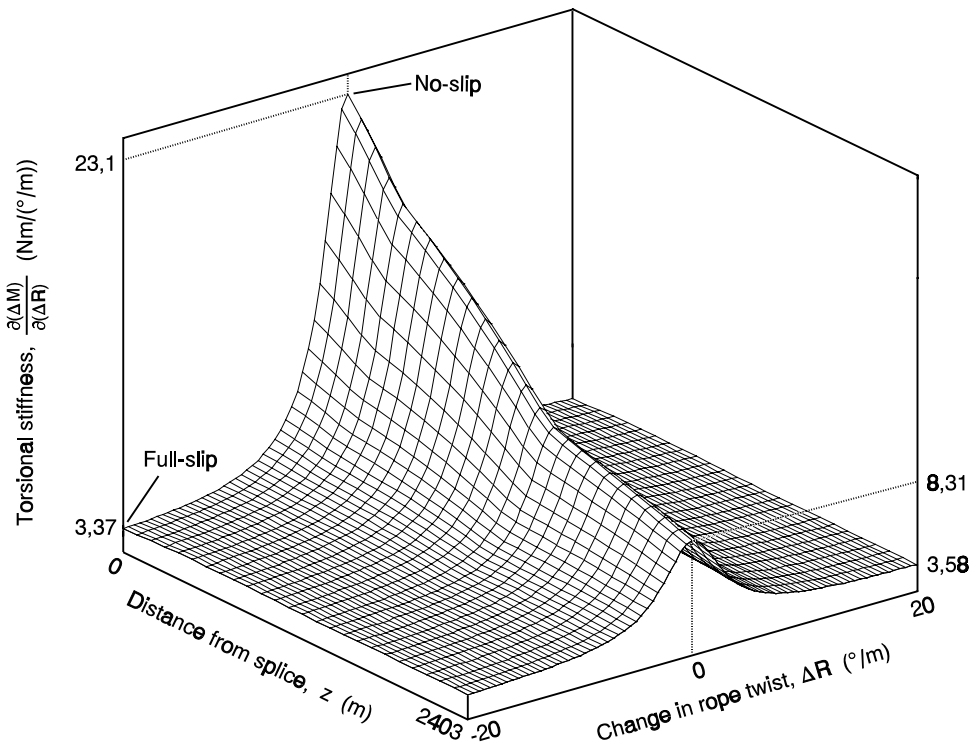

Figure 6.5 - Variation in torsional stiffness for changes in twist from a stationary position, rope S13. Calculated by differentiation of the data in figure 6.4.

Starting twist values corresponding to the rows of a_{cl}, b_{cl} and c_{cl} :

$$R_{cl0} = \begin{bmatrix} (474) \\ 271 \\ 68 \\ -135 \\ -338 \end{bmatrix} \quad (°/m) \qquad [6.8]$$

Knowing the response of the rope to changes in twist (figure 6.4) and the required change in torque, ΔM, the twist during loading, ΔR, was calculated (equation [5.28]). Figure 6.6a shows the change in twist for rope S13 for three different payloads. The payloads are equal to the actual payload (67,7 kN) and fifteen percent increase and decrease from this value. Integration of the twist during loading results in the rope rotation which is compared to the measured rotation values in figure 6.6b. There is considerable scatter in the measured rotation results in spite of the fact that a locomotive of constant weight was used for each loading cycle. It is believed that the dynamic variability in the loading process (figure 4.7) combined with the hysteretic nature of the torsional response caused the differences in the observed rotation.

Figure 6.6c shows the rotation distributions for the rope as it was received by the mine ($\Phi_{coil} = R_{coil}.z$) and after installation for an empty conveyance (Φ_{ei}). The empty (Φ_e) and loaded (Φ_f) rotation distributions at the time of the measurements are also shown. The difference between Φ_e and Φ_f corresponds to the solid line in figure 6.6b. For each rotation distribution, the associated twists and lay lengths were calculated (equation 5.2). Figure 6.6d compares the calculated lay lengths to the lay lengths which were measured after installation and at the time of the measurements for this investigation.

The actual amount of rotation lost from the rope during maintenance operations is not known since rope maintenance staff do not always take note of this. In figure 6.6d, the change in lay length from installation (LL_{ei}) to the time of measurements (LL_e) is a direct result of deliberate unlaying of the rope. It was mentioned earlier that unlaying of the rope can be simulated by increasing the rotation boundary condition at the splice. It was therefore shown that, at some point of unlaying, the calculated lay length values correspond to the measured

values. Through this process, the variable Φ_{lost} was determined. Table 6.1 lists the data relevant to the rotation and lay length analysis for rope S13. Similar tables for the other 21 ropes are contained in appendix C.

Table 6.1 - Analysis and torsion test data for rope S13 relating to figures 6.3 to 6.7.

Shaft analysis data, rope S13, shaft E		**Torsion test data, rope T9**	
Rope coil number	016289	Torsion test rope coil number	137944/001
Date of rope installation	14/5/89	d_{nom} (mm)	46
Date of measurements	27/9/95	d_0 (mm)	47,0
q (kN/m)	0,0895	LL_0 (mm)	392,4
P_e (kN)	70,0	LL_{nom} (mm)	348
P_f (kN)	137,7	l_0 (mm)	2661
Payload, P_f - P_e (kN)	67,7	Lay type	RHL
Payload envelope (%)	15	K_{LL} (1/(°/m))	3,8011e-4
Lay type	RHL	A_{met} (mm²)	970,3
Construction	6x31(13/12/6 + 3Δ)/F	Construction	6x31(13/12/6 + 3Δ)/F
LL_{nom} (mm)	348	$S_{u,wire}$ (MPa)	1800
$S_{u,wire}$ (MPa)	2150		
z_{max} (m)	2824		
L (m)	2403		
Df	1		
R_{coil} (°/m)	90		
$SWbc$ (°/360 = turns)	802,4		
$R_{coil} . z_{max}$ (turns)	706,0		
z for R_{coil} (m) at installation equilibrium (% of L)	1323 55,04		
Φ_{lost} (turns)	1406,7		
$\Delta\Phi_{max}$ (turns)	13,03		
z for $\Delta\Phi_{max}$ (m) (% of L)	1273,6 53,0		
$LL_{ei}(0)$ (% change from nominal)	-21,55		
$LL_{ei}(L)$ (% change from nominal)	24,43		
$LL_e(0)$ (% change from nominal)	-3,74		
$LL_e(L)$ (% change from nominal)	66,38		
$LL_f(0)$ (% change from nominal)	-2,87		
$LL_f(L)$ (% change from nominal)	63,79		
Rotation error range (turns)	-2,76 → 1,62		
Lay length error range (% of nominal)	-3,32 → 3,28		
M_{ei} (Nm)	1191,5		
M_e (Nm)	650,5		
M_f (Nm)	955,7		

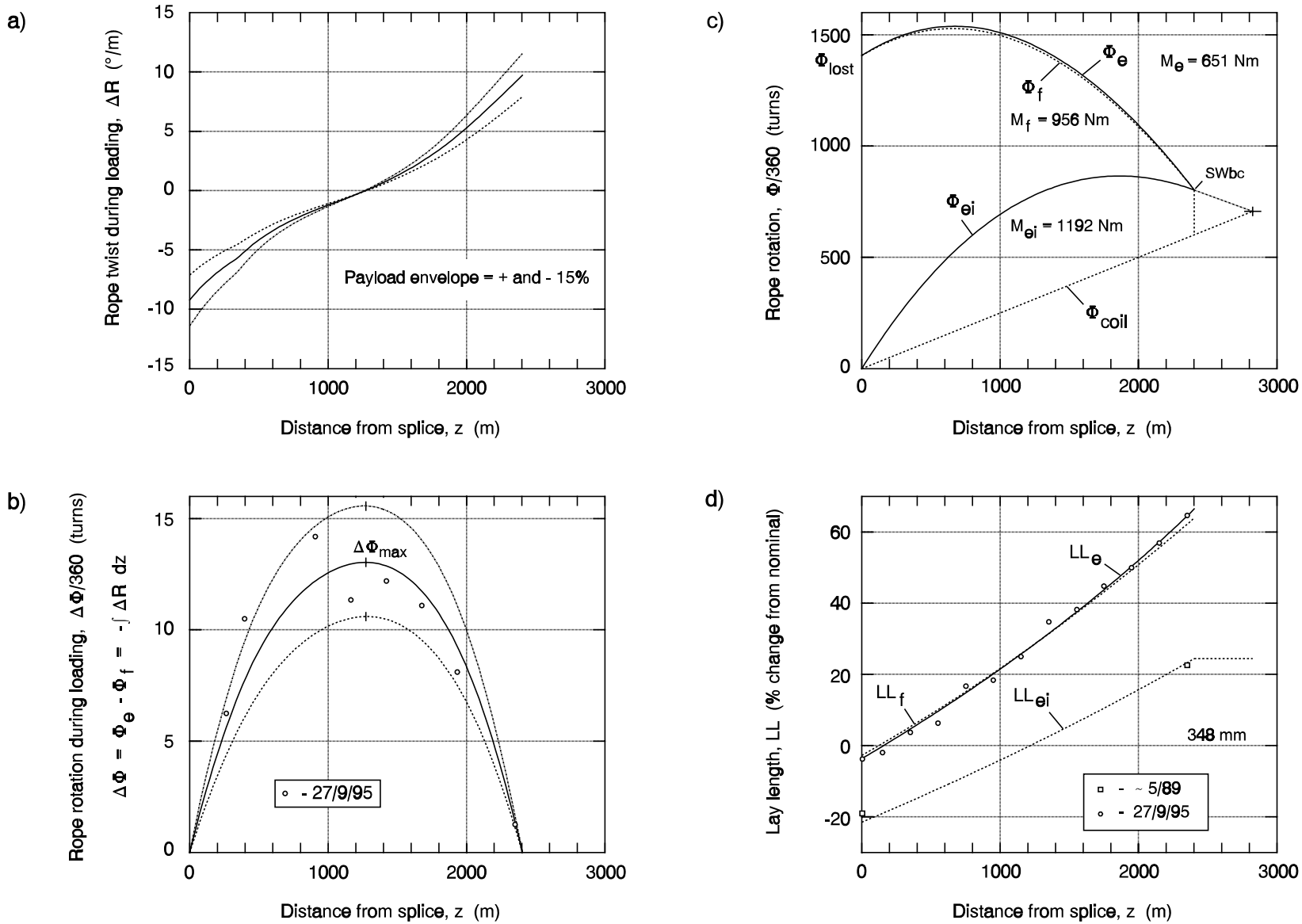

Figure 6.6 - Measurement and analysis results for rope S13, service period = 76,5 months. Additional information contained in table 6.1.

The date of rope installation and of the measurements conducted for this study are given in the left hand section of table 6.1. These are followed by the rope weight per unit length, q, and the empty and loaded conveyance weights, P_e and P_f. The pay load envelope refers to the variation in payload used to calculate the data in figures 6.6a and 6.6b. Rope construction details, the nominal lay length (LL_{nom}) and the wire tensile grade ($S_{u,wire}$) are also listed. As regards the shaft geometry, z_{max} is the total rope length installed on the winder and L is the maximum suspended length. The ratio between twist at the sheave and twist at the drum connection point for the installation equilibrium state is given by Df. The twist, R_{coil}, is associated with the manufactured lay length (LL_m) determined using equation [5.2] and the torsion test constants for rope T9 listed on the right of the table. The sheave wheel rotation boundary condition, $SWbc$, was calculated by the numerical procedure described in table 5.2 as was the position where the manufactured lay length occurred at installation, z for R_{coil}. The remainder of the items in the left hand section are complementary to the data shown in figure 6.6. Where applicable, the subscripts denote the state of loading and are associated with specific stages in the service period :

ei	=	empty conveyance at installation
e	=	empty conveyance at measurement date
f	=	loaded conveyance at measurement date

Figures 6.6b and 6.6d (and similar figures for the other 21 ropes) represent the most important results in this chapter. They show how the calculated rope torsional response compares to the values measured in service. For rope S13, the lay lengths for the loaded conveyance were also recorded and figure 6.7 indicates how these compare to the calculated lay length distribution, L_f. Lay lengths for the empty conveyance correspond to those in figure 6.6d (27/9/95). The measured lay length values of rope S13, for the loaded conveyance, show good correlation with the calculated data. The changes in lay length from the empty to loaded conveyance state are however of a similar magnitude to the scatter in the measured data. This was found to be the case for all the in-service ropes. The loaded conveyance lay lengths therefore provided no additional information and are not be presented for the remaining 21 ropes.

It is important to restate that the values depicted in figures 6.3 (constant torques), 6.4, 6.5, 6.6 and 6.7 are unique to rope S13 subject to the conditions defined by the values listed in table 6.1.

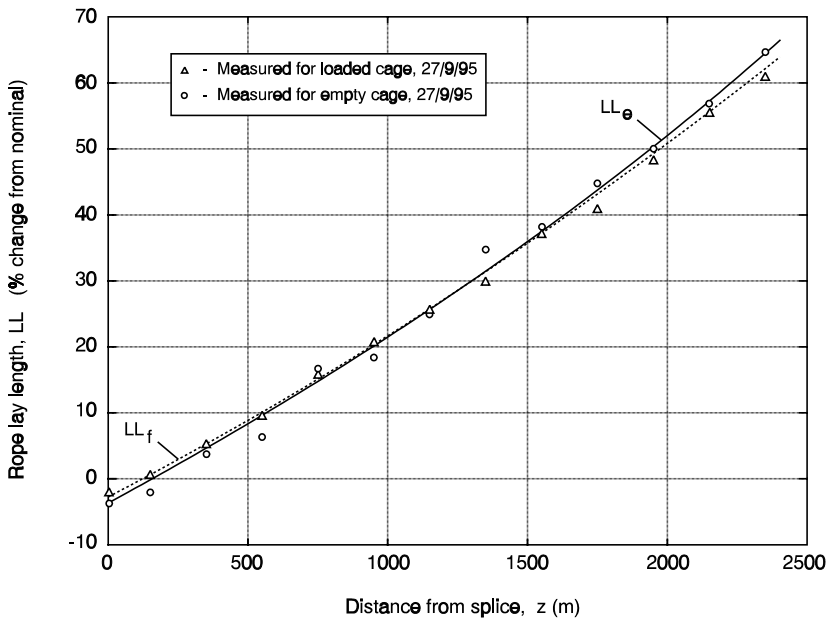

Figure 6.7 - Detail of calculated and measured lay lengths for rope S13. Empty and loaded conveyance.

For rope S13, figure 6.6c, it was calculated that 1407 turns were lost to effect the change from the installation lay lengths (LL_{ei}) to the lay lengths at the time of measurements (LL_e). This value may seem large but it is apparent that the splice end lay length at the measurement date ($LL_e(0)$ = -3,74 percent less than nominal) was still less than the lay length to which the splice end would unwind if it was unrestrained (figure 5.15). Examination of the statutory test records for rope S13 showed that the free lay length of the splice end was on average equal to the nominal lay length plus 8,48 percent. Only if 2147 turns had been released from the rope would the constrained splice end lay length equal this value. The rope would then seem to be torsionally "dead" when detached from the conveyance at the surface level. With the splice end lay length at 8,48 percent longer than nominal, the sheave end would be (substantially) increased to 101,6 percent. In contrast, if the maximum suspended length was only 1000 m (with all other parameters remaining constant) the splice end lay length at installation would be 11,1 percent shorter than nominal (as opposed to -21,55 percent). The release of 531 turns would increase the splice end to 8,48 percent. The corresponding sheave end lay length would be 40,3 percent increase which is well within the current range of sheave end lay lengths found on existing drum winders. It is therefore apparent that on shallower shafts, unlaying of the rope in service will eventually result in the

splice end appearing to be torsionally inactive without experiencing excessively long lay lengths at the sheave (drum) end. This is however not the case in deeper shafts.

The difference in tensile grade between rope T9 (1800 MPa) and rope S13 (2150 MPa) is noted. The torsional properties of rope T9 were used in the calculations for rope S13. This difference did not negatively affect the accuracy of the calculations. Yiassoumis (1992) reported that non-spin ropes of identical construction but different tensile grades have similar torsional properties. It appears as if differences in tensile grade are also not significant as regards the torsional behaviour of single layer triangular strand ropes.

6.3 Summary of the results for ropes S1 to S12 and S14 to S22

Figures 6.8 to 6.21 contain the most relevant data for the remainder of the ropes on which shaft measurements were conducted. The main details of each winding installation are given prior to each figure as are general comments relating to the results (where applicable).

The winders for shafts **A** and **B** are of the BMR type and therefore use both left and right hand lay ropes (table 4.1). The rotation of a LHL rope during installation and conveyance loading is in the opposite direction to that of a RHL rope. For the purposes of presentation, the rotation results for the four LHL ropes (S1, S4, S6 and S8) are displayed as if the ropes were of the RHL construction.

6.3.1 Shaft A, 41 mm ropes at 1071 m

Sub-vertical BMR rock winder

Ropes S1 (LHL), S2 (RHL), S3 (RHL) and S4 (LHL)

41 mm, 6x29(11/12/6 + 3Δ)/F, 1800 MPa

Maximum suspended length, L = 1071,3 m

Empty conveyance weight,	P_e = 48,9 kN per rope
Conveyance payload,	P_f - P_e = 61,5 kN per rope
Rope service periods :	27,8 months

For ropes S1, S2, S3 and S4 (figures 6.8d and 6.9d) the rope manufacturer was unable to supply the manufactured on-tension lay lengths (LL_m). It was therefore assumed that the ropes were manufactured at their nominal lay length plus 3,71 percent (average for the ropes considered in this project, figure 5.2). The differences between the calculated lay length at installation (LL_{ei}) and the values measured by the mine could be attributed to not using the true values of LL_m. It should also be noted that the shaft is a sub-vertical one in which the distance between the bank and headgear sheaves (107,3 m) is considerably greater than on a surface shaft. Normally the distance on surface shafts is between 40 m and 50 m. With rope maintenance and installation taking place from the sub-vertical shaft bank area, there is a greater possibility for rotation to be lost than on a surface shaft. The relatively short rope length (z_{max} = *1460 m*) would have increased the effect of lost rotation on lay length changes.

In the case of ropes S1 to S4, the lay length values were measured one and a half months prior to the rotation recordings. The torsional stiffness values used for calculating the rotation during loading were determined for a specific lay length distribution ($LL_e \propto R_e$). It is possible that in the period between the two sets of measurements the ropes were unlaid further, altering their torsional stiffness characteristics and increasing the rotations evident during conveyance loading. It is known that on the morning of the lay length measurements rotation was released from the ropes when sections were cut from the conveyance ends for statutory testing. The lost rotation may not have taken full effect by the time of the lay length measurements. It was calculated that if the measured lay lengths were increased by 6 percent (1,06.LL_e) then the measured and calculated rotation values would correlate more accurately, figures 6.8b and 6.9b.

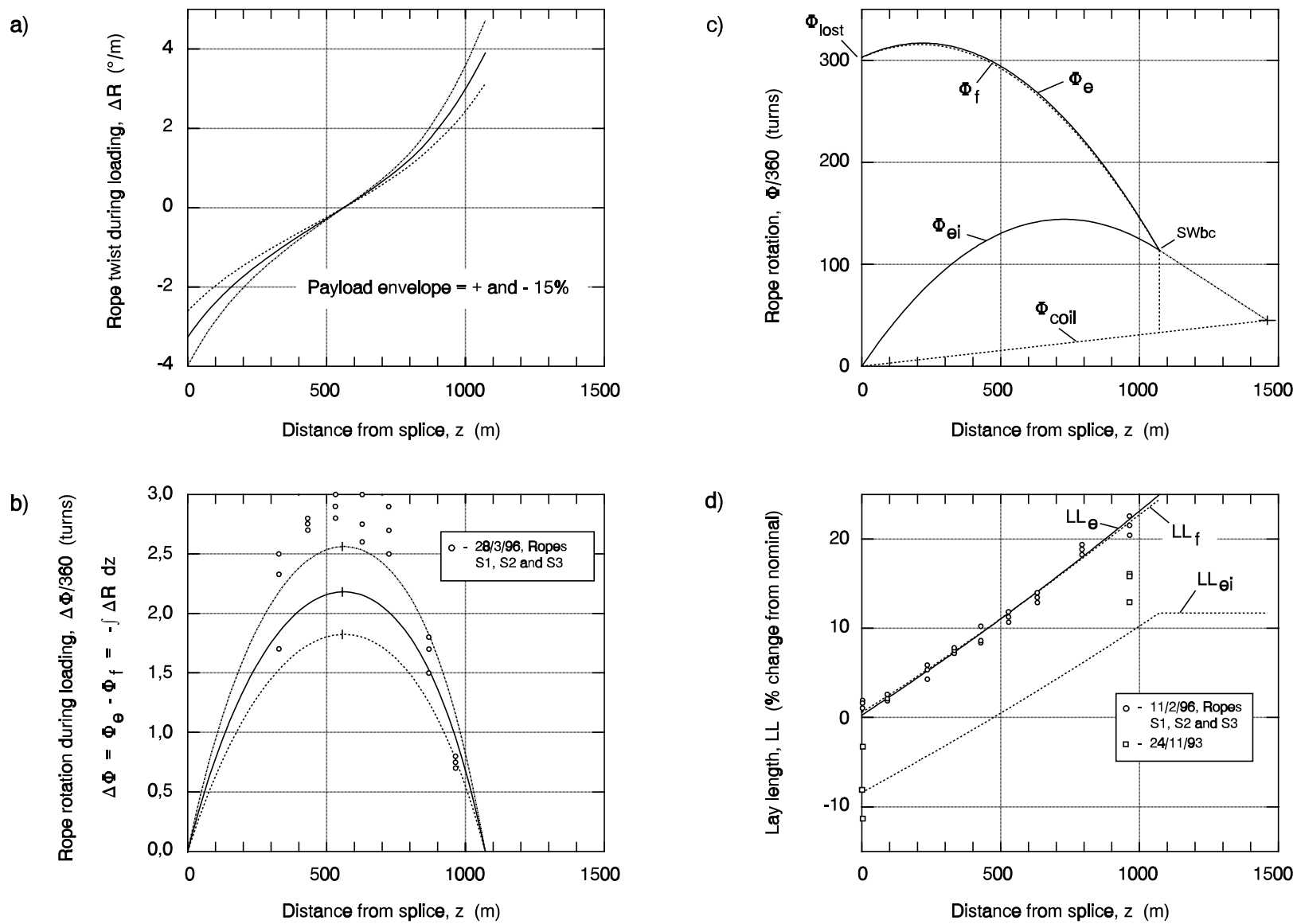

Figure 6.8 - Measurement and analysis results for ropes S1, S2 and S3. Additional information in table C.1, figure C.1 and section C.2.1

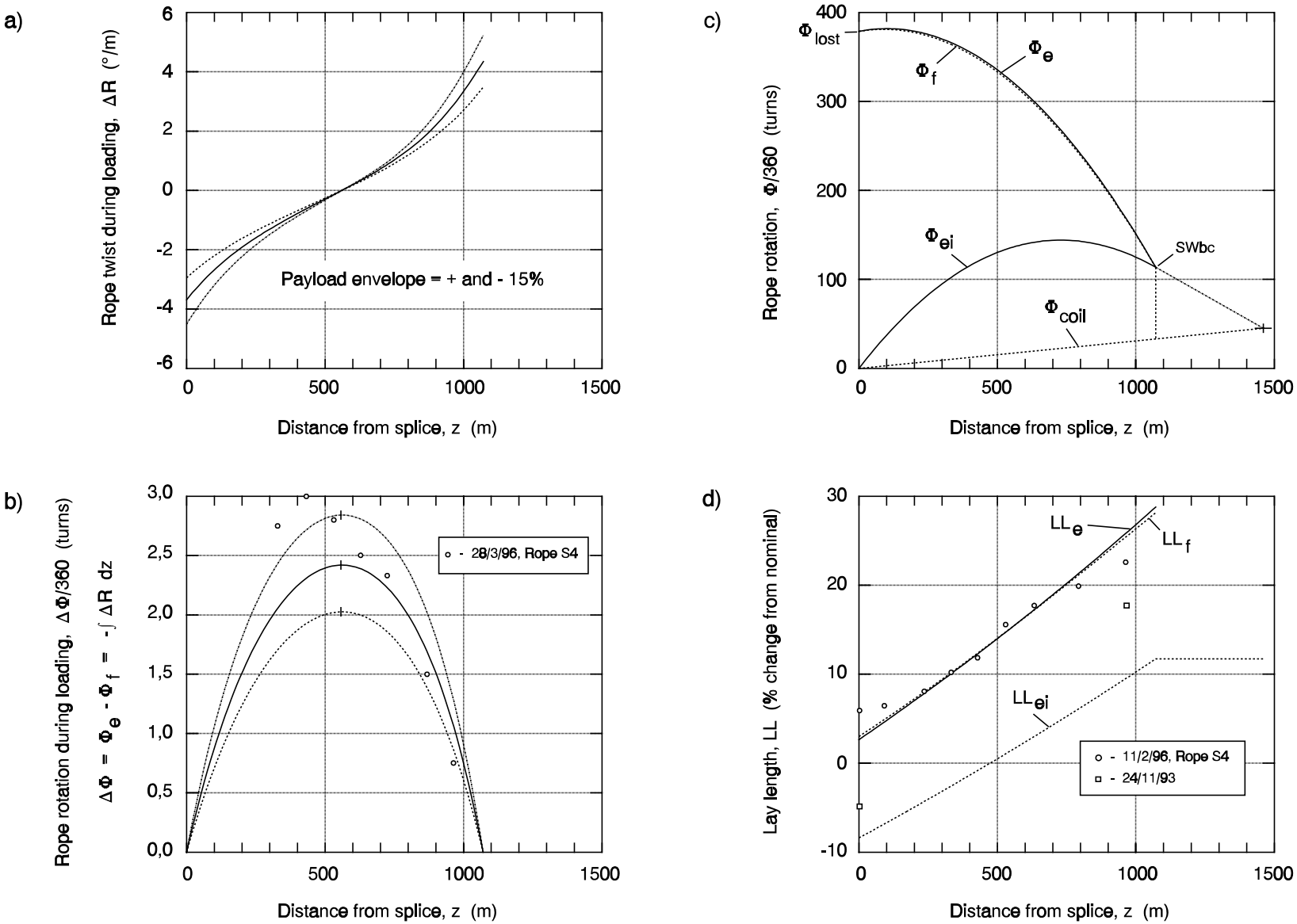

Figure 6.9 - Measurement and analysis results for rope S4. Additional information in table C.2, figure C.2 and section C.2.1

6.3.2 Shaft B, 41 mm ropes at 1529 m

Sub-vertical BMR rock winder

Ropes S5 (RHL), S6 (LHL), S7 (RHL) and S8 (LHL)

41 mm, 6x29(11/12/6 + 3Δ)/F, 1900 MPa

Maximum suspended length, L = 1528,6 m

Empty conveyance weight, P_e = 66,6 kN per rope

Conveyance payload, P_f - P_e = 63,8 kN per rope

Rope service periods : 8,1 months

It is known that rope S5, figure 6.10d, was deliberately unlaid by the shaft's rope maintenance personnel in order to lengthen the rope (BMR winder). Compensating head sheaves were used as opposed to a compensating sheave on the conveyance. The head sheave for rope S6 had reached the limit of its travel implying that rope S5 was too short. Time constraints did not allow for releasing rope S5 from the drum end (to lengthen it) so the unlaying option was chosen. It was not possible for the mine to indicate the amount of rotation released from rope S5. The deliberate unlaying explains the notable difference in the lay length results presented in figures 6.10d and 6.11d. The installation lay lengths for ropes S5 to S8 were measured within 24 hours after the ropes were put on and in this period it is unlikely that a state of equilibrium (LL_{ei}) would have been reached. The larger errors for the rotation results of these ropes (figures 6.10b and 6.11b) are probably a result of applying a static rotation analysis to a dynamic event. The analysis showed that 445,4 turns were lost from rope S5 and only 108,5 from ropes S6 to S8. In comparing these values it must be noted that the sheave wheel boundary condition (*SWbc*) for rope S5 was double the value for the other three ropes. This implies that the tendency for the rope to unlay when detached from the conveyance was greater in the case of rope S5. For both the measured and calculated results, the rotation during loading of ropes S6 to S8 were less than that for rope S5 since their lay lengths were generally shorter.

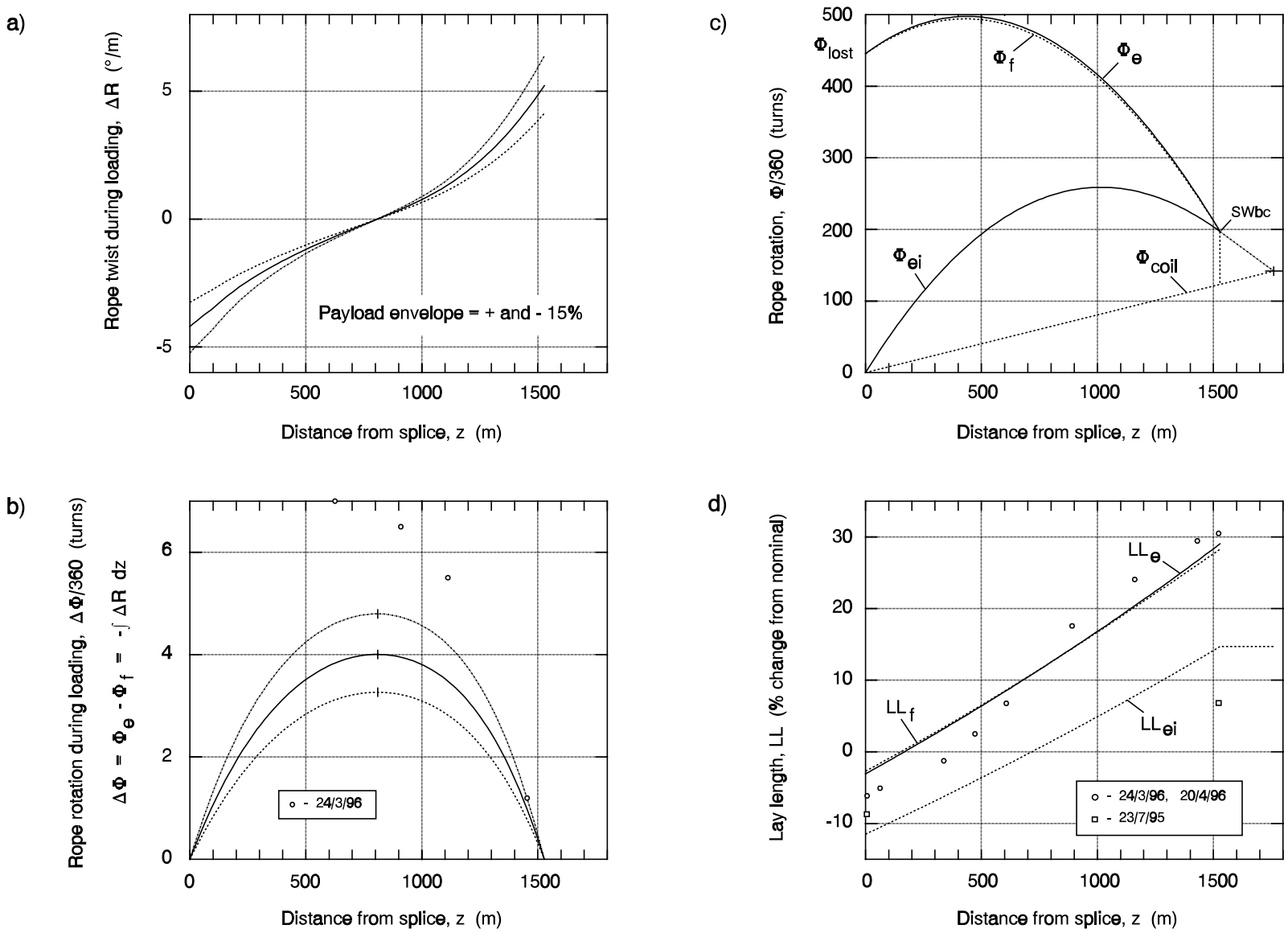

Figure 6.10 - Measurement and analysis results for rope S5. Additional information in table C.3, figure C.3 and section C.2.1

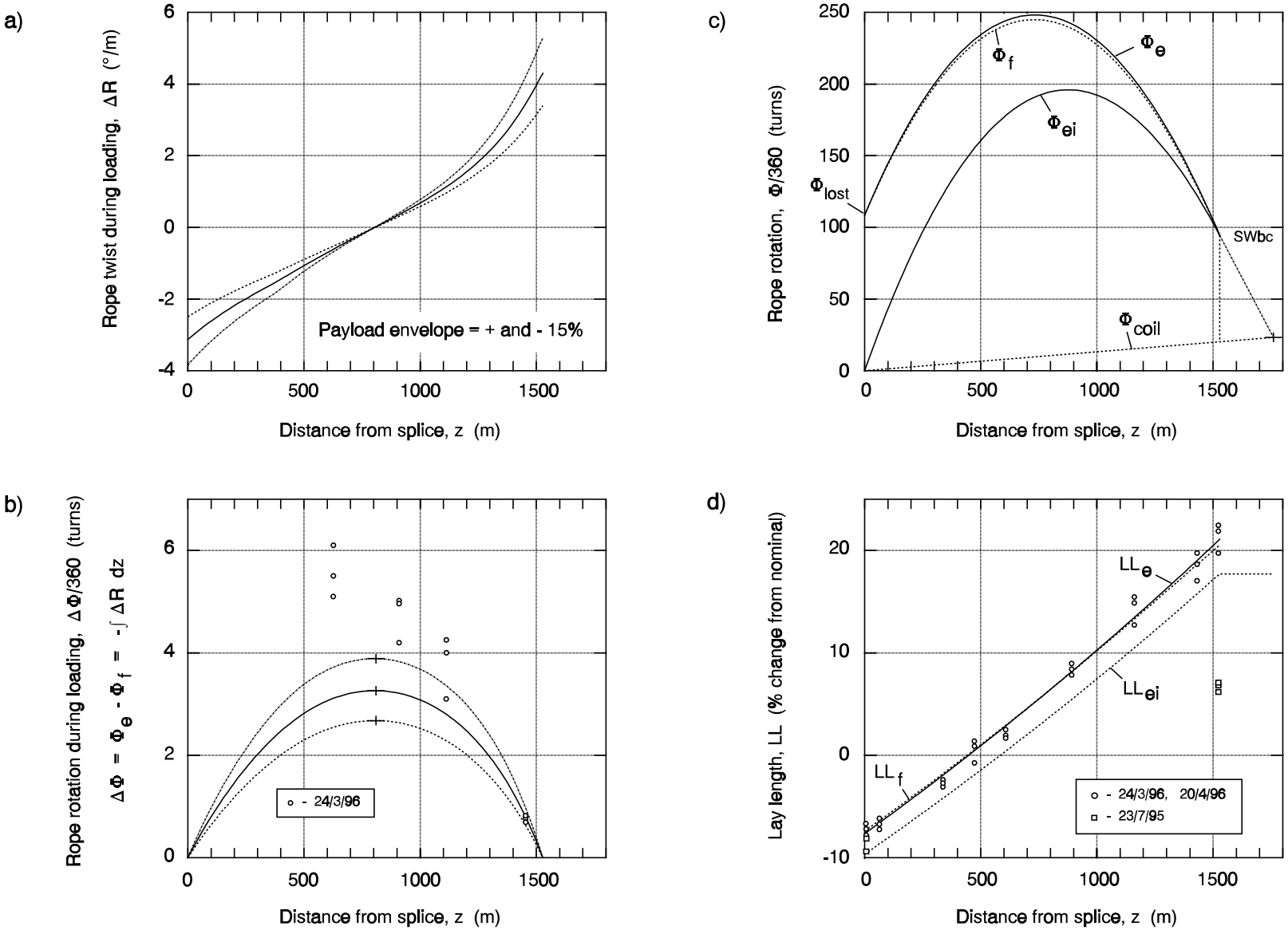

Figure 6.11 - Measurement and analysis results for ropes S6, S7 and S8. Additional information in table C.4, figure C.4 and section C.2.1

6.3.3 Shaft C, 46 mm ropes at 1426 m

Surface double drum rock winder (old ropes)

Ropes S9 and S10

46 mm, 6x31(13/12/6 + 3Δ)/F, RHL, 1800 MPa, Galvanised

Maximum suspended length, L = 1425,5 m

Empty conveyance weight, P_e = 70,5 kN

Conveyance payload, P_f - P_e = 83,4 kN

Rope service periods : 62,2 months

The relatively large scatter in the measured lay lengths for ropes S9 and S10 are as a result of only considering the lay length across 6 strands, figure 6.12d. The measurement instrument was that of the shaft rigger and repeatability was questionable. In the subsequent measurements conducted on the new ropes in the same shaft (S11 and S12) a tape was used over 18 strands with noticeably improved results, figure 6.13d. The mine was not able to provide the lay length values measured after installation for figure 6.12d.

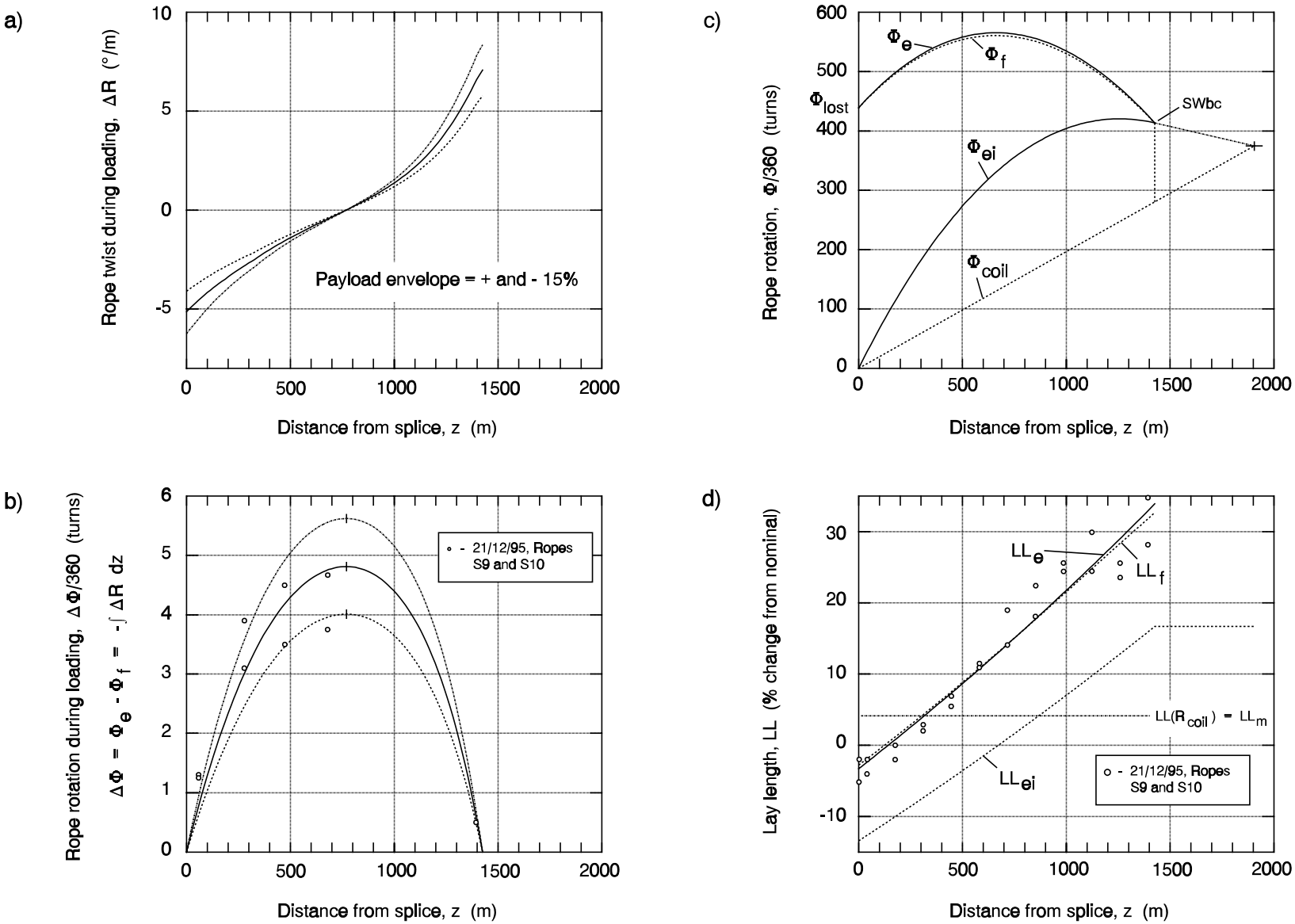

Figure 6.12 - Measurement and analysis results for ropes S9 and S10. Additional information in table C.5 and figure C.6

6.3.4 Shaft D, 46 mm ropes at 1426 m

Surface double drum rock winder (new ropes)

Ropes S11 and S12

46 mm, 6x31(13/12/6 + 3Δ)/F, RHL, 1800 MPa, Galvanised

Maximum suspended length, L = 1425,5 m

Empty conveyance weight, P_e = 70,5 kN

Conveyance payload, P_f - P_e = 83,4 kN

Rope service periods : 0,6 months

The lay lengths measurements on ropes S11 and S12 (figure 6.13d) were conducted two weeks after their installation. In the analysis algorithm it was assumed that no rotation was lost from the ropes during the installation procedure. It was however found that the removal of 75 turns (Φ_{lost}) from the rope resulted in the most accurate representation of the measured lay lengths. It is likely that this quantity of rotation could have been lost during installation. It must however be assumed that the manufactured lay length (LL_m) used to calculated the twist at installation (R_{coil}) was measured accurately. From the data in figure 6.13d it can be seen that two weeks of operation is sufficient for a rope to reach an equilibrium state as far as lay length changes are concerned. This observation is in accordance with the studies of Kuun et al. (1993) who referred to a two week settling in period after installation.

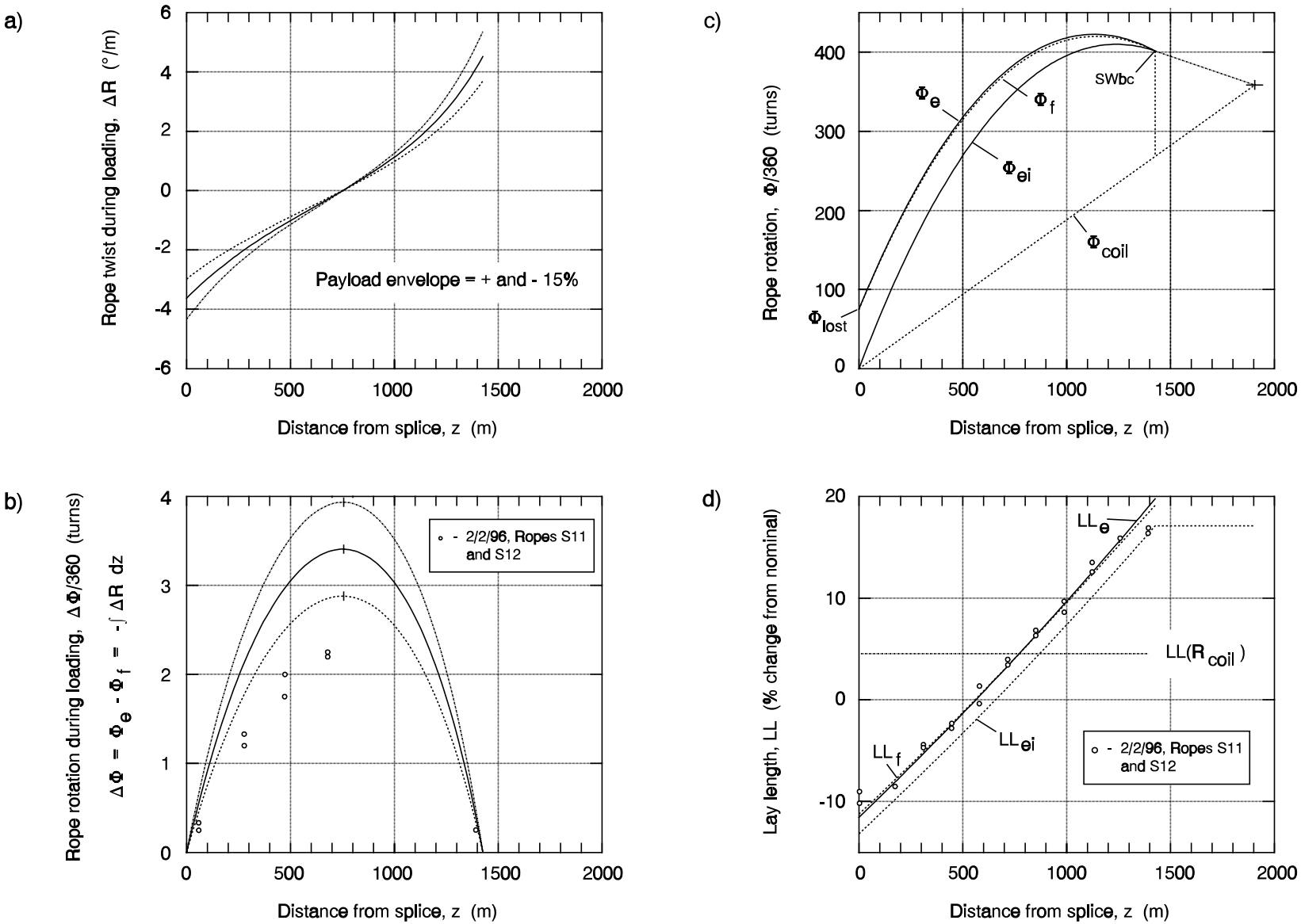

Figure 6.13 - Measurement and analysis results for ropes S11 and S12. Additional information in table C.6 and figure C.7

6.3.5 Shaft F, 48 mm ropes at 2196 m

Surface double drum rock winder

Ropes S14 and S15

48 mm, 6x32(13/12/6 + 3Δ)/F, RHL, 1800 MPa

Maximum suspended length, L = 2196 m

Empty conveyance weight, P_e = 96,0 kN

Conveyance payload, P_f - P_e = 138,0 kN (for rope S15 only)

Rope service periods : 15,3 months

Only one rotation measurement was available for rope S15 and none for rope S14. The data was extracted from the work of Hecker and van Zyl (1993). The lay length measurements for these ropes were taken by the shaft maintenance personnel and were reproduced by Borello (1991). Two sets of installation lay lengths are shown in figure 6.15d which vary considerably. Since the ropes were installed on the 4/10/89, it is assumed that the measurements of the 19/10/89 were measured inaccurately. Encouraging correlation is noted between the calculated torques for rope S15 and the values measured by Hecker and van Zyl (1993). For the empty conveyance the calculated value was 1203 Nm compared to 1270 Nm. For the loaded conveyance 1984 Nm was calculated compared to a measured value of 2020 Nm (figure 2.16).

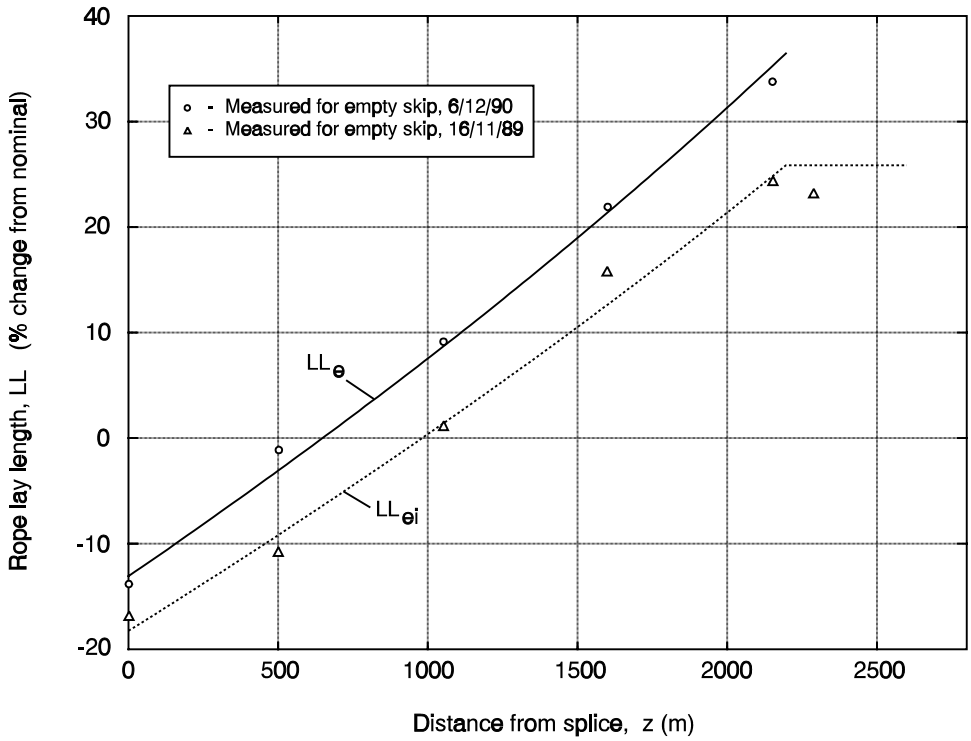

Figure 6.14 - Calculated and measured lay lengths for rope S14. No rotation measurements were available. Additional information in table C.7 and section C.5.1.

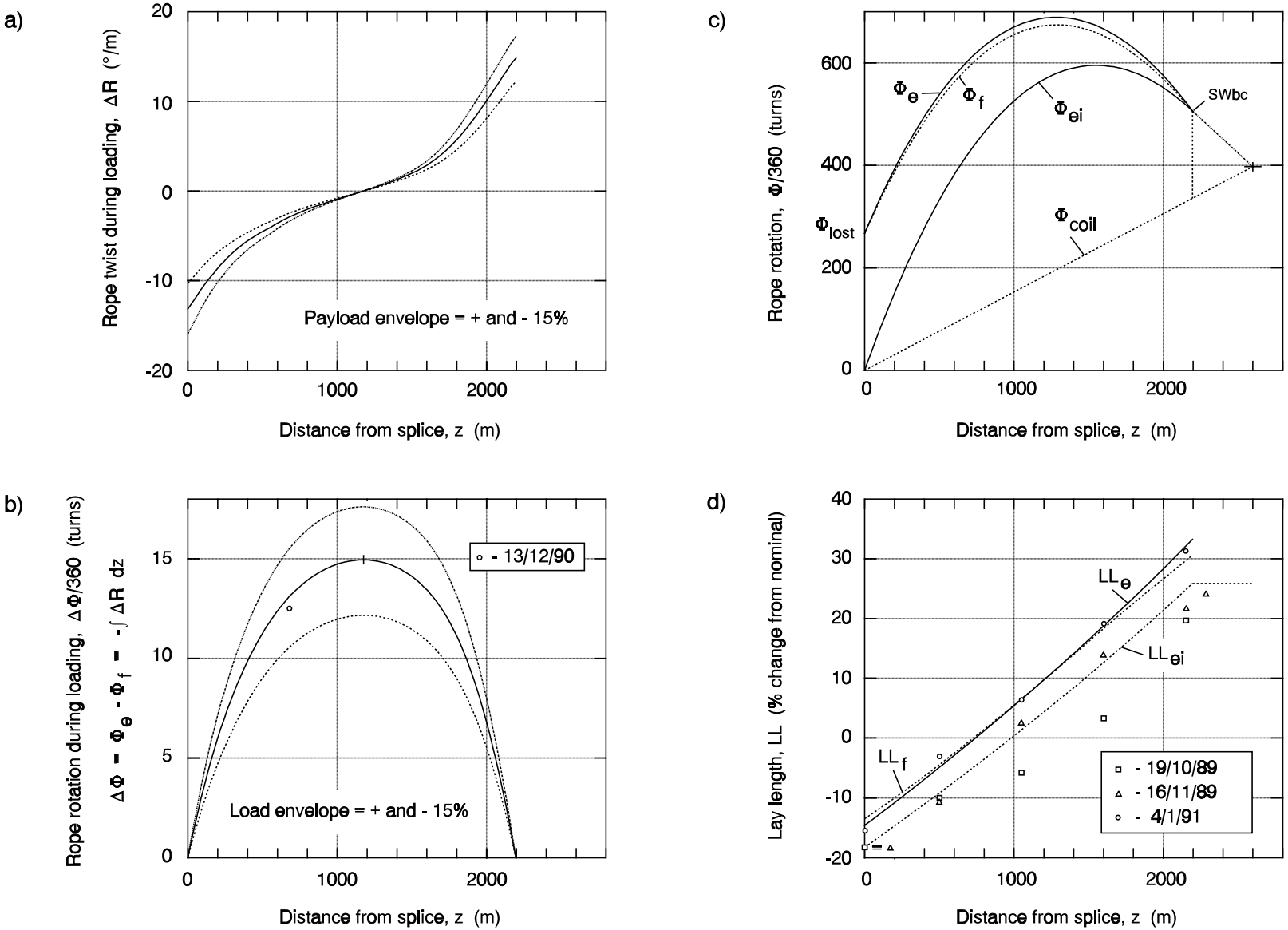

Figure 6.15 - Measurement and analysis results for rope S15. Additional information in table C.7, figure C.8 and section C.5.1.

6.3.6 Shaft G, 49 mm ropes at 1126 m

Surface double drum rock winder

Ropes S16 and S17

49 mm, 6x32(13/12/6 + 3Δ)/F, RHL, 1900 MPa

Maximum suspended length, L = 1126 m

Empty conveyance weight, P_e = 86,7 kN

Conveyance payload, P_f - P_e = 96,3 kN (for rope S16 only)

Rope service periods : 23,4 months (S16 and S17, figure 6.16)
18,5 months (S16, figure 6.17)

Figure 6.16 indicates the combined lay length data for ropes S16 and S17 one month after installation and just before discard. It was calculated that 385 turns were lost from the ropes in the two year period. In contrast, at the time of measurements for this study (5 months before discard) only 156.4 turns had been lost from rope S16. The shaft engineer indicated that it was the practice to return rotation to the ropes prior to reattachment to the conveyance after maintenance. It was not possible to determine why relatively large changes in lay length occurred in the last five months of service.

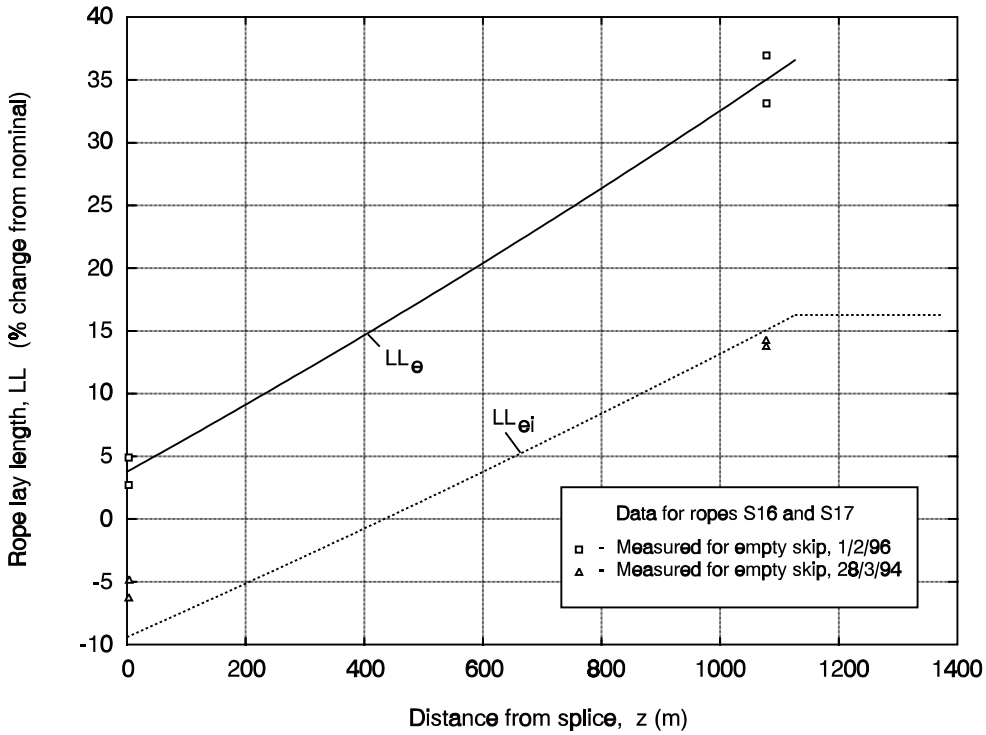

Figure 6.16 - Calculated and measured lay lengths for rope S16 and S17, at installation and at discard. Additional information in table C.8 and section C.9.1. No rotation data was available for rope S17.

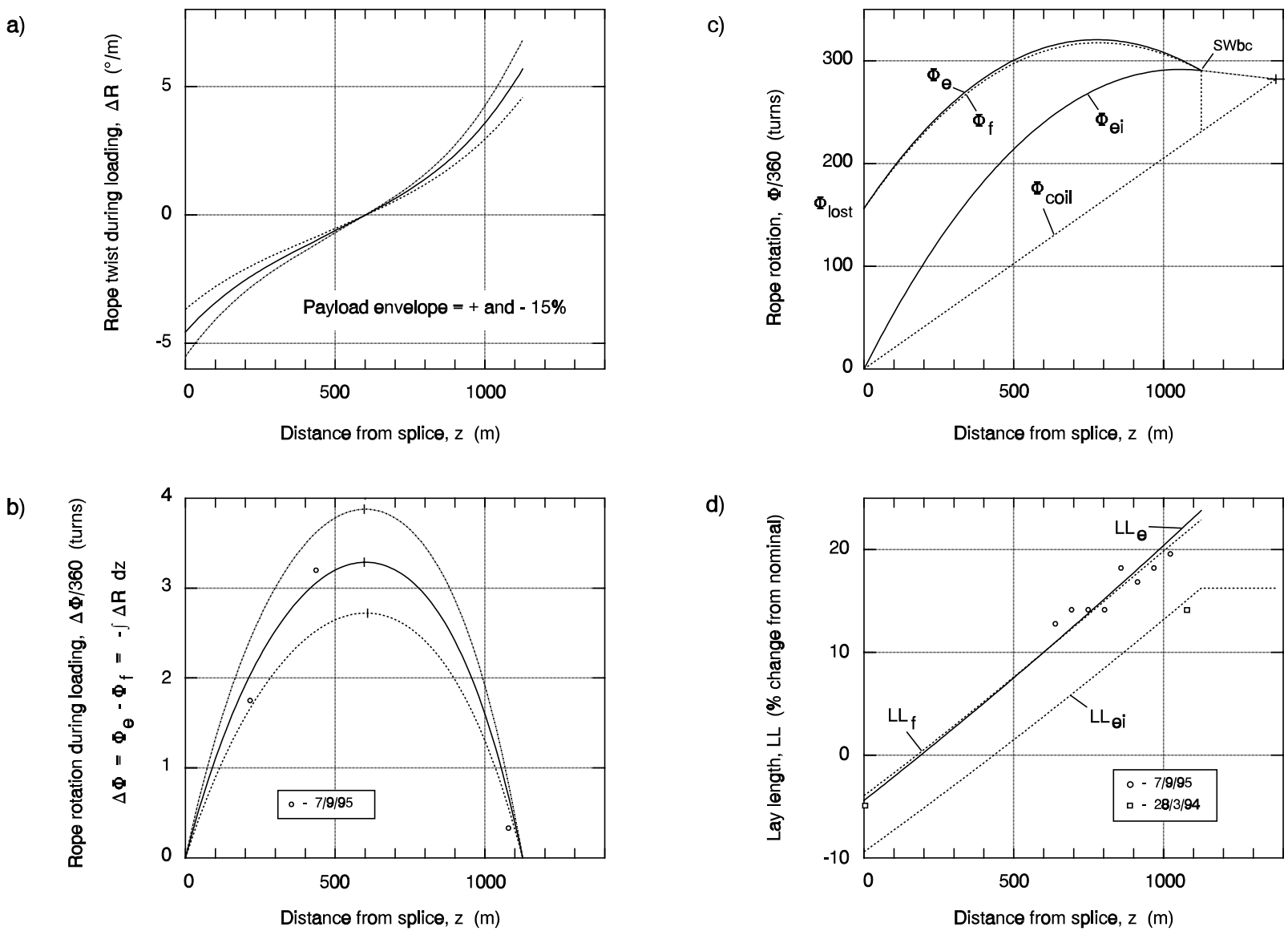

Figure 6.17 - Measurement and analysis results for rope S16. Additional information in table C.8, figure C.10 and section C.9.1.

6.3.7 Shaft H, 49 mm ropes at 1068 m

Sub-vertical double drum rock winder

Ropes S18 and S19

49 mm, 6x32(13/12/6 + 3Δ)/F, RHL, 1800 MPa

Maximum suspended length, L = 1068,1 m

Empty conveyance weight, P_e = 55,2 kN

Conveyance payload, P_f - P_e = 89,1 kN

Rope service periods : 75,3 months

The large changes in lay length of ropes S18 and S19 from the installation values (LL_{ei}) to the date of measurements (LL_e) are attributed to the long service period and the great distance (105,2 m) between the bank and the headgear sheaves (sub–vertical shaft).

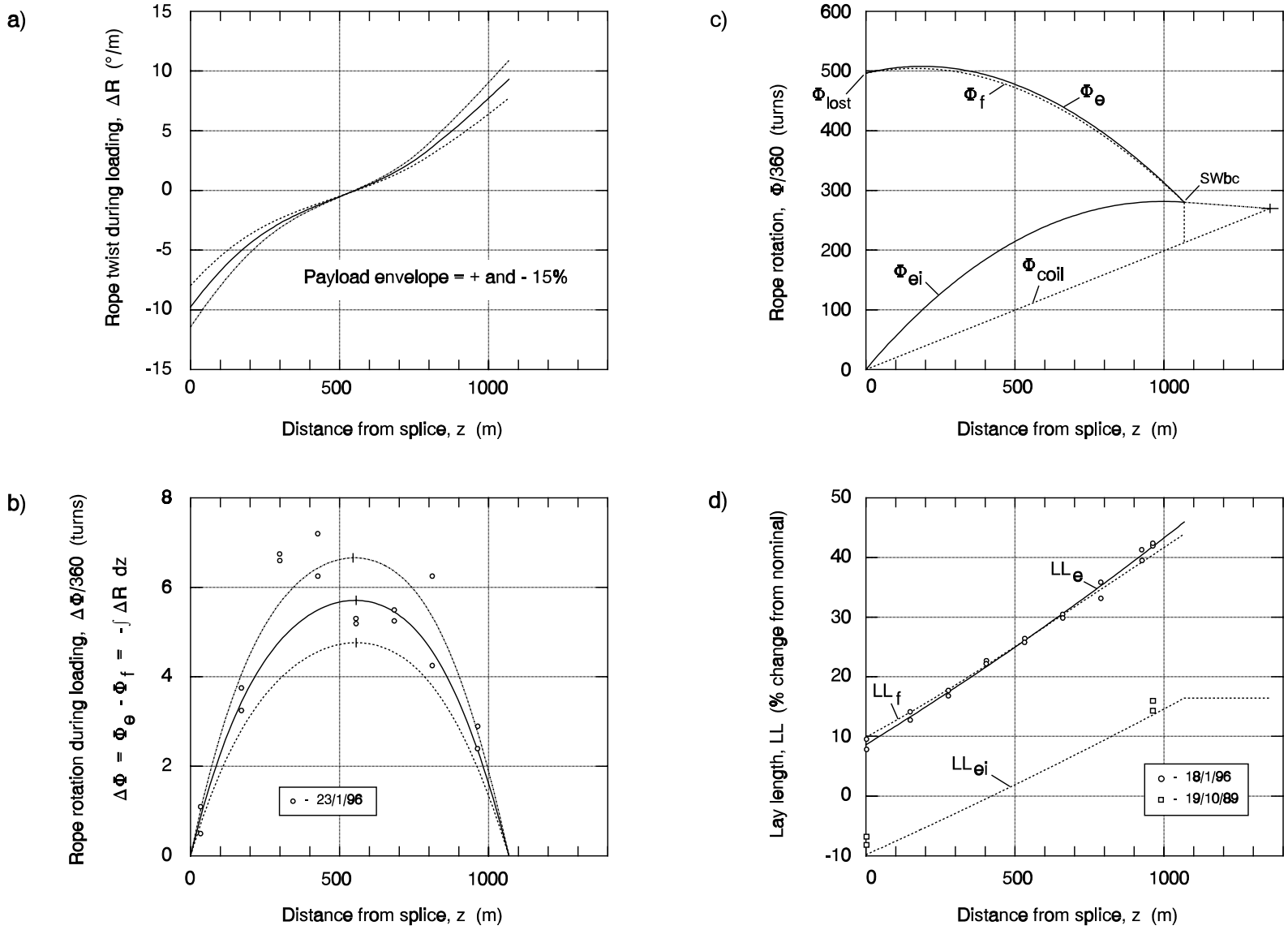

Figure 6.18 - Measurement and analysis results for ropes S18 and S19. Additional information in table C.9, figure C.11 and section C.9.1.

6.3.8 Shaft J, 49 mm rope at 1599 m

Surface double drum man winder

Rope S20

49 mm, 6x32(13/12/6 + 3Δ)/F, RHL, 1800 MPa

Maximum suspended length, L = 1598,6 m

Empty conveyance weight, P_e = 73,0 kN

Conveyance payload, P_f - P_e = 40,9 kN (locomotive)

Rope service period : 21,6 months

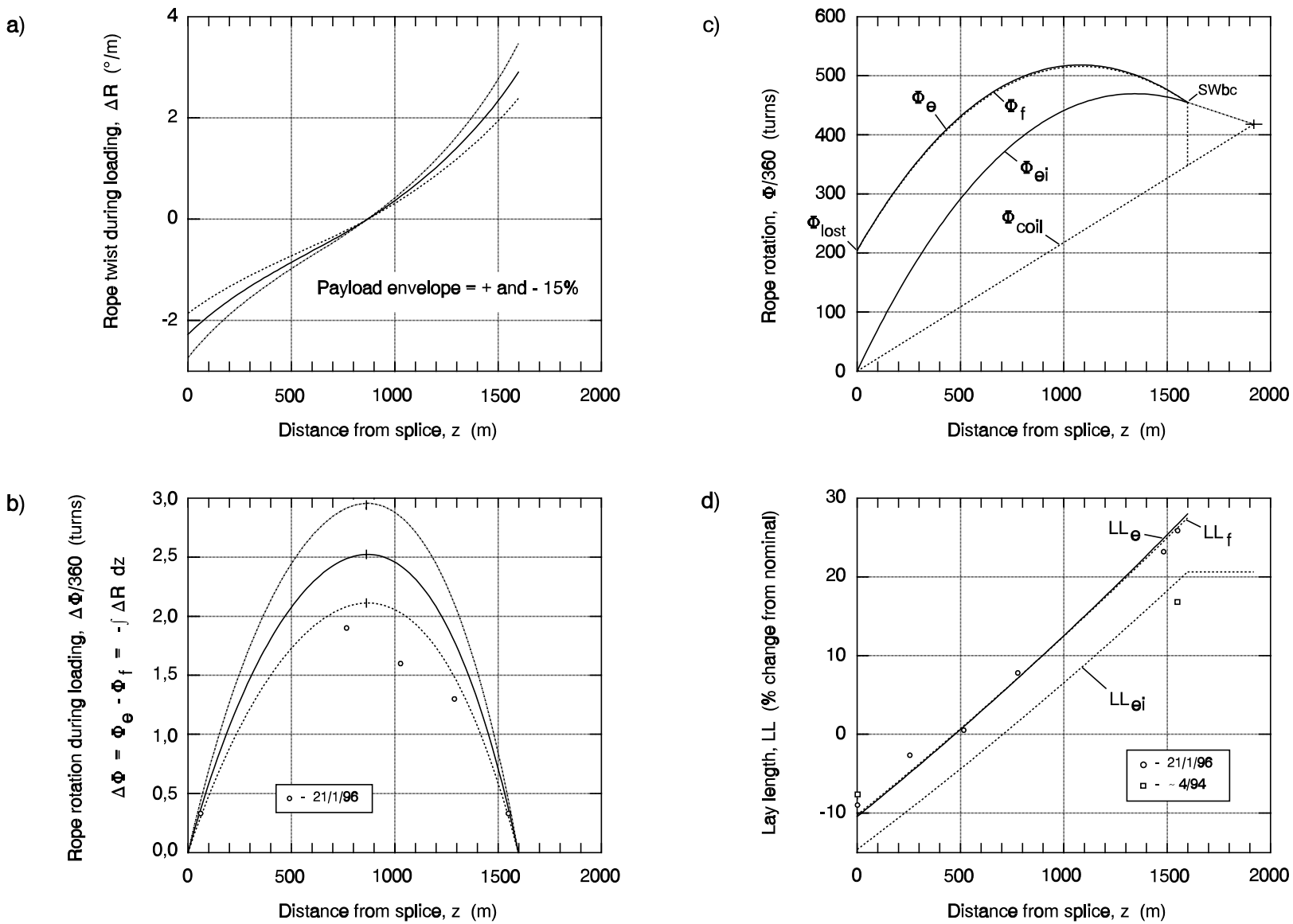

Figure 6.19 - Measurement and analysis results for rope S20. Additional information in table C.10, figure C.12 and section C.9.1.

6.3.9 Shaft K, 49 mm rope at 1935 m

Surface double drum man winder

Rope S21

49 mm, 6x32(13/12/6 + 3Δ)/F, RHL, 1800 MPa

Maximum suspended length, L = 1935,4 m

Empty conveyance weight, P_e = 55,2 kN

Conveyance payload, P_f - P_e = 40,8 kN (locomotive)

Rope service period : 12,4 months

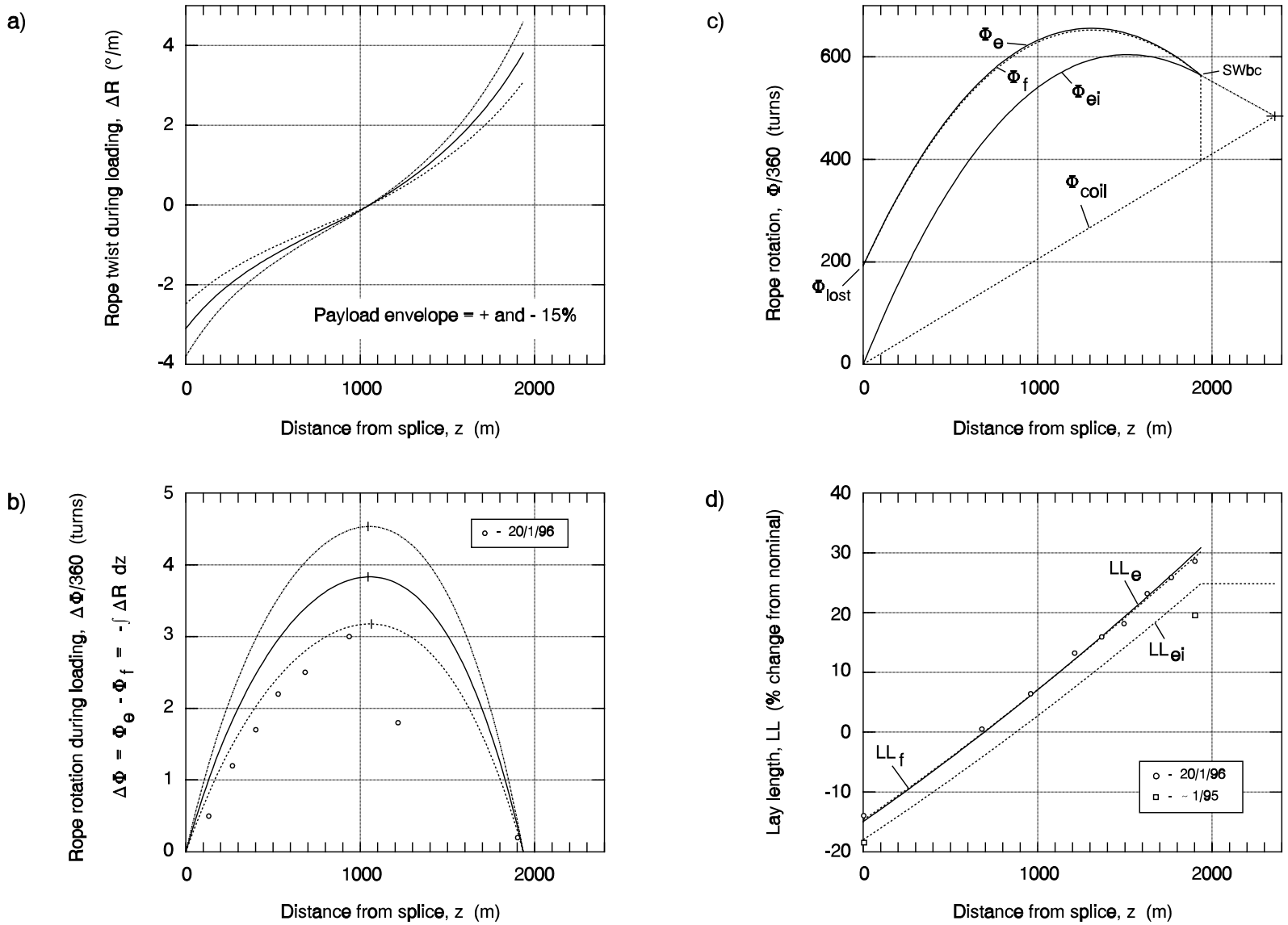

Figure 6.20 - Measurement and analysis results for rope S21. Additional information in table C.11, figure C.13 and section C.9.1.

6.3.10 Shaft L, 54 mm rope at 1887 m

Surface double drum man winder

Rope S22

54 mm, 6x32(13/12/6 + 3Δ)/F, RHL, 1950 MPa

Maximum suspended length, L = 1886,9 m

Empty conveyance weight, P_e = 85,9 kN

Conveyance payload, P_f - P_e = 45,5 kN (locomotive)

Rope service period : 8,0 months

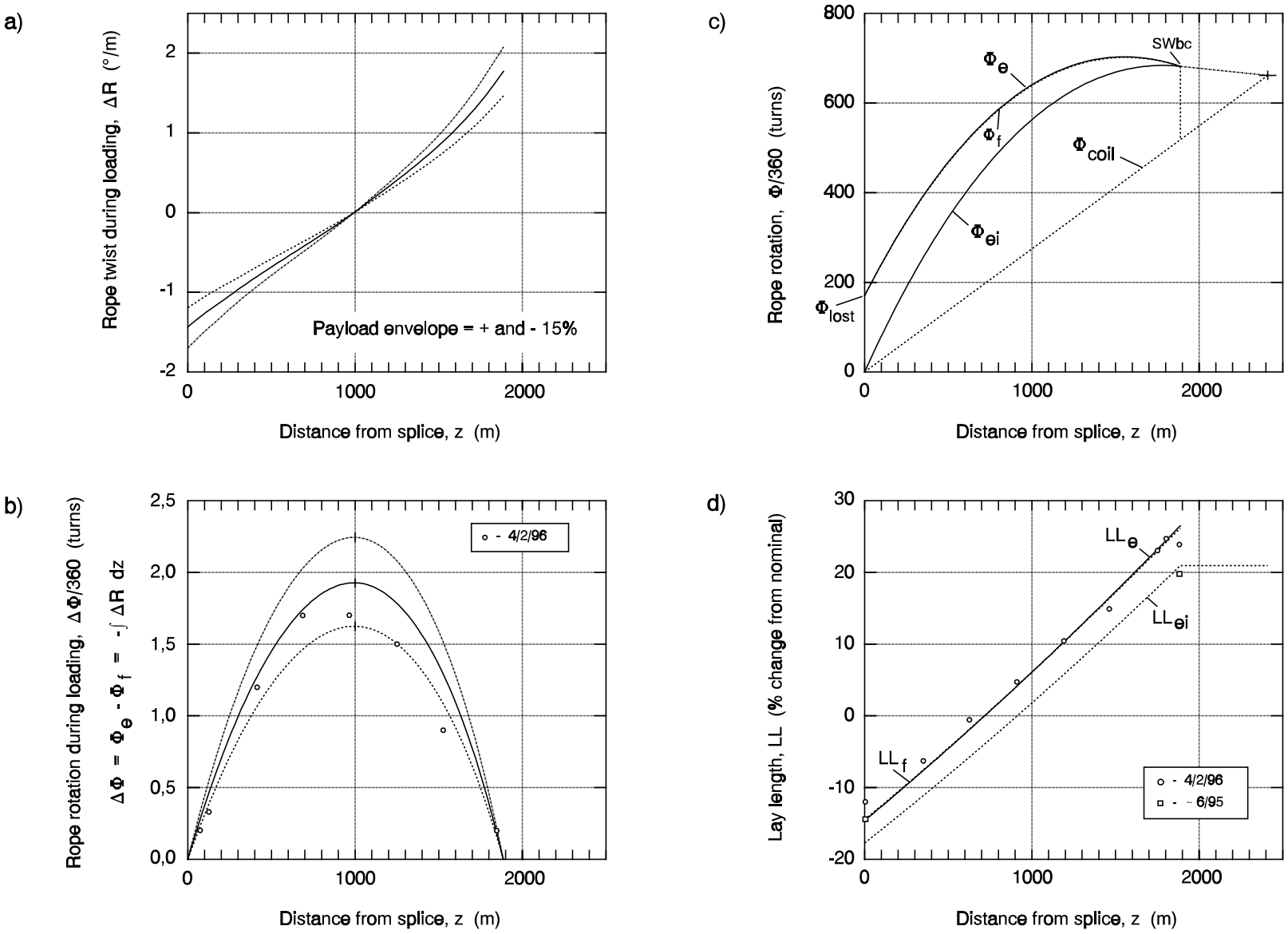

Figure 6.21 - Measurement and analysis results for rope S22. Additional information in table C.12, figure C.15 and section C.10.1.

6.4 Accuracy of the modelling approach

6.4.1 In-service lay length and rotation measurements

Figures 6.22 and 6.23 show the error values calculated from the lay length and rotation predictions for ropes S1 to S22. The error values were determined by subtracting the measured values from the calculated data. In the case of the lay lengths, 86,1 percent of the errors lie in the range plus and minus two percent of the particular nominal lay lengths. For the rotation errors, 80,5 percent are in the range plus and minus one turn. It was known that the rotation at the splice and sheave ends of a rope are zero during conveyance loading. These points were therefore not considered in the calculations for figure 6.23.

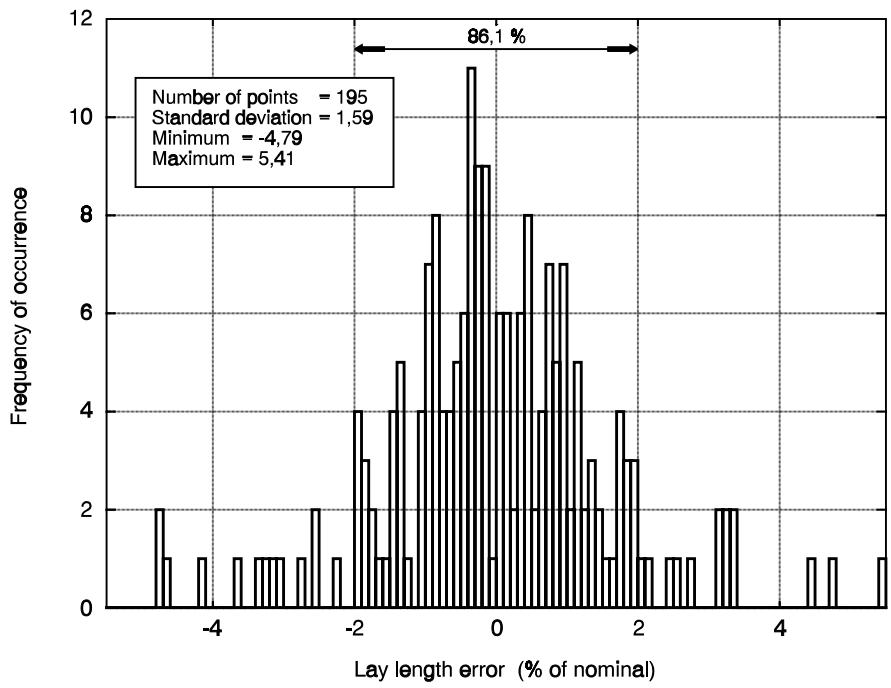

Figure 6.22 - Differences between the calculated (LL_e) and measured lay lengths for ropes S1 to S22 (empty conveyance).

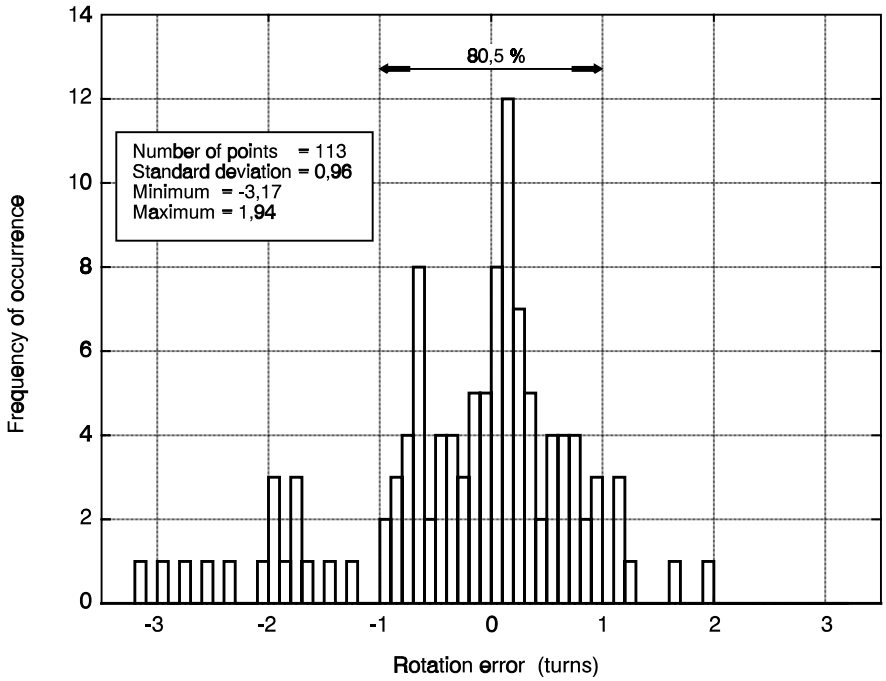

Figure 6.23 - Differences between the calculated ($\Delta\Phi$) and measured rope rotations during conveyance loading for ropes S1 to S22.

6.4.2 Installation lay lengths and loss of rotation

In general it has been observed that rope lay lengths are measured with considerable haste by rope maintenance personnel, usually over six strands. Other than statutory monitoring and recording, the lay length values are seldom used for further decision making. There is therefore little motivation to obtain accurate values. In comparison, rope diameter values are later compared to sheave groove radii and the matching of these are important from a rope endurance point of view. Lay length discard criteria for triangular strand ropes of 30 percent shortening and 100 percent lengthening from nominal were given by Kuun et al. (1993). This represents a very wide range of values covering all the measurements conducted in this study.

For all the lay length results presented, where ropes had been in service for some time, the measured splice and sheave end lay lengths were greater than the lay lengths measured by the shaft engineering personnel just after installation. The sheave end lay length always increases at a more rapid rate than the splice end due

to the nonlinear relationship between twist and lay length (equation 5.2). The changes in lay length result directly from the maintenance practice of allowing the ropes to gradually unlay. The rotation lost from each rope during the service period was calculated by the analysis algorithm. Figure 6.24 indicates that there is a correlation between the period of operation and the rotation lost per unit length of suspended rope (Φ_{lost}/L). It was stated in section 5.4 that the rotation of the splice end of the rope during detachment from the conveyance is partly dependant on the distance between the bank and head sheave (L_b). These distances for the various shafts are also shown in figure 6.24. The outlying points are individually marked. Ropes S1 to S4 of shaft **A** (41 mm at 1071 m) were unlaid considerably. Being a BMR winder with conveyance mounted compensating sheaves, the rope tangent points to the sheaves were cut on a three monthly basis. The regular detachment from the conveyance combined with the great distance between the bank and the headgear sheaves is thought to be the reason for the substantial unlaying.

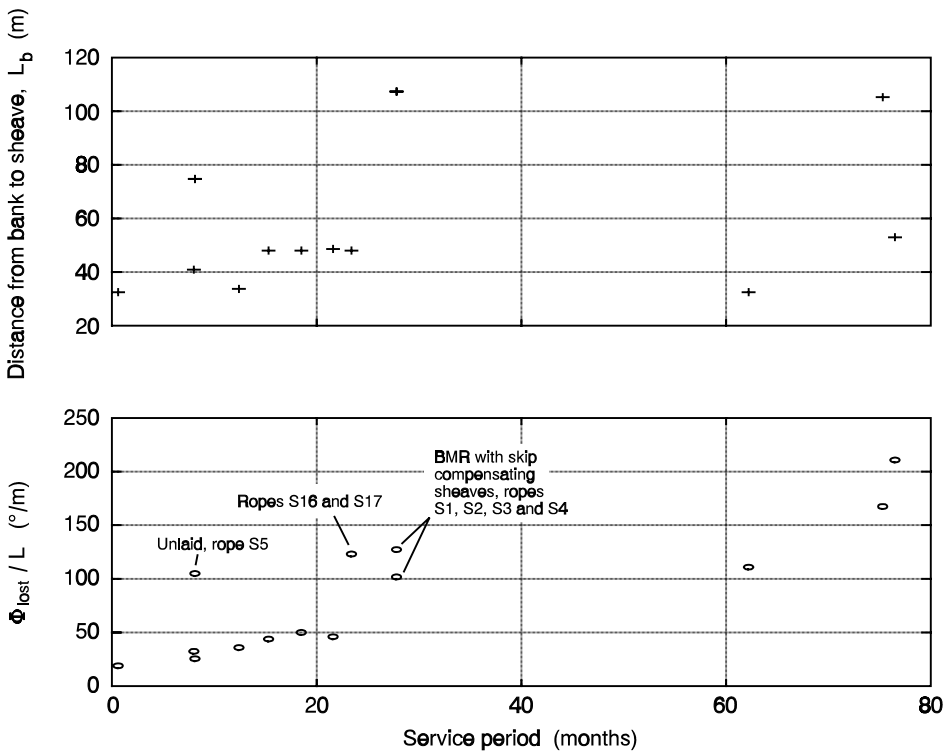

Figure 6.24 - Correlation between service period and the (calculated) rotation lost per unit length of suspended rope, for ropes S1 to S22.

6.4.2 Torsion test lay length measurements

For the twelve ropes on which torsion tests were conducted, the relationship between lay length and twist was determined, equation [5.2]. The lay length factor K_{LL} for each rope was calculated to satisfy the least squares criterion of fit, table 6.2. Error values were defined by subtracting the measured data from the fitted curve and expressing the differences as percentages of the nominal lay lengths of the respective ropes. Figure 6.25 indicates the distribution of these errors for the twelve ropes. Of the 118 measurements, 95,8 percent lie in the range plus and minus one percent. The lay lengths were all measured at a load of 30 kN using the lay length gauge shown earlier in figures 3.14 and 3.15. The data of figure 6.25 can be compared to the lay length errors for the in-service measurements, figure 6.22. The errors for the in-service measurements are considerably larger with 86.1 percent in the range plus and minus two percent of nominal. Movement of the in-service ropes during the measurements and the use of a measuring tape (over three lay lengths) were probably the main reasons for incurring the larger errors.

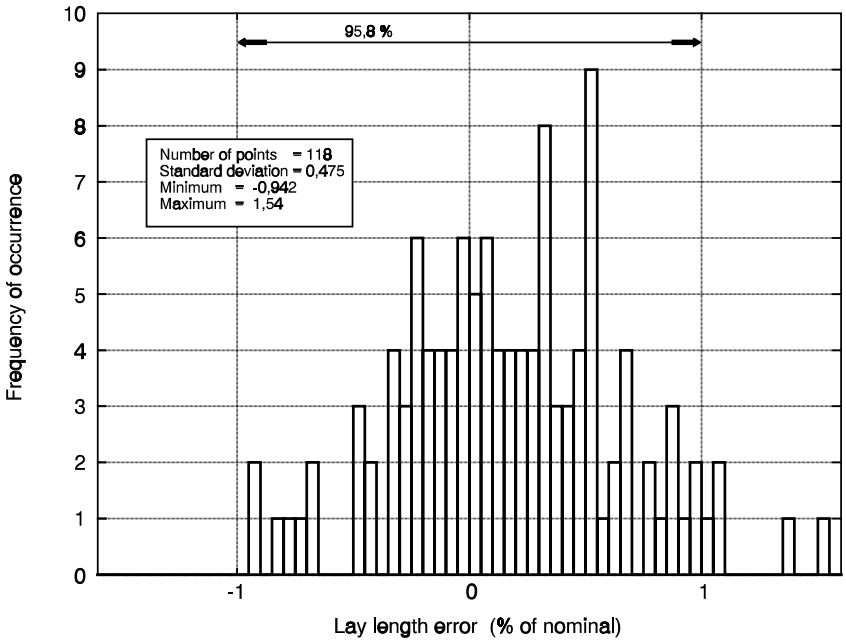

Figure 6.25 - Distribution of torsion test lay length errors determined by subtracting the measured lay lengths from the lay lengths defined by equation [5.2]. Details of ropes T1 to T12 are listed in table 6.2.

Table 6.2 - Constants of the lay length versus twist equation for the twelve torsion test ropes. Some data duplicated from tables 4.3 and 4.4.

Rope number	Nominal diameter, d_{nom} (mm)	Zero twist gauge length, l_0 (mm)	Zero twist diameter, d_0 (mm)	Zero twist lay length, LL_0 (mm)	Least squares lay length factor, K_{LL} (1/(°/m))
T1	25	2670	24,90	203,8	2,0412e-4
T2	40	2676	40,95	353,0	3,2744e-4
T3	40	2649	41,15	342,0	3,2889e-4
T4	40	2651	41,40	331,7	3,3620e-4
T5	40	2650	40,85	339,0	3,3118e-4
T6	40	2663	40,65	334,0	3,2849e-4
T7	40	2655	40,60	332,4	3,3028e-4
T8	41	2670	42,60	325,0	3,4426e-4
T9	46	2661	47,00	392,4	3,8011e-4
T10	48	2670	49,55	402,8	3,9799e-4
T11	49	2669	50,40	421,5	4,0519e-4
T12	54	2666	55,95	485,0	4,4986e-4

6.4.4 Empirical equation for torsion test lay lengths

In planning tension-torsion tests on triangular strand ropes it is useful to have an equation with which to determine the effect of end rotation on changes in lay length. From the tests conducted, it was found that equation 5.2a accurately describes the relationship over a wide range of lay length changes :

$$LL = \frac{\pi . d_0}{tan\left[\arctan\left(\frac{\pi . d_0}{LL_0}\right) + \frac{1000 . k_{LL} . \Phi_t}{l_0}\right]} \quad \text{(mm)} \qquad [5.2a]$$

where :

d_0	=	measured diameter at zero twist	(mm)
LL_0	=	measured lay length at zero twist	(mm)
l_0	=	measured gauge length at zero twist	(mm)
Φ_t	=	test specimen end rotation	(°)

It was determined that the lay length factor can be approximated by :

$$K_{LL} \approx \frac{d_0}{108105} . \cos^2\left[\arctan\left(\frac{\pi . d_0}{LL_0}\right)\right] \quad (1/(°/m)) \qquad [6.9]$$

Therefore, by measuring the diameter, lay length and gauge length of a specimen at installation into a torsion testing machine (with a 10 kN to 30 kN preload) it is possible to determine an estimate of the end rotation required to achieve specific changes in the lay length. Once the test has been completed (constant twist) then the accurate value of K_{LL} can be calculated from the known applied twists ($R_i = \Phi_i / l_0$) and the actual measured lay lengths (least squares fit). Figure 6.26 shows that the lay length errors for the twelve ropes are not significantly different using the estimated values of K_{LL} compared to the least squares values (figure 6.25). This would be expected since equation [6.9] is based on consideration of helix geometry.

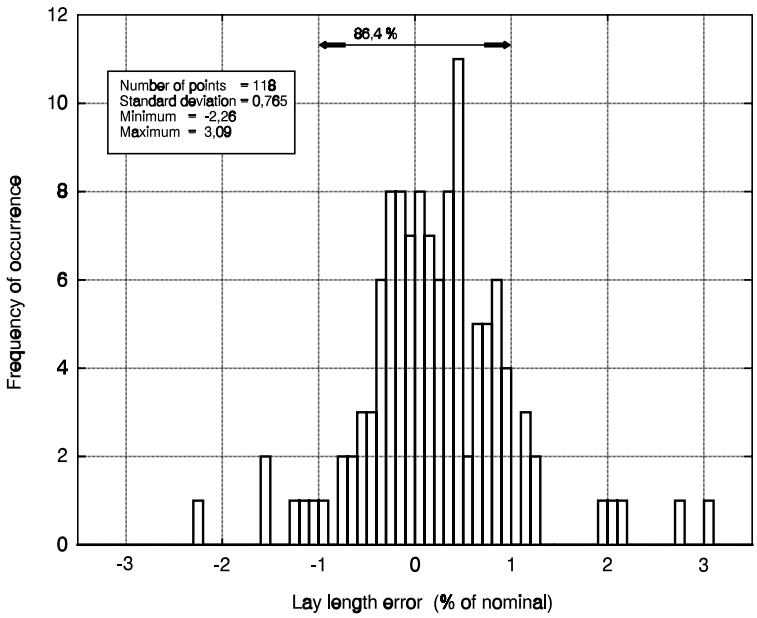

Figure 6.26 - Distribution of torsion test lay length errors calculated by comparing the lay length estimate, equations [5.2a] and [6.9], to the actual measured lay lengths for ropes T1 to T12.

6.5 Factors influencing the calculated results

6.5.1 The effect of galvanised wires on torsional hysteresis

Torsion tests at constant load and twist were also conducted on six 40 mm triangular strand rope samples (table 4.3). Two of the ropes had galvanised wires which resulted in considerably increased torsional hysteresis in the results of the constant load tests. Figures 6.27 and 6.28 compare constant load curves for the samples without and those with galvanised wires. There is a significant difference between the hysteresis areas of the two figures for each constant load value. The four ropes of figures 6.27 and 6.28 were all of very similar dimensions and so the lay lengths corresponding to the applied twists were comparable. At a twist of 300 °/m, the lay lengths were within a range of 7 mm and at -300 ° they were within 15 mm. Prior to conducting the measurements, 150 bedding in load cycles (150 kN to 450 kN at 0 °/m) and 50 rotation cycles (-68°/m to 68 °/m at 300 kN) were run.

The observations regarding the effect of galvanised wires on torsional hysteresis have relevance to the results for shafts **C** and **D** (46 mm ropes at 1426 m). The torsion tests for the ropes of these shafts (analysis for ropes S9 to S12) were carried out on a 46 mm rope which was not galvanised. The in-service ropes however were galvanised. The rotation prediction for the ropes which had been in service for over five years (figure 6.12b) are more accurate than the prediction for the newly installed ropes (figure 6.13b).

It is proposed that the old ropes had accumulated sufficient wear at their inter-wire contact points that the hysteretic torsional stiffness properties were similar to an ungalvanised specimen. In the case of the newly installed ropes, the galvanising would have contributed significantly to the torsional hysteresis resulting in a stiffer rope which rotated less during the conveyance loading than predicted.

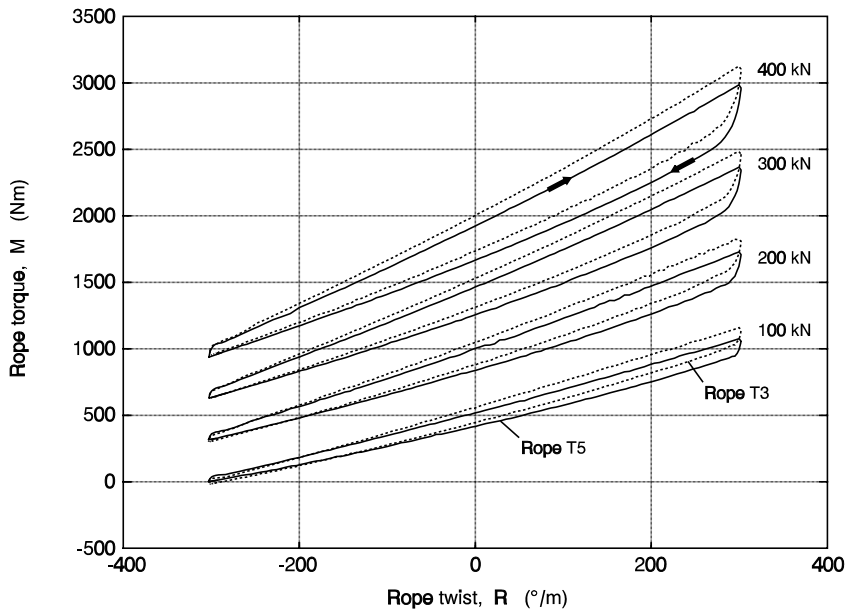

Figure 6.27 - Measured torsional hysteresis at constant load for **ungalvanised**, 40 mm, triangular strand ropes, rope T3 = 6x28(10/12/6 + 3Δ)/F, 1900 MPa.
Rope T5 = 6x29(11/12/6 + 3Δ)/F, 1800 MPa.

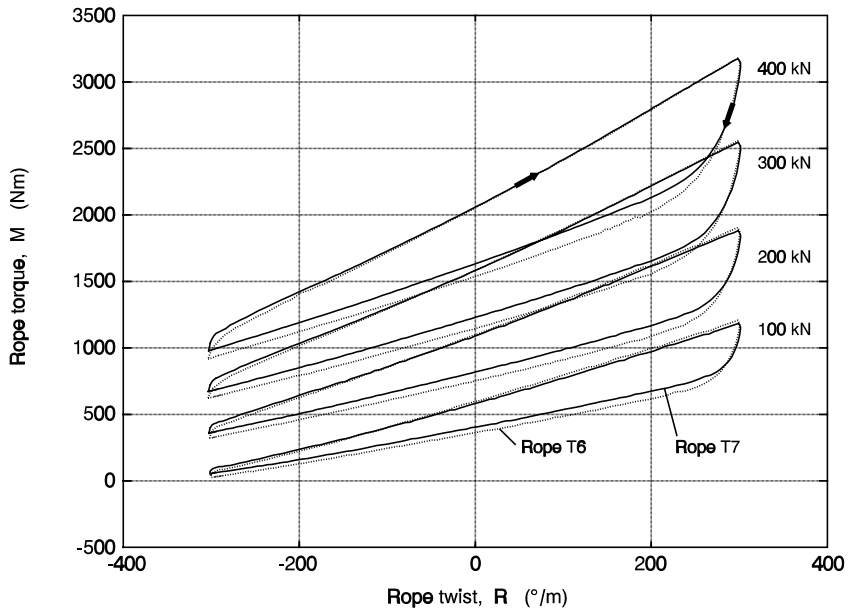

Figure 6.28 - Measured torsional hysteresis at constant load for **galvanised**, 40 mm, triangular strand ropes. Ropes T6 and T7 = 6x30(12/12/6 + 3Δ)/F, 1800 MPa.

6.5.2 Torsional stiffness variation with changes in lubrication

The rope samples received from the manufacturer were lubricated internally during the closing process but external dressing had not been applied. The ends of the specimens were completely degreased (with trichloroethylene) during preparation for casting of the white metal end cones. This resulted in a length of approximately 300 mm on either end of a made-up specimen being without any lubrication. It was anticipated that any end effects resulting from a twist discontinuity at the terminations (figure A.12) would be amplified by the localised lack of lubrication. Therefore, for all the torsion tests conducted, low viscosity hydraulic oil was applied by brush to the rope samples during the bedding in cycles. Particular attention was given to the areas adjacent to the end cones.

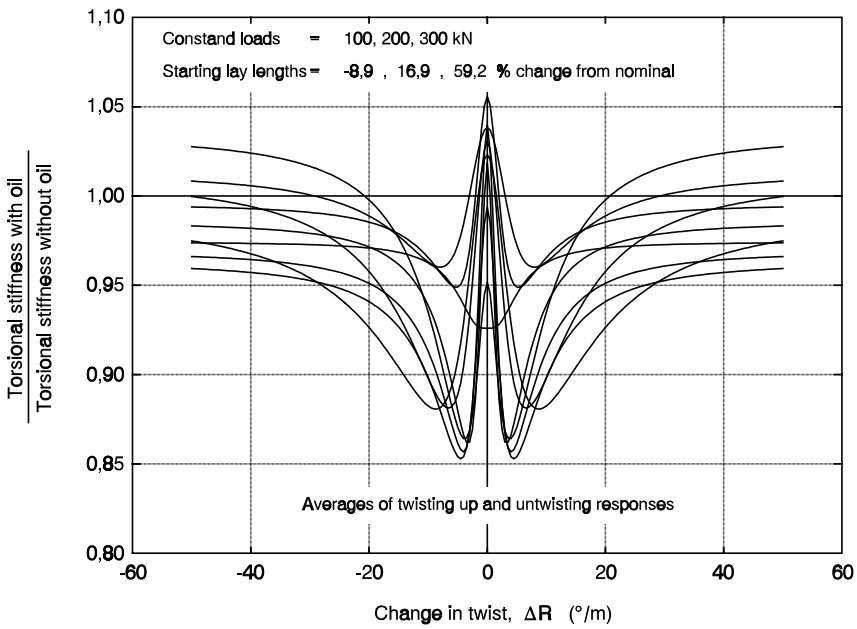

Figure 6.29 - Ratio of measured torsional stiffness for a specimen with and without lubricating oil applied. Rope T2, 40 mm, 6x28(10/12/6 + 3Δ)/F, 1900 MPa, zero twist gauge length = 2679 mm.

For one of the 40 mm ropes, T2, torsional stiffness tests were conducted before and after the application of the hydraulic oil in order to establish an indication of the effect. Figure 6.29 shows the ratio of the measured stiffnesses with oil to those without. In general, the stiffness with oil tends to be less than without, which is expected. The differences are most evident in the area of transition from no slippage between the wires to full slippage, -10 °/m to + 10 °/m. For the results

presented in chapter six, the majority of changes in twist (ΔR) during conveyance loading were within this range (figures 6.6a to 6.21a). The decrease in stiffness with increased lubrication was expected to result in greater rope rotation during conveyance loading. Table 6.3 lists the results of calculations conducted using the two sets of stiffness data.

Table 6.3 - Calculated variation in the maximum rotation during conveyance loading for increased lubrication of a torsion test specimen.

Rope T2, d_{nom} = 40 mm, EBL = 1168 kN (1800 MPa),

R_{coil} = 123 °/m (LL_{nom} + 3.71 % = 313.2 mm), RSF = 25000/(4000 + L)

f_s = 0.68, q = 0.0669 kN/m, z_{max} - L = 370 m

L **(m)**	***RSF***	LL_{ei} **(0)** **(% change from** LL_{nom} **)**	LL_{ei} **(L)** **(% change from** LL_{nom} **)**	$\Delta\Phi_{max}$ **without oil (turns)**	$\Delta\Phi_{max}$ **with oil (turns)**	**Increase in maximum rotation with added lubrication (%)**
1000	5,00	-8,2	11,0	1,87	1,87	0,0
1500	4,55	-12,5	15,5	4,05	4,21	4,0
2000	4,17	-16,4	19,9	6,87	7,37	7,3
2500	3,85	-20,0	24,3	9,93	10,86	9,4

The effect of the state of torsion test specimen lubrication becomes more evident at depth. A difference of ten percent in rotation is however not significant compared to the inherent scatter in rotation data observed even with fixed payloads (locomotive) as in figure 6.6b. It is recommended that torsion test specimens should always be well lubricated since this would mostly be the condition under which ropes operate.

6.5.3 Reasons for considering the loading values of torque from the constant twist tests

The constants in the matrix *N* of equation [5.3] are determined from the torsion test data (constant twist). It is possible to consider both the loading and unloading data (N_{avg}) or only the loading values of torque (N_{load}). For the analysis conducted to determine the in-service predictions, sections 6.2 and 6.3, the loading data was used exclusively. It was found that if both are considered the resulting fitted curve (least squares) is dependant on the maximum load during the torsion test as illustrated in figure 6.30. In the case of the loading data, the same path is followed irrespective of the maximum load. Not all of the ropes were tested to the same loads and in some cases the torque limitation resulted in differing maximum loads in a single test (example, figure C.14). It was therefore more consistent to consider only the loading values and less errors were expected when the data was linearly extrapolated.

It was also found that a second order equation such as [5.3] is prone to instability when extrapolating to loads higher than those for which data was obtained in the torsion tests. An approach was therefore adopted whereby the measured data was extended linearly based only on the upper 20 percent of the measured values as shown in figure 6.31. The subsequent second order fit considered both the measured data and the linearly extended data.

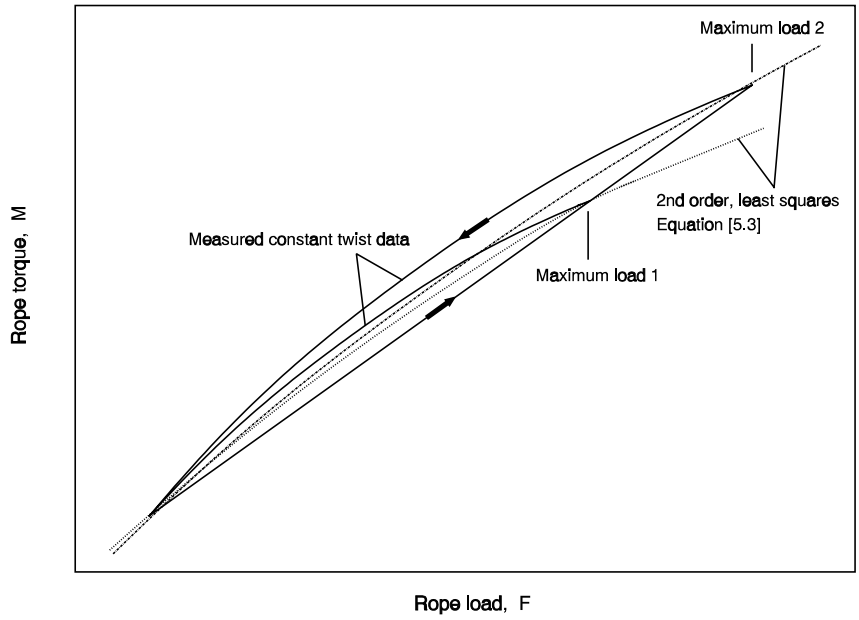

Figure 6.30 - Illustration of the effect of maximum load during a constant twist test on the shape of the fitted torque curves. Loading and unloading data are taken into account.

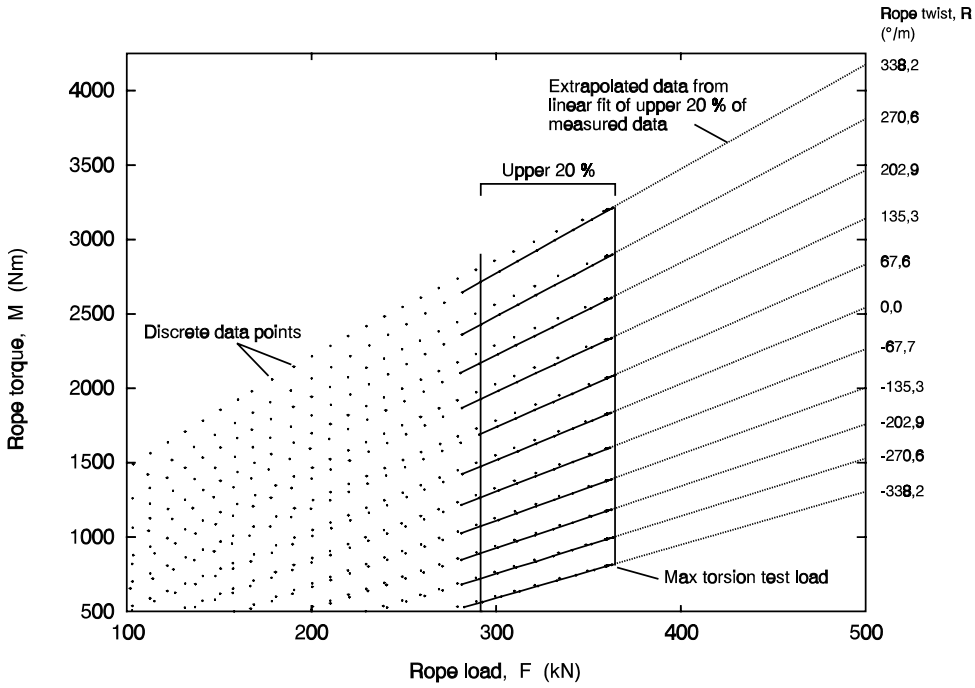

Figure 6.31 - Linear extrapolation of torque versus load data based on the upper 20 percent of the measured results, rope T9, 46 mm, 6x31(13/12/6 + 3Δ)/F, 1800 MPa. Figure 6.2 shows the complete constant twist test results for this rope.

6.5.4 Calculation of intermediate values of the torsional stiffness constants a_{cl}, b_{cl} and c_{cl}

In the rope rotation analysis presented in chapter five, the values for a_{cl}, b_{cl} and c_{cl} at constant loads and starting twists, different from those at which the torsion tests were conducted, were determined by double linear interpolation within the a_{cl}, b_{cl} and c_{cl} matrices. This approach was also applied to the calculations of the results presented in sections 6.2 and 6.3. From the general form of a_{cl}, b_{cl} and c_{cl} shown earlier (figure 5.23) it is apparent that a_{cl} and c_{cl} are approximately continuous and b_{cl} is not. Interpolation in matrix b_{cl} can therefore result in errors in the torsional response for the specific intermediate load and twist value. It would be more accurate to interpolate the torsional response at the intermediate point and then solve for the values of a_{cl}, b_{cl} and c_{cl} numerically from the interpolated torque versus twist data. This concept is illustrated in figure 6.32.

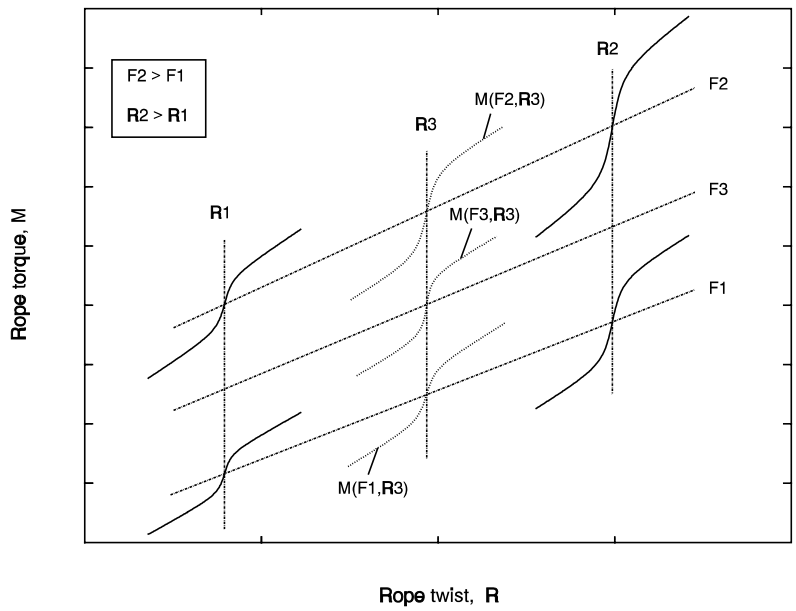

Figure 6.32 - Accurate method of determining the torsional response constants at an intermediate constant load and starting twist.

As an example, it could be assumed that the interpolation point of interest is associated with starting twist, R3, and constant load, F3 and that torsion test data exists at (F1,R1), (F1,R2), (F2,R1) and (F2,R2). The linearly interpolated torsional responses M(F1,R3) and M(F2,R3) would first be determined followed by the response M(F3,R3). From the interpolated response the accurate values of a_{cl}, b_{cl} and c_{cl} at F3 and R3 are then determined using a nonlinear optimisation routine.

To determine whether the error between the approximate and accurate interpolation methods is significant calculations were conducted for ropes T8, T9 and T11. These all have 5x5 a_{cl}, b_{cl} and c_{cl} matrices. At all the intermediate constant load and starting twist values approximate and accurate a_{cl}, b_{cl} and c_{cl} interpolations were conducted. The intermediate loads and twist were calculated from the mean values of the test loads and starting twist :

$$(F_{cl\,(i)} + F_{cl\,(i+1)}) / 2 \qquad [6.10]$$

$$(R_{cl0\,(i)} + R_{cl0\,(i+1)}) / 2 \qquad [6.11]$$

It follows that from the original 5x5 matrices, sixteen interpolation points resulted. At each interpolation point the approximate and accurate torsional stiffness characteristics were calculated and compared. Figure 6.33 shows the torsional stiffness errors for the sixteen interpolation points for the three ropes. The variations in torsional stiffness between the two interpolation methods results primarily from the differences in the values of b_{cl}. For all three ropes the largest errors occur at low loads and positive twists where b_{cl} is more unstable (figure 5.23). For the three ropes, the torsional stiffness errors lie in a range -10 percent to +25 percent. To determine the effect of these errors the accurate interpolation method was applied to the rotation predictions for ropes S5, S11, S12, S18, S19 and S20. Table 6.4 lists the maximum calculated rotation during conveyance loading for the two interpolation methods.

Table 6.4 - Examples of variations in the calculate maximum rotation using accurate and approximate a_{cl}, b_{cl} and c_{cl} interpolation.

Rope	$\Delta\Phi_{max}$ **approximate interpolation (turns)**	$\Delta\Phi_{max}$ **accurate interpolation (turns)**	**percentage change, approximate to accurate**
S5 (41 mm at 1529 m)	4,00	4,19	+4,75
S11 and S12 (46 mm at 1426 m)	3,40	3,55	+4,41
S18 and S19 (49 mm at 1068 m)	5,71	5,65	-1,05
S20 (49 mm at 1599 m)	2,52	2,72	+7,94

Rope T8 - 41 mm
6x29(11/12/6+3Δ)/F
1800 MPa

$$\text{Error} = \left(\frac{\text{approximate}}{\text{accurate}} - 1 \right) . 100$$

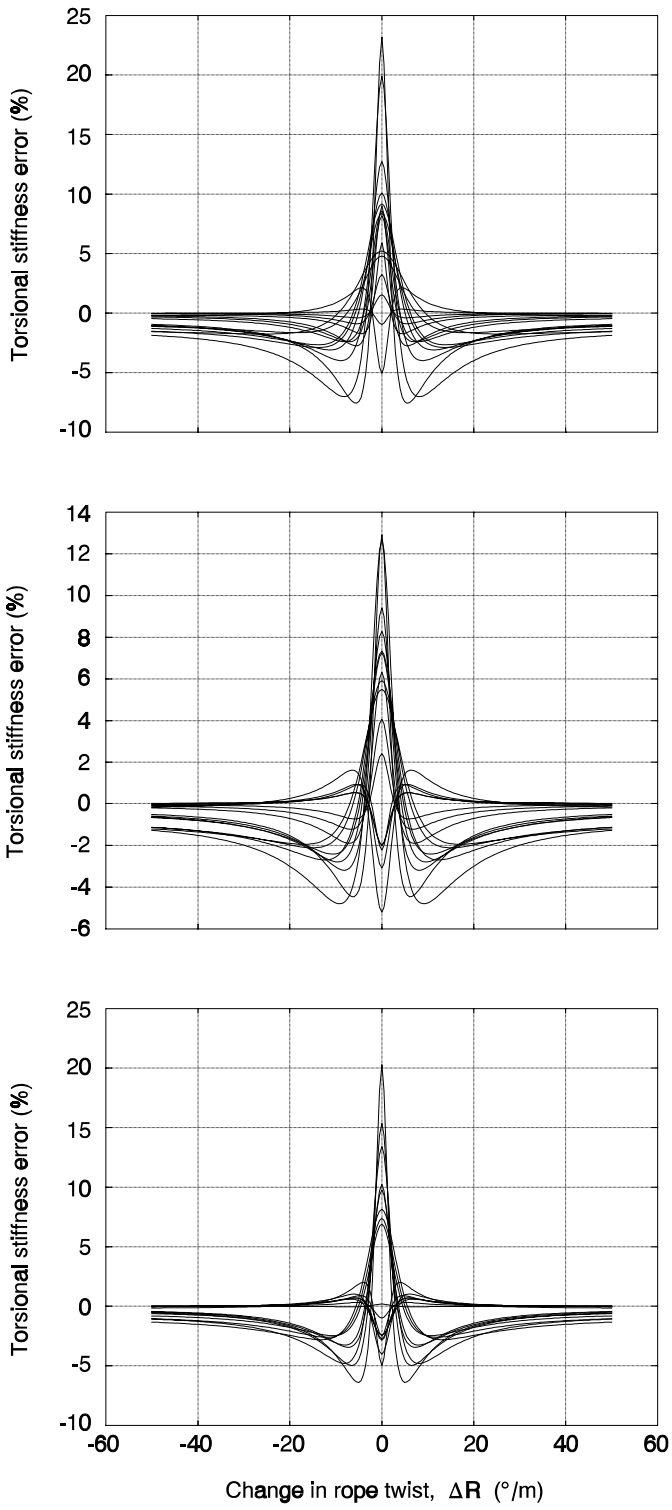

Rope T9 - 46 mm
6x31(13/12/6+3Δ)/F
1800 MPa

Rope T11 - 49 mm
6x32(14/12/6+3Δ)/F
1800 MPa

Figure 6.33 - Torsional stiffness errors resulting from interpolation within the matrices a_{cl} , b_{cl} and c_{cl} . In general the approximate interpolation method results in a higher no-slip stiffness.

Table 6.4 illustrates that the error in torsional stiffness does not significantly affect the calculated rotation during loading. In general the approximate interpolation method results in a higher no-slip torsional stiffness than the accurate method (figure 6.33). It follows that the calculated rotation would be slightly more in the case where the accurate method is applied. This proved true in three of the four cases in table 6.3. Figure 6.34 compares the calculated values of a_{cl}, b_{cl} and c_{cl} along the suspended rope length for ropes S11 and S12. As would be expected, the values for a_{cl} and c_{cl} are very similar for the two interpolation methods. However in the case of b_{cl} the difference is larger.

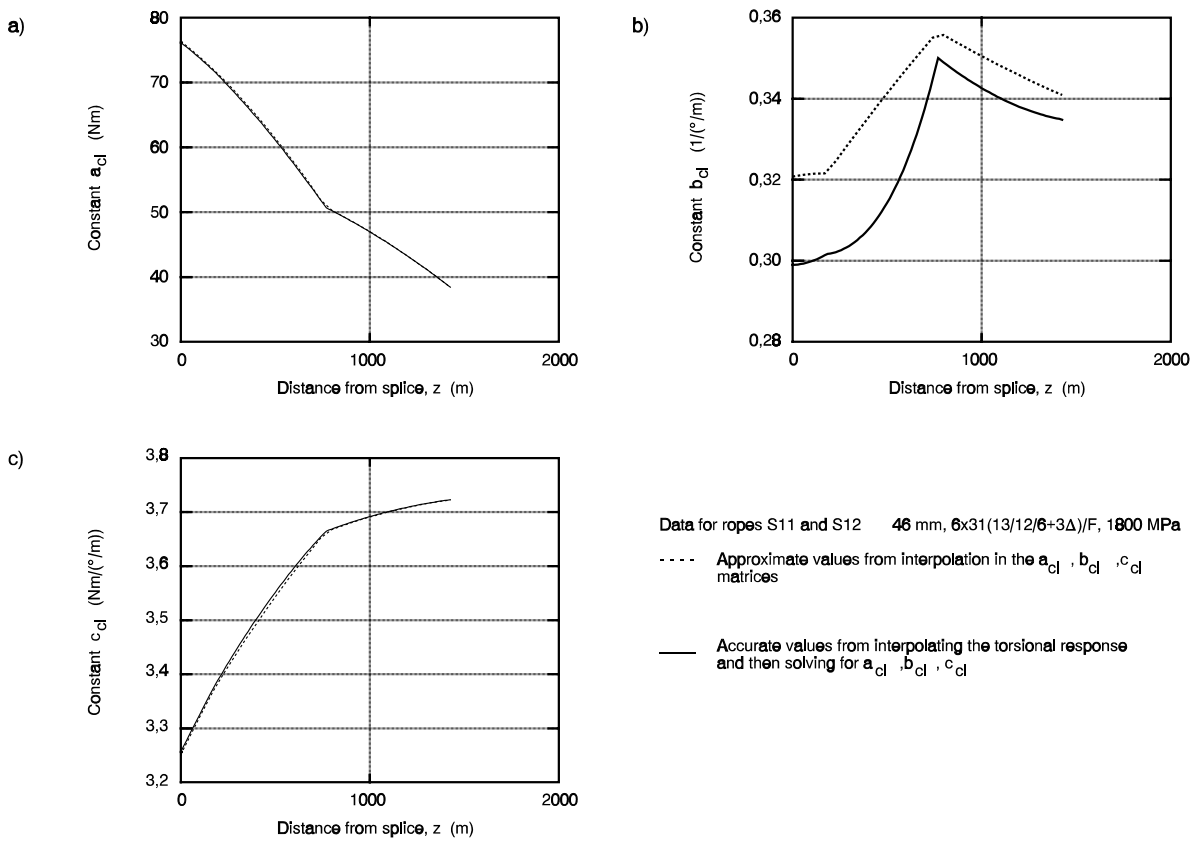

Figure 6.34 - Accurate and approximate methods of determining the torsional response constants at intermediate loads and starting twist values applied to the calculations for ropes S11 and S12.

Interpolation within the a_{cl}, b_{cl} and c_{cl} matrices can result in errors in the calculated torsional response since b_{cl} is not necessarily continuous. These errors are however unlikely to effect the rotation calculations by any order of magnitude. Interpolation within the matrices results in a less complicated and more speedy analysis algorithm compared to one which interpolates the torsional response and then solves for the stiffness constants.

6.5.5 Use of the average twisting up and untwisting torsional responses

Conveyance loading is inevitably a dynamic event. Figure 6.35 was extracted from the data of figure 2.16 and shows detail of the variation in rope end load and torque for a 50 second interval during skip loading. The shaft parameters are identical to those of rope S15 (table C.7) with a maximum suspended rope length of 2196 m.

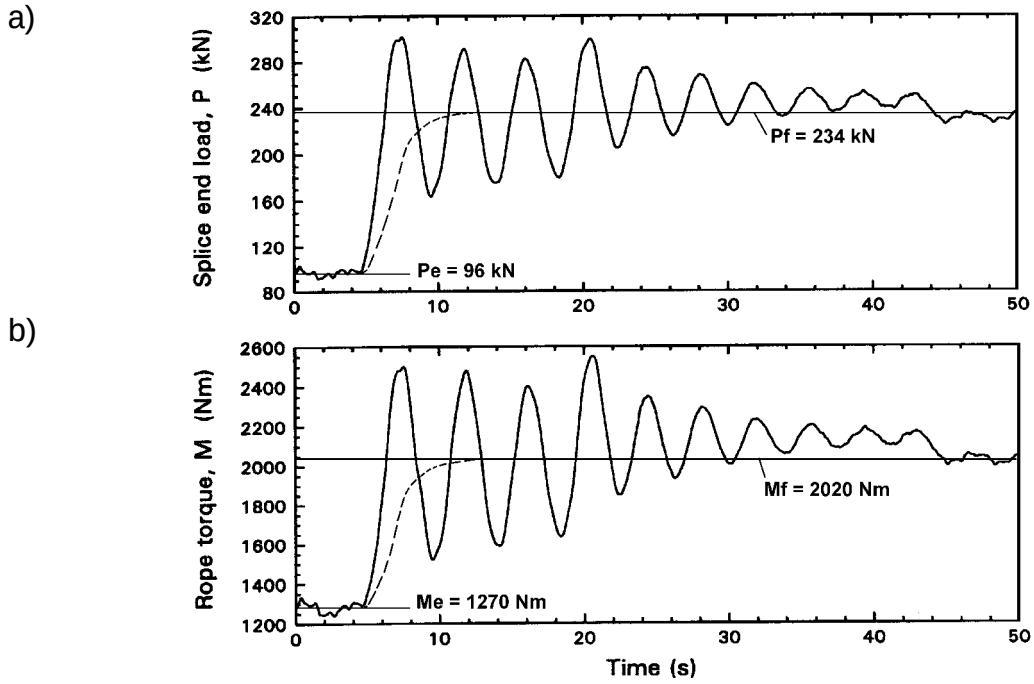

Figure 6.35 - Measured rope end load and rope torque during conveyance loading (Hecker and van Zyl, 1993). Data for rope S15, 48 mm 6x32(14/12/6 + 3Δ)/F, 1800 MPa, RHL. Extracted from measurements of figure 2.16.

It was observed that ropes show torsional oscillation during conveyance loading which are coupled to the longitudinal oscillations. As the rope end load increases at the start of conveyance loading, the lower half of the rope untwists and the upper half twists up from the initial stationary position. The twisting then reverses as the load decreases again. The changes in torque at each position along the rope are greater for twisting up than for untwisting since the rope shows higher torsional stiffness in the twisting up direction (both no-slip and full-slip). Since the analysis presented in chapter five is a static one, it was considered reasonable that the average of the twisting up and untwisting stiffness should be used to determine the final static change in rotation. The favourable comparison between the measured

and calculated rotation results indicates that this assumption is acceptable (figure 6.23). The greater the dynamic oscillations, the more accurate the results should tend to be using the average stiffness values.

If the loading occurred according to the dashed line in figure 6.35a then the torque would probably have increased as shown by the dashed line in figure 6.35b. Under these circumstances the rope would not show torsional oscillations and the untwisting stiffness could be used for the lower half and the twisting up stiffness could be used for the upper half. The calculations for all the results in sections 6.2 and 6.3 were repeated using the different stiffness values for untwisting and twisting up. It was found that in some cases the correlation between the measured and calculated data improved but in other cases it worsened. In general the range of errors increased above that shown earlier in figure 6.23.

It was however apparent that an analysis which takes into account both stiffness values produces a more accurate shape of the rotation along the rope during loading. Figures 6.36 and 6.37 contain examples of the changes in twist and rotation for ropes S4, S18 and S19. Since the splice end untwists, the extent of the twisting is greater to achieve the required change in torque as the torsional stiffness is less than for twisting up. This results in the maximum rotation being displaced towards the splice end of the rope which is more representative of the site observations.

For a static analysis, using the average of the measured twisting up and untwisting stiffness results in the most accurate results. A dynamic analysis, which incorporates the detailed torsional damping properties, would probably return similar values for rope rotation magnitudes but improved general shape of the rotation curves (i.e. skewed towards the splice end).

a)

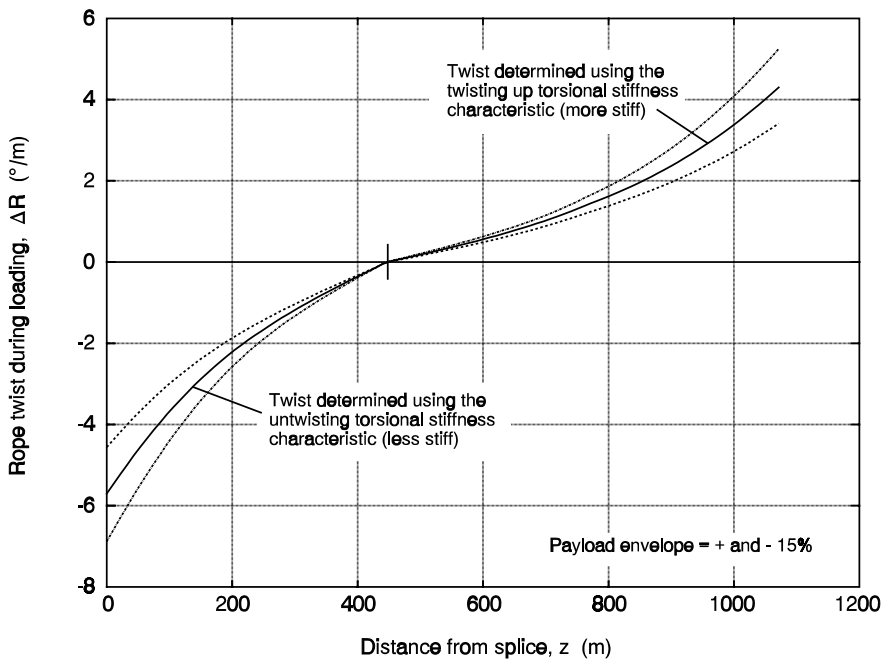

b)

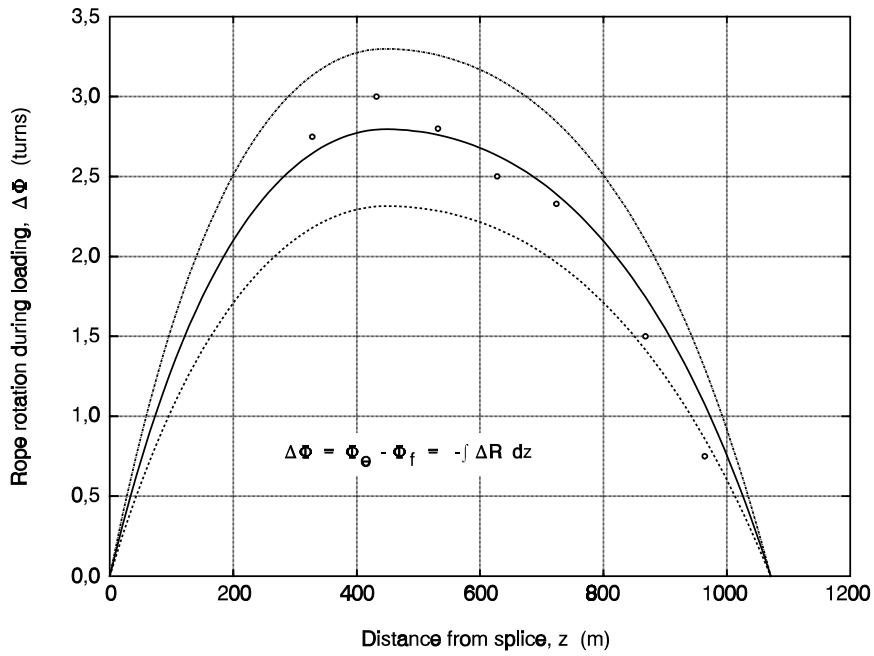

Figure 6.36 - Rope rotation and twist during loading determined using the twisting up and untwisting rope stiffness characteristics. Data for rope S4, 41 mm 6x29(11/12/6 + 3Δ)/F, 1800 MPa, RHL. Compare to figures 6.9a and 6.9b.

a)

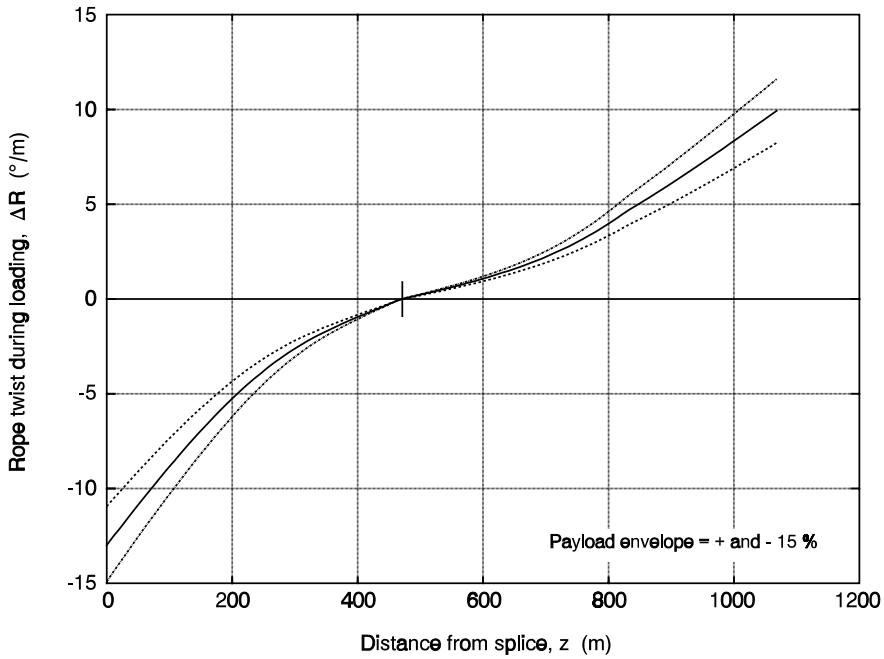

b)

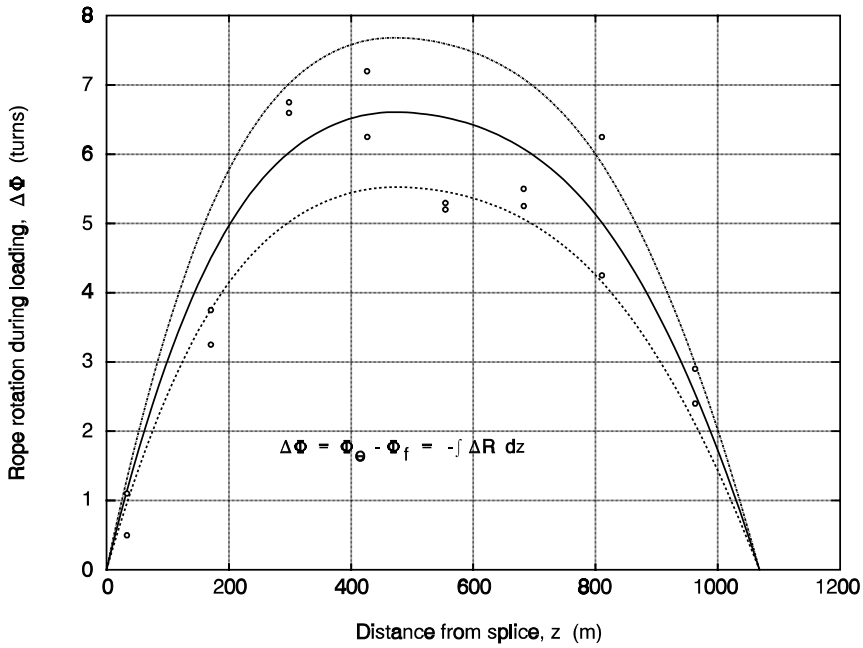

Figure 6.37 - Rope rotation and twist during loading determined using the twisting up and untwisting rope stiffness characteristics. Data for ropes S18 and S19, 49 mm, 6x32(14/12/6 + 3Δ)/F, 1800 MPa, RHL. Compare to figures 6.18a and 6.18b.

6.6 Additional results regarding rope torsional behaviour in general

6.6.1 Rotation of the splice end during detachment from the conveyance

From the empty rotation distribution, Φ_e, it is possible to determine an estimate of the rotation at the splice end when a rope is disconnected form the conveyance as described in section 5.5. Data was obtained from two shafts which are shown in figure 6.38. The twists (42,4 °/m and 62,0 °/m), corresponding to the unconstrained states, were calculated knowing the statutory test lay lengths of the samples cut from the splice ends of the respective ropes. For both examples, the calculated rotation is less than the measured (observed) values. It is likely that the weight of the rope attachments and safety detaching hook caused additional rotation to occur.

a)

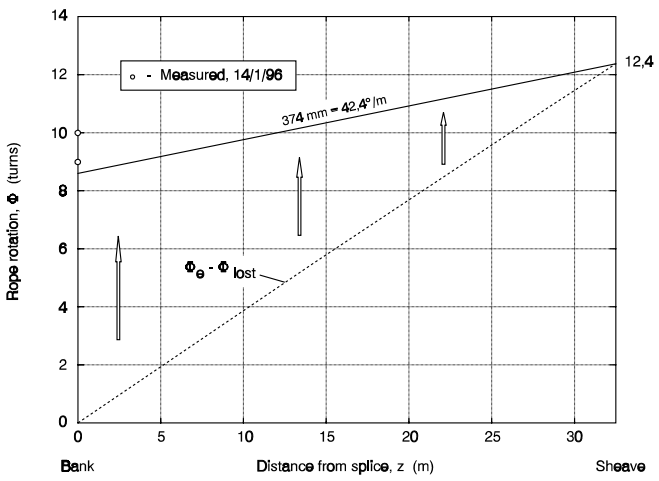

b)

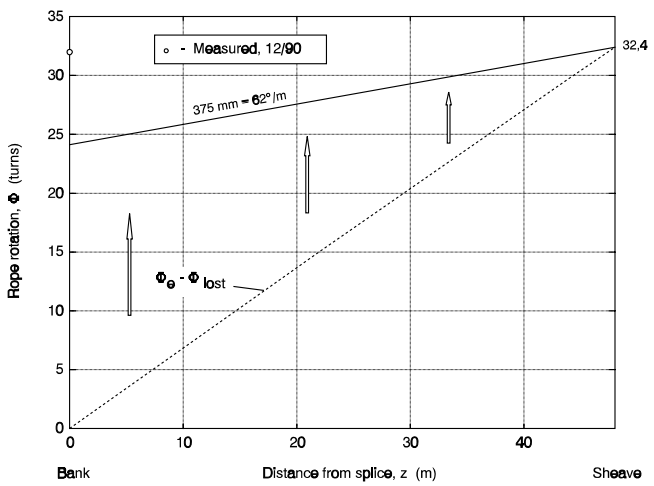

Figure 6.38 - Calculated and measured rotation of the splice end during detachment from the conveyance for a) ropes S9, S10 and b) rope S15, a) refer to figure 6.12c. b) refer to figure 6.15c.

6.6.2 Rope rotation and lay length changes as a result of load release

It has been shown that a rope rotates in the opposite direction (compared to reaching the empty equilibrium state) when the end load is increased above that of the empty conveyance (i.e. $\Phi_f < \Phi_e$, figure 5.27). The opposite is true if the end load is decreased to a value less than the empty conveyance weight. The most likely cause of such a decrease is an abnormal slack rope condition resulting from tight conveyance guides or a foreign object wedging the conveyance in guides. Figure 6.39 compares the lay lengths for an empty conveyance and zero end load for rope S13 at installation and at the date of measurements. It is evident that in both cases the splice end lay length shortens and the sheave end lay length increases as the end load is decreased to zero. The changes in lay length were determined taking full account of the detailed torsional stiffness variation along the rope length. The maximum calculated rotation (Φ_e - Φ_f) is also indicated for both empty conveyance lay length distributions (LL_{ei} and LL_e).

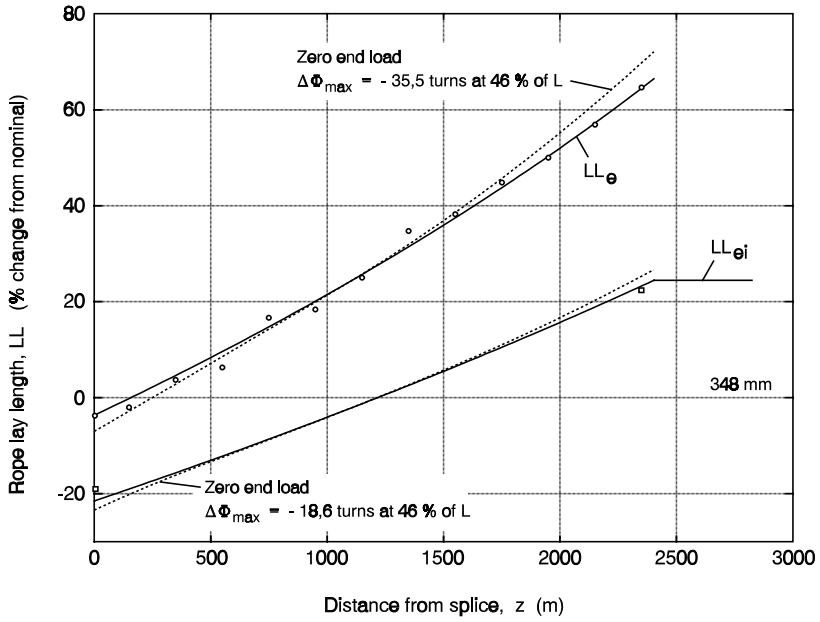

Figure 6.39 - Lay length distributions for an empty conveyance and for zero end load, rope S13, 46 mm, 6x31(12/12/6 + 3Δ)/F, 2150 MPa, RHL. Based on data in figure 6.6d and table 6.1.

The primary concern with slack rope incidents is the formation of kinks and corkscrews at the splice end. With a decrease in end load the splice end lay length shortens which, combined with the low or zero load, makes a rope particularly

prone to distortion. Slack rope conditions are more critical in new ropes (LL_{ei}) than for ropes which have been allowed to unlay (LL_e) since the initial lay length prior to the decrease in end load is shorter. It was noted during the breaking strength tests conducted at different lay lengths (section 1.4) that for lay lengths in the order of 20 percent shortening from nominal, the rope sections were extremely prone to corkscrew formation near zero loads.

6.6.3 Calculation of rope rotation during winder emergency braking

It was shown in section 1.3, figure 1.8, that the maximum rope rotation amplitude during emergency braking increase significantly with an increase in the suspended rope length. The rotation analysis presented in chapter five can be used to calculate expected rotation amplitudes under emergency braking conditions.

As an approximation, it can be assumed that the weight of the empty conveyance (P_e) and the rope weight per unit length (q) would be affected by the system acceleration (a) as follows :

$$P_e = m_e.(g + a) \qquad [6.12]$$

$$q = m_r.(g + a) \qquad [6.13]$$

where : m_e is the conveyance mass and m_r is the rope mass per unit length.

In the case of emergency braking, with the conveyance moving up the shaft, a would assume a negative value. This would have the effect of reducing the apparent weight of the conveyance and the rope weight per unit length. Just as the rope rotation during conveyance loading was calculated by increasing the end load from P_e to P_f, so the rotation during braking can be determined by reducing the load P_e and weight per unit length, q, under the action of negative acceleration.

The torsional hysteresis constants (a_{cl}, b_{cl}, c_{cl}) are calculated using the load distribution, $(P_e + q.z).(g + a)/g$, and the empty conveyance twist distribution before braking, R_e.

Calculations were conducted for rope T9, 46 mm, 6x31(13/12/6 + 3Δ)/F, 1800 MPa for a = -g/4, -g/3, -g/2 m/s² and at suspended lengths of L = 760, 2000, 3000 and 3500 m. Hamilton (1997) reported that the nominal acceleration during emergency braking for drum winders in South Africa is 2,5 m/s². Stewart (1993) stated that in general, the acceleration at the conveyance should not exceed 5 m/s². Based on these references a range of acceleration between -g/4 to -g/2 m/s² was considered realistic. The empty conveyance weight (P_e) was calculated according to a rope selection factor of 25000/(4000 + L) an a skip weight to payload ratio of 0.68.

In conducting the site experiments for section 1.3, it was noticed that the rotation of the ropes during braking occurred initially in one direction only until the maximum amplitude was reached (to the left for the RHL ropes). Thereafter, rotation was in the opposite direction by an equivalent amount with subsequent decay as the system reached a steady state. Figure 6.40 illustrates the time based response of the rope under emergency braking conditions as observed on site.

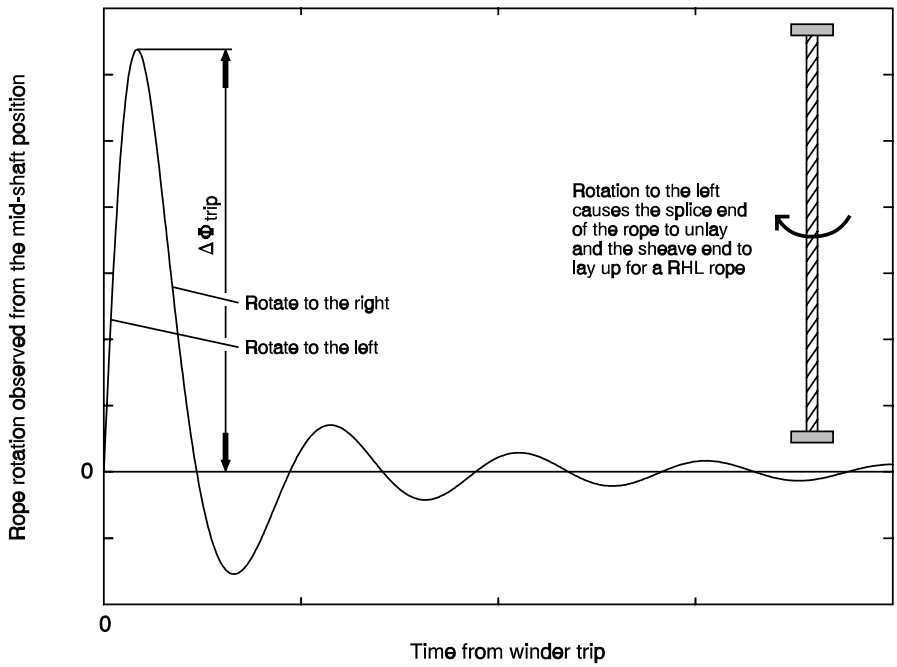

Figure 6.40 - Schematic illustration of the mid-shaft rope rotation during winder emergency braking. The response represents the rope rotation behaviour observed during the site experiments conducted for section 1.3. The skips were hoisted empty from the loading stations and the winders were tripped at rope speeds of approximately 10 m/s.

Since the rotation, in reaching the maximum amplitude $\Delta\Phi_{trip}$, is in one direction only the rotation calculation must consider the untwisting and twisting up hysteretic properties for the lower and upper halves of the suspended rope respectively.

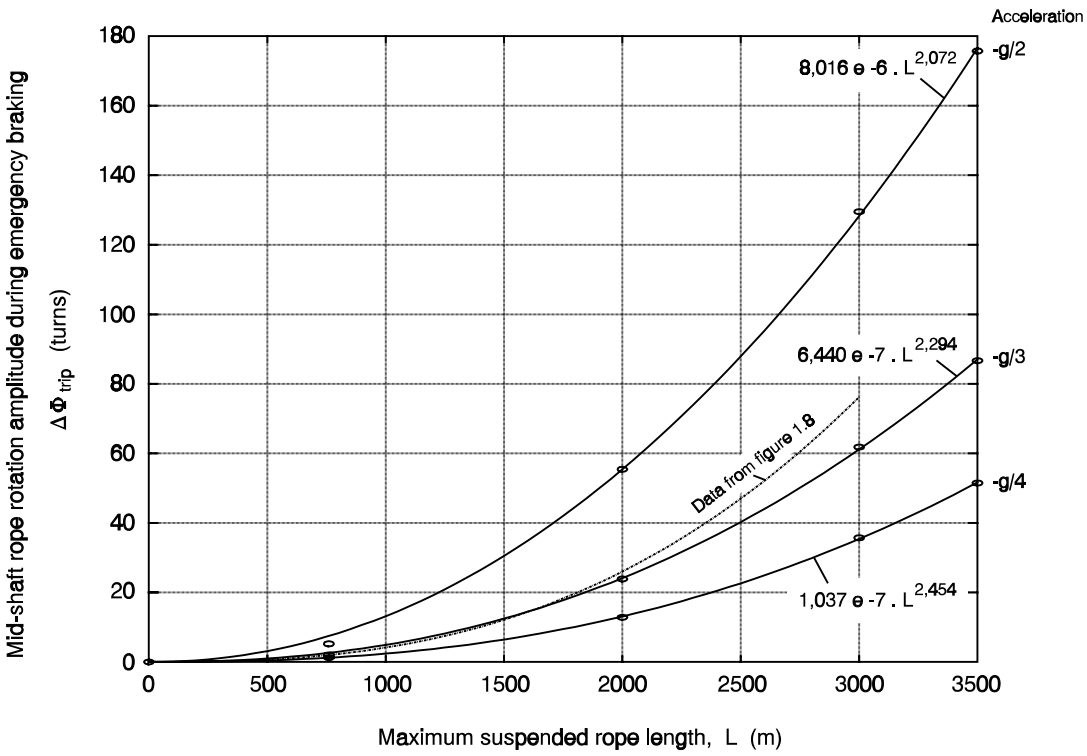

Figure 6.41 - Calculated maximum rope rotation amplitude during winder emergency braking for an empty conveyance being hoisted up the shaft. Rope T9, 46 mm, 6x31(13/12/6 + 3Δ)/F, 1800 MPa. Refer to figure 1.8.

Figure 6.41 shows the results of the calculations on the 46 mm rope at the various depths and accelerations. Equations of the form [1.1] were fitted though the calculated data. The line representing the observations of figure 1.8 is also shown. It was not possible to determine the exact acceleration values for the two systems discussed in section 1.3 but the data shows good correlation to the line representing 3,27 m/s². This example demonstrates the suitability of the modelling approach described in chapter five for simple investigation of rope behaviour under dynamic conditions. The information of figure 6.41 suggests that quite substantial rotation amplitudes could be expected at 3500 m which would be very much dependant on the system acceleration. The effects of large rotation amplitudes on rope endurance have not been quantified but intuitively it is expected that they could be detrimental to rope life (torsional fatigue). Careful consideration of winder

brake control is therefore required for very deep shafts to limit the actual acceleration values. It is understood form investigations such as those of Hamilton (1997) that sophisticated winder brake control systems are being considered for the very deep shafts to limit the peak rope loads associated with emergency breaking. These systems will also result in lower torsional oscillations of the hoisting ropes.

It is noted that the direction of rope rotation during emergency braking with the conveyance moving up the shaft is opposite to the case where only the rope end load is decreased (section 6.6.2). The 46 mm rope was chosen for this analysis because of it being the largest diameter for which hysteresis data (a_{cl}, b_{cl}, c_{cl}) was available up to 3500 m suspended length (twist and load range).

7 DISCUSSION

Chapter summary : It has been found that torsional hysteresis, which is evident when triangular strand ropes are twisted at constant load, has a very significant effect on the rotational behaviour of ropes operating in mine shafts. An example is given which shows that substantial errors can result if the hysteretic behaviour is ignored when calculating rope rotation during conveyance loading. Equally important in the modelling of torsional deformation of suspended triangular strand ropes is the determination of realistic in-service rotation boundary conditions. These are a function of the difference between the free lay length of the torsion test specimen and the manufactured lay length of the in-service rope. Maintenance practices can also have a major influence on the rotation boundary conditions which in turn result in variations of the rope lay lengths as the service period progresses. The results of an analysis identifying the parameters which are most important as regards rope torsional behaviour are presented. Based on the conclusions drawn from the parametric analysis, a discussion on the probable depth limit of application for triangular strand ropes operating on drum winders is given. Possible solutions to the problems which may be encountered at depths of up to 3500 m are considered. The information contained in this chapter is intended to be of practical interest as it gives insight into the likely torsional behaviour of triangular strand ropes in future shaft systems.

7.1 The importance of considering torsional hysteresis

Through this study it has become clear that torsional hysteresis constitutes a first order effect, as regards the rotational behaviour of triangular strand ropes, which cannot be ignored. Laboratory torsion tests, which were discussed in chapter four, showed that inter-wire friction can result in an order of magnitude difference in the measured torsional stiffness of a rope, depending on the extent of the applied twist, under conditions of constant load.

Hecker and van Zyl (1993) and Rebel et al. (1996a) presented rope rotation calculations in which the rotation distribution for the loaded conveyance was determined using the same method as for the empty conveyance (i.e. P_e replaced with P_f in equation [5.8]). The change in rotation during loading was determined by subtracting the loaded rotation from the empty rotation distribution. This approach neglected hysteresis effects in the torsional response resulting in considerable errors since only data from the constant twist tests were taken into account. Torsional stiffness data can be inferred from the constant twist test results, equation [5.15]. However, the values represent the full-slip stiffnesses which may be substantially less than the no-slip stiffnesses. During the constant twist tests, the change in twist for each load cycle occurs at relatively low load (≈ 30 kN, figure 3.21) where inter–wire friction does not contribute significantly to the change in torque. In theory, the full-slip stiffnesses determined from the constant load tests (c_{cl}) should be very similar to the stiffness values calculated by equation [5.15]. The data presented earlier in figure 4.12 are a further contribution to the same argument. It was shown that the change in torque for large angles of twist in a constant load test correspond closely to the changes in torque at the same constant loads and twist ranges in the constant twist test.

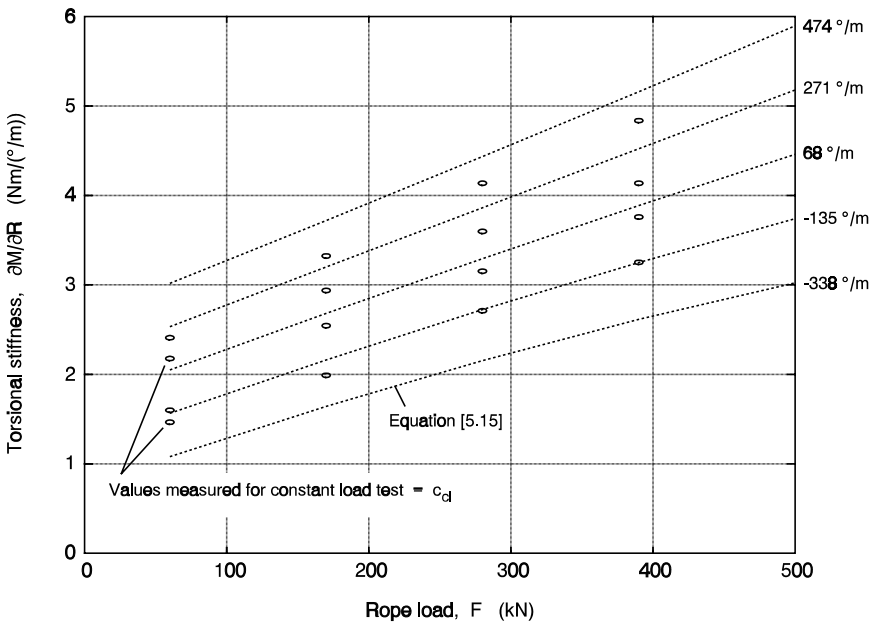

Figure 7.1 - Comparison between torsional stiffness inferred from the constant twist test and the full slip stiffness (c_{cl}) determined from the constant load tests, 46 mm, rope T9, 6x31(13/12/6 + 3Δ)/F, 1800 MPa. The individual data points represent the untwisting full-slip stiffness values measured for the starting twists indicated on the right. Dashed lines from equation [5.15].

Figure 7.1 indicates that the difference between the full-slip stiffness values for the two tests types are small. The constant load test stiffnesses were determined for untwisting only and the twist increments for the constant twist test were in the untwisting direction. For rope S13, figure 6.6b, the maximum rotation during loading ($\Delta\Phi_{max}$) was calculated to be 46,7 turns (as opposed to 13,0) using only the relationships described by equation [5.3]. Figure 7.2 compares the rotation prediction based on the method of Hecker and van Zyl (1993) and the method presented in chapter 5 which takes full account of torsional hysteresis. In general, it was found that ignoring the non-linear relationship between torque and twist at constant load resulted in rotation predictions which were between 3 to 5 times greater than the rotations observed on site.

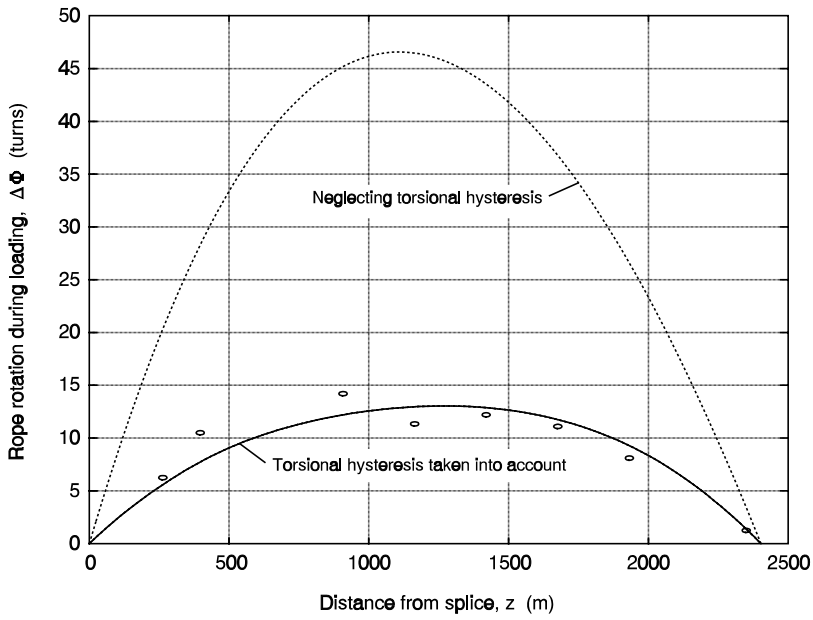

Figure 7.2 - Effect of torsional hysteresis on the calculation of rope rotation during conveyance loading, rope S13, 46 mm , 6x31(13/12/6 + 3Δ)/F, 2150 MPa, measured data from figure 6.6b.

Torsional hysteresis is however not taken into account in determining the empty conveyance lay length distributions (example, figure 6.6c). The changes in rotation (or twist) from the manufactured state (Φ_{coil}) to the installation equilibrium values (Φ_{ei}) are large in comparison to the rope rotation during conveyance loading and are therefore dominated by the full-slip torsional stiffness values. It was shown in figure 7.1 that the full-slip stiffness measured under constant load conditions is comparable to the torsional stiffness inferred from the constant twist tests. It is

therefore acceptable to calculate in-service lay length changes using only the constant twist test data.

7.2 Effects of in-service rotation boundary conditions

Hermes and Bruens (1957), Hankus (1995), Hecker and van Zyl (1993) and Rebel et al. (1996a) all assumed that, in the general case of a suspended rope, the rotation boundary conditions at the bottom (splice) and top (sheave) ends are zero. The theory presented in sections 5.3 and 5.4 showed that this assumption was not realistic for a drum winding installation. The rotation distribution after installation for the 46 mm rope data (S13) of figure 6.6c is reproduced in figure 7.3 along with the rotation distribution for the approximate boundary conditions.

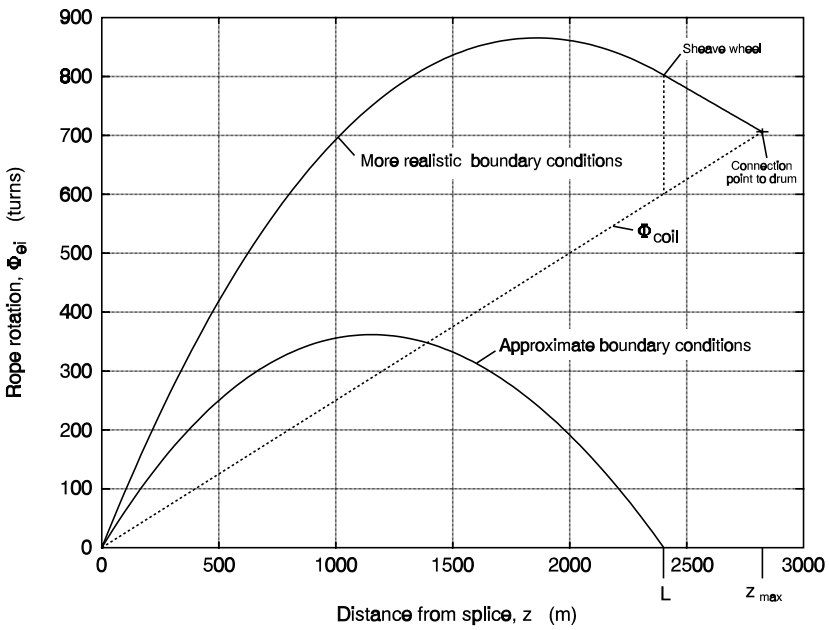

Figure 7.3 - Comparison of the effect of rotation boundary conditions on the general rotation distribution in a suspended rope, data for a 46 mm rope, S13, 6x31(13/12/6 + 3Δ)/F, 2150 MPa, more realistic data from figure 6.6c. $\Phi_{coil} = R_{coil}.z$.

The noticeably different slopes of the curves are evident. This affects the calculated lay lengths which are shown in figure 7.4. It is important to determine the boundary conditions accurately as these have a significant effect on the lay length distribution. The hysteretic torsional properties are in turn dependant on the rope

lay length, therefore the rotation calculations will also be affected by incorrectly calculated lay length values. The accuracy of the calculated rotation boundary conditions depends on the accuracy of the "on-tension" lay length measurement during manufacture (figure 5.1) and on the amount of rotation that is lost from the rope during the installation process. In both cases, if care is taken, the respective values can be accurately quantified.

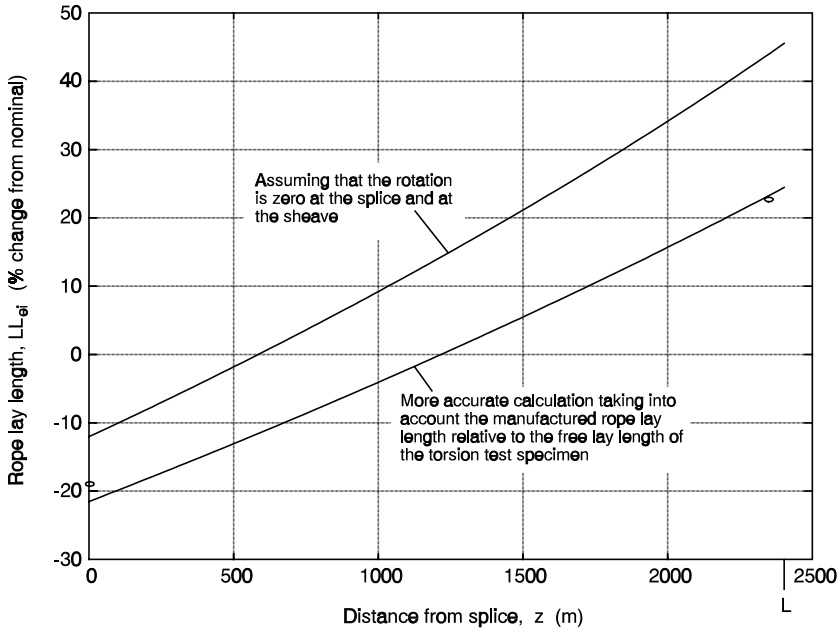

Figure 7.4 - Effect of rotation boundary conditions on the calculated lay lengths at installation, data for the 46 mm rope, S13, 6x31(13/12/6 + 3Δ)/F, 2150 MPa, more accurate data from figure 6.6d.

Even in the case where the twist (R_{coil}) associated with the manufactured lay length is zero the rotation boundary condition at the sheave (*SWbc*) would assume a positive value (figure 5.13).

The errors associated with assuming zero rotation boundary conditions are evident in the analysis of Hecker and van Zyl (1993). In their calculations, the splice and sheave end lay lengths were determined to be -11,4 percent and + 28,8 percent different from the nominal values compared to -18,3 and + 25,8 percent by the more accurate method (rope S15, figure 6.15d, LL_{ei}). The empty torque at installation was calculated as 1055 Nm compared to 1345 Nm when taking full account of the difference between the manufactured and zero twist lay lengths. The sheave end value (28,8 percent) is only coincidentally close to the more accurate

value and could have been quite different had the same torsional properties been used as was the case for the calculations of figure 7.4. Using the 48 mm rope (T10) torsional properties determined in this study and the zero boundary conditions, the splice and sheave end lay lengths were found to be -11,15 percent and +40,6 percent. These values represent substantial errors compared to those produced by using the realistic boundary conditions. A further limitation of the investigations of Hecker and van Zyl (1993) was that relatively small twists were applied during the torsion testing, –75 °/m to +75°/m, compared to –337 °/m to +270 °/m for this investigation (rope T10). The considerably larger twist range is more representative of in–service torsional deformations.

It must be noted that the difference between the zero twist lay length (LL_0) and the manufactured lay length (LL_m) is the most significant factor in the preceding argument. Also, if the zero twist lay length and the free lay length of the in-service rope (when new) are very different then the calculated torque prediction may be affected. At some point of unlaying, during the service period, the splice and sheave end rotation values will be equal (Φ_{lost} = *SWbc*). This condition then represents the same lay length distribution as when the rotation values at either end are assumed to be zero.

7.3 Factors influencing in-service torsional behaviour and the implications for future shaft systems

The encouraging correlation between the measured and calculated results presented in chapter six (figures 6.22 and 6.23) showed that the analysis method of chapter five is capable of producing acceptably accurate predictions of in-service torsional behaviour for varying shaft depths and rope diameters. Such a verified modelling approach is a most useful tool for investigating the behaviour of triangular strand ropes in future applications. The large variability in the parameters of the eleven shaft installations did not allow for conclusions to be drawn directly from the measured site data. A study of how variations in the parameters affect in-service behaviour was therefore necessary to determine which are most important as regards torsional deformations.

It is evident, from the analysis presented in chapter five, that there are a number of factors which have an influence on the in-service lay length changes, rope rotation during conveyance loading and the associated constant rope torques. For a particular rope construction with certain characteristic torsional properties, these factors include :

- Rope weight per unit length (q)
- Empty conveyance weight (P_e)
- Loaded conveyance weight (P_f)
- Maximum suspended length (L)
- Lay length at which the rope was manufactured ($LL_m \equiv R_{coil}$)
- The length of rope from the sheave to the drum connection point (z_{max} - L)
- Rope diameter (d_{nom})
- Amount of rotation released from the rope during installation and maintenance operations (Φ_{lost})

7.3.1 Selection of shaft parameters for analysis

Amongst others, Laubscher (1995) presented a new equation, [7.4], for calculating rope selection factors (*RSF*) for drum winders. Although this equation has not yet been fully implemented in practice, it soon will thereby enabling the maximum utilisation of drum winder rope load carrying capacity. It was therefore assumed that all payloads and conveyance weights calculated should be based on the new rope selection factor equation. The selection factor reduces as the suspended length of the rope increases :

$$RSF = \frac{25000}{4000 + L} = \frac{EBL}{F_{max}} \qquad [7.4]$$

where : L = maximum suspended length (m)

EBL = estimated rope breaking load (kN)

F_{max} = maximum static load applied to the rope, including rope weight (kN)

It is common practice in the mining industry to measure the efficiency of conveyance design by the ratio of conveyance weight to the payload which it can carry :

$$f_s = \frac{weight\ of\ conveyance}{payload} = \frac{P_e}{P_f - P_e} \qquad [7.5]$$

The ratio, f_s, is often termed the "skip factor". Examination of the design records of a major South African mining company revealed that on average the value of f_s is 0,68 for rock skips and between 1,0 and 1,1 for man cages. The ratios examined included all safety and rope attachments as well as the conveyance guide roller sets in their calculation.

The maximum static load applied to the rope would be in the case of maximum suspended rope length with a fully loaded conveyance :

$$F_{max} = Payload.(1 + f_s) + q.L \qquad [7.6]$$

Combining equations [7.4] and [7.6] yields an equation for the allowable payload which can be carried :

$$Payload = P_f - P_e = \frac{\frac{EBL.(4000 + L)}{25000} - q.L}{(1 + f_s)} \qquad [7.7]$$

Therefore, for the all the analyses in this section the following two equations were used to calculate the empty and loaded conveyance rope end loads :

$$P_e = \frac{\frac{EBL.(4000 + L)}{25000} - q.L}{(1 + f_s)} . f_s \qquad [7.8]$$

$$P_f = \frac{EBL.(4000 + L)}{25000} - q.L \qquad [7.9]$$

The relevant parameters of the ropes considered in the investigation are listed in table 7.1. Calculations were conducted for each of the seven rope diameters for which torsion test data was available. The suspended lengths were taken at 500, 1000, 1500, 2000, 2500, 3000 and 3500 m. The ratio f_s was set equal to 0,68. It was initially assumed that the ropes were all manufactured (closed) at their nominal lay lengths plus 3,71 percent which is the average value of the 122 ropes considered in figures 5.2 and 5.3. The distance between the sheave and the drum connection point (z_{max} - L) was set equal to 370 m which is equal to the average length for the 32 winding installations associated with the 122 ropes of figures 5.2 and 5.3. For q and EBL the catalogue values were used (Haggie Rand, 1987).

Table 7.1 - Details of ropes considered in investigating the factors influencing torsional behaviour. The rope numbers (T#) correspond to the ropes listed in tables 4.3 and 4.4.

Nominal diameter d_{nom} (mm)	Weight per unit length q (kN/m)	Tensile grade $S_{u,wire}$ (MPa)	Nominal lay length LL_{nom} (mm)	Estimated breaking load EBL (kN)	Measured new rope breaking load (kN)
25 (T1)	0,0257	1800	188	451,3	471
40 (T4)	0,0665	1800	300	1160	1243
41 (T8)	0,0705	1800	309	1231	1292
46 (T9)	0,0887	1800	348	1541	1594
48 (T10)	0,0962	1800	361	1669	1708
49 (T11)	0,0995	1800	368	1727	1826
54 (T12)	0,1229	1950	409	2257	2369

An estimate of the lay length variation along a suspended length of rope at installation can also be determined by a graphical method which is described in detail in Appendix D. The graphical method was found to return the same results as the numerical scheme (section 5.3, table 5.2) used for the calculations shown in chapter 6. The difference is that the numerical method calculates the lay length distributions knowing the in-service boundary conditions. The graphical method relies on empirical knowledge of the position along the suspended length at which the manufactured lay length (LL_m) occurs. During the parametric study for this section, these values were determined and are presented in appendix D.

There is an obvious practical application for a graphical approach since it eliminates the need for numerical schemes to calculate lay length distributions. It can also be used in reverse, i.e. if the lay lengths and the splice and sheave end loads of an in–service rope are known then the equilibrium torque in can be determined. The data required for the graphical method can readily be generated using the torsion testing machine described in section 3 (constant twist tests).

7.3.2 Rope diameter

Figure 7.5 shows how the calculated rope lay lengths vary at installation for increasing depth for the seven diameters (table 7.1). Although there is not a distinct pattern, the ropes of smaller diameter exhibit smaller variations in the splice and sheave end lay lengths than those of larger diameter. The difference increases as the maximum suspended length increases. In the case of the 40 mm rope, the constant twist test was conducted starting at the most unlaid position, with the twist increments in the laying up direction. For all the other ropes the twist increments were in the unlaying direction. It is believed that this affected the results for the 40 mm rope.

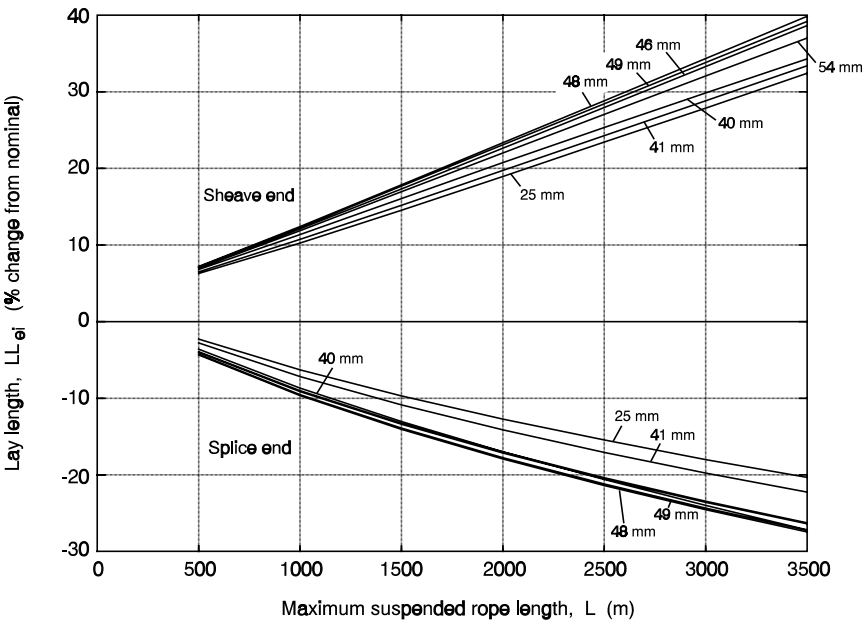

Figure 7.5 - Calculated variation in splice and sheave end lay lengths for different rope diameters and shaft depths, z_{max} - L = 370 m, LL_m = 1,0371.LL_{nom}, f_s = 0,68. Empty conveyance end load according to equation [7.8]. Nominal weight per unit length, q, used.

For lay length shortening at the splice end, it can be seen that a 41 mm rope would show approximately the same change in lay length at 3500 m that the 48 mm and 49 mm ropes would have at 2650 m. Similar observations can be made at the sheave end, but the differences there are less because of the increased slope of the lines.

Figure 7.6 indicates the maximum rope rotation values calculated for the diameters from 41 mm to 54 mm. Detailed torsional stiffness data (a_{cl}, b_{cl} and c_{cl}) for the 25 mm and 40 mm rope were not available. Where the curves are truncated, either the load or twist values exceeded the ranges for which values of a_{cl}, b_{cl} and c_{cl} had been determined. The trend is for the rotation to increase with an increase in diameter except in the case of the 54 mm rope. The larger diameter (54 mm) could have a higher stiffness as a result of a size effect. The tensile grade of the rope wires for the 54 mm specimen was 1950 MPa compared to 1800 MPa for the other specimens which is unlikely to have influenced the results (Yiassoumis, 1992). For all the diameters shown in figure 7.6, the maximum rotation increases with the square of depth up to 2000 m. Between 2000 m and 3500 m the further increase in rotation with depth tends to be linear.

If the earlier analyses discussed in sections 7.1 and 7.2 had been applied to these calculations, very short lay lengths at 2500 m suspended length would not have been identified. The errors would have arisen since the previous methods did not recognise that ropes may be installed on winders with considerably shorter lay lengths than the zero twist lay lengths of the tension-torsion tests. At the sheave end, the calculated lay lengths would have been longer than is the case in figure 7.5. Values for the rotation calculations would in general have been 3 to 5 times greater as was shown in the example of section 7.1.

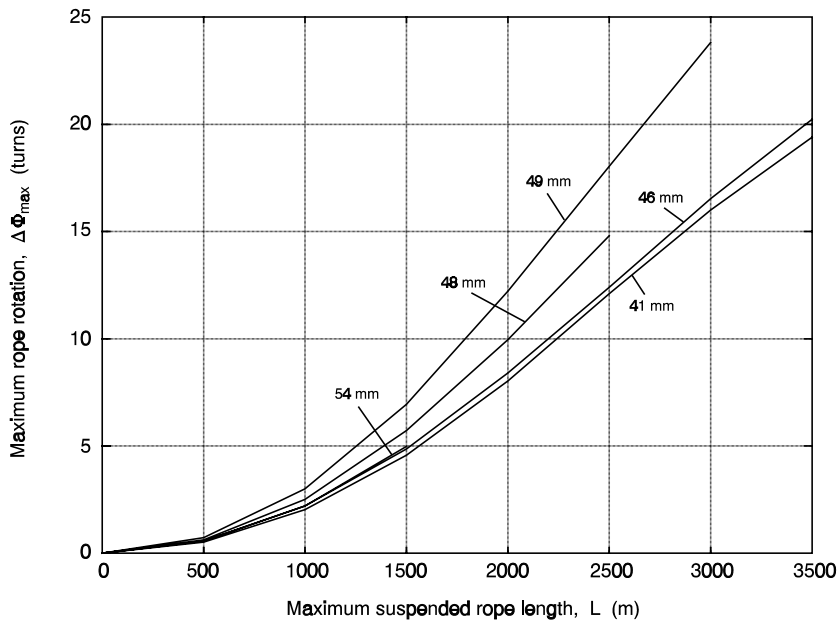

Figure 7.6 - Calculated variation in the maximum rope rotation during conveyance loading for different rope diameters and shaft depths, z_{max} - L = 370 m, LL_m = 1,0371.LL_{nom} , f_s = 0,68. Payload according to equation [7.7].

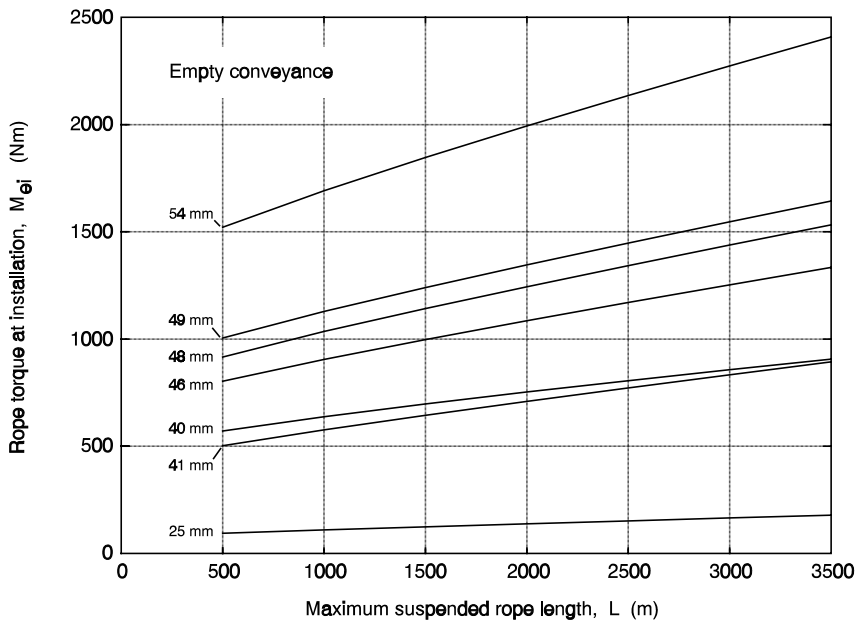

Figure 7.7 - Calculated variation in rope torque for different rope diameters and shaft depths, $z_{max} - L$ = 370 m, LL_m = 1,0371.LL_{nom}, f_s = 0,68. Empty conveyance end load according to equation [7.8]. Nominal weight per unit length, q, used.

Figure 7.7 shows the variation of the equilibrium rope torque for an empty conveyance for the seven rope diameters and changing depth. For a given diameter, the increase in torque is approximately linearly related to the maximum suspended length. At a given suspended length, the torque increases with diameter to the power of 3,28 ($M_{ei} \approx Constant.d_{nom}^{3.28}$). It was found that the average ratio of loaded torque to empty torque (M_{fi} / M_{ei}) equalled 1,98 at 500 m; 1,60 at 2000 m and 1,38 at 3500 m.

Figure 7.8 indicates that the maximum allowable load which can be attached to the end of a rope decreases with an increase in the suspended length, equation [7.9].

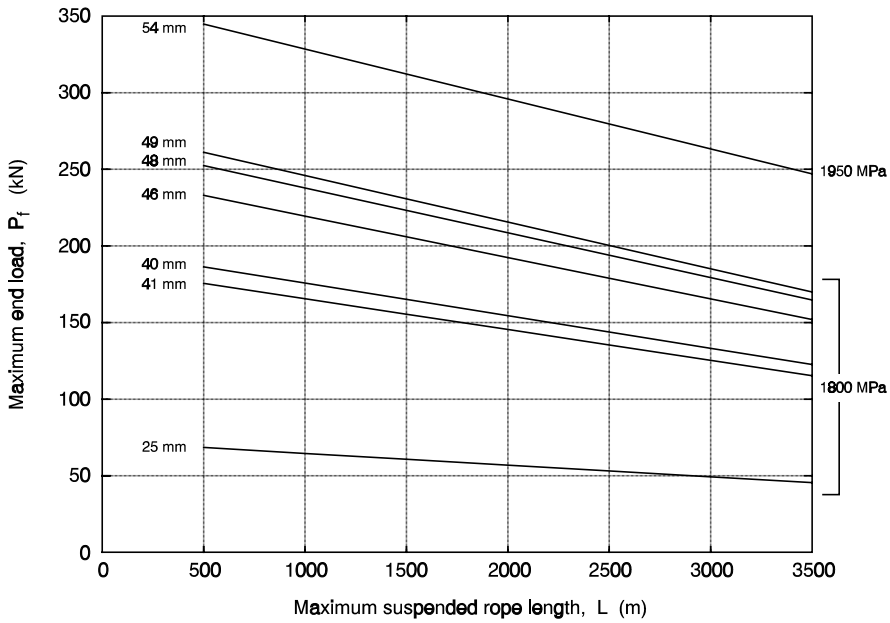

Figure 7.8 - Calculated variation in the maximum allowable end load for different rope diameters and shaft depths, equation [7.9].

7.3.3 Rope weight per unit length

It was also of interest to investigate the effect of varying the rope weight per unit length for a constant diameter. The 46 mm rope was chosen for this purpose as it was the largest diameter for which torsional stiffness data was available up to 3500 m suspended length. Calculations were conducted with the rope weight per unit length, *q*, increased and decreased by 10 percent. The estimated breaking load (*EBL*) was not altered. A variation in *q* implies a variation in the strength to weight ratio of the rope. Figure 7.9 shows the influence which changes in *q* has on the

installation lay lengths at different depths. A rope of lighter weight per unit length (0,9.*q*) shows smaller changes in lay length both at the splice and sheave ends, as would be expected.

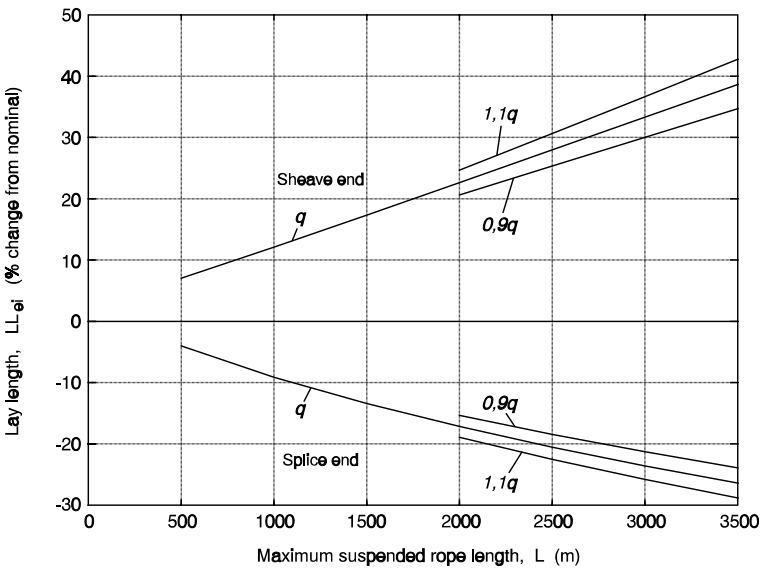

Figure 7.9 - Calculated variation in splice and sheave end lay lengths for changes in the rope weight per unit length at different depths. 46 mm, rope T9, z_{max} - L = 370 m, LL_m = 1,0371.LL_{nom} , f_s = 0,68

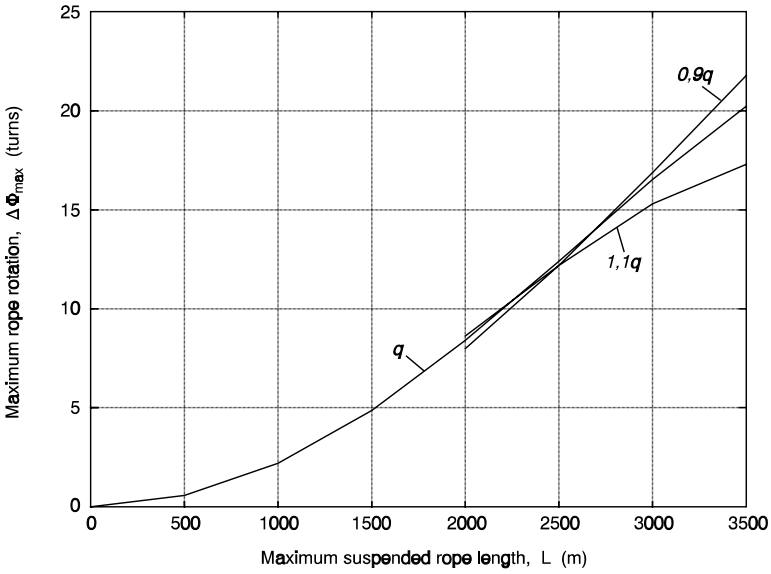

Figure 7.10 - Calculated variation in the maximum rope rotation during conveyance loading for changes in the rope weight per unit length at different depths. 46 mm, rope T9, z_{max} - L = 370 m, LL_m = 1,0371.LL_{nom} , f_s = 0,68

The effect of q on rope rotation is shown in figure 7.10. The lighter rope is capable of supporting larger payloads and therefore the rope rotation during loading would be greater. The increase in rope rotation due to the higher payloads is however opposed by the decreased rotation resulting from the smaller lay length differentials. Therefore, rotation during conveyance loading varies only marginally for the differing rope weights per unit length. In terms of minimising lay length changes, ropes with higher strength to weight ratios would be preferred. For a given diameter and construction, improvements are usually achieved by increasing the tensile grade of the rope wires (Fuller and Wainwright, 1967).

7.3.4 Influence of conveyance weight to payload ratio

It was stated earlier that the ratio of conveyance weight to payload was assumed to be 0,68 based on mining company records for rock hoisting. It is possible to improve this ratio and values as low as 0,42 can be achieved with the use of aluminium alloys as the primary conveyance construction material (Albert and McIvor, 1988). In the case of a poorly designed rock skip, or one which is required to carry heavy loads from the underside the ratio can exceed 1. As mentioned earlier, man cages typically would have ratios above 1. For this section, a range for f_s from 0,4 to 1,4 was therefore assumed. Figure 7.11 shows the effect which the ratio has on the installation lay lengths.

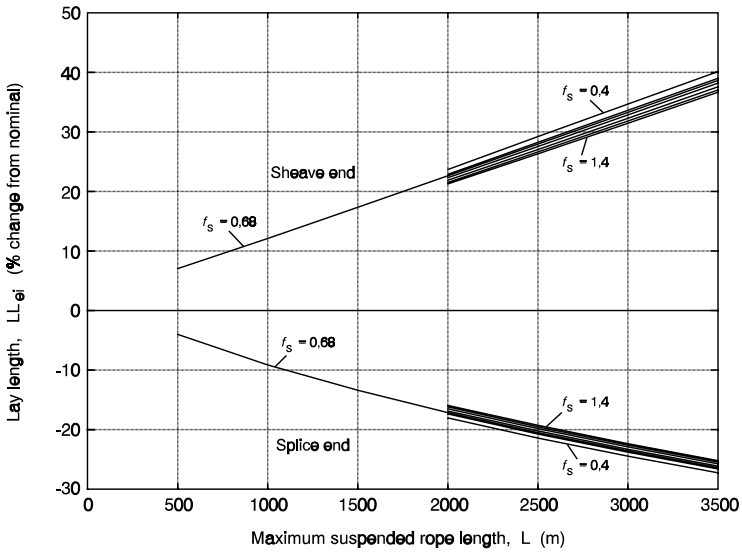

Figure 7.11 - Calculated variation in splice and sheave end lay lengths for changes in the conveyance weight to payload ratio at different depths. 46 mm, rope T9, $z_{max} - L$ = 370 m, LL_m = 1,0371.LL_{nom} .

The heaviest conveyance (f_s = 1,4) results in the least changes in lay length at all depths with the opposite being true for the lightest conveyance (f_s = 0,4). The variation is however not very significant. Rope rotation, figure 7.12, is more markedly affected by the ratio, f_s. For a given rope breaking strength, the lighter the conveyance, the heavier the payload would be. Larger payloads give rise to increased rope rotation during loading.

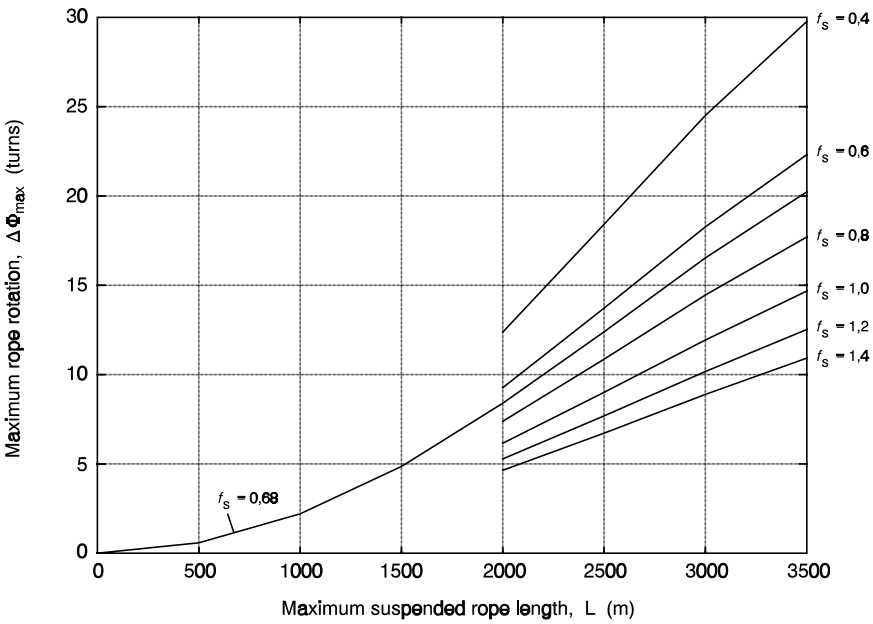

Figure 7.12 - Calculated variation in the maximum rope rotation during conveyance loading for changes in the conveyance weight to payload ratio at different depths.
Rope T9, 46 mm, z_{max} - L = 370 m, LL_m = 1,0371.LL_{nom} .

7.3.5 Manufactured lay length

Lang's lay triangular strand ropes can be manufactured (closed) with different lay lengths. In the preceding sections, it was assumed that the ropes were all manufactured at their nominal lay lengths (LL_{nom}) plus 3,71 percent. The manufactured lay length (LL_m) has a significant effect on the lay length changes at installation, figure 7.13. Although the rope closing specifications allow for the lay length to be in the range LL_{nom} to 1,05.LL_{nom} it is possible to exceeded this range. Other than manufacturing anomalies, the most probable cause of an increases in lay length is the loss of rotation from the rope during installation. A longer rope will however be less affected by a given loss in rotation than a shorter rope. If rotation is lost from a rope, it has the same effect as if the rope was manufactured (closed)

with a longer lay length. Figure 7.13 shows that the sheave end lay length is affected considerably more than the splice end by changes in LL_m .

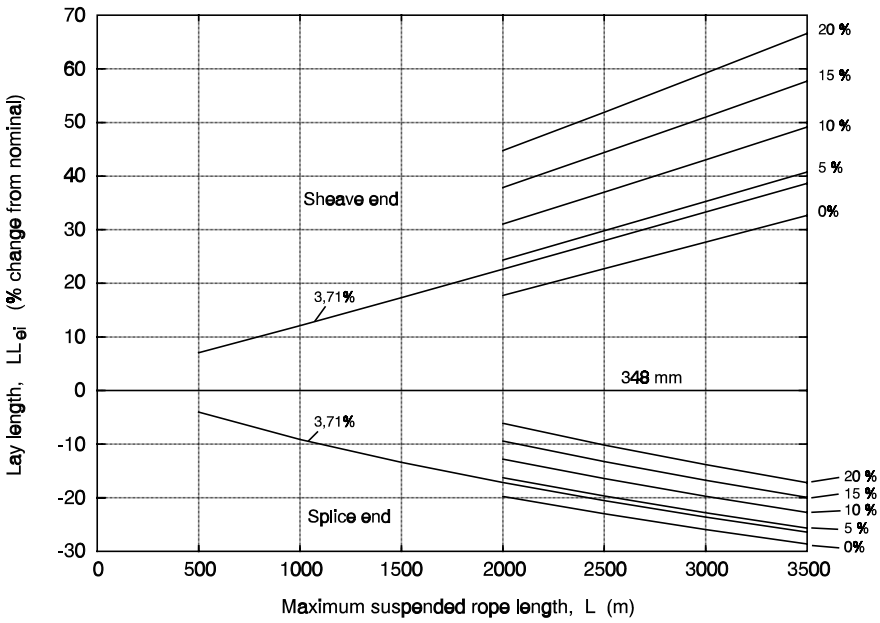

Figure 7.13 - Calculated variation in splice and sheave end lay lengths for changes in the manufactured lay length at different depths. In all cases, the percentage values indicate the increase in LL_m from LL_{nom} , 46 mm, rope T9, z_{max} - L = 370 m, f_s = 0,68.

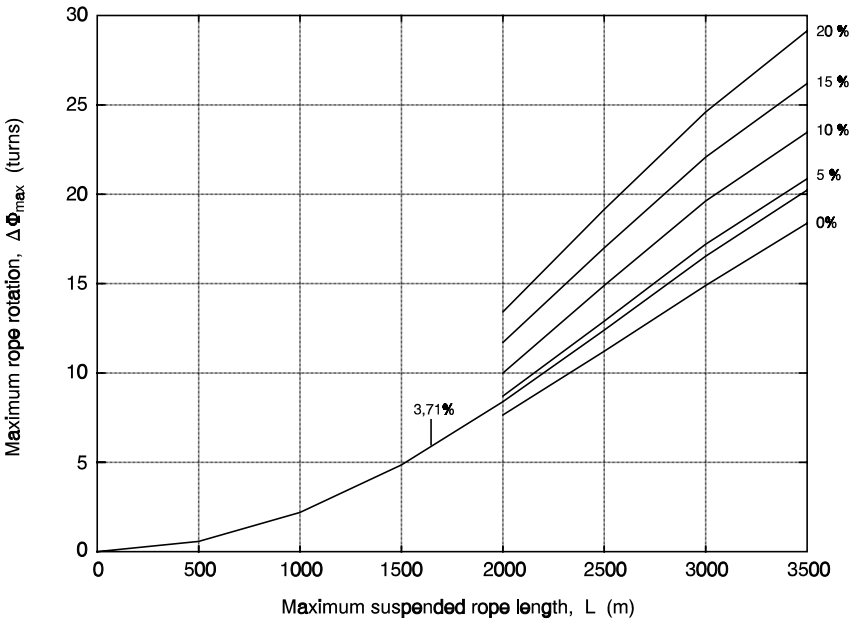

Figure 7.14 - Calculated variation in the maximum rope rotation during conveyance loading for changes in the manufactured lay length at different depths. In all cases, the percentage values indicate the increase in LL_m from LL_{nom} , 46 mm, rope T9, $z_{max} - L$ = 370 m, f_s = 0,68.

Figure 7.14 demonstrates how the rope rotation during conveyance loading increases with an increase in the manufactured lay length. At 3000 m, a 15 percent increase in the lay length (from 5 percent to 20 percent) results in a 43 percent increase in rope rotation during conveyance loading.

7.3.6 Total installed rope length

The total length of a drum winder rope (z_{max}) is mainly dependant on the geometry of the winding system and the expected service life of the rope. The service life will determine the number of times that the splice end would have to be cut for a statutory tensile test. The winder duty would influence the number of times which the drum end would have to be pulled in to move the points of layer crossover damage. The length of rope from the sheave to the drum connection point (z_{max} - L) has an influence on the lay lengths at installation as was shown in section 5.3. It was therefore necessary to consider the effect which changes in this length have on the torsional behaviour. Figure 7.15 shows the changes in the installation lay lengths and figure 7.16 shows the effect on rope rotation, neither of which are very significant.

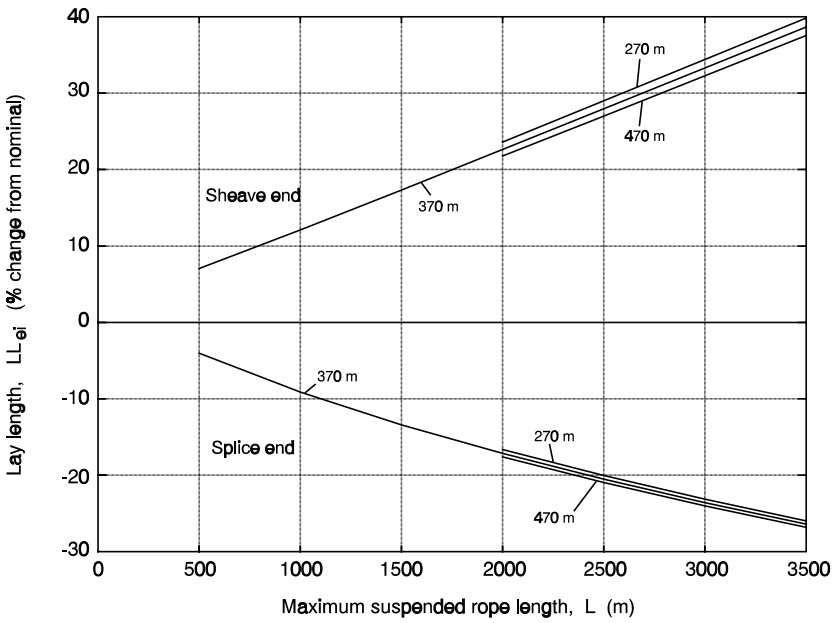

Figure 7.15 - Calculated variation in splice and sheave end lay lengths for changes in the length of rope between the sheave and drum connection point, z_{max} - L, 46 mm, rope T9, f_s = 0,68 , LL_m = 1,0371.LL_{nom} . Nominal weight per unit length, q, used. The distances (m) indicated refer to z_{max} - L.

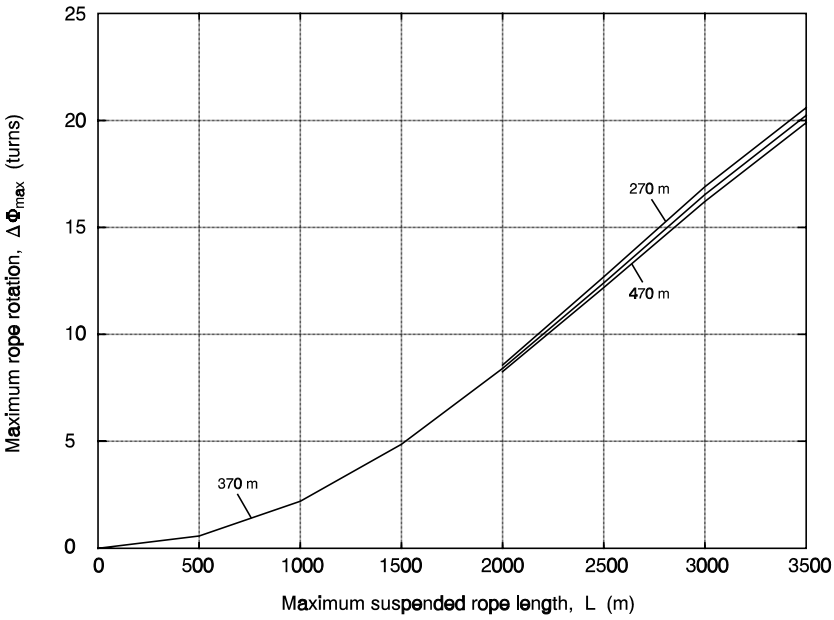

Figure 7.16 - Calculated variation in the maximum rope rotation during conveyance loading for changes in the length of rope between the sheave and drum connection point, $z_{max} - L$. 46 mm rope, T9, $f_s = 0{,}68$, $LL_m = 1{,}0371.LL_{nom}$. Nominal weight per unit length, q, used. The distances indicated refer to $z_{max} - L$.

7.3.7 Parameters which have the greatest effect on the static rope torsional behaviour

Suspended rope length, diameter, manufactured lay length, deliberate loss in rotation and rope weight per unit length were identified as being most important as regards the torsional behaviour of Lang's lay triangular strand ropes.

Other than the inherent torsional properties, the primary cause of lay length variations and rotation of Lang's lay ropes used on drum winders is the load differential along the length of the rope. This differential is dependant on the rope weight per unit length, q. It was shown in figure 7.9 that if the rope weight is reduced without reducing the breaking strength, then the in–service lay length changes are reduced (at installation). It was also shown in figure 7.5 that smaller diameter ropes are less prone to lay length changes than ones of larger diameter. It follows that if smaller diameter ropes of reduced weight per unit length (compared to current designs) were used in very deep shafts, there could be considerable benefits in terms of lay length changes.

To demonstrate this, further calculations were conducted on the 41 mm rope at a ten and twenty percent reduction in rope weight, with the *EBL* remaining constant. The results are shown in figure 7.17. As was indicated earlier, it can be seen that the a standard 41 mm rope would have the same splice end lay length at 3500 m that the larger ropes (48 mm and 49 mm) have at 2650 m. The sheave end lay length of the standard 41 mm rope at 3500 m would occur at approximately 2940 m if the larger ropes were used. If the weight of the 41 mm rope could be reduced by ten percent, without changing the torsional properties, or the breaking strength, then the splice and sheave end lay lengths at 3500 m projected back to the larger ropes occur at 2330 m and 2640 m respectively. If the weight per unit length could be reduced by twenty percent then the values would be 2000 m and 2340 m for the splice and sheave end respectively.

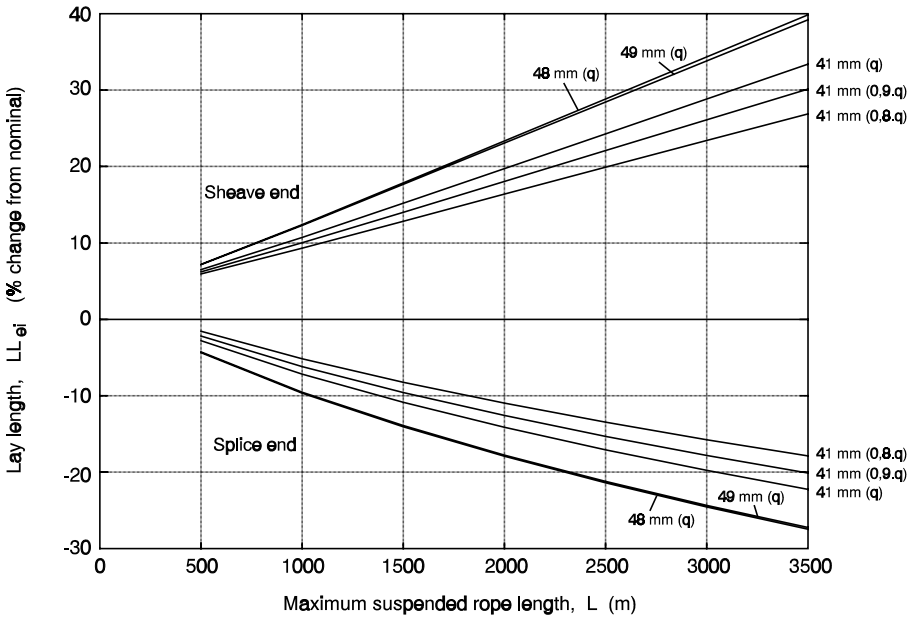

Figure 7.17 - Calculated variation in splice and sheave end lay lengths for changes in rope weight per unit length. z_{max} - L = 370 m, f_s = 0,68, q = nominal weight per unit length.

The reduction in rope weight per unit length at constant breaking load implies that the attached mass and payload should increase. The reduction in rope rotation due to the reduction in rope weight is again opposed by the increase in payload. Therefore the rotation during conveyance loading, figure 7.18, varies only marginally for the differing rope weights. This was also the case with the 46 mm data shown in earlier in figure 7.10.

There appears to be great potential for extending the limit of application of Lang's lay triangular strand ropes by using more smaller diameter ropes and focusing on the reduction of the rope weight per unit length while maintaining the current breaking loads. In this regard, Blair Multi-Rope drum winders with two or even three ropes per drum would be preferred to a single (larger diameter) rope system for very deep shafts.

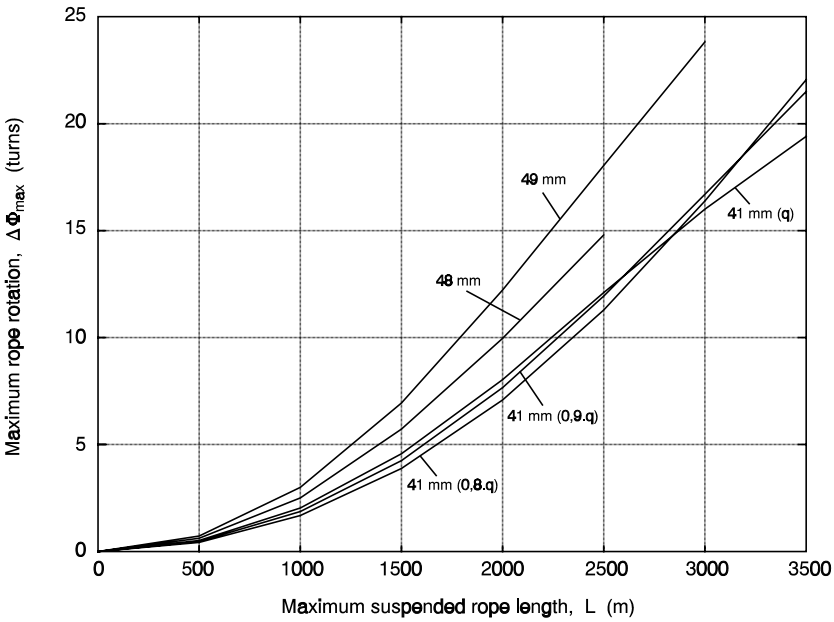

Figure 7.18 - Calculated variation in the maximum rope rotation during conveyance loading for changes in rope weight per unit length. z_{max} - L = 370 m, f_s = 0,68, q = nominal weight per unit length.

7.4 The limit of triangular strand rope application and possible solutions

In-service lay length data for more than 120 ropes were examined and it was found that in very few cases the splice end was shorter than 20 percent decrease from nominal and none of the lay lengths exceeded a 70 percent increase at the sheave end. Very short lay lengths at the splice end (< -20%) would make that portion of the rope extremely prone to distortion in the form of kinks and corkscrews. These distortions are mostly reason for immediate discard.

It is proposed that the splice end lay length should not be operated at more than 20 percent shortening from nominal. It is now possible to calculate the lay length at

which a rope should be manufactured so that upon installation the splice end lay length has the desired value. For example, in the case of the 46 mm rope data shown in figure 7.13, if the rope was manufactured at the nominal lay length plus ten percent then at 3000 m the lay lengths at installation would be approximately correct. No rotation would have to be released from the rope after installation and the lay lengths could be more or less maintained for the entire service life.

Considerable increases in lay length may affect the endurance. Although this has not been quantified, Rebel et al. (1996b) cited numerous references which suggested that unlaying of Lang's lay ropes has a negative influence on endurance. Further references to support this view included Haller (1989) and Oplatka (1994). Investigations should be conducted to determine whether the effects of lay length on endurance are significant under tension-tension and bending fatigue (*D/d* ratios from 80 to 120). If the effects are significant then rope life could be improved on existing installations by altering the rope maintenance practices.

It was shown in figure 7.14 that rope rotation during conveyance loading increases significantly with increases in lay length, particularly at depth. The implications of increased cyclic torsional activity on rope endurance also have to be considered especially in the case of rock winders where the conveyance may be loaded between 300 and 600 times per day. If the increased cyclic rotation is regarded as detrimental then there is further argument against allowing deliberate unlaying. For the example shown in figure 6.6c, the calculated rotation at installation was 6,59 turns (Φ_{ei} - Φ_{fi}). The unlaying ($LL_{ei} \rightarrow LL_e$) therefore resulted in a doubling of the maximum rope rotation (to 13 turns) for the particular payload (67,7 kN).

If the current practice of allowing ropes to unlay in service is adopted for very deep shafts then 3000 m suspended length may not even be possible. By altering the lay lengths at which ropes are closed (figure 7.13) and modifying the maintenance practices, 3500 m could well be achieved. Reductions in rope weight per unit length of the order of 20 percent could make suspended lengths of greater than 3500 m viable. This forecast does not take into account the amplitude of torsional oscillations associated with dynamic events which was discussed in section 6.6.3.

Figure 7.19 shows the cross-section of a triangular strand rope in which the "Plaited" triangular cores have been replaced by a polymer profile or polymer-fibre

matrix. McKenzie (1990b) proposed that extruded polymer profiles or polymer strands could be used to replace wires in the inner triangular strand ropes of multi–layer non-spin ropes. This concept should also be applicable to triangular strand ropes on their own. It was suggested that stranded polypropylene (rope) cores with an extruded polypropylene jacket may be particularly suited for triangular strand ropes operating at great depths (McKenzie, 1990a).

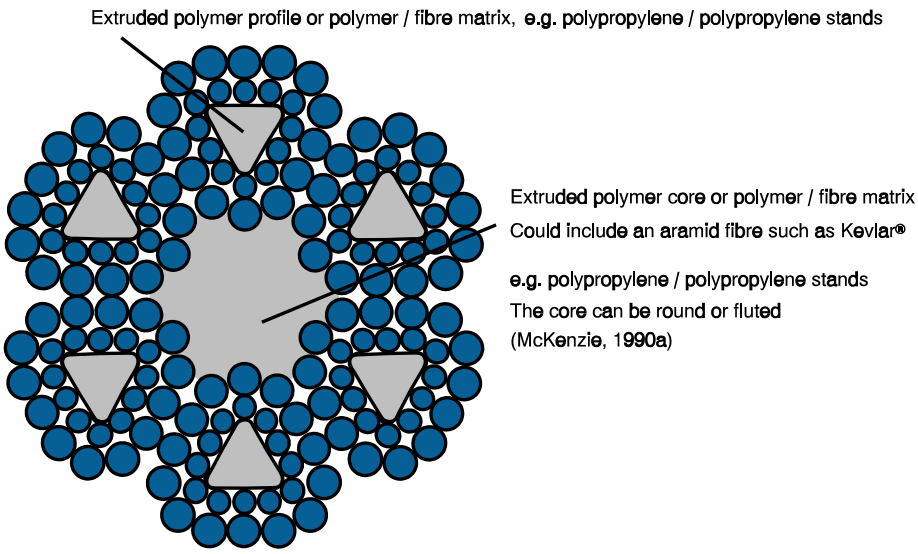

Figure 7.19 - Option for reducing the weight of triangular strand ropes while maintaining the breaking strength and diameter. The polymer profile concept is based on the reduced mass rope patent of McKenzie (1990b).

It is probable that the weight of a triangular strand rope could be reduced by almost ten percent by replacing the "Plaited" core with a polymer profile and increasing the tensile grade of the remaining wires to maintain the breaking load. For a 41 mm 6x29 rope, the core represents approximately 9,7 percent of the metallic area. It is however expected that a twenty percent reduction in weight per unit length would require the addition of light weight, high strength material into the rope cross-section. In such a case, it would be best to maintain the outer wire diameters so as not to affect the abrasion resistance of the rope (required for drum winding). The diameter of the second layer of strand wires could be reduced to reduce the metallic content (may also be required for ten percent reduction). Both the extruded polymer strand core and the rope core could incorporate aramid type fibres such as Kevlar®. In the past, Kevlar® has been used for ropes particularly where rope weight

is problematic. Examples are given by Anon. (1990) and McGrath (1995). Kevlar® has a relatively low resistance to abrasion but this can be overcome by protecting the fibres with a suitable matrix. In the triangular strand rope the protective matrix could be formed by the outer extruded jacket of the strand and rope cores.

Attempts at including non-metallic components in a rope must not result in any significant loss in transverse stiffness. Considerable variations in diameter could negatively affect the coiling patterns on a winder drum. The introduction of non–metallic strength components into the rope cross-section could also complicate the condition assessment of the rope in service as conventional magnetic inspection techniques would not be able to detect broken fibres. A further concern would be the differences in moduli between the fibres and the rope wires as this would affect the load sharing for a given rope strain. A possible solution to this problem would be to ensure that the fibres in the rope core are parallel to the axis of the rope (i.e. no helix geometry). The fibre stiffness would then remain constant whereas the effective stiffness of the wires (forming the strands and rope) are reduced as a result of the helical lay.

8 CONCLUSIONS AND RECOMMENDATIONS

8.1 Torsional properties of triangular strand ropes

A computer controlled machine for tension-torsion testing of steel wire ropes has been developed. The machine is capable of automatic manipulation and recording of rope torque, load and twist. Constant twist and load tests were conducted on twelve triangular strand rope specimens in a diameter range from 25 mm to 54 mm. A marked variation in the measured torsional stiffness was observed when the ropes were twisted at constant load. The change in stiffness is ascribed to a transition from no-slippage between the rope wires to full slippage which occurs as the angle of applied twist increases. This explanation is based on the theory of Raoof and Hobbs (1989). It was found that there can be an order of magnitude difference between the no-slip and full-slip torsional stiffnesses especially in the case of higher rope loads and short lay lengths.

The measured torsional stiffness (both no-slip and full-slip) increases with increases in the constant load and shortening of the lay length. In general, lay length has a greater affect on rope torsional stiffness properties than load. For all loads and starting values of twist, triangular strand ropes show a higher torsional stiffness in the twisting up direction of rotation compared to untwisting, for both the no-slip and full-slip cases.

Constant load tests, with varying twist should always be used if the torsional stiffness of a rope needs to be quantified. The proportionality between rope load and torque should be determined by means of the constant twist test as has been the case in the past.

There exists a correlation between the torsional stiffness inferred from the constant twist tests and the full-slip torsional stiffness determined from the constant load tests. This is assuming that the changes in twist for the different load cycles of the constant twist tests occur at relatively low loads (in the order of 30 kN for ropes with breaking strengths in excess of 1000 kN). It is not possible to quantify the hysteretic torsional response of a rope by the constant twist method alone.

8.2 Modelling of rope torsional behaviour

A method of modelling the static torsional behaviour of Lang's lay triangular strand ropes operating on drum winders has been developed. It is possible to calculate the lay length changes which occur at installation based on tension-torsion test data determined under conditions of constant rope twist. In-service rotation boundary conditions are determined by comparison of the relationship between twist and lay length of the test specimen with the manufactured lay length of the in-service rope. Rope rotation during conveyance loading is determined by first considering the constant twist tests data, for an increase in load at constant twist and then the hysteretic torsional response from the constant load tests, for the subsequent change in twist at constant load. To determine the validity of the rope lay length and rotation analyses, they were applied to 22 operating ropes at depths between 1000 m and 2500 m and acceptable correlation was noted.

The modelling approach differs from previous work in that it takes full account of the load and lay length dependant torsional hysteresis in the calculation of rope rotation due to changes in end load. As far as could be established, rope lay length calculations, which have been verified with in-service measurement, have not been published before.

8.3 In-service torsional behaviour

In general, the splice and sheave end lay lengths of ropes operating on drum winders are at their shortest after installation. Both tend to increase as the service period progresses since ropes are normally allowed to unlay during maintenance operations. The sheave end lay lengths increase at a more rapid rate than those at the splice end due to the nonlinear relationship between twist and lay length.

As the overall lay length of a rope increases, the extent of rope rotation due to changes in end load also increases. It was noted, at some sites, that unlaying caused the rope rotation during conveyance loading to double over the service period.

Rope rotation during conveyance loading is such that the splice end lay length

increases and the sheave end lay length decreases. In the case of emergency braking with a conveyance moving up the shaft, the initial rotation was found to have the same effect. If only the rope end load is decreased, then the rope rotates in the opposite direction causing the splice end lay length to decrease and the sheave end lay length to increase. Under abnormal conditions of slack rope, this rotation behaviour would promote distortion of the splice end.

During emergency braking, the system acceleration was found to have a significant effect on the amplitude of torsional oscillations in the rope. Torsional oscillations under braking conditions are expected to increase with at least the square of the maximum suspended length.

Smaller diameter triangular strand ropes are expected to show less changes in lay length at the splice and sheave end than larger diameters, at a given depth. The rotation of smaller diameter ropes due to changes in end loads also appear to be less and therefore these would be preferred for very deep shafts. Two or three rope BMR winders would thus be the best machines for such installations.

The lay length at which a triangular strand rope is manufactured can have a notable effect on the equilibrium lay lengths which the rope shows after installation on a drum winding system in a vertical shaft. It is therefore possible for a rope manufacturer to have control over the lay lengths at installation by altering the lay length at which the rope is closed. Using the verified analysis methods, it was found that the splice end lay lengths at installation for depths greater than 2500 m are extremely short (< -20 percent from nominal) if the ropes are manufactured within the range 0 to 5 percent longer than the nominal value. Current experience shows that a splice end lay length of -20 percent can be tolerated without the danger of distortion under normal operating conditions. For a 3500 m deep shaft, a rope would have to be closed at about 15 percent longer than nominal to achieve an installed splice end value of -20 percent. The sheave end lay length at installation is then expected to be between 50 and 60 percent greater than the nominal lay length. There are numerous examples of ropes currently operating in this lay length extension range (due to deliberate unlaying) without signs of instability.

8.4 Recommendations relating to modelling of rope torsional behaviour

It may be considered to develop a dynamic analysis for calculating rope rotation during conveyance loading. Such an analysis would take into account the different torsional stiffness properties which triangular strand ropes show depending on whether they are twisted up or untwisted. It is expected that in general a dynamic analysis would return similar rotation amplitudes as the static analysis developed in this study. The most probable difference would lie in the shape of the curve representing the rotation along the rope during loading. A dynamic analysis would also allow more detailed investigation of rope rotation during emergency braking which could become significant at depths greater than 2500 m.

The effect of detaching the drum end of the rope from the drum (for pulling in of the back end) on the rotation boundary condition at the sheave should be investigated. This would require observations to be made on site as to the direction of rotation (if at all) of the free drum end of the rope. The change rope length between the sheave and the drum connection point (conveyance at lowest position) as the service period progresses also needs to be taken into account in modelling the changes in the rotation boundary condition at the sheave.

Using the testing and analysis methods presented in this thesis, it is possible to determine a non-dimensional set of equations for the torsional response, at constant twist and load, for a range of diameters in the compound triangular strand construction. These equations would then remove the necessity for further torsion testing of the specific triangular strand ropes or any other intermediate diameters. For consistency, it may be necessary to define the zero twist lay lengths for the various specimens at the same percentage change from their nominal lay lengths (e.g. plus 15 percent).

8.5 Recommendations relating to the operation of triangular strand ropes

Since release of rotation from in-service ropes during maintenance procedures can significantly affect the lay length distributions, it should be considered to implement measures which would make it mandatory for maintenance personnel to monitor

and record the rotation lost. If such records are kept then it would be possible to determine whether the calculated rotation lost from a rope for a given change in lay length is correct. This would be particularly relevant to ropes operating at suspended lengths in excess of 2500 m.

In very deep shafts the sheave end lay lengths at installation would be relatively long for splice end lay lengths of around -20 percent. If these rope were allowed to unlay, the sheave end lay lengths would rapidly lengthen and could lead to instability of the construction. Systems must therefore be developed which will allow the lay lengths to be maintained at the installations values throughout the service period of a rope. This will probably require all rotation that is lost from the rope be returned prior to reattachment of the rope to the conveyance. It may not be possible to return rotation at the drum end but whatever amount is lost there, can be put back at the splice end.

8.6 Recommendations relating to the design and manufacture of triangular strand ropes

Triangular strand rope development should focus on the reduction of rope weight per unit length while maintaining the diameter and breaking strength. Indications are that a 10 percent reduction in weight per unit length could delay certain lay length changes at installation by 500 m. Replacement of metallic components in the rope cross-section with light weight material is required for the reduction of the weight per unit length. Polymer fibres or extruded profiles can be used which do not contribute to the rope strength. In such cases the tensile grade of the remaining wires would have to be increased. An alternative solution would be to include high strength aramid type fibres into the cross-section which contribute to the rope strength.

Rope manufacturing techniques may need to be altered to allow the closing of triangular strand ropes at lay lengths outside of the usual range of 0 to 5 percent greater than nominal.

APPENDIX A : THE EFFECT OF LAY LENGTH ON ROPE TENSILE PROPERTIES

The details contained in this appendix relate to the investigation described in section 1.4. It was shown that variations in lay length can have a significant effect on rope properties determined by means of a destructive tensile test.

A.1 Equipment

Further to the information presented in section 1.4, figure A.1 shows a rope mounted in the 15 MN tensile testing machine with the torque clamp attached. Detail of the torque clamp is contained in figure A.2.

Figure A.1 - The use of a collar mounted torque clamp for altering rope lay length prior to tensile testing. The twist in the section of rope shown was approximately -734 °/m which corresponds to 1,89.LL_{nom} . 25 mm rope, 6x27(9/12/6 + 3Δ)/F, RHL, 1800 MPa, cut from the same coil as rope T1.

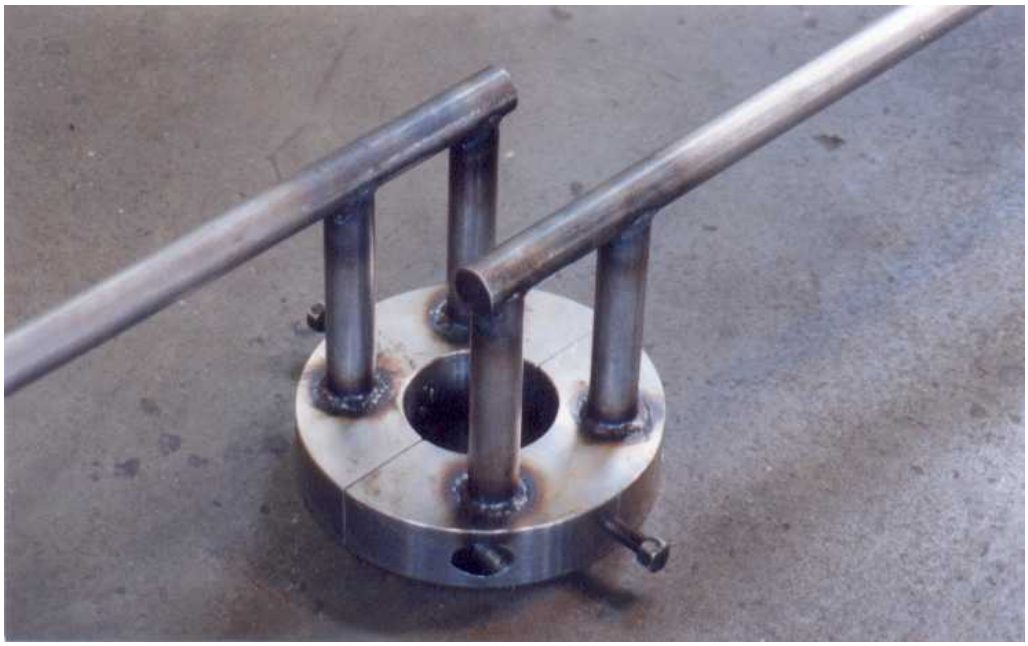

Figure A.2 - Detail of the collar mounted torque clamp. The clamp was manufactured specifically for investigation of the effects of lay length on rope tensile properties.

A.2 Tensile test results

Figure A.3 shows the variation in breaking strength with a variation in lay length. Three reference tests were conducted at the free lay length (torsionally unrestrained state after being cut from the coil). The average of the three reference tests were used to calculate the percentage variations.

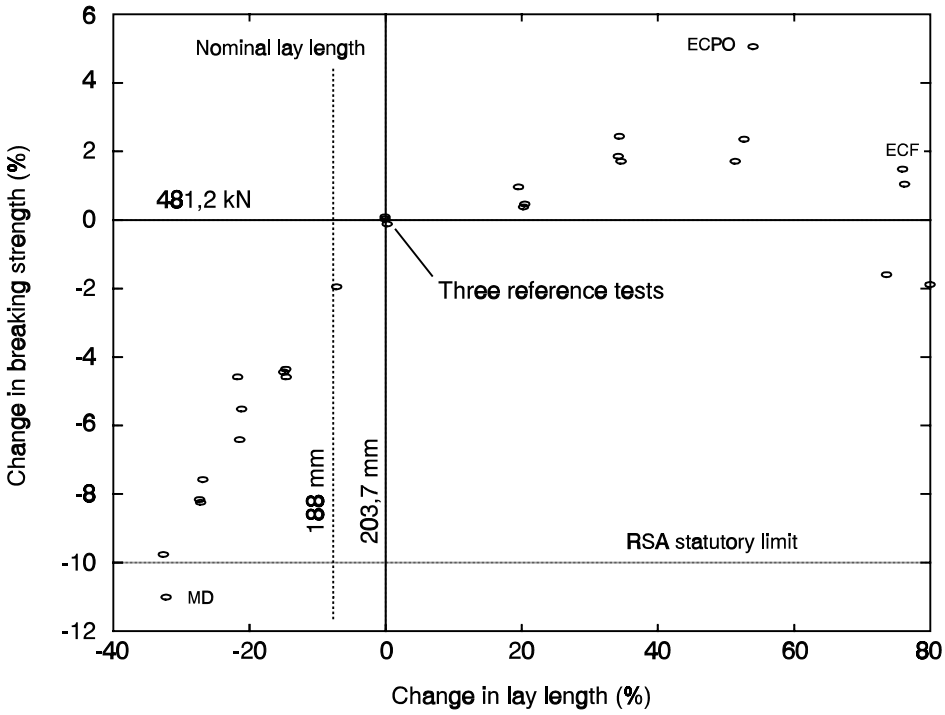

Figure A.3 - Variation in breaking strength with lay length for a 25 mm diameter Lang's lay triangular strand rope, 6x27(9/12/6 + 3Δ)/F, RHL, 1800 MPa, cut from the same coil as rope T1.

As with the twelve preliminary tests of this type (Rebel, 1995) there is a sharp decrease in breaking strength with a decrease in lay length. The strength increases marginally with an increase in lay length and thereafter tends to decrease. This is expected since there is a limit to which the construction can be upset before the benefits of reduced spinning losses are outweighed by the additional wire stresses imposed. Three of the tests results are marked :

MD Mechanical Damage : three outer wires in one strand showed transverse abrasion marks along approximately 6 mm of the wire axes. These marks originated when the blade of the cut-off machine came into contact with the wires during specimen preparation.

ECPO End Cap Pull Out : strands failed inside the white metal cone.

ECF End Cap Failure : strands failed at the white metal collar.

A line corresponding to the nominal lay length of the rope (LL_{nom} = 188 mm) is indicated in figure A.3. A decrease in nominal lay length of 30 percent corresponds to a decrease in breaking strength of approximately 10 percent (from nominal). This gives a quantified justification for the South African specification that a 30 percent decrease in lay length from nominal is reason for discard of a hoisting rope. Discard criteria for drum winder ropes have been discussed by Kuun et al. (1993).

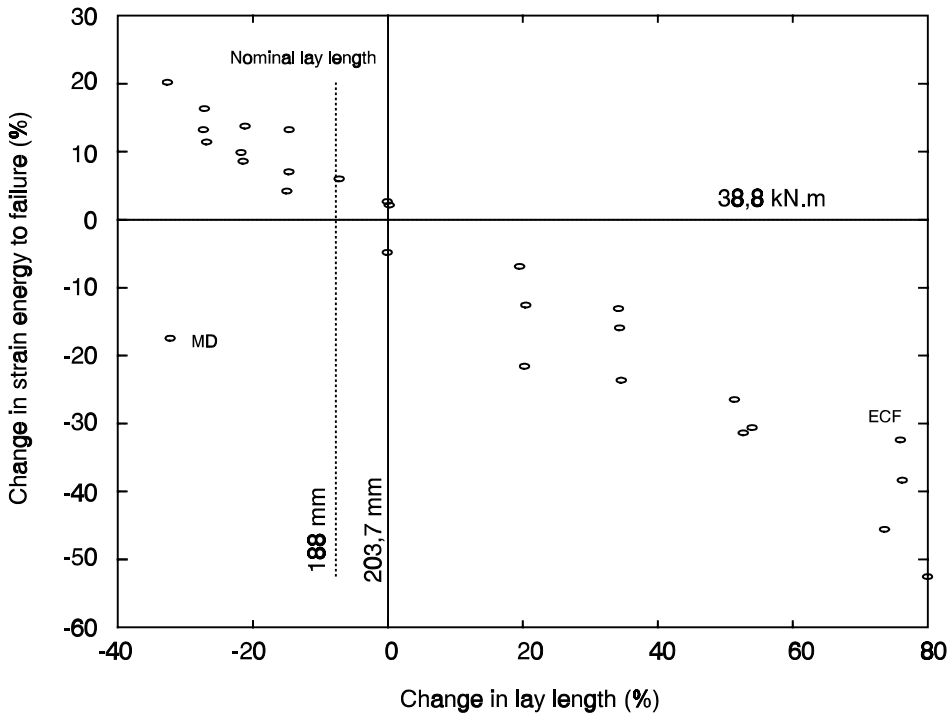

Figure A.4 - The effect of lay length on energy absorption at failure for a 25 mm diameter Lang's lay triangular strand rope, 6x27(9/12/6 + 3Δ)/F, RHL, 1800 MPa, cut from the same coil as rope T1.

Figure A.4 shows the variation of strain energy to failure with a variation in lay length. Strain energy to failure is defined as the total area under the load elongation diagram. It is an indication of the work done in breaking the specimen and the energy absorbtion capabilities of the rope. The ability of the rope to absorb energy decreases with an increase in lay length and the relationship is approximately linear. The specimen with mechanical damage (MD) showed a sharp decrease in strain energy to failure.

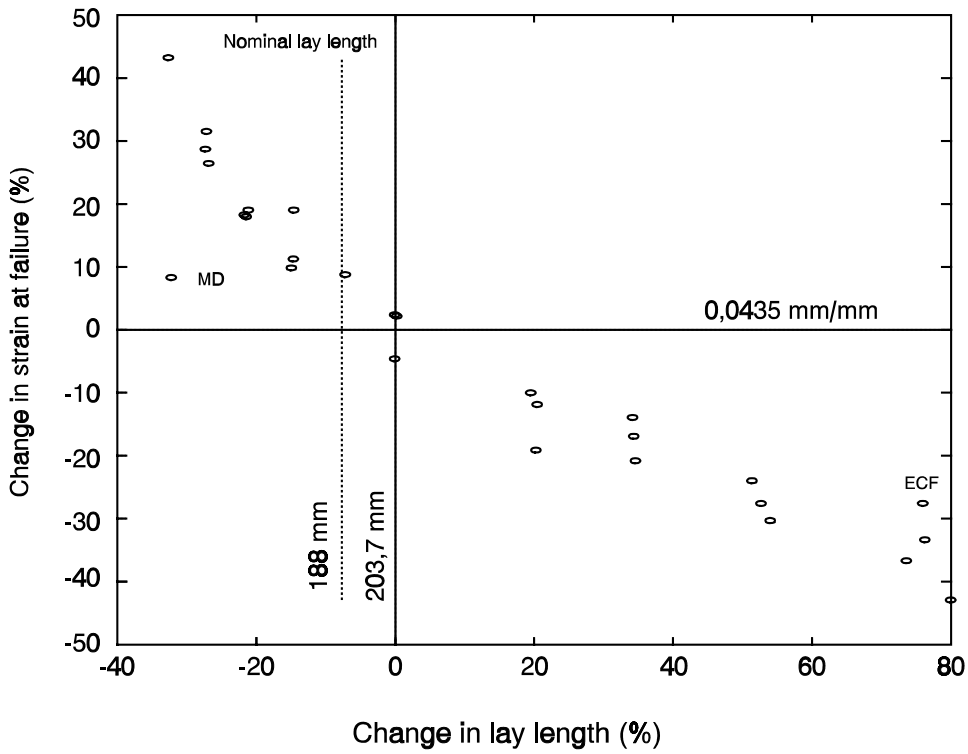

Figure A.5 - Total strain at failure for a 25 mm diameter Lang's lay triangular strand rope with different lay lengths, 6x27(9/12/6 + 3Δ)/F, RHL, 1800 MPa, cut from the same coil as rope T1.

Materials which undergo large strains before failure are classified as ductile. An indication of ductility can therefore be determined by dividing the elongation at failure by the gauge length (measured after the lay length change), figure A.5. The elongation measurement includes elastic deformation of the testing machine as well as settling in of the cones into the grips. Since all the specimens were prepared in the same manner it is assumed that results are subject to the same errors and can therefore be compared with reasonable accuracy. The specimen with mechanical damage (MD) also showed a considerable decrease in strain at failure compared to the other specimens with similar lay lengths.

A.3 Torsion test results for calculating failure torque

In addition to the 28 breaking strength tests, a constant twist test was conducted to allow calculation of the estimated rope torque at failure for the tensile tests specimens. Figure A.6 shows the measured torque in the rope for varying tensile loads. From the measured data it was possible to determine the constants matrix, *N*, for equation [5.3] which describes torque in terms of load and twist.

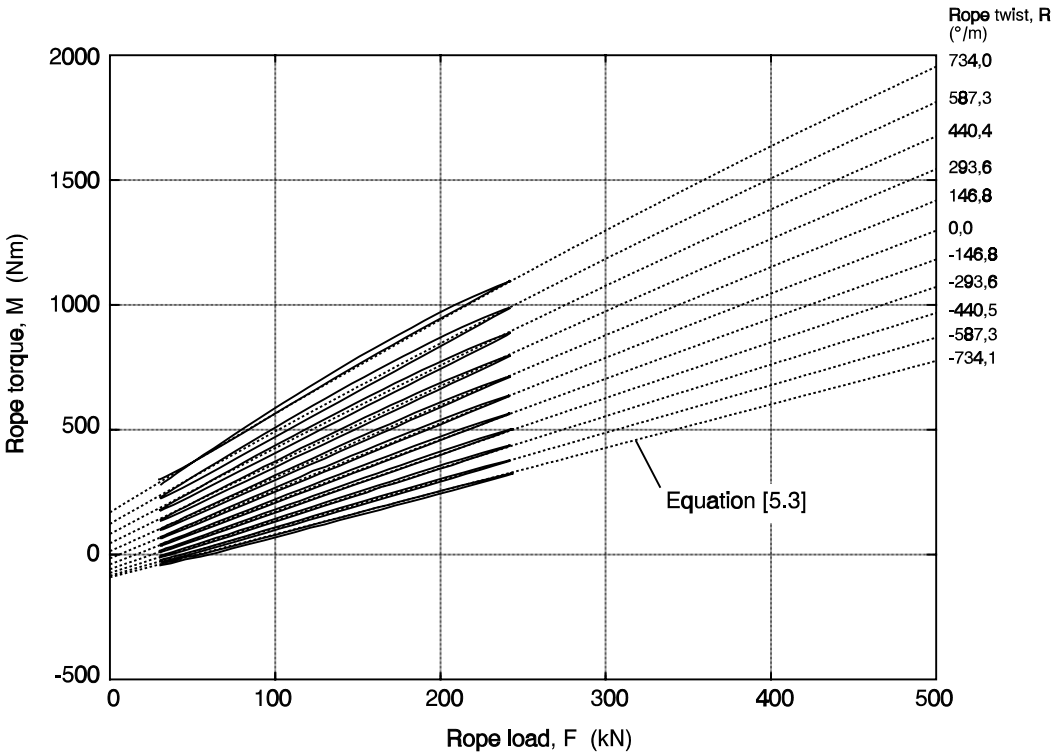

Figure A.6 - Torque versus load response for rope T1, 25 mm, 6x27(9/12/6 + 3Δ)/F, RHL, 1800 MPa. The maximum load applied during the tension-torsion test was approximately half the rope breaking load.

From the constant twist test data for rope T1, 25 mm, 6x27(9/12/6 + 3Δ)/F, RHL, 1800 MPa :

$$N = \begin{bmatrix} -3{,}5977e-010 & 2{,}3030e-007 & 1{,}0078e-004 \\ -6{,}7943e-007 & 1{,}5914e-003 & 1{,}7691e-001 \\ -2{,}7132e-004 & 2{,}7617e+000 & -1{,}5419e+001 \end{bmatrix} \qquad [A.1]$$

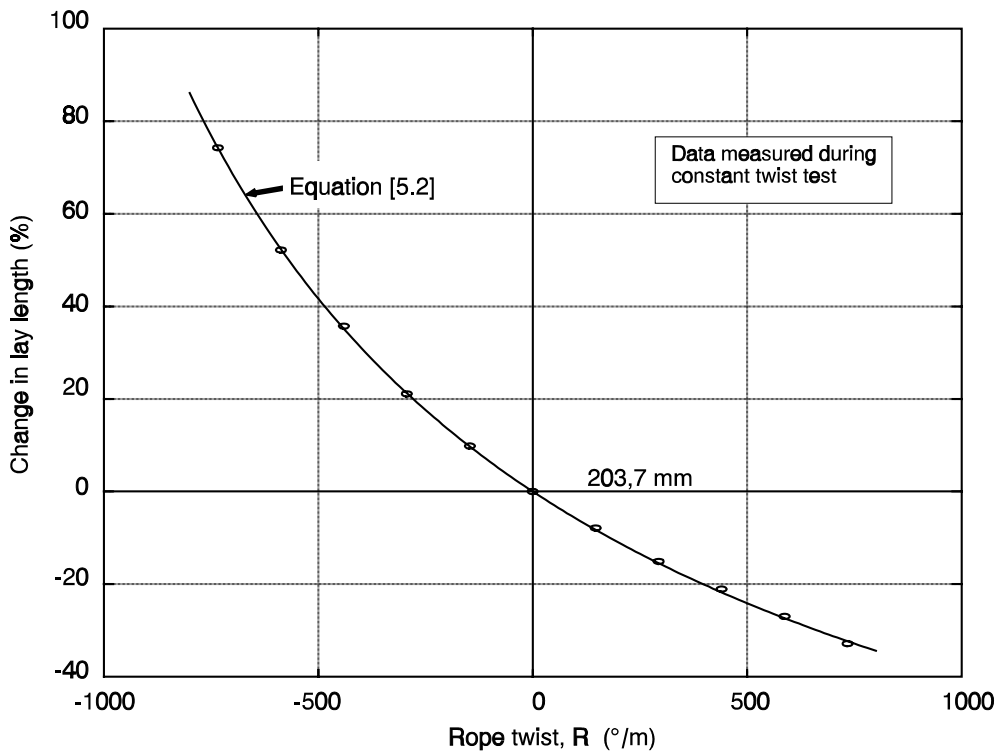

Figure A.7 - Relationship between the applied twist and lay length for rope T1, 25 mm, 6x27(9/12/6 + 3Δ)/F, RHL, 1800 MPa.

During the constant twist test, the relationship between lay length and applied twist was determined and is shown in figure A.7. Using equation [5.2] and the lay lengths measured on the tensile test specimens, the accurate twist values, *R*, were calculated. Substituting these values of twist and the failure loads into equation [5.3] yielded the estimated failure torques shown in figure A.8. There is little scatter in the failure torque data which suggests that for a given lay length there is a specific torque at which the rope will fail.

Constants for rope T1, 25 mm, 6x27(9/12/6 + 3Δ)/F, RHL, 1800 MPa relating to equation [5.2] :

d_0 = 24,9 mm

LL_0 = 203,8 mm

k_{LL} = 2,0412e-4 (1/(°/m))

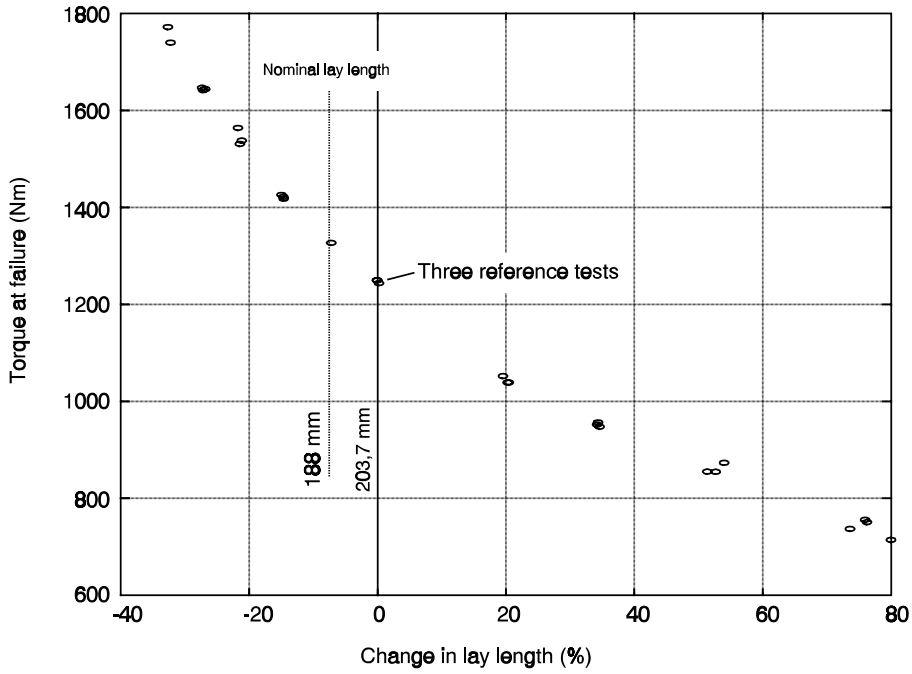

Figure A.8 - Estimated failure torque for a 25 mm diameter Lang's lay triangular strand rope with different lay lengths, 6x27(9/12/6 + 3Δ)/F, RHL, 1800 MPa, cut from the same coil as rope T1.

A.4 Comments relating to the tensile test results

In one test, with a decreased lay length, the rope showed sensitivity to slight mechanical damage (MD). This result could be significant for future cut wire tests conducted on new triangular strand ropes. i.e. The effect of one or two cut wires with a short lay length may be quite different to the effect of the same cut wires with a longer lay length.

It is probable that all splice and BMR compensating sheave tangent point tests in the past were conducted with the specimens at their free lay lengths. It must be questioned how the results would have been affected if the tests were conducted at the lay lengths which the sections operated at in service. This is particularly relevant in deeper shafts where the conveyance end lay lengths would be shorter than in shallower shafts. It may be considered in future to conduct all splice and BMR compensating sheave tangent point tests at the operating lay lengths as opposed to the free lay lengths. This can be achieved using a manually operated, torque clamp (figures A.1 and A.2) and statutory lay length information supplied by the shaft engineer.

A.5 Rope modulus calculation

It was found that equation [A.2] accurately describes the average strain versus stress curve shown by the dashed line in figure A.9. The five constants in the equation were solved for numerically for each of the eleven curves determined during the constant twist test on rope T1, table A.1.

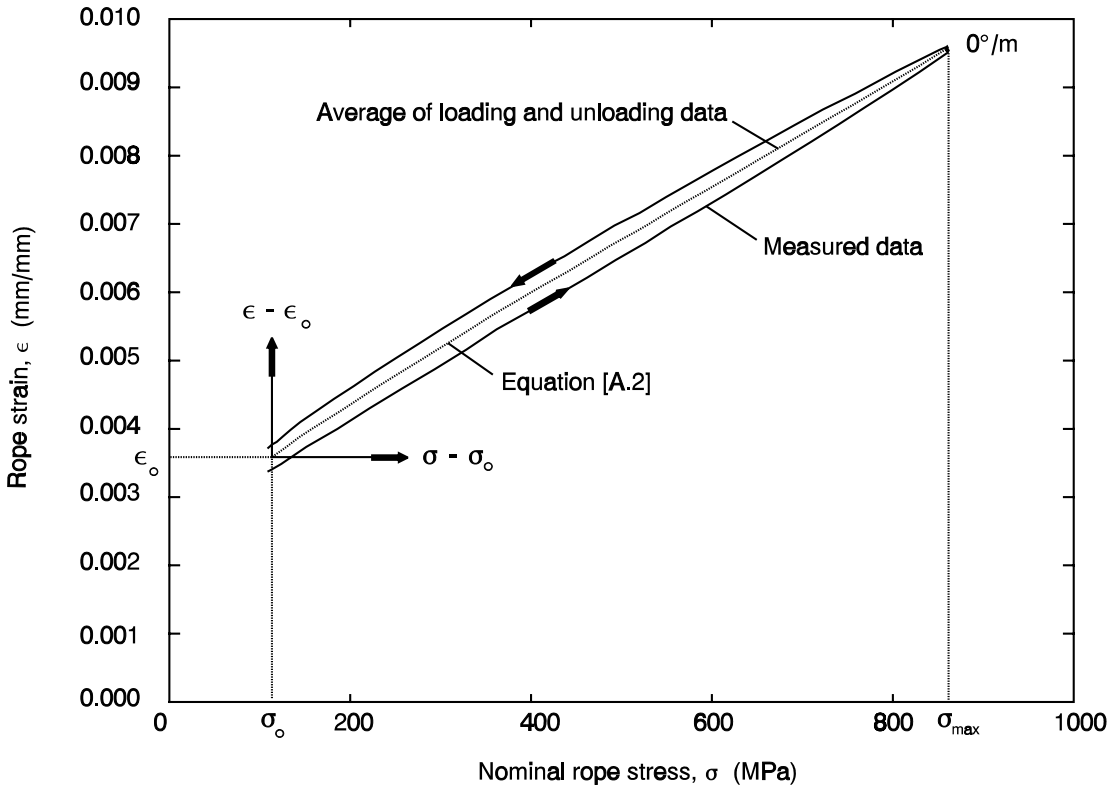

Figure A.9 - Strain versus stress for zero twist, rope T1, 25 mm, 6x27(9/12/6 + 3Δ)/F, RHL, 1800 MPa. Data from elongation measurement during the constant twist test.

$$\varepsilon - \varepsilon_0 = a_\varepsilon.(\sigma - \sigma_0) + b_\varepsilon.\ln(\, c_\varepsilon.\,(\sigma - \sigma_0) + 1\,) + d_\varepsilon.\arctan(\, f_\varepsilon.(\,\sigma - \sigma_0\,)\,) \qquad [A.2]$$

where :	ε	=	rope strain (mm/mm)
		=	$\Delta l \,/\, l_0$
	Δl	=	measured rope elongation (mm)
	l_0	=	0°/m gauge length (mm)
		=	2670 mm for rope T1
	σ	=	nominal rope stress (MPa)
		=	$1000\,.\,F \,/\, A_{met}$
	F	=	applied load (kN)

A_{met}	=	metallic cross-sectional area determined from the number of wires and the wire diameters (mm²)
	=	280,6 mm² for rope T1
$a_\varepsilon, b_\varepsilon, c_\varepsilon, d_\varepsilon, f_\varepsilon$	=	equation constants listed in table A.1 (the values vary depending on the applied twist)
σ_0 , ε_0	:	figure A.9, starting values of stress and strain for each curve

The modulus of the rope can be determined within the stress range σ_0 to σ_{max} (table A.1) using equation [A.3] :

$$E = \frac{d\,\sigma}{d\,\varepsilon} = \left[\frac{d(\varepsilon - \varepsilon_0)}{d(\sigma - \sigma_0)}\right]^{-1} \qquad [A.3]$$

therefore :

$$E = \frac{1}{\left[a_\varepsilon + \dfrac{b_\varepsilon . c_\varepsilon}{1 + c_\varepsilon . (\sigma - \sigma_0)} + \dfrac{d_\varepsilon . f_\varepsilon}{1 + (f_\varepsilon . (\sigma - \sigma_0))^2}\right]} \qquad [A.3a]$$

Equation [A.3a] was used to determine the variation in modulus for different rope lay lengths and applied stresses, shown in figure A.10.

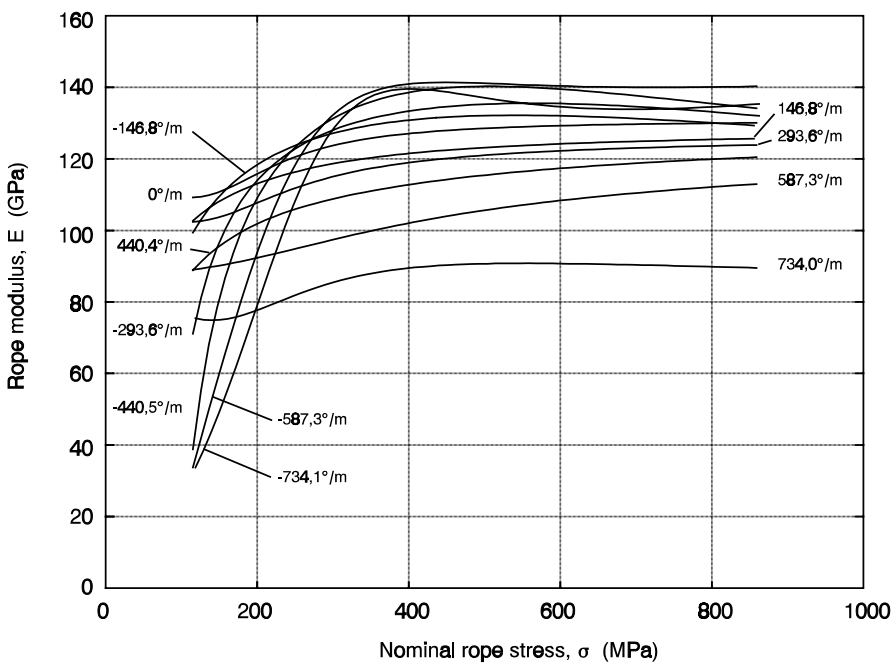

Figure A.10 - Rope modulus variation with applied stress for different lay lengths, rope T1, 25 mm, 6x27(9/12/6 + 3Δ)/F, RHL, 1800 MPa. Data from elongation measurement during the constant twist test.

Table A.1 - Strain versus stress constants for equation [A.2], rope T1, 25 mm, 6x27(9/12/6 + 3Δ)/F, RHL, 1800 MPa.

Twist R (°/m)	Lay length (mm)	ε_0 (mm/mm)	σ_0 (MPa)	σ_{max} (MPa)	a_ε	b_ε	c_ε	d_ε	f_ε
734,0	137,7	-4,40e-02	118	859	1,2388e-05	-1,6570e-03	2,3689e-03	-7,5500e-04	-6,3362e-03
587,3	147,9	-3,16e-02	114	859	7,7897e-06	1,2067e-03	1,7709e-03	-3,3888e-04	-3,8731e-03
440,4	159,3	-2,15e-02	114	859	7,7539e-06	4,8847e-04	7,7434e-03	4,3787e-05	-6,2997e-03
293,6	172,1	-1,25e-02	114	859	7,8476e-06	2,0801e-04	2,2901e-03	-1,9807e-04	-7,2874e-03
146,8	186,8	-4,15e-03	114	855	7,7627e-06	1,5356e-04	1,1073e-02	-4,0902e-05	-6,9137e-03
0,0	203,7	3,59e-03	114	859	7,6520e-06	6,2774e-05	4,3030e-09	-1,7630e-04	-8,5085e-03
-146,8	223,5	1,06e-02	114	855	8,9591e-06	3,0237e-04	1,1165e-02	2,5903e-03	-8,6933e-04
-293,6	247,0	1,70e-02	114	862	1,0376e-05	2,6688e-04	2,8592e-02	6,1307e-03	-6,2436e-04
-440,5	275,4	2,28e-02	114	859	8,5201e-06	3,4034e-04	6,0546e-02	2,2677e-03	-1,1974e-03
-587,3	310,5	2,80e-02	114	859	6,2833e-06	1,3115e-03	2,2861e-02	1,8115e-03	-3,4713e-03
-734,1	355,1	3,29e-02	118	862	4,4735e-06	4,3840e-03	9,5661e-03	4,8842e-03	-3,3816e-03

Figure A.11 shows the maximum and minimum moduli and the stresses at which they occur. For a shortening in lay length the modulus decreases. For increased lay lengths the maximum modulus increases however the minimum modulus decreases significantly. When a rope is severely unwound, the construction adjacent to the white metal collars and end cones is upset to such an extent that the wires and strands separate. In figure A.1 it can be seen that the strands separated adjacent to the torque clamp. As the load is increased, the separation reduces and if the load is high enough, the wires will return to their original positions.

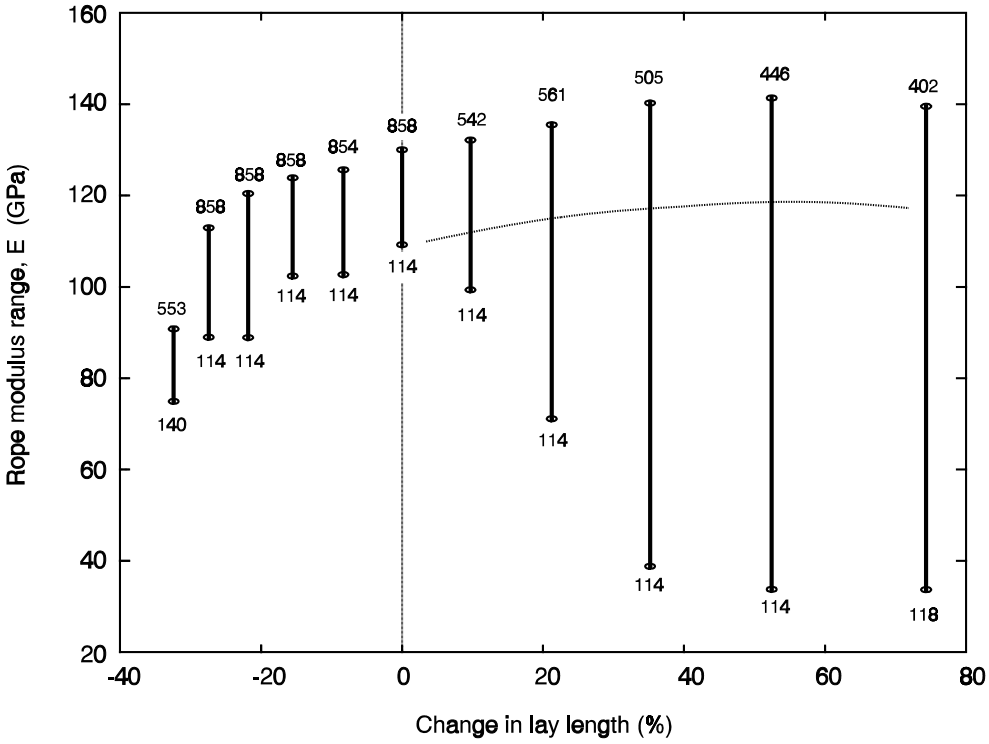

Figure A.11 - Modulus range for different lay lengths, rope T1, 25 mm, 6x27(9/12/6 + 3Δ)/F, RHL, 1800 MPa. Values determined from the data in figure A.10. The nominal rope stresses (MPa), at which the maximum and minimum moduli occurred, are indicated.

Figure A.12 illustrates the approximate and expected actual rotation and twist distribution in a torsion test specimen. It is apparent that there must exist a twist transition area where the twist changes from zero within the white metal cone to a maximum value some distance from the collar. It is proposed that the construction upset in the twist transition area results in a significantly reduced modulus at lower rope loads. Once the load increases to the point where the wires and strands close up, the effect of the upset on the modulus is reduced. If it were not for the end effects, the minimum moduli in the increased lay length region would probably

follow the dashed line in figure A.11, based on the same trend as in the reduced lay length region.

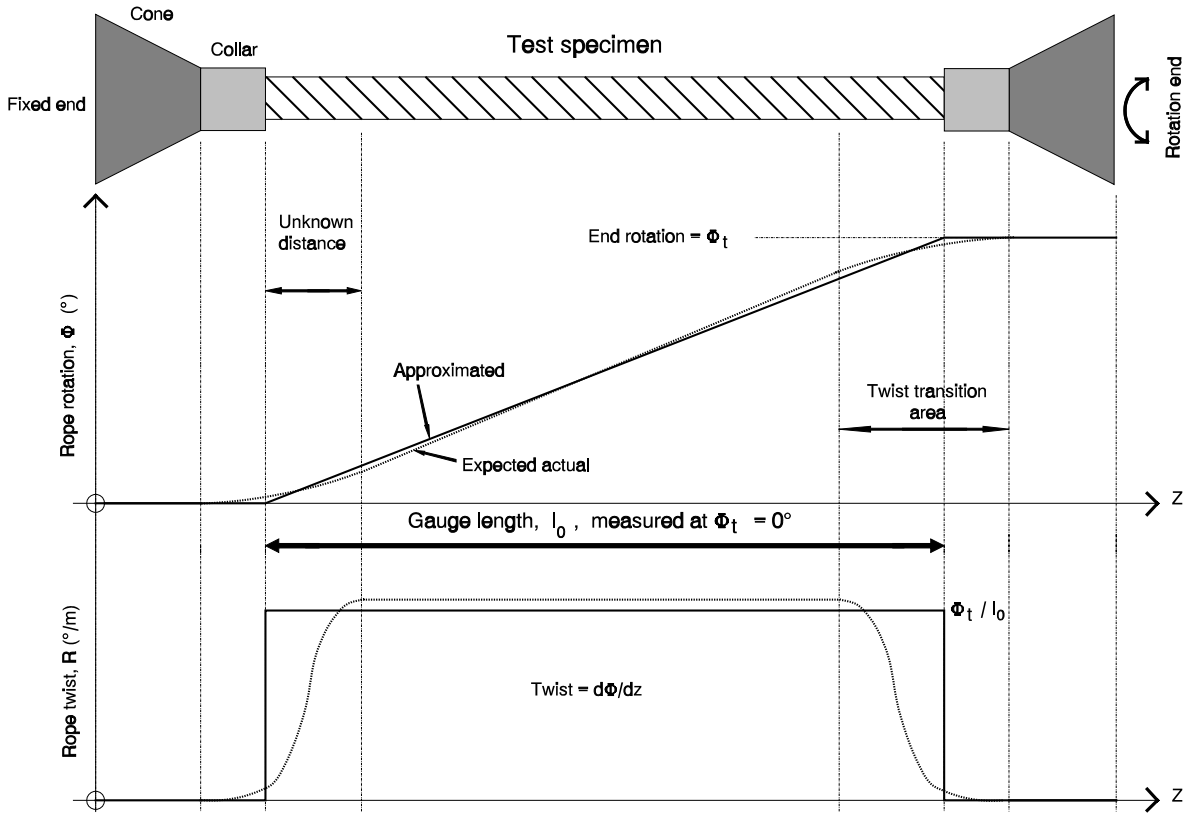

Figure A.12 - Approximated and expected actual rotation and twist distribution for a torsion test specimen.

Winding up a rope to shorten the lay length does not result in any visual distortion of the construction in the twist transition area, nor does the existence of the twist transition area seem to have an effect on the shortened lay length moduli values.

APPENDIX B : VARYING TWIST BETWEEN THE SHEAVE WHEEL AND DRUM CONNECTION POINT

In the analysis presented in chapter five it was assumed that, for equilibrium at installation, the rope twist between the sheave wheel and the drum connection point is constant and equal to the twist in the vertical section at the sheave. The equations presented in this appendix allow for a linear variation in twist between the sheave and the drum connection point. It is therefore possible for the drum connection point lay length to be shorter than the lay length at the sheave while satisfying the rotation boundary conditions.

To accommodate a variation in lay length between the sheave and drum connection point, it is necessary to define the change in twist as indicated in figure B.1. If R_2 is the twist at the sheave then ($R_2.Df$) would be the twist at the drum. In an equilibrium condition the twists on the vertical and drum sides of the sheave would be equal, $R_1 = R_2$. Equation [B.1] describes the relationship between twist and the distance, z_1, measured from the sheave towards the drum.

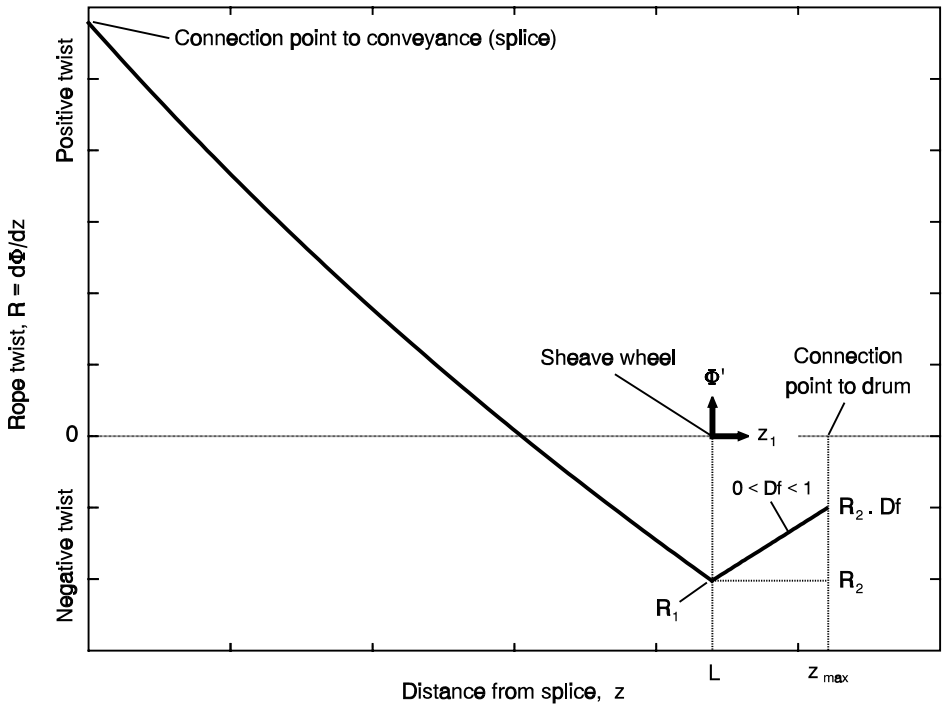

Figure B.1 - Twist variation along the length of a rope, with a linear change in twist from the sheave wheel to the drum connection point.

$$\Phi' = R_2 + \left[\frac{R_2.Df - R_2}{z_{max} - L}\right].z_1 \qquad (°/m) \qquad [B.1]$$

The purpose of the numerical scheme listed in table 5.2 was to solve for the sheave wheel rotation boundary condition (*SWbc*) so that the constant twist between the sheave and the drum equalled the twist at the sheave in the vertical section. The boundary condition ($R_{coil}.z_{max}$) at the drum connection point also had to be satisfied, figure 5.13. For a varying twist between the sheave and drum, the following conditions are required for equilibrium :

Twist at the drum connection point as a function of twist at the sheave :

$$R(z_{max}) \quad = \quad R(L_{drum}).Df \qquad [B.2]$$

Rotation boundary condition at the drum connection point :

$$\Phi(z_{max}) \quad = \quad R_{coil}.z_{max} \qquad [B.3]$$

Rotations must be equal at the sheave :

$$\Phi(L_{vertical}) \quad = \quad \Phi(L_{drum}) \qquad [B.4]$$

Twists must be equal at the sheave :

$$R(L_{vertical}) \quad = \quad R(L_{drum}) \qquad [B.5]$$

where : L_{drum} is at the sheave on the drum side
$L_{vertical}$ is at the sheave on the vertical side

From equation [B.1] the rotation between the sheave and drum can be determined :

$$\int \Phi' \, dz_1 \quad \Rightarrow \quad \Phi = R_2.z_1 + \left[\frac{R_2.(Df - 1)}{2.(z_{\max} - L)}\right] z_1^2 + K \qquad [B.6]$$

at $z_1 = 0$: $\Phi = SWbc$ from [B.4]

therefore : $K = SWbc$ (°) [B.7]

at $z_1 = z_{max} - L$: $\Phi = R_{coil}.z_{max}$ [B.3]

(K = the constant of integration)

substituting [B.3] and [B.7] into [B.6] gives :

$$R_2 = \frac{R_{coil}.z_{\max} - SWbc}{\left[(z_{\max} - L) + \frac{(Df - 1).(z_{\max} - L)}{2}\right]} \qquad (°/m) \qquad [B.8]$$

The correct value of *SWbc* needs to be determined so that $R_1 = R_2$. Note that R_1 is a function of the *SWbc*, since each time the *SWbc* is changed a new equilibrium torque in the vertical section must be calculated. The change in torque results in a change in the twist distribution, $R(z)$. The procedure described in table 5.2 can be used to determine the value of the *SWbc*. The only difference is that line 8 would read :

8. Calculate R_2 using equation [B.8]

Df is a defined value, which can be changed to produce different results. Figure B.2 shows how changing the value of *Df* affects the overall rotation distribution.

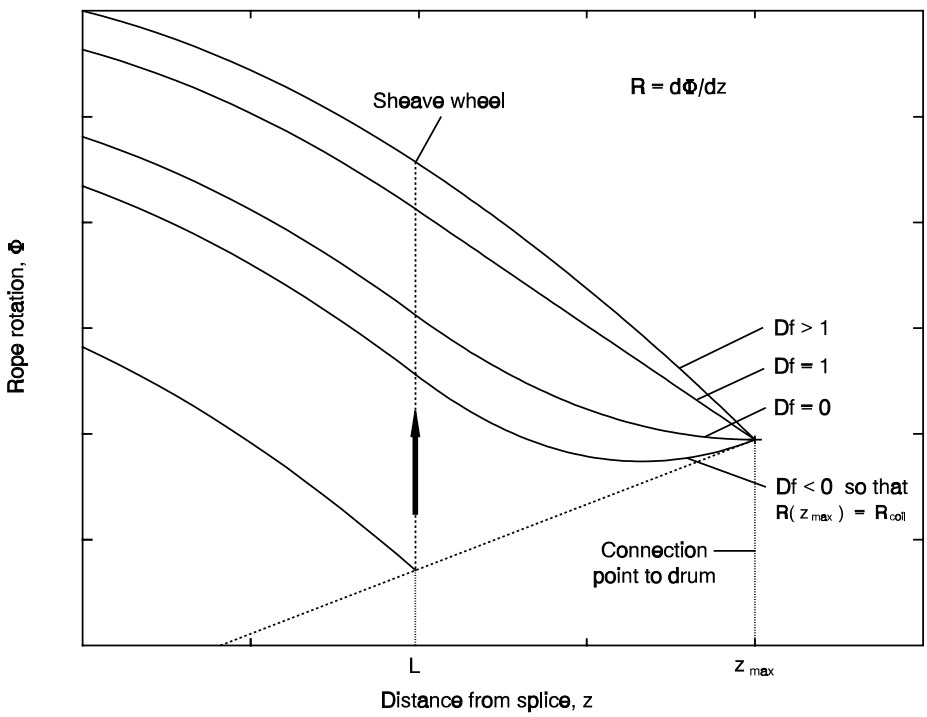

Figure B.2 - The effect of varying *Df* on the rotation distribution between the sheave and drum connection point. The conveyance is at the lowest position in the shaft.

If $Df = 0$, it follows from equation [B.2] that the twist at the drum connection point would also equal zero. If *Df* is reduced to a value below zero, then zero twist occurs at some point between L and z_{max}. The resulting slope (twist) at the drum is positive. It would be reasonable to assume that the minimum value which *Df* could have would be such that the twist at the drum connection point equals the manufactured twist :

$$R(z_{max}) \quad = \quad R_{coil} \qquad [B.9]$$

Stated in other words, the lay length at the drum connection point of an operating rope is unlikely to be shorter than the manufactured lay length, LL_m. In terms of lay lengths, $Df > 1$ implies that the lay length at the drum connection point is longer than the lay length at the sheave. Based on site observations it is most likely that the true value of Df lies in the range 0 to +1. There are two ways in which the value of *Df* could be determined with the first being most practical :

1. Measure the sheave and drum connection point lay lengths on operating ropes that have recently been installed and appear to have reached a lay length equilibrium condition (minimum two weeks operation). The measured lay length ratios can be used to calibrate Df. (Note that $LL_{drum} / LL_{sheave} \neq Df$ since there is a nonlinear relationship between lay length and twist, described by equation [5.2])

2. Calculate the rotation distribution analytically, using a cycle by cycle approach until equilibrium is reached. The rope load variation between the sheave and drum connection point would have to be quantified, as would the coefficient of friction between the rope and the drum surface and between the rope layers. This would most likely be similar to the "back slip" analysis approach presented by Chaplin (1993). The exact details of the effect of doubling down on rope rotation, would also have to be taken into account.

Probably the best analysis algorithm would be one where the lay length ratio is defined in the numerical scheme. *Df* would then be adjusted automatically until the desired lay length ratio was achieved.

APPENDIX C : IN-SERVICE ANALYSIS DETAILS

The information contained in this appendix is complimentary to the measured and calculated results presented in chapter six.

C.1 Analysis details for shaft A, ropes S1 to S4, 41 mm at 1071,3 m

Table C.1 - Analysis data for ropes S1, S2 and S3 relating to figure 6.8

Shaft analysis data, ropes S1, S2 and S3 shaft A	
Rope coil numbers	S1 - 020712 S2 - 020957 S3 - 020646
Date of rope installation	17/10/93
Date of measurements	11/2/96, 28/3/96
q (kN/m)	0,0705
P_e (kN)	48,9
P_f (kN)	110,4
Payload, P_f - P_e (kN)	61,5
Payload envelope (%)	15
Lay type	RHL / LHL
Construction	6x29(11/12/6 + 3Δ)/F
LL_{nom} (mm)	309
$S_{u,wire}$ (MPa)	1800
z_{max} (m)	1460
L (m)	1071,3
Df	1
R_{coil} (°/m)	11,12 *
$SWbc$ (°/360 = turns)	113,7
$R_{coil}.z_{max}$ (turns)	45,1
z for R_{coil} (m) at installation equilibrium (% of L)	670 62,54
Φ_{lost} (turns)	302,8
$\Delta\Phi_{max}$ (turns) calculated	2,18
z for $\Delta\Phi_{max}$ (m) (% of L)	557,1 52,0
$LL_{ei}(0)$ (% change from nominal)	-8,09
$LL_{ei}(L)$ (% change from nominal)	11,97
$LL_e(0)$ (% change from nominal)	0,647
$LL_e(L)$ (% change from nominal)	25,24
$LL_f(0)$ (% change from nominal)	0,971
$LL_f(L)$ (% change from nominal)	24,92
Rotation error range (turns)	-0,889 → 0,259
Lay length error range (% of nominal)	-1,43 → 1,80
M_{ei} (Nm)	474,8
M_e (Nm)	299,1
M_f (Nm)	580,0

Torsion test data, rope T8	
Torsion test rope coil number	136053/001
d_{nom} (mm)	41
d_0 (mm)	42,6
LL_0 (mm)	325
LL_{nom} (mm)	309
l_0 (mm)	2670
Lay type	RHL
K_{LL} (1/(°/m))	3,4426e-4
A_{met} (mm²)	773,2
Construction	6x29(11/12/6 + 3Δ)/F
$S_{u,wire}$ (MPa)	1800

* = Nominal plus 3,71 percent since no manufacturing information (LL_m) was available, figure 5.2.

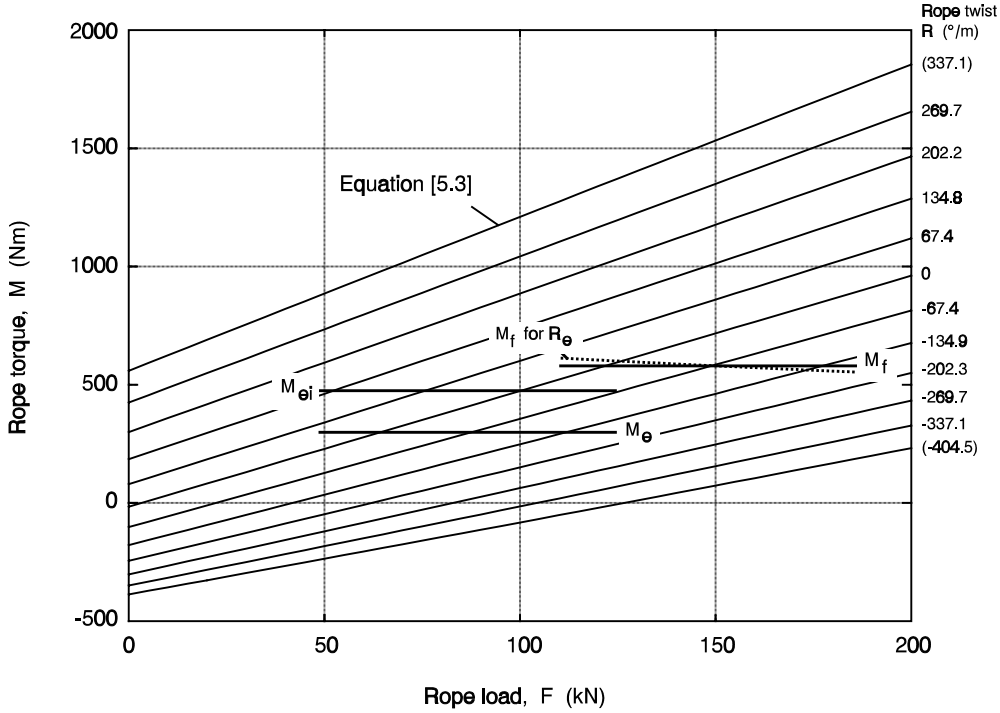

Figure C.1 - Equilibrium rope torques for ropes S1, S2 and S3 in relation to the torsion test data. Torsion test data for rope T8, 41 mm, 6x29(11/12/6 + 3Δ)/F, 1800 MPa. N_{load} according to equation [C.2].

Table C.2 - Analysis data for rope S4 relating to figure 6.9.

Shaft analysis data, rope S4 shaft A (all other data as per ropes S1 to S3)	
Rope coil number	020648
Φ_{lost} (turns)	378,6
$\Delta\Phi_{max}$ (turns)	2,42
$LL_e(0)$ (% change from nominal)	2,91
$LL_e(L)$ (% change from nominal)	29,13
$LL_f(0)$ (% change from nominal)	3,24
$LL_f(L)$ (% change from nominal)	28,48
Rotation error range (turns)	-0,698 → 0,309
Lay length error range (% of nominal)	-3,23 → 3,26
M_e (Nm)	258,7
M_f (Nm)	532,6

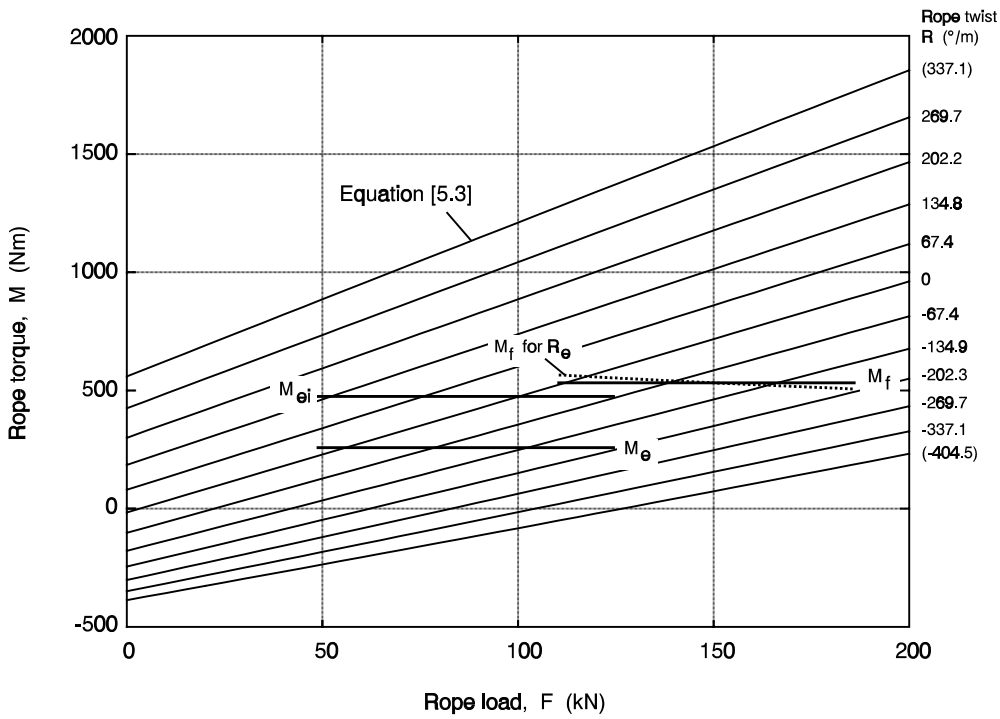

Figure C.2 - Equilibrium rope torques for rope S4 in relation to the torsion test data. Torsion test data for rope T8, 41 mm, 6x29(11/12/6 + 3Δ)/F, 1800 MPa. N_{load} according to equation [C.2].

C.2 Analysis details for shaft B, ropes S5 to S8, 41 mm at 1528,6 m

Table C.3 - Analysis data for rope S5 relating to figure 6.10.

Shaft analysis data, rope S5 shaft B	
Rope coil numbers	135575/001
Date of rope installation	22/7/95
Date of measurements	24/3/96, 20/4/96
q (kN/m)	0.0705
P_e (kN)	66,6
P_f (kN)	130,4
Payload, P_f - P_e (kN)	63,8
Payload envelope (%)	15
Lay type	RHL
Construction	6x29(11/12/6 + 3Δ)/F
LL_{nom} (mm)	309
$S_{u,wire}$ (MPa)	1900
z_{max} (m)	1760
L (m)	1528,6
Df	1
R_{coil} (°/m)	29,01
$SWbc$ (°/360 = turns)	196,9
$R_{coil}.z_{max}$ (turns)	141,8
z for R_{coil} (m) at installation equilibrium (% of L)	849,6 55,6
Φ_{lost} (turns)	445,4
$\Delta\Phi_{max}$ (turns) calculated	4,0
z for $\Delta\Phi_{max}$ (m) (% of L)	810,2 53,0
$LL_{ei}(0)$ (% change from nominal)	-11,65
$LL_{ei}(L)$ (% change from nominal)	14,56
$LL_e(0)$ (% change from nominal)	-3,23
$LL_e(L)$ (% change from nominal)	29,13
$LL_f(0)$ (% change from nominal)	-2,59
$LL_f(L)$ (% change from nominal)	28,16
Rotation error range (turns)	-3,16 → 0
Lay length error range (% of nominal)	-3,7 → 4,5
M_{ei} (Nm)	660,1
M_e (Nm)	461,4
M_f (Nm)	753,2

Torsion test data, rope T8	
Torsion test rope coil number	136053/001
d_{nom} (mm)	41
d_0 (mm)	42,6
LL_0 (mm)	325
LL_{nom} (mm)	309
l_0 (mm)	2670
Lay type	RHL
K_{LL} (1/(°/m))	3,4426e-4
A_{met} (mm²)	773,2
Construction	6x29(11/12/6 + 3Δ)/F
$S_{u,wire}$ (MPa)	1800

Table C.4 - Analysis data for ropes S6, S7 and S8 relating to figure 6.11.

Shaft analysis data, ropes S6, S7 and S8 shaft B	
Rope coil numbers	S6 - 135576/002 S7 - 135575/002 S8 - 134826/001
Date of rope installation	22/7/95
Date of measurements	24/3/96, 20/4/96
q (kN/m)	0,0705
P_e (kN)	66,6
P_f (kN)	130,4
Payload, P_f - P_e (kN)	63,8
Payload envelope (%)	15
Lay type	RHL, LHL
Construction	6x29(11/12/6 + 3Δ)/F
LL_{nom} (mm)	309
$S_{u,wire}$ (MPa)	1900
z_{max} (m)	1760
L (m)	1528,6
Df	1
R_{coil} (°/m)	4,74 *
$SWbc$ (°/360 = turns)	94,3
$R_{coil}.z_{max}$ (turns)	23,2
z for R_{coil} (m) at installation equilibrium (% of L)	849,6 55,6
Φ_{lost} (turns)	108,5
$\Delta\Phi_{max}$ (turns)	3,26
z for $\Delta\Phi_{max}$ (m) (% of L)	810,2 53
$LL_{ei}(0)$ (% change from nominal)	-9,71
$LL_{ei}(L)$ (% change from nominal)	17,8
$LL_e(0)$ (% change from nominal)	-7,77
$LL_e(L)$ (% change from nominal)	21,04
$LL_f(0)$ (% change from nominal)	-7,44
$LL_f(L)$ (% change from nominal)	20,39
Rotation error range (turns)	-2,99 → 0,09
Lay length error range (% of nominal)	-1,99 → 1,95
M_{ei} (Nm)	612,4
M_e (Nm)	562,9
M_f (Nm)	870,4

Torsion test data, rope T8	
Torsion test rope coil number	136053/001
d_{nom} (mm)	41
d_0 (mm)	42,6
LL_0 (mm)	325
LL_{nom} (mm)	309
l_0 (mm)	2670
Lay type	RHL
K_{LL} (1/(°/m))	3,4426e-4
A_{met} (mm²)	773,2
Construction	6x29(11/12/6 + 3Δ)/F
$S_{u,wire}$ (MPa)	1800

* = Twist for average manufactured lay length (LL_m) of the three coils (320, 326 and 324,5 mm).

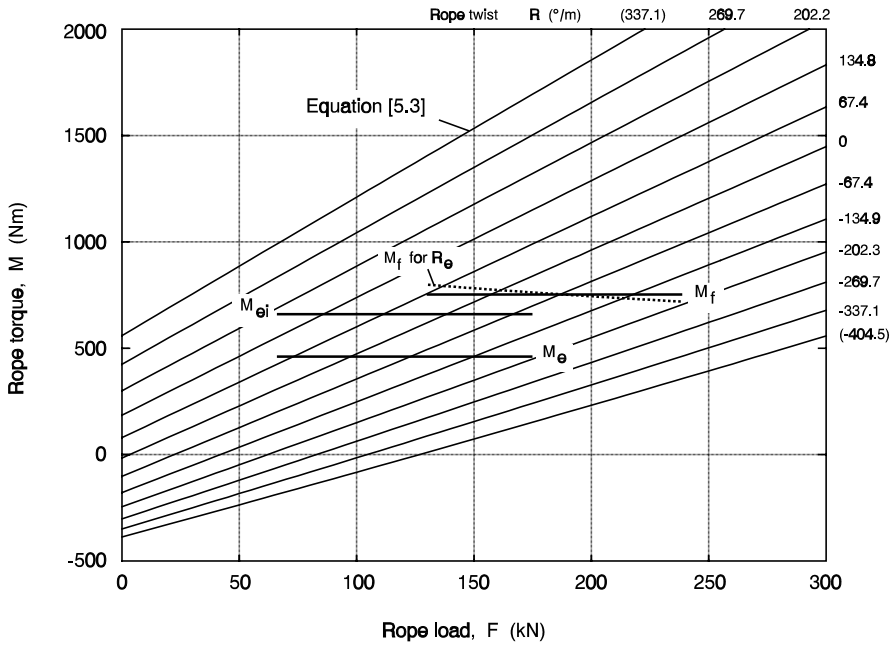

Figure C.3 - Equilibrium rope torques for rope S5 in relation to the torsion test data. Torsion test data for rope T8, 41 mm, 6x29(11/12/6 + 3Δ)/F, 1800 MPa. N_{load} according to equation [C.2].

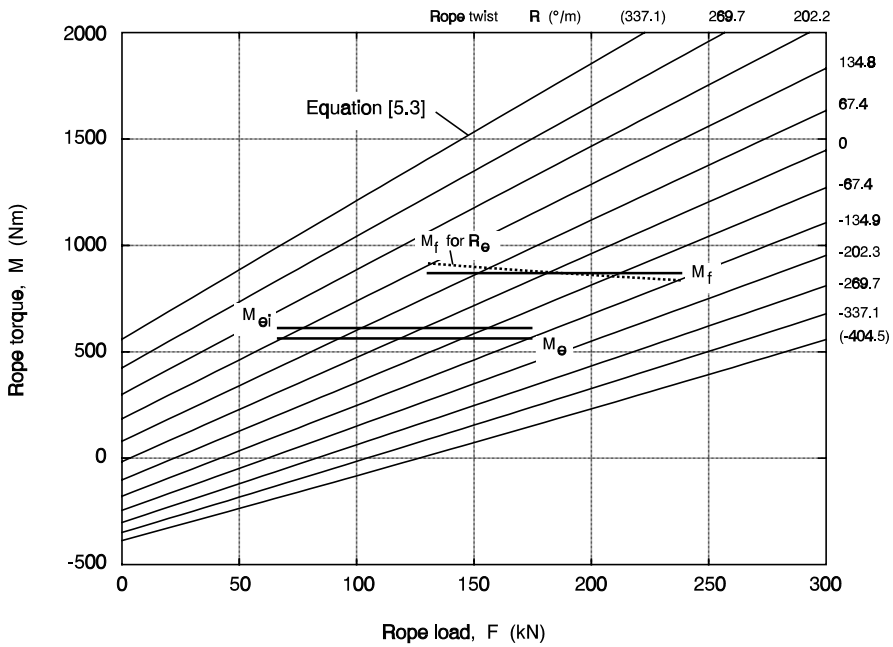

Figure C.4 - Equilibrium rope torques for ropes S6, S7 and S8 in relation to the torsion test data. Torsion test data for rope T8, 41 mm, 6x29(11/12/6 + 3Δ)/F, 1800 MPa. N_{load} according to equation [C.2].

C.2.1 Torsion test constants for rope T8, 41 mm, 6x29(11/12/6 + 3Δ)/F, 1800 MPa

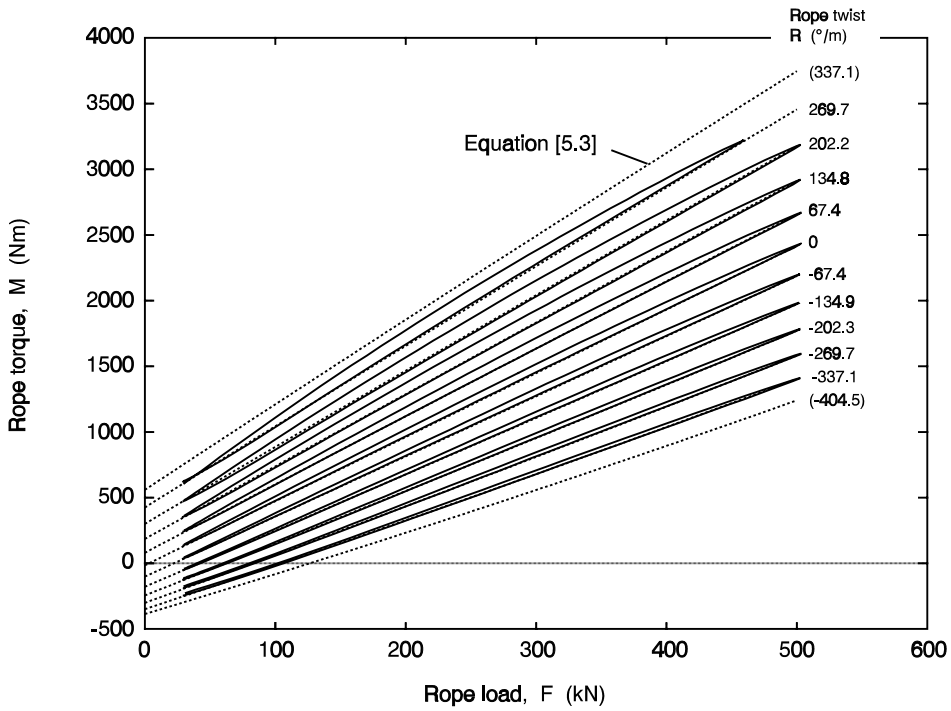

Figure C.5 - Measured and calculated rope torque versus load for rope T8, 41 mm, 6x29(11/12/6 + 3Δ)/F, 1800 MPa. N_{load} according to equation [C.2].

The torsion tests data for rope T8 was used in the analysis for ropes S1 to S8.

From the constant twist test on rope T8 :

$$N_{avg} = \begin{bmatrix} -1.9172e-009 & 1.4803e-006 & 1.0164e-003 \\ -3.1247e-006 & 5.8210e-003 & 1.3161e+000 \\ -6.3402e-004 & 5.1944e+000 & -1.8946e+001 \end{bmatrix} \qquad [C.1]$$

$$N_{load} = \begin{bmatrix} 9.7771e-010 & 1.9844e-007 & 1.0648e-003 \\ -1.1115e-006 & 4.8126e-003 & 1.3472e+000 \\ -7.4563e-005 & 4.9014e+000 & -1.5882e+001 \end{bmatrix} \qquad [C.2]$$

From the constant load tests on rope T8:

$$a_{cl} = \begin{bmatrix} 62.4519 & 121.0152 & 183.8956 & 228.7990 & 289.5209 \\ 36.2797 & 71.5503 & 108.0805 & 137.5938 & 173.4942 \\ 17.6365 & 34.8536 & 51.3723 & 67.3611 & 84.2290 \\ 7.9216 & 15.9170 & 23.2816 & 33.4792 & 41.1592 \\ 5.0021 & 7.5859 & 10.3565 & 14.5197 & 17.1969 \end{bmatrix} \qquad [C.3] \quad (Nm)$$

$$b_{cl} = \begin{bmatrix} 0.4043 & 0.2058 & 0.1438 & 0.1202 & 0.0970 \\ 0.5179 & 0.2690 & 0.1876 & 0.1611 & 0.1321 \\ 0.7357 & 0.3954 & 0.3035 & 0.2425 & 0.2094 \\ 0.4323 & 0.5365 & 0.4278 & 0.3429 & 0.3583 \\ 0.1547 & 0.4003 & 0.3765 & 0.4138 & 0.4403 \end{bmatrix} \qquad [C.4] \quad (1/(°/m))$$

$$c_{cl} = \begin{bmatrix} 2.0020 & 2.8344 & 3.4441 & 4.3599 & 5.0809 \\ 2.0119 & 2.7720 & 3.3551 & 4.0620 & 4.7336 \\ 1.8790 & 2.5921 & 3.1845 & 3.7803 & 4.4331 \\ 1.6771 & 2.3772 & 2.8722 & 3.3263 & 3.9239 \\ 1.3097 & 2.0184 & 2.4997 & 2.9511 & 3.5462 \end{bmatrix} \qquad [C.5] \quad (Nm/(°/m))$$

Constant loads corresponding to the columns of a_{cl} , b_{cl} and c_{cl} :

$$F_{cl} = [\ 60 \quad 170 \quad 280 \quad 390 \quad (500)\ ] \qquad (kN) \qquad [C.6]$$

Starting twists corresponding to the rows of a_{cl} , b_{cl} and c_{cl} :

$$R_{cl0} = \begin{bmatrix} (474) \\ 270 \\ 67 \\ -135 \\ -337 \end{bmatrix} \qquad (°/m) \qquad [C.7]$$

C.3 Analysis details for shaft C, ropes S9 and S10, 46 mm at 1425,5 m

Table C.5 - Analysis data for ropes S9 and S10 relating to figure 6.12.

Shaft analysis data, ropes S9 and S10 shaft C	
Rope coil numbers	121047/001 121047/002
Date of rope installation	14/10/90
Date of measurements	21/12/95
q (kN/m)	0,0887
P_e (kN)	70,5
P_f (kN)	153,9
Payload, P_f - P_e (kN)	83,4
Payload envelope (%)	15
Lay type	RHL
Construction	6x31(13/12/6 + 3Δ)/F
LL_{nom} (mm)	348
$S_{u,wire}$ (MPa)	1800 Drawn galvanised
z_{max} (m)	1905
L (m)	1425,5
Df	1
R_{coil} (°/m)	70,78
$SWbc$ (°/360 = turns)	413,5
$R_{coil}.z_{max}$ (turns)	374,5
z for R_{coil} (m) at installation equilibrium (% of L)	868,9 60,95
Φ_{lost} (turns)	439
$\Delta\Phi_{max}$ (turns)	4,81
z for $\Delta\Phi_{max}$ (m) (% of L)	769,8 54,0
$LL_{ei}(0)$ (% change from nominal)	-13,51
$LL_{ei}(L)$ (% change from nominal)	16,67
$LL_e(0)$ (% change from nominal)	-3,16
$LL_e(L)$ (% change from nominal)	33,91
$LL_f(0)$ (% change from nominal)	-2,87
$LL_f(L)$ (% change from nominal)	32,76
Rotation error range (turns)	-0,899 → 1,003
Lay length error range (% of nominal)	-4,79 → 5,41
M_{ei} (Nm)	913,5
M_e (Nm)	645,2
M_f (Nm)	1060,3

Torsion test data, rope T9	
Torsion test rope coil number	137944/001
d_{nom} (mm)	46
d_0 (mm)	47,0
LL_0 (mm)	392,4
LL_{nom} (mm)	348
l_0 (mm)	2661
Lay type	RHL
K_{LL} (1/(°/m))	3,8011e-4
A_{met} (mm²)	970,3
Construction	6x31(13/12/6 + 3Δ)/F
$S_{u,wire}$ (MPa)	1800

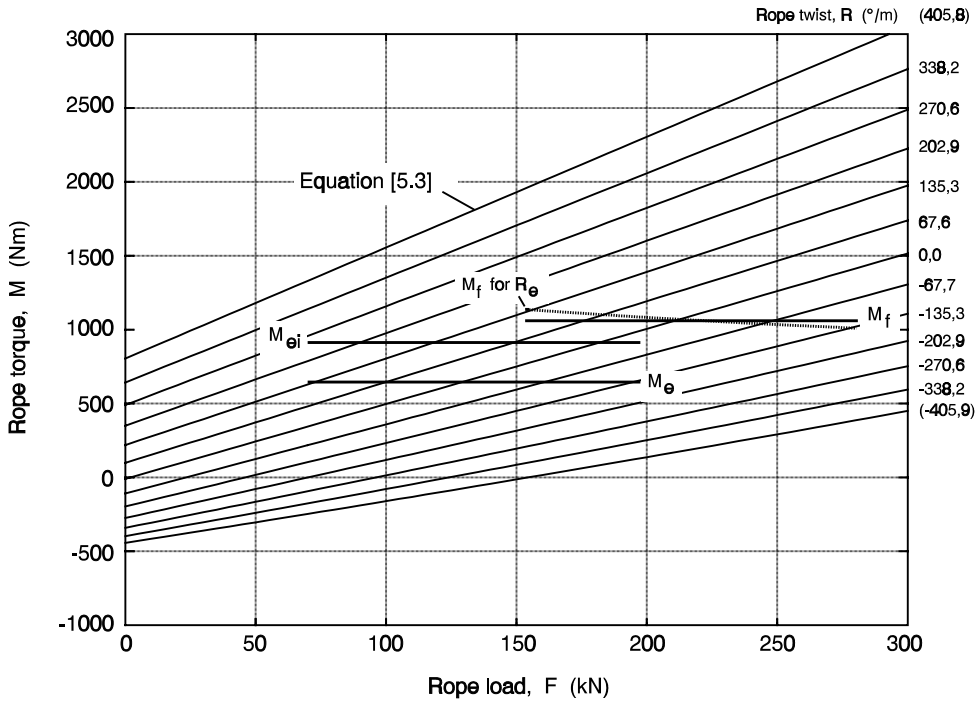

Figure C.6 - Equilibrium rope torques for ropes S9 and S10 in relation to the torsion test data. Torsion test data for rope T9, 46 mm, 6x31(13/12/6 + 3Δ)/F, 1800 MPa. N_{load} according to equation [6.2].

For ropes S9 and S10 : N_{avg} , N_{load} , a_{cl} , b_{cl} , c_{cl} , F_{cl} and R_{cl0} are the same as for rope S13, as given in equations [6.1], [6.2], and [6.4] to [6.8].

C.4 Analysis details for shaft D, ropes S11 and S12, 46 mm at 1425,5 m

Table C.6 - Analysis data for ropes S11 and S12 relating to figure 6.13.

Shaft analysis data, ropes S11 and S12 shaft D	
Rope coil numbers	122312/001 122312/002
Date of rope installation	14/1/96
Date of measurements	2/2/96
q (kN/m)	0,0887
P_e (kN)	70,5
P_f (kN)	153,9
Payload, P_f - P_e (kN)	83,4
Payload envelope (%)	15
Lay type	RHL
Construction	6x31(13/12/6 + 3Δ)/F
LL_{nom} (mm)	348
$S_{u,wire}$ (MPa)	1800 Drawn galvanised
z_{max} (m)	1905
L (m)	1425,5
Df	1
R_{coil} (°/m)	67,75
$SWbc$ (°/360 = turns)	401,5
$R_{coil}.z_{max}$ (turns)	358,5
z for R_{coil} (m) at installation equilibrium (% of L)	868,9 60,95
Φ_{lost} (turns)	75,1
$\Delta\Phi_{max}$ (turns) calculated	3,41
z for $\Delta\Phi_{max}$ (m) (% of L)	755,5 53,0
$LL_{ei}(0)$ (% change from nominal)	-13,22
$LL_{ei}(L)$ (% change from nominal)	16,95
$LL_e(0)$ (% change from nominal)	-11,49
$LL_e(L)$ (% change from nominal)	19,83
$LL_f(0)$ (% change from nominal)	-11,21
$LL_f(L)$ (% change from nominal)	19,25
Rotation error range (turns)	0 → 1,22
Lay length error range (% of nominal)	-2.52 → 2.59
M_{ei} (Nm)	905,7
M_e (Nm)	857,8
M_f (Nm)	1315,8

Torsion test data, rope T9	
Torsion test rope coil number	137944/001
d_{nom} (mm)	46
d_0 (mm)	47,0
LL_0 (mm)	392,4
LL_{nom} (mm)	348
l_0 (mm)	2661
Lay type	RHL
K_{LL} (1/(°/m))	3,8011e-4
A_{met} (mm²)	970,3
Construction	6x31(13/12/6 + 3Δ)/F
$S_{u,wire}$ (MPa)	1800

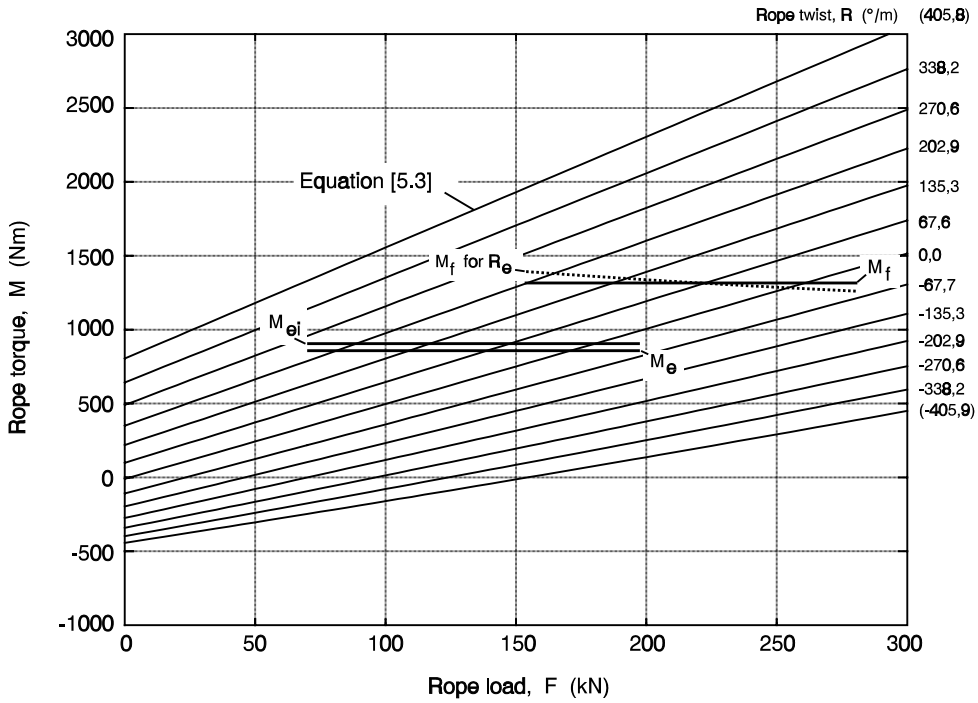

Figure C.7 - Equilibrium rope torques for rope S11 and S12 in relation to the torsion test data. Torsion test data for rope T9, 46 mm, 6x31(13/12/6 + 3Δ)/F, 1800 MPa. N_{load} according to equation [6.2].

For ropes S11 and S12 : N_{avg} , N_{load} , a_{cl} , b_{cl} , c_{cl} , F_{cl} and R_{cl0} are the same as for rope S13, as give in equations [6.1], [6.2], and [6.4] to [6.8].

C.5 Analysis details for shaft F, ropes S14 and S15, 48 mm at 2196 m

Table C.7 - Analysis data for ropes S14 and S15 relating to figures 6.14 and 6.15

Shaft analysis data, rope S15 shaft F, figure 6.15	
Rope coil number	124930/002
Date of rope installation	4/9/89
Date of measurements	13/12/90, 4/1/91
q (kN/m)	0,096
P_e (kN)	96,0
P_f (kN)	234,0
Payload, P_f - P_e (kN)	138,0
Payload envelope (%)	15
Lay type	RHL
Construction	6x32(14/12/6 + 3Δ)/F
LL_{nom} (mm)	361
$S_{u,wire}$ (MPa)	1800
z_{max} (m)	2600
L (m)	2196
Df	1
R_{coil} (°/m)	55,0
$SWbc$ (°/360 = turns)	506,4
$R_{coil}.z_{max}$ (turns)	397,2
z for R_{coil} (m) at installation equilibrium (% of L)	1217 55,4
Φ_{lost} (turns)	267,2
$\Delta\Phi_{max}$ (turns)	14,95
z for $\Delta\Phi_{max}$ (m) (% of L)	1185,8 54,0
$LL_{ei}(0)$ (% change from nominal)	-18,28
$LL_{ei}(L)$ (% change from nominal)	25,76
$LL_e(0)$ (% change from nominal)	-14,68
$LL_e(L)$ (% change from nominal)	33,24
$LL_f(0)$ (% change from nominal)	-13,57
$LL_f(L)$ (% change from nominal)	30,75
Rotation error range (turns)	0,0 → 0,603
Lay length error range (% of nominal)	-1,838 → 0,926
M_{ei} (Nm)	1344,8
M_e (Nm) Measured (Hecker, van Zyl, 1993)	1203,1 (1270,0)
M_f (Nm) Measured (Hecker, van Zyl, 1993)	1984,4 (2020,0)

Torsion test data, rope T10	
Torsion test rope coil number	140156/001
d_{nom} (mm)	48,0
d_0 (mm)	49,55
LL_0 (mm)	402,8
LL_{nom} (mm)	361
l_0 (mm)	2670
Lay type	RHL
K_{LL} (1/(°/m))	3,9799e-4
A_{met} (mm²)	1051,3
Construction	6x32(14/12/6 + 3Δ)/F
$S_{u,wire}$ (MPa)	1800

Shaft analysis data, rope S14 shaft F, figure 6.14 (all other data as per rope S15)	
Shaft rope coil number	124930/001
Date of measurements	6/12/90
Φ_{lost} (turns)	374,5
$LL_e(0)$ (% change from nominal)	-13,02
$LL_e(L)$ (% change from nominal)	36,57
Lay length error range (% of nominal)	-1.96 → 1.47
M_e (Nm)	1148

Note : The data for rope S15 is also applicable to figure 2.16 and figure 6.35

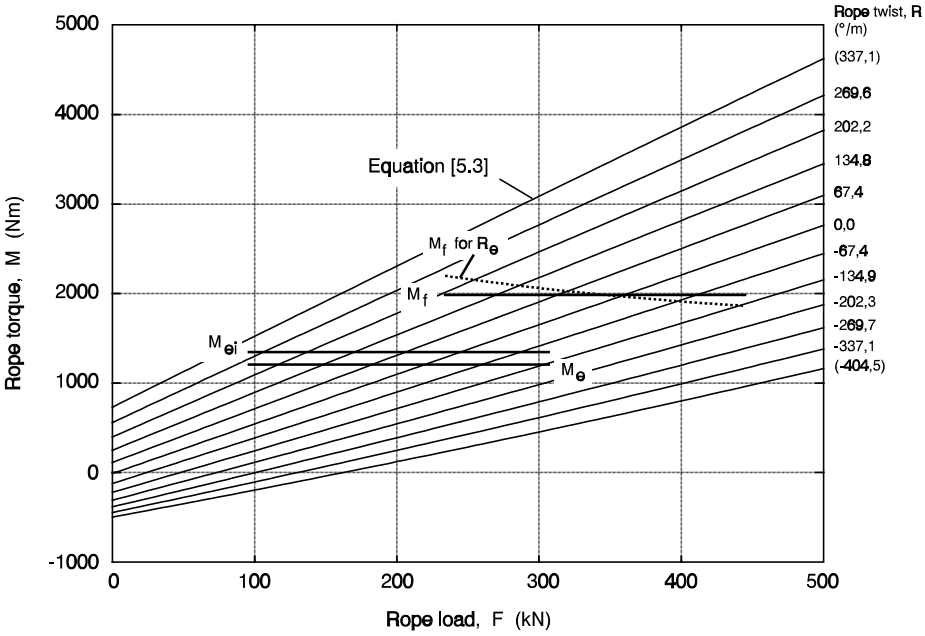

Figure C.8 - Equilibrium rope torques for rope S15 in relation to the torsion test data. Torsion test data for rope T10, 48 mm, 6x32(14/12/6 + 3Δ)/F, 1800 MPa. N_{load} according to equation [C.9].

C.5.1 Torsion test constants for rope T10, 48 mm, 6x32(14/12/6 + 3Δ)/F, 1800 MPa

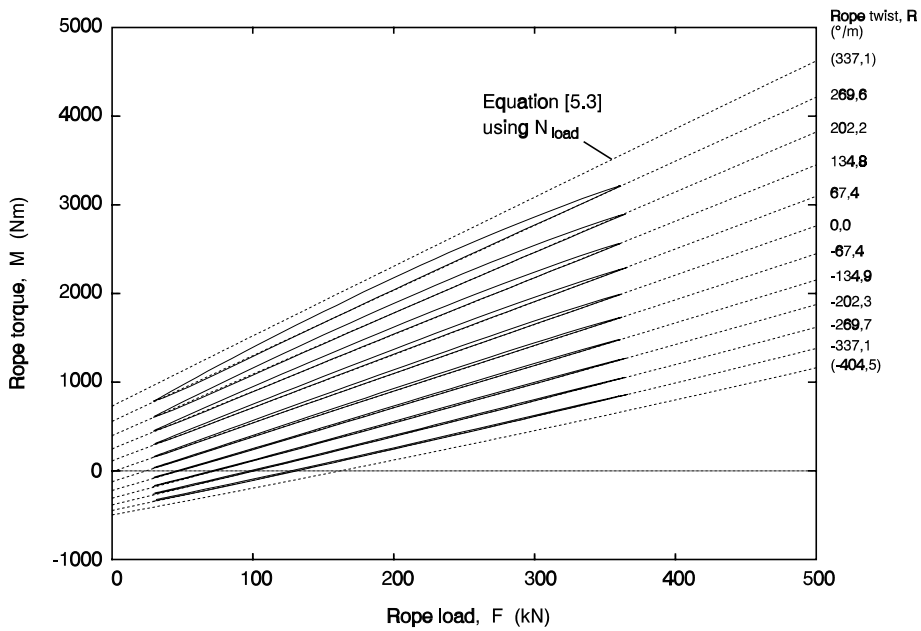

Figure C.9 - Measured and calculated rope torque versus load for rope T10. Torsion test data for rope T10, 48 mm, 6x32(14/12/6 + 3Δ)/F, 1800 MPa. N_{load} according to equation [C.9].

From the constant twist test on rope T10 :

$$N_{avg} = \begin{bmatrix} -3.1372e-009 & 2.5175e-006 & 1.3984e-003 \\ -4.4020e-006 & 8.0255e-003 & 1.7297e+000 \\ -5.8787e-004 & 5.7667e+000 & -1.1472e+001 \end{bmatrix} \qquad [C.8]$$

$$N_{load} = \begin{bmatrix} 9.8555e-010 & 1.0320e-006 & 1.3445e-003 \\ -1.3989e-006 & 6.8321e-003 & 1.7450e+000 \\ 2.4826e-005 & 5.5357e+000 & -1.1802e+001 \end{bmatrix} \qquad [C.9]$$

From the constant load tests on rope T10 :

$$a_{cl} = \begin{bmatrix} 3.9581 & 6.5089 & 9.8847 & 12.1324 & 18.2342 \\ 8.0538 & 13.4211 & 19.0387 & 25.3375 & 37.2952 \\ 18.2685 & 29.0869 & 40.4925 & 53.6558 & 77.9941 \\ 41.4891 & 61.0532 & 84.1025 & 107.6228 & 153.8426 \\ 45.5727 & 90.5333 & 124.1378 & 165.1217 & 248.5326 \\ 64.4109 & 129.8753 & 177.8494 & 235.4161 & 355.2467 \end{bmatrix} \qquad [C.10] \quad (\text{Nm})$$

$$b_{cl} = \begin{bmatrix} 0.5450 & 0.4463 & 0.3441 & 0.4187 & 0.3699 \\ 0.5083 & 0.6587 & 0.5637 & 0.4550 & 0.4711 \\ 0.7302 & 0.5682 & 0.4665 & 0.3808 & 0.3317 \\ 0.7032 & 0.4264 & 0.3260 & 0.2692 & 0.1832 \\ 0.6503 & 0.3592 & 0.2735 & 0.2519 & 0.1929 \\ 0.5946 & 0.2989 & 0.2285 & 0.1970 & 0.1421 \end{bmatrix} \qquad [C.11] \quad (1/(°/\text{m}))$$

$$c_{cl} = \begin{bmatrix} 2.0412 & 2.7123 & 3.2666 & 3.7958 & 5.0631 \\ 2.5557 & 3.2490 & 3.7803 & 4.2524 & 5.4971 \\ 2.8822 & 3.5512 & 4.1494 & 4.6897 & 6.0005 \\ 2.8760 & 3.6457 & 4.2490 & 4.8454 & 6.2645 \\ 2.9162 & 3.7197 & 4.4169 & 5.2509 & 6.8677 \\ 2.6984 & 3.5856 & 4.3583 & 5.4081 & 7.2395 \end{bmatrix} \qquad [C.12] \quad (\text{Nm}/(°/\text{m}))$$

Constant loads corresponding to the columns of a_{cl}, b_{cl} and c_{cl} :

$$F_{cl} = [\ 90 \quad 170 \quad 250 \quad 330 \quad (500)\ ] \qquad (\text{kN}) \qquad [C.13]$$

Starting twists corresponding to the rows of a_{cl}, b_{cl} and c_{cl} :

$$R_{cl0} = \begin{bmatrix} -270 \\ -135 \\ 0 \\ 135 \\ 243 \\ (351) \end{bmatrix} \qquad (°/\text{m}) \qquad [C.14]$$

C.6 Analysis details for shaft G, ropes S16 and S17, 49 mm at 1126 m

Table C.8 - Analysis data for rope S16 relating to the results in figures 6.16 and 6.17.

Shaft analysis data, rope S16 shaft G, figure 6.17	
Rope coil number	131275/001
Date of rope installation	20/2/94
Date of measurements	7/9/95
q (kN/m)	0,0995
P_e (kN)	86,7
P_f (kN)	183,0
Payload, P_f - P_e (kN)	96,3
Payload envelope (%)	15
Lay type	RHL
Construction	6x32(14/12/6 + 3Δ)/F
LL_{nom} (mm)	368
$S_{u,wire}$ (MPa)	1900
z_{max} (m)	1375
L (m)	1126
Df	1
R_{coil} (°/m)	73,86
$SWbc$ (°/360 = turns)	290,4
$R_{coil} \cdot z_{max}$ (turns)	282,1
z for R_{coil} (m) at installation equilibrium (% of L)	649,1 57,7
Φ_{lost} (turns)	156,4
$\Delta\Phi_{max}$ (turns)	3,29
z for $\Delta\Phi_{max}$ (m) (% of L)	596,8 53
$LL_{ei}(0)$ (% change from nominal)	-9,51
$LL_{ei}(L)$ (% change from nominal)	16,30
$LL_e(0)$ (% change from nominal)	-4,35
$LL_e(L)$ (% change from nominal)	23,91
$LL_f(0)$ (% change from nominal)	-3,80
$LL_f(L)$ (% change from nominal)	22,83
Rotation error range (turns)	-0,14 → 0,36
Lay length error range (% of nominal)	-1,80 → 1,45
M_{ei} (Nm)	1037,0
M_e (Nm)	886,0
M_f (Nm)	1431,0

Torsion test data, rope T11	
Torsion test rope coil number	135197/001
d_{nom} (mm)	49
d_0 (mm)	50,4
LL_0 (mm)	421,5
LL_{nom} (mm)	368
l_0 (mm)	2669
Lay type	RHL
K_{LL} (1/(°/m))	4,0519e-4
A_{met} (mm²)	1088,2
Construction	6x32(14/12/6 + 3Δ)/F
$S_{u,wire}$ (MPa)	1800

Shaft analysis data, rope S16 and S17 combined, Shaft G, figure 6.16	
Coil numbers	16 - 131275/001 17 - 131275/002
Date of measurements	1/2/96
Φ_{lost} (turns)	385,0
$LL_e(0)$ (% change from nominal)	3,80
$LL_e(L)$ (% change from nominal)	36,69
M_e (Nm)	678,7

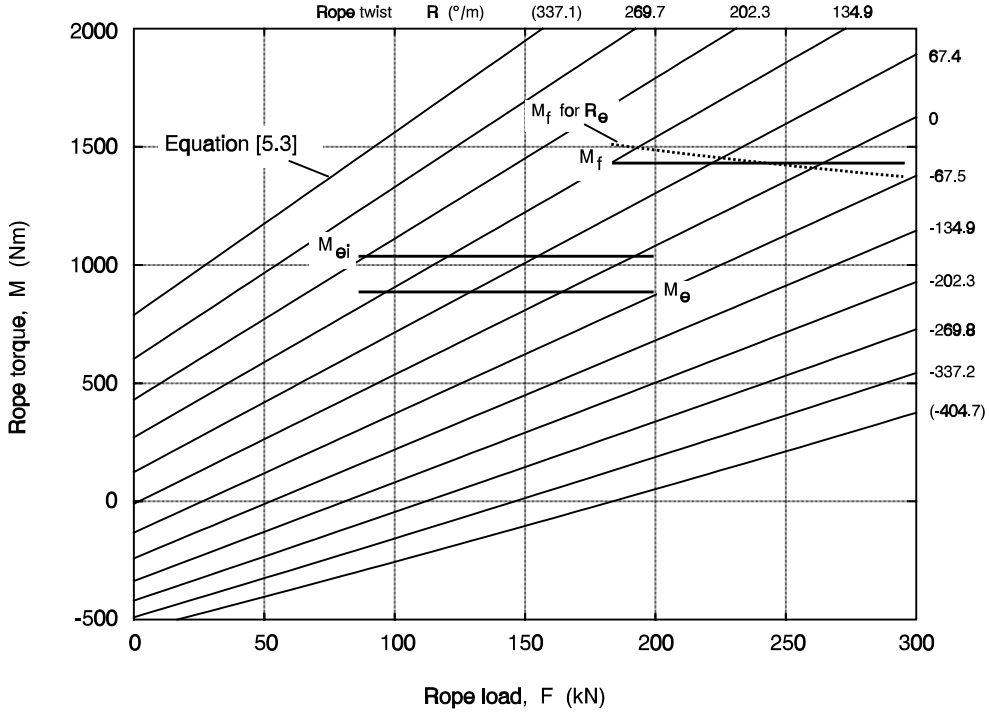

Figure C.10 - Equilibrium rope torques for rope S16 in relation to the torsion test data. Torsion test data for rope T11, 49 mm, 6x32(14/12/6 + 3Δ)/F, 1800 MPa. N_{load} according to equation [C.16].

C.7 Analysis details for shaft H, ropes S18 and S19, 49 mm at 1068 m

Table C.9 - Analysis data for ropes S18 and S19 relating to the results in figure 6.18

Shaft analysis data, ropes S18 and S19 shaft H	
Rope coil number	S18 - 021079 S19 - 021183
Date of rope installation	8/10/89
Date of measurements	18/1/96, 23/1/96
q (kN/m)	0,0995
P_e (kN)	55,2
P_f (kN)	144,3
Payload, P_f - P_e (kN)	89,1
Payload envelope (%)	15
Lay type	RHL
Construction	6x32(14/12/6 + 3Δ)/F
LL_{nom} (mm)	368
$S_{u,wire}$ (MPa)	1800
z_{max} (m)	1356
L (m)	1068,1
Df	1
R_{coil} (°/m)	71,62
$SWbc$ (°/360 = turns)	280,2
$R_{coil}.z_{max}$ (turns)	269,8
z for R_{coil} (m) at installation equilibrium (% of L)	632,3 59,2
Φ_{lost} (turns)	496,6
$\Delta\Phi_{max}$ (turns)	5,71
z for $\Delta\Phi_{max}$ (m) (% of L)	555,4 52
$LL_{ei}(0)$ (% change from nominal)	-9,78
$LL_{ei}(L)$ (% change from nominal)	16,30
$LL_e(0)$ (% change from nominal)	8,70
$LL_e(L)$ (% change from nominal)	45,92
$LL_f(0)$ (% change from nominal)	9,78
LL_f(L) (% change from nominal)	44,02
Rotation error range (turns)	-1,96 → 0,51
Lay length error range (% of nominal)	-1,05 → 2,11
M_{ei} (Nm)	833,6
M_e (Nm)	393,6
M_f (Nm)	835,4

Torsion test data, rope T11	
Torsion test rope coil number	135197/001
d_{nom} (mm)	49
d_0 (mm)	50,4
LL_0 (mm)	421,5
LL_{nom} (mm)	368
l_0 (mm)	2669
Lay type	RHL
K_{LL} (1/(°/m))	4,0519e-4
A_{met} (mm²)	1088,2
Construction	6x32(14/12/6 + 3Δ)/F
$S_{u,wire}$ (MPa)	1800

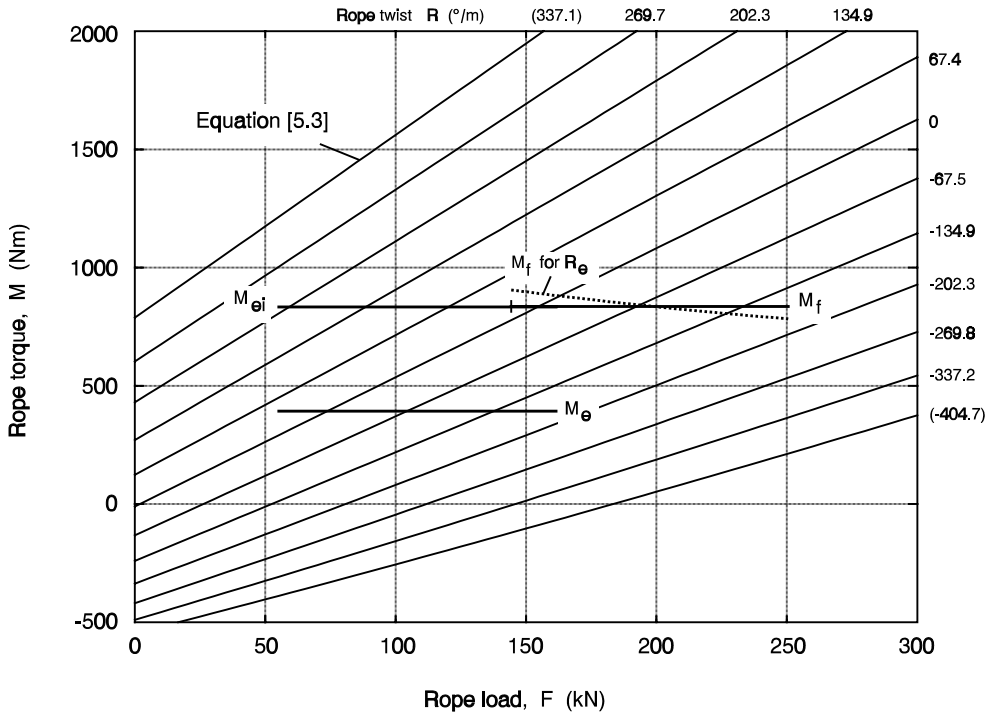

Figure C.11 - Equilibrium rope torques for ropes S18 and S19 in relation to the torsion test data. Torsion test data for rope T11, 49 mm, 6x32(14/12/6 + 3Δ)/F, 1800 MPa. N_{load} according to equation [C.16].

C.8 Analysis details for shaft J, rope S20, 49 mm at 1598,6 m

Table C.10 - Analysis data for rope S20 relating to the results in figure 6.19

Shaft analysis data, rope S20 shaft J	
Rope coil number	018434
Date of rope installation	3/4/94
Date of measurements	21/1/96
q (kN/m)	0,0995
P_e (kN)	73,0
P_f (kN)	113,9
Payload, P_f - P_e (kN)	40,9
Payload envelope (%)	15
Lay type	RHL
Construction	6x32(14/12/6 + 3Δ)/F
LL_{nom} (mm)	368
$S_{u,wire}$ (MPa)	1800
z_{max} (m)	1920
L (m)	1598,6
Df	1
R_{coil} (°/m)	78,37
$SWbc$ (°/360 = turns)	454,9
$R_{coil}.z_{max}$ (turns)	418,0
z for R_{coil} (m) at installation equilibrium (% of L)	902 56,43
Φ_{lost} (turns)	204,3
$\Delta\Phi_{max}$ (turns)	2,52
z for $\Delta\Phi_{max}$ (m) (% of L)	863,2 54,0
$LL_{ei}(0)$ (% change from nominal)	-14,67
$LL_{ei}(L)$ (% change from nominal)	20,65
$LL_e(0)$ (% change from nominal)	-10,33
$LL_e(L)$ (% change from nominal)	27,99
$LL_f(0)$ (% change from nominal)	-10,33
$LL_f(L)$ (% change from nominal)	27,45
Rotation error range (turns)	0 → 0,827
Lay length error range (% of nominal)	2,27 → 1,71
M_{ei} (Nm)	1119,3
M_e (Nm)	976,0
M_f (Nm)	1209,0

Torsion test data, rope T11	
Torsion test rope coil number	135197/001
d_{nom} (mm)	49
d_0 (mm)	50,4
LL_0 (mm)	421,5
LL_{nom} (mm)	368
l_0 (mm)	2669
Lay type	RHL
K_{LL} (1/(°/m))	4,0519e-4
A_{met} (mm²)	1088,2
Construction	6x32(14/12/6 + 3Δ)/F
$S_{u,wire}$ (MPa)	1800

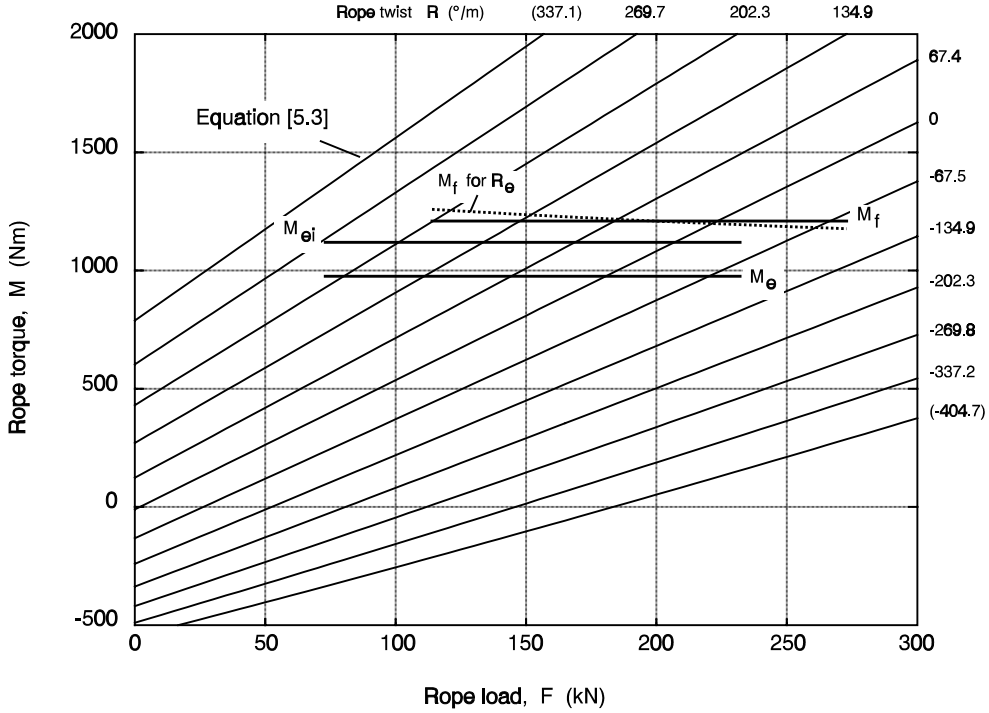

Figure C.12 - Equilibrium rope torques for rope S20 in relation to the torsion test data. Torsion test data for rope T11, 49 mm, 6x32(14/12/6 + 3Δ)/F, 1800 MPa. N_{load} according to equation [B.16].

C.9 Analysis details for shaft K, rope S21, 49 mm at 1935,4 m

Table C.11 - Analysis data for rope S21 relating the results in figure 6.20.

Shaft analysis data, rope S21 shaft K	
Rope coil number	116724/002
Date of rope installation	8/1/95
Date of measurements	20/1/96
q (kN/m)	0,0995
P_e (kN)	55,2
P_f (kN)	96,0
Payload, P_f - P_e (kN) locomotive	40,8
Payload envelope (%)	15
Lay type	RHL
Construction	6x32(14/12/6 + 3Δ)/F
LL_{nom} (mm)	368
$S_{u,wire}$ (MPa)	1800
z_{max} (m)	2360
L (m)	1935,4
Df	1
R_{coil} (°/m)	73,86
$SWbc$ (°/360 = turns)	564,1
$R_{coil}.z_{max}$ (turns)	484,2
z for R_{coil} (m) at installation equilibrium (% of L)	1096 56,6
Φ_{lost} (turns)	192,7
$\Delta\Phi_{max}$ (turns)	3,83
z for $\Delta\Phi_{max}$ (m) (% of L)	1045,1 54,0
$LL_{ei}(0)$ (% change from nominal)	-17,93
$LL_{ei}(L)$ (% change from nominal)	24,73
$LL_e(0)$ (% change from nominal)	-14,95
$LL_e(L)$ (% change from nominal)	30,97
$LL_f(0)$ (% change from nominal)	-14,67
$LL_f(L)$ (% change from nominal)	30,16
Rotation error range (turns)	0 → 1,94
Lay length error range (% of nominal)	-1,01 → 1,31
M_{ei} (Nm)	1113,8
M_e (Nm)	1001,8
M_f (Nm)	1236,2

Torsion test data, rope T11	
Torsion test rope coil number	135197/001
d_{nom} (mm)	49
d_0 (mm)	50,4
LL_0 (mm)	421,5
LL_{nom} (mm)	368
l_0 (mm)	2669
Lay type	RHL
K_{LL} (1/(°/m))	4,0519e-4
A_{met} (mm²)	1088,2
Construction	6x32(14/12/6 + 3Δ)/F
$S_{u,wire}$ (MPa)	1800

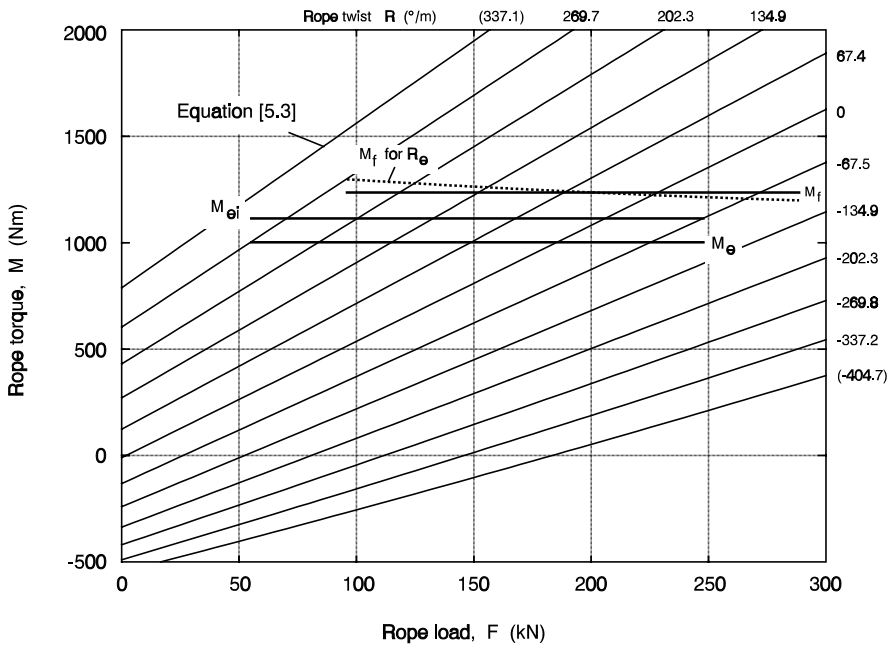

Figure C.13 - Equilibrium rope torques for rope S21 in relation to the torsion test data. Torsion test data for rope T11, 49 mm, 6x32(14/12/6 + 3Δ)/F, 1800 MPa. N_{load} according to equation [C.16].

C.9.1 Torsion test constants for rope T11, 49 mm, 6x32(14/12/6 + 3Δ)/F, 1800 MPa

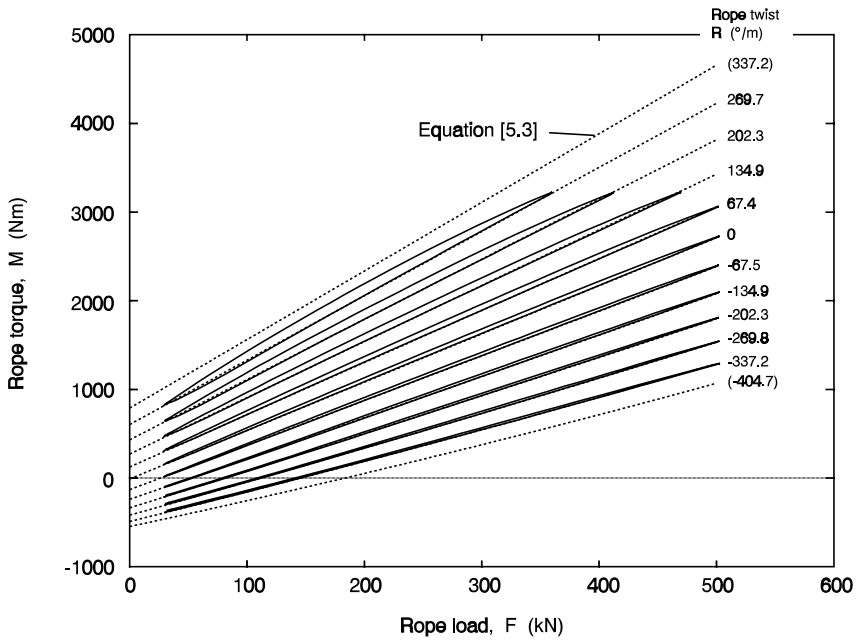

Figure C.14 - Measured and calculated rope torque versus load for rope T11, 49 mm, 6x32(14/12/6 + 3Δ)/F, 1800 MPa. N_{load} according to equation [C.16].

From the constant twist test on rope T11 :

$$N_{avg} = \begin{bmatrix} -3.4791e-009 & 2.1676e-006 & 1.4449e-003 \\ -3.8159e-006 & 7.7773e-003 & 1.8855e+000 \\ -5.1633e-004 & 5.7112e+000 & -1.1622e+001 \end{bmatrix} \qquad [C.15]$$

$$N_{load} = \begin{bmatrix} 3.1040e-009 & 2.5798e-007 & 1.4042e-003 \\ -8.1895e-007 & 6.6079e-003 & 1.8954e+000 \\ -6.0227e-005 & 5.4740e+000 & -1.0498e+001 \end{bmatrix} \qquad [C.16]$$

From the constant load tests on rope T11 :

$$a_{cl} = \begin{bmatrix} 84.9550 & 144.0455 & 213.8942 & 281.3532 & 372.1846 \\ 46.0228 & 79.1470 & 116.1578 & 151.6922 & 200.9204 \\ 18.1044 & 30.7573 & 42.1261 & 54.3698 & 71.1872 \\ 7.1317 & 12.5926 & 17.7421 & 22.5282 & 29.8870 \\ 4.7705 & 5.6577 & 7.3284 & 10.5310 & 12.5680 \end{bmatrix} \qquad [C.17] \quad (\text{Nm})$$

$$b_{cl} = \begin{bmatrix} 0.3299 & 0.2188 & 0.1854 & 0.1717 & 0.1528 \\ 0.4737 & 0.2924 & 0.2720 & 0.2598 & 0.2327 \\ 0.7026 & 0.5423 & 0.4119 & 0.3740 & 0.3313 \\ 0.2540 & 0.3202 & 0.3712 & 0.3351 & 0.3589 \\ 0.2155 & 0.1842 & 0.2391 & 0.2541 & 0.2597 \end{bmatrix} \qquad [C.18] \quad (1/(°/\text{m}))$$

$$c_{cl} = \begin{bmatrix} 2.8680 & 3.7886 & 5.1385 & 6.4351 & 8.0524 \\ 2.7686 & 3.7444 & 4.7188 & 5.7121 & 7.0793 \\ 2.6523 & 3.6124 & 4.3486 & 5.0938 & 6.2644 \\ 2.2063 & 3.0735 & 3.7150 & 4.3277 & 5.3622 \\ 1.8500 & 2.5570 & 3.2349 & 3.7473 & 4.6945 \end{bmatrix} \qquad [C.19] \quad (\text{Nm}/(°/\text{m}))$$

Constant loads corresponding to the columns of a_{cl} , b_{cl} and c_{cl} :

$$F_{cl} = [\ 60 \quad 160 \quad 260 \quad 360 \quad (500)\ ] \qquad (\text{kN}) \qquad [C.20]$$

Starting twists corresponding to the rows of a_{cl} , b_{cl} and c_{cl} :

$$R_{cl0} = \begin{bmatrix} (474) \\ 270 \\ 67 \\ -135 \\ -337 \end{bmatrix} \qquad (°/\text{m}) \qquad [C.21]$$

C.10 Analysis details for shaft L, rope S22, 54 mm at 1886,9 m

Table C.12 - Analysis data for rope S22 relating to figure 6.21

Shaft analysis data, rope S22 shaft L	
Rope coil number	129020/001
Date of rope installation	4/6/95
Date of measurements	4/2/96
q (kN/m)	0,1229
P_e (kN)	85,9
P_f (kN)	131,4
Payload, P_f - P_e (kN) locomotive	45,5
Payload envelope (%)	15
Lay type	RHL
Construction	6x32(14/12/6 + 3Δ)/F
LL_{nom} (mm)	409
$S_{u,wire}$ (MPa)	1950
z_{max} (m)	2410
L (m)	1886,9
Df	1
R_{coil} (°/m)	98,84
$SWbc$ (°/360 = turns)	681,8
$R_{coil}.z_{max}$ (turns)	661,7
z for R_{coil} (m) at installation equilibrium (% of L)	1102 58,4
Φ_{lost} (turns)	169,9
$\Delta\Phi_{max}$ (turns)	1,93
z for $\Delta\Phi_{max}$ (m) (% of L)	1000 53
$LL_{ei}(0)$ (% change from nominal)	-17,85
$LL_{ei}(L)$ (% change from nominal)	21,03
$LL_e(0)$ (% change from nominal)	14,67
$LL_e(L)$ (% change from nominal)	26,41
$LL_f(0)$ (% change from nominal)	14,43
$LL_f(L)$ (% change from nominal)	26,16
Rotation error range (turns)	-0,01 → 0,39
Lay length error range (% of nominal)	-2,55 → 2,50
M_{ei} (Nm)	1761,5
M_e (Nm)	1601,4
M_f (Nm)	1889,7

Torsion test data, rope T12	
Torsion test rope coil number	139666/001
d_{nom} (mm)	54
d_0 (mm)	55,95
LL_0 (mm)	485
LL_{nom} (mm)	409
l_0 (mm)	2666
Lay type	RHL
K_{LL} (1/(°/m))	4,4986e-4
A_{met} (mm²)	1344,0
Construction	6x32(14/12/6 + 3Δ)/F
$S_{u,wire}$ (MPa)	1950

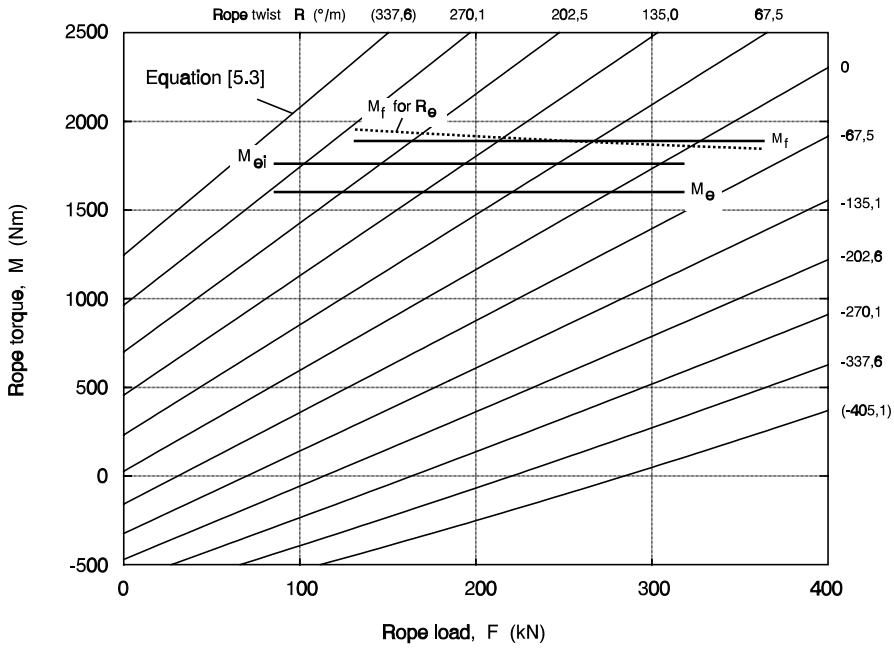

Figure C.15 - Equilibrium rope torques for rope S22 in relation to the torsion test data. Torsion test data for rope T12, 54 mm, 6x32(14/12/6 + 3Δ)/F, 1950 MPa. N_{load} according to equation [C.23].

C.10.1 Torsion test constants for rope T12, 54 mm, 6x32(14/12/6 + 3Δ)/F, 1950 MPa :

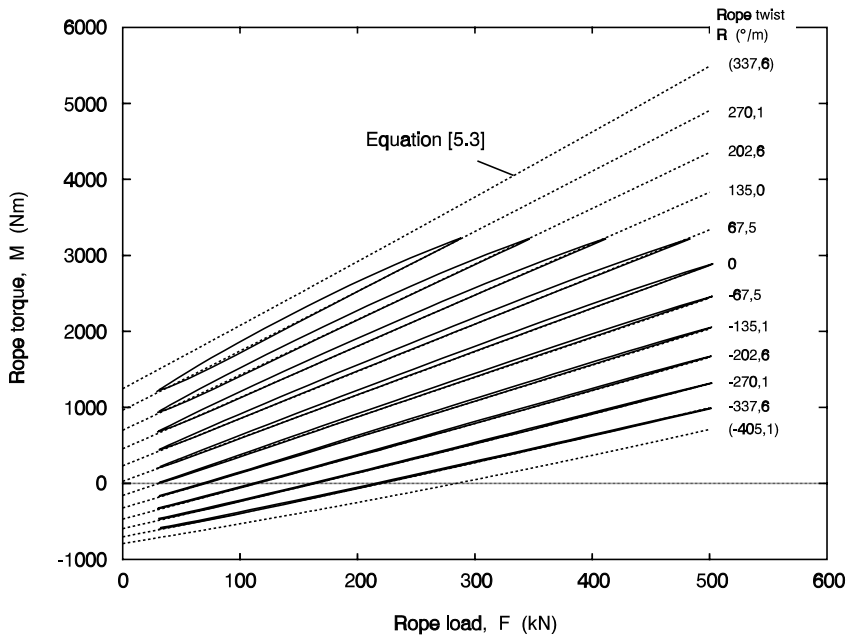

Figure C.16 - Measured and calculated rope torque versus load for rope T12, 54 mm, 6x32(14/12/6 + 3Δ)/F, 1950 MPa. N_{load} according to equation [C.23].

From the constant twist test on rope T12 :

$$N_{avg} = \begin{bmatrix} -1.0887e-009 & -2.4555e-012 & 2.3197e-003 \\ -4.0047e-006 & 8.7853e-003 & 2.9119e+000 \\ -5.8154e-004 & 5.9779e+000 & 2.6777e+001 \end{bmatrix} \qquad [C.22]$$

$$N_{load} = \begin{bmatrix} 4.8719e-009 & -2.2754e-007 & 2.1428e-003 \\ -4.7611e-007 & 7.7704e-003 & 2.8885e+000 \\ 2.1348e-005 & 5.6813e+000 & 2.6947e+001 \end{bmatrix} \qquad [C.23]$$

From the constant load tests on rope T12 :

$$a_{cl} = \begin{bmatrix} 71.2810 & 110.5330 & 145.2549 & 182.8773 & 234.6446 \\ 31.3190 & 49.4362 & 66.7132 & 83.8785 & 108.5738 \\ 15.2804 & 24.3076 & 33.1556 & 41.9466 & 54.4381 \\ 7.4373 & 11.2160 & 14.0543 & 18.5332 & 23.2867 \end{bmatrix} \qquad [C.24] \quad (Nm)$$

$$b_{cl} = \begin{bmatrix} 0.5851 & 0.4152 & 0.3247 & 0.2699 & 0.2261 \\ 0.7901 & 0.5570 & 0.4396 & 0.3803 & 0.3235 \\ 0.6553 & 0.5618 & 0.5537 & 0.4511 & 0.4473 \\ 0.2636 & 0.3003 & 0.4465 & 0.4297 & 0.4706 \end{bmatrix} \qquad [C.25] \quad (1/(°/m))$$

$$c_{cl} = \begin{bmatrix} 3.7479 & 5.4321 & 6.9268 & 8.4984 & 10.7176 \\ 3.9294 & 5.2284 & 6.2247 & 7.1706 & 8.7471 \\ 3.6496 & 4.7655 & 5.6381 & 6.4057 & 7.7656 \\ 3.0464 & 4.0349 & 4.9481 & 5.7247 & 7.0335 \end{bmatrix} \qquad [C.26] \quad (Nm/(°/m))$$

Constant loads corresponding to the columns of a_{cl}, b_{cl} and c_{cl} :

$$F_{cl} = [\ 60 \quad 160 \quad 260 \quad 360 \quad (500)\ ] \qquad (kN) \qquad [C.27]$$

Starting twists corresponding to the rows of a_{cl}, b_{cl} and c_{cl} :

$$R_{cl0} = \begin{bmatrix} (270) \\ 67 \\ -67 \\ 202 \end{bmatrix} \qquad (°/m) \qquad [C.28]$$

APPENDIX D : GRAPHICAL METHOD FOR DETERMINING ROPE LAY LENGTHS AT INSTALLATION

Details of an approximate graphical solution method for determining rope lay lengths changes at installation and the corresponding equilibrium rope torque are given in this appendix. The method relies on rope data measured during constant twist tests. Empirical knowledge of the position at which the manufactured lay length occurs at installation equilibrium is also required. During the parametric study reported in chapter seven, such information was determined for a wide variety of in-service conditions and is included in this appendix.

D.1 Theory

It is possible do determine the approximate equilibrium lay length distribution at installation by a graphical method. Equation [5.2] can be rewritten as twist in terms of lay length :

$$R = \frac{\arctan(\frac{\pi.d_0}{LL}) - \arctan(\frac{\pi.d_0}{LL_0})}{k_{LL}} \qquad [5.2b]$$

Combining [5.2b] with [5.3] results in an equation for torque in terms of load and lay length, $M = f(F,LL)$. Sectioning the surface, M, in the load - lay length plane will produce a family of curves for constant torque, as shown in figure D.1.

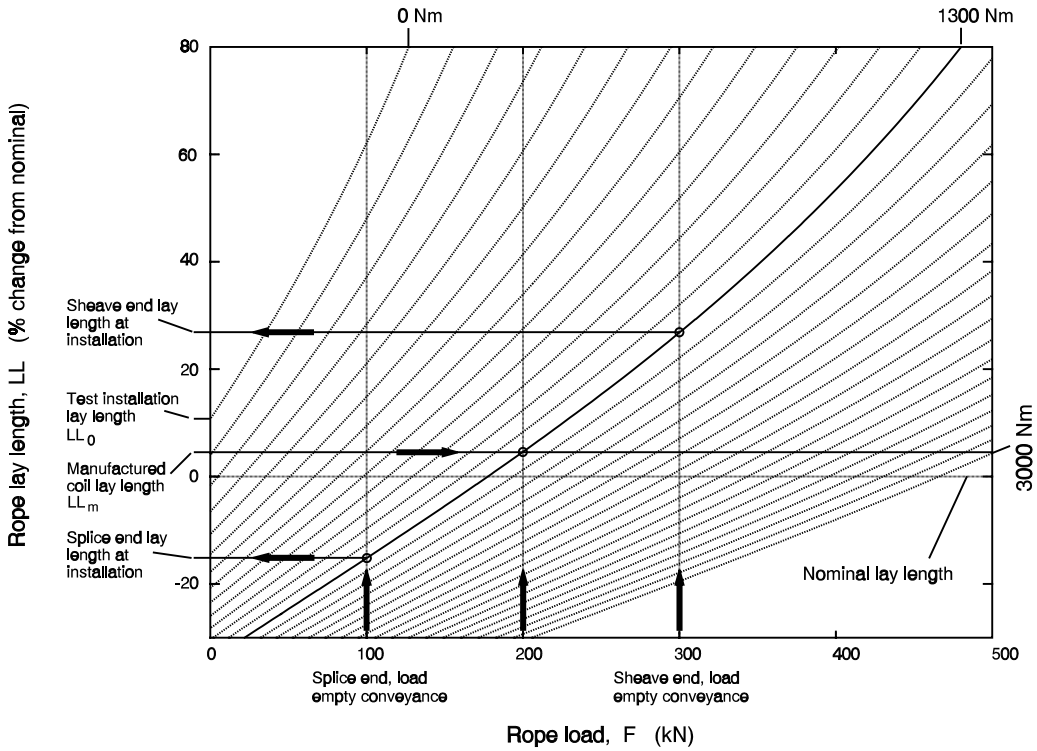

Figure D.1 - A graphical method for determining the equilibrium lay length distribution in a suspended rope at installation.

As an example, assuming that the manufactured lay length (LL_m) occurs at the midpoint of the suspended section, the equilibrium torque can be identified.
If the empty conveyance weight is say 100 kN and the rope load at the sheave (including rope weight) is 300 kN then the load at the midpoint would be 200 kN.

The intersection of the horizontal line, corresponding the manufactured lay length, and the vertical line for the midpoint load identifies the equilibrium torque line (1300 Nm). Projecting (horizontally) the intersection points of the vertical lines corresponding to the splice and sheave end loads to the vertical axis gives the splice and sheave end lay lengths. The complete lay length distribution can be determined by this method.

D.2 Position at which the manufactured lay length occurs

For the graphical method of determining in-service lay length changes at installation, it is necessary to know the point along the suspended rope at which the manufactured lay length occurs. Figure D.2 shows the results for the seven diameters considered in section 7.3.2. Figure D.3 contains the results for the all the parametric analyses conducted on the 46 mm rope, sections 7.3.3 to 7.3.6.

For the 46 mm rope analyses, only the rope length, $z_{max} - L$, had a more significant effect on the position at which the manufactured lay length occurs. The influence decreases with an increase in the suspended length.

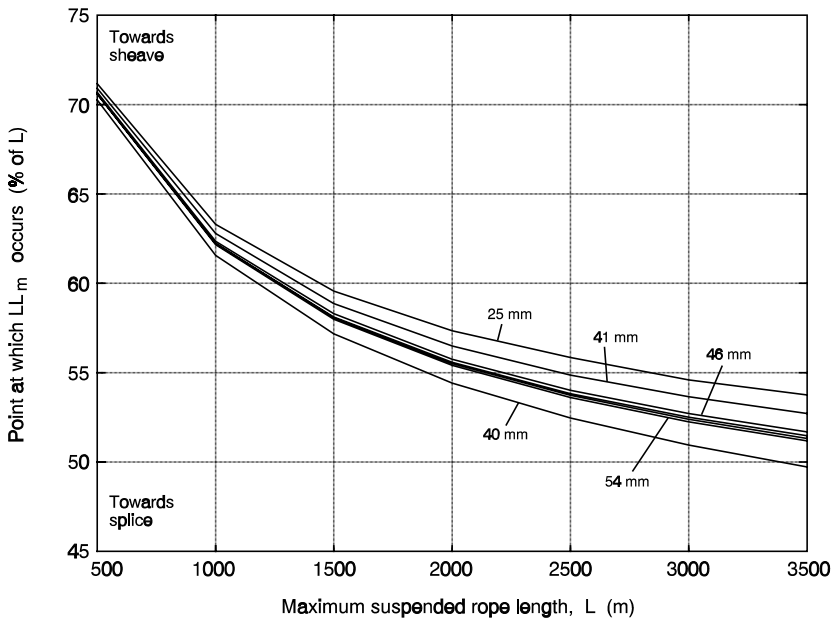

Figure D.2 - Position along the suspended rope length at which the manufactured lay length occurs (distance from splice). $z_{max} - L$ = 370 m, LL_m = 1,0371.LL_{nom}, f_s = 0,68 , nominal weight per unit length, q, used. The test method for the 40 mm rope differed from that for the other ropes.

This observation indicates that at as depth increases, the torsional behaviour of the suspended section becomes more dominant, as would be expected. The 46 mm data for 370 m (figure D.3) also corresponds to the average of the values in figure D.2.

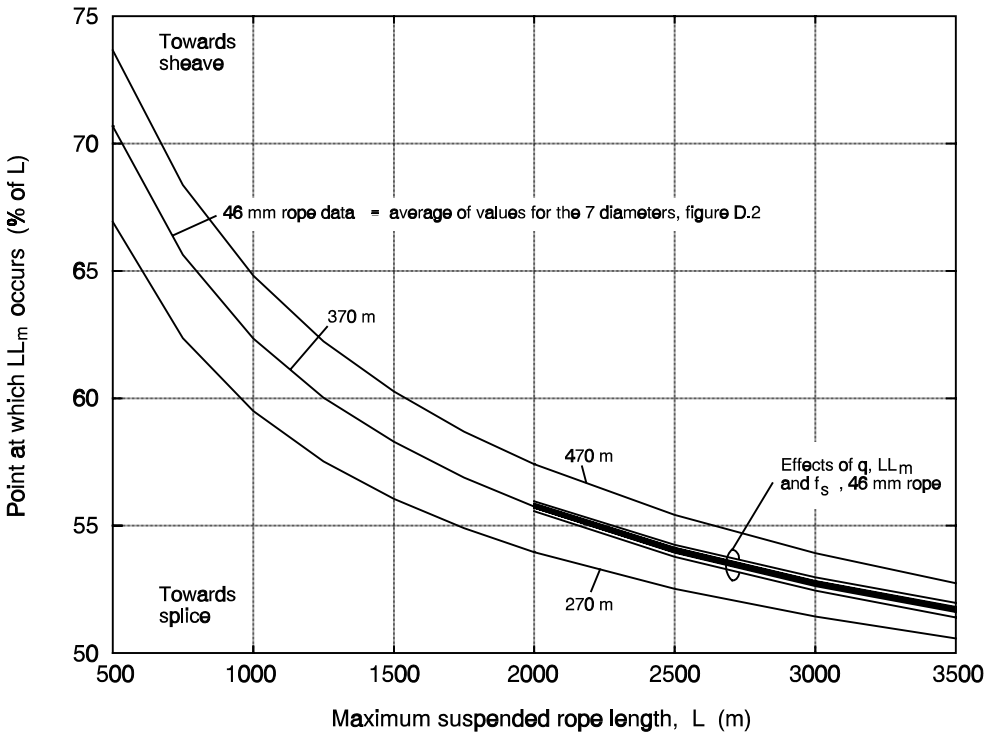

Figure D.3 - Position along the suspended rope length at which the manufactured lay length occurs (distance from splice). All the results of the calculations on the 46 mm rope are included, sections 7.3.3 to 7.3.6. The distances indicated refer to the lengths, z_{max} - L.

D.3 Information required for the graphical solution :

1. The accurate on-tension lay length (LL_m, figure 5.1) obtained from the manufacturer and converted to a percentage change from nominal :

$$(LL_m / LL_{nom} - 1).100 \qquad [D.1]$$

(The average value for the triangular strand ropes considered in this project was 3,71 percent)

2. Maximum suspended length, L (m).

3. Empty conveyance weight including all attachments, P_e (kN)

4. Rope weight per unit length, q (kN/m)

5. Point at which the on-tension lay length will occur at installation assuming that no rotation is lost from the rope during the installation process. Figure D.4 (data from figure D.3) gives approximate values of r_{LLm} which is the ratio of the position of the manufactured lay length to the total suspended length, L. Note that r_{LLm} is a function of the maximum suspended length and the difference between the maximum suspended length and the total rope length installed (z_{max} - L).

D.4 Procedure for determining estimates of the installation lay lengths :

1. For the specific rope diameter (figures D.5 to D.11), draw a horizontal line at LL_m as a percentage change from the nominal lay length.

2. Draw a vertical line at the load : P_e.

3. Draw a vertical line at the load : $P_e + q.L$.

4. Draw a vertical line at the load : $P_e + q.L.r_{LLm}$.

5. The point of intersection of the vertical line from 4 and the horizontal line from 1 defines the value of constant torque. Graphical, linear interpolation may be required if the intersection point lies in between two lines of constant torque.

6. The intersections of the line of constant torque (from 5) with the vertical lines from 2 and 3 projected back to the vertical axis gives the lay lengths at the splice and sheave ends respectively. Any other point, on the line of constant torque, projected back to the vertical axis will give the lay length at that specific position along the suspended length.

If the accurate lay length at a specific position along a suspended rope is known, then the rope torque can be determined for an empty conveyance and so can the lay lengths at all other position along the rope.

D.5 Curves for graphical lay length solution

Figures D.4 to D.11 contain the data required for the graphical lay length solution method for ropes T1, T4, T8, T9, T10, T11 and T12. Refer also to tables 4.3, 4.4 and 7.1.

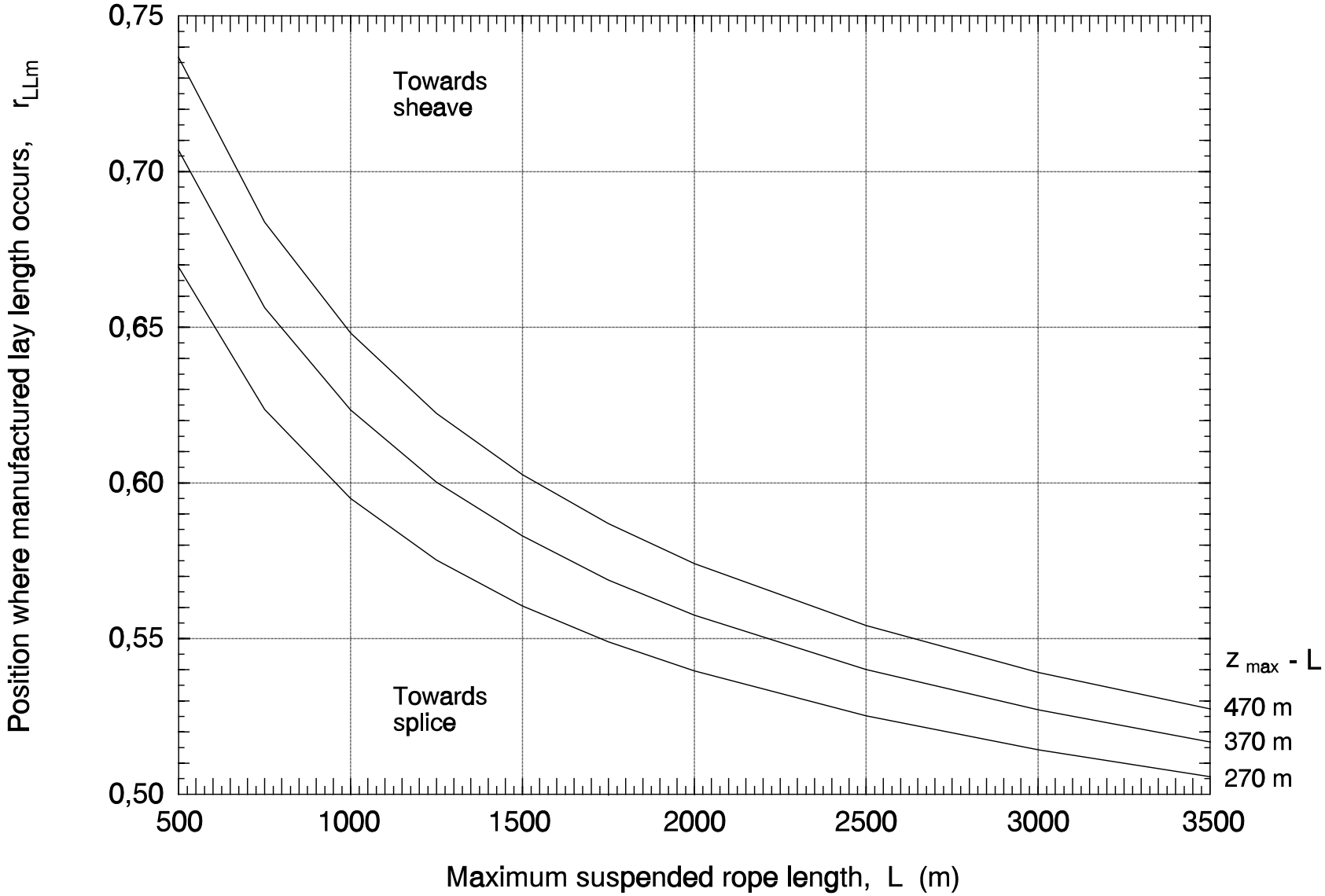

Figure D.4 - Approximate values of r_{LLm} for graphical lay length solution method (equivalent to the value [z for R_{coil}]/L).

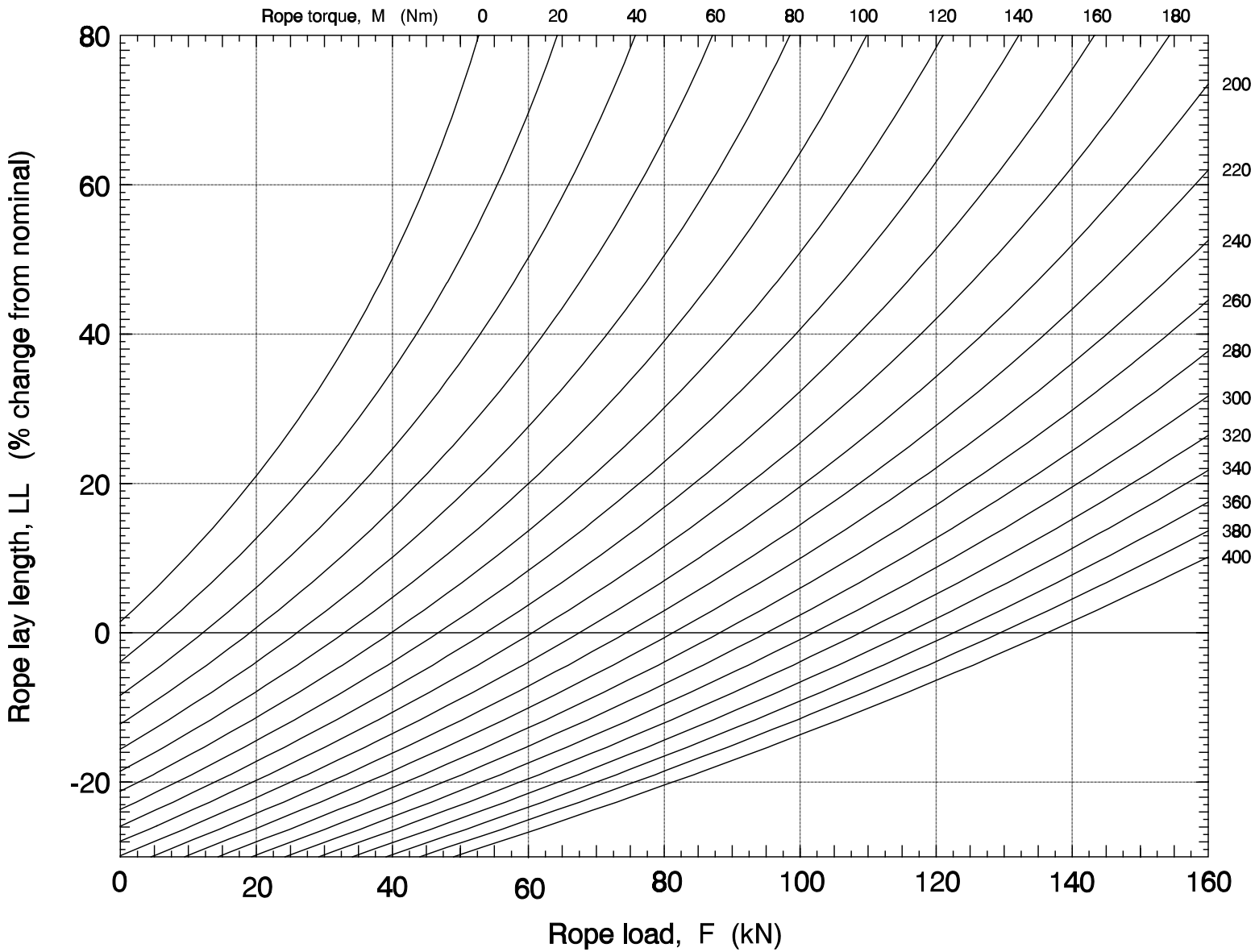

Figure D.5 - Data for graphical lay length solution method, rope T1, 25 mm, 6x27(9/12/6 + 3Δ)/F, 1800 MPa, q = 0,0257 kN/m.

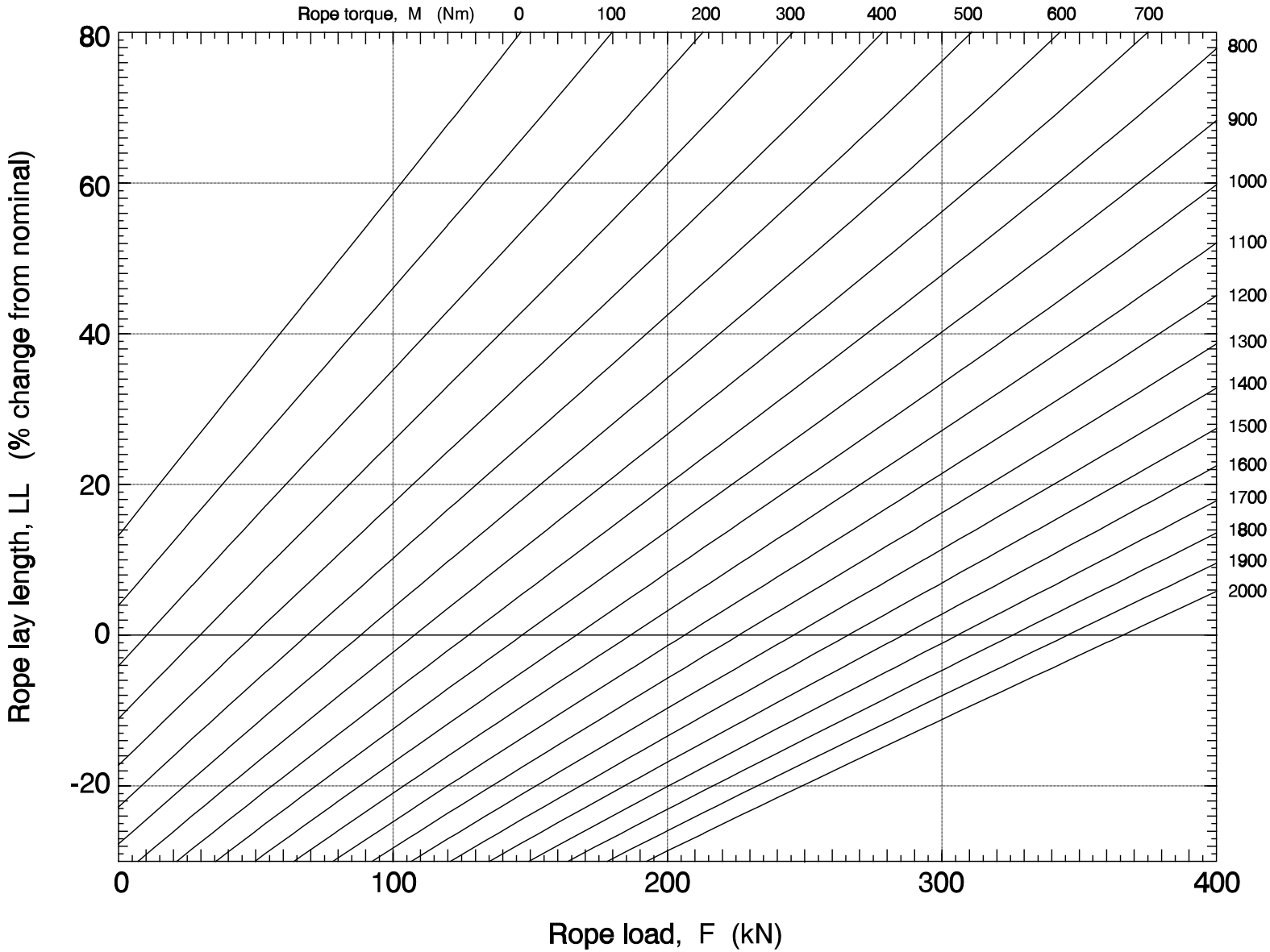

Figure D.6 - Data for graphical lay length solution method, rope T4, 40 mm, 6x29(11/12/6 + 3Δ)/F, 1800 MPa, q = 0,0665 kN/m.

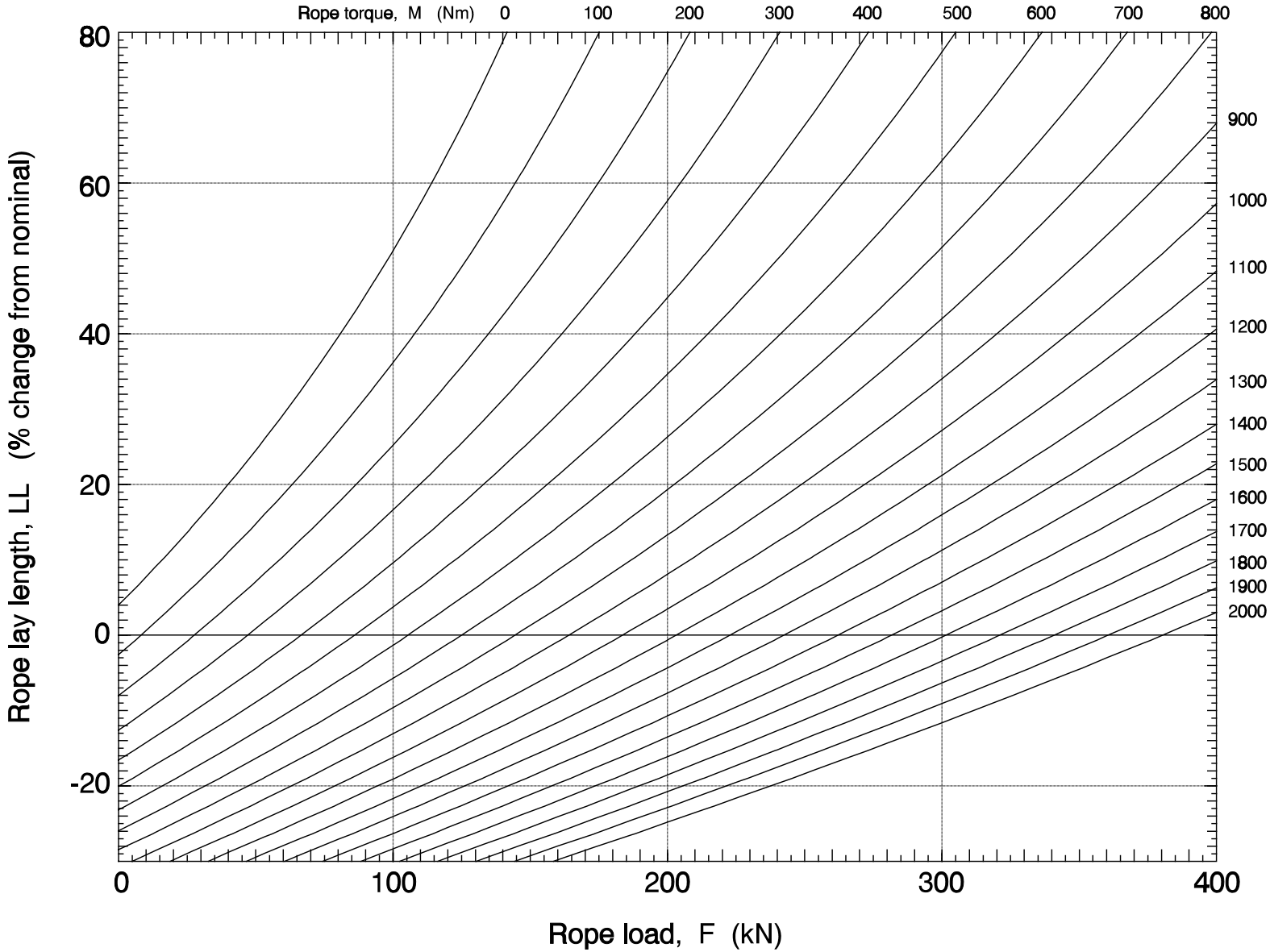

Figure D.7 - Data for graphical lay length solution method, rope T8, 41 mm, 6x29(11/12/6 + 3Δ)/F, 1800 MPa, q = 0,0705 kN/m.

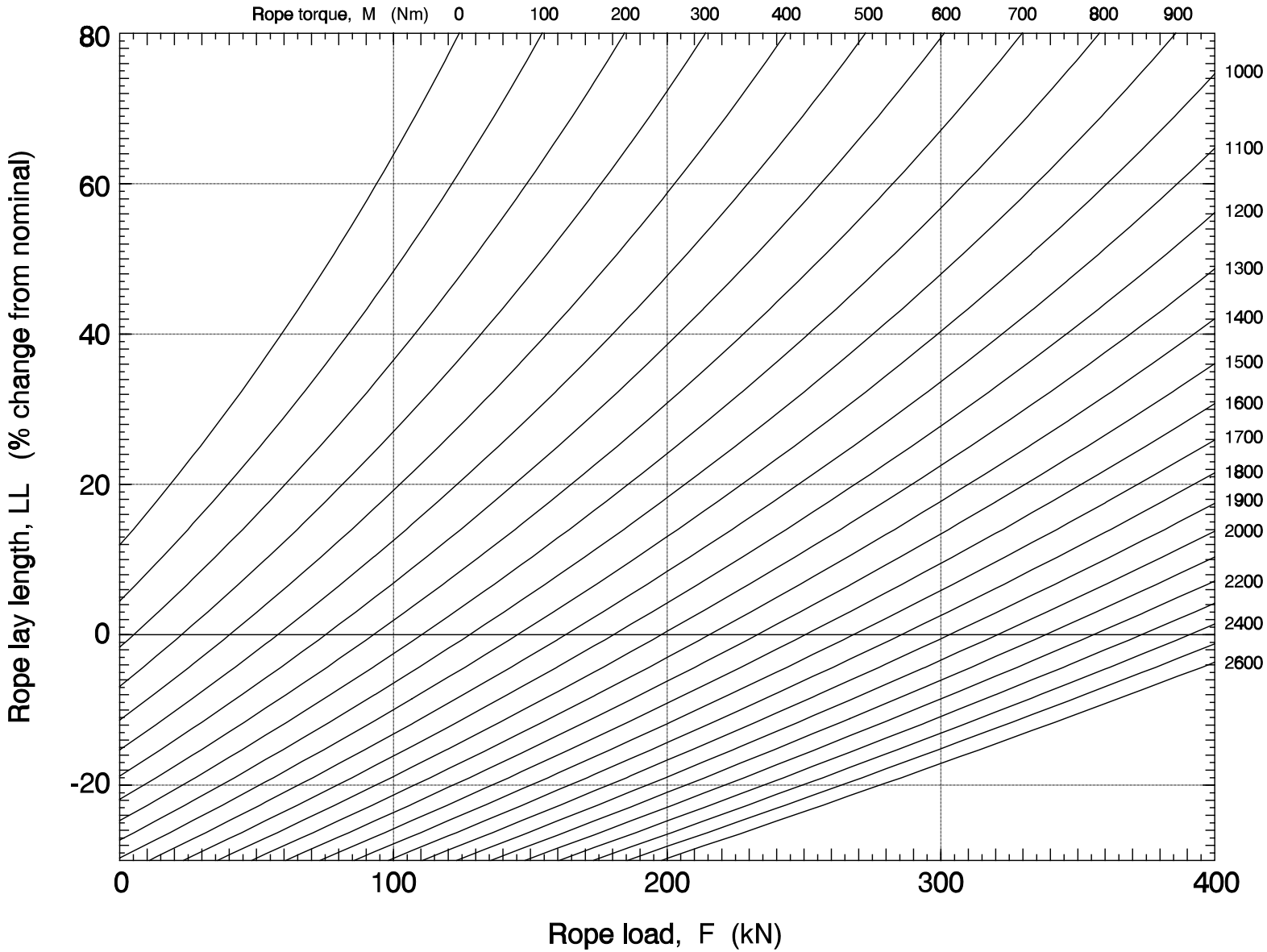

Figure D.8 - Data for graphical lay length solution method, rope T9, 46 mm, 6x31(13/12/6 + 3Δ)/F, 1800 MPa, q = 0,0887 kN/m.

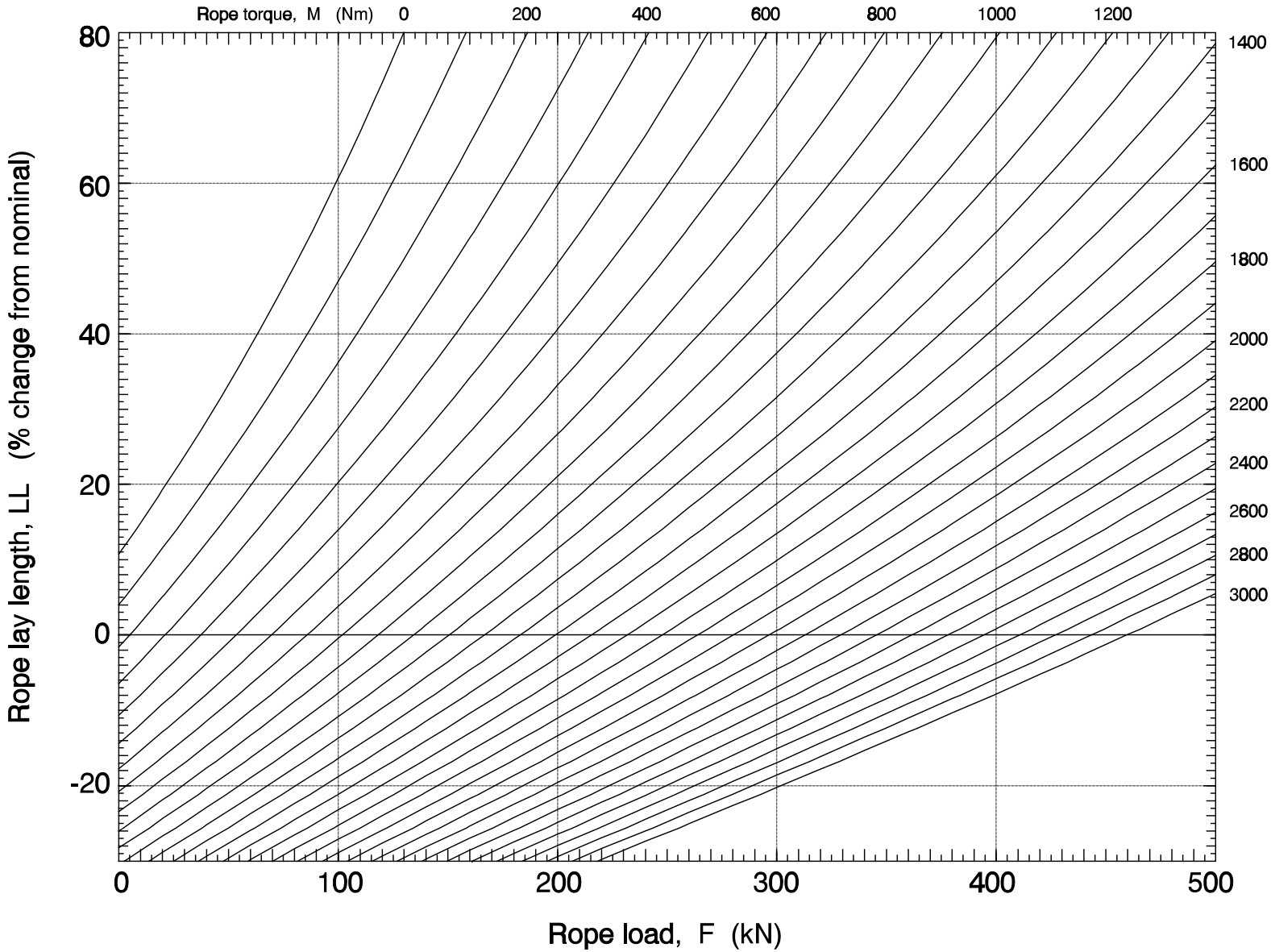

Figure D.9 - Data for graphical lay length solution method, rope T10, 48 mm, 6x32(14/12/6 + 3Δ)/F, 1800 MPa, q = 0,096 kN/m.

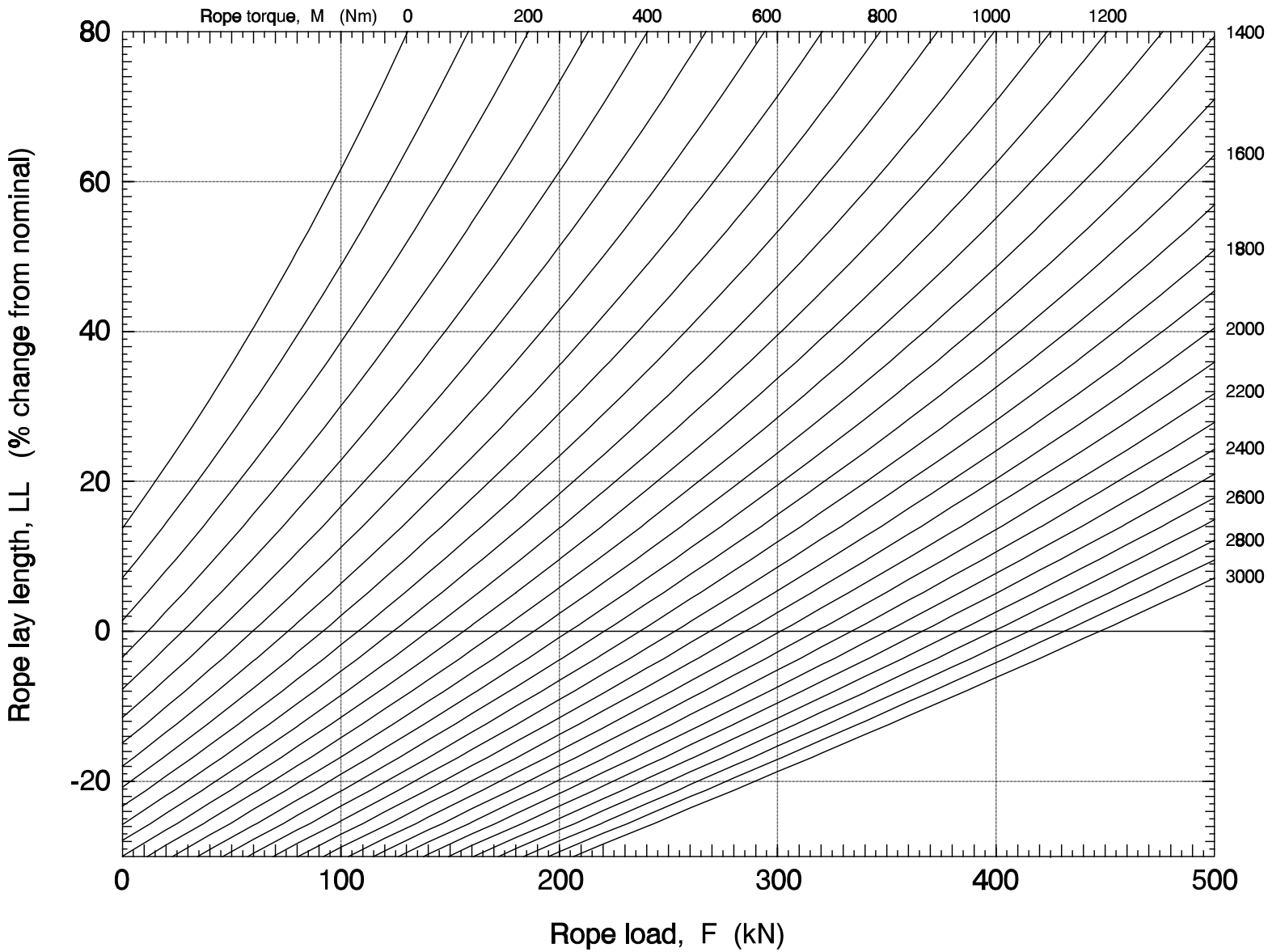

Figure D.10 - Data for graphical lay length solution method, rope T11, 49 mm, 6x32(14/12/6 + 3Δ)/F, 1800 MPa, q = 0,0995 kN/m.

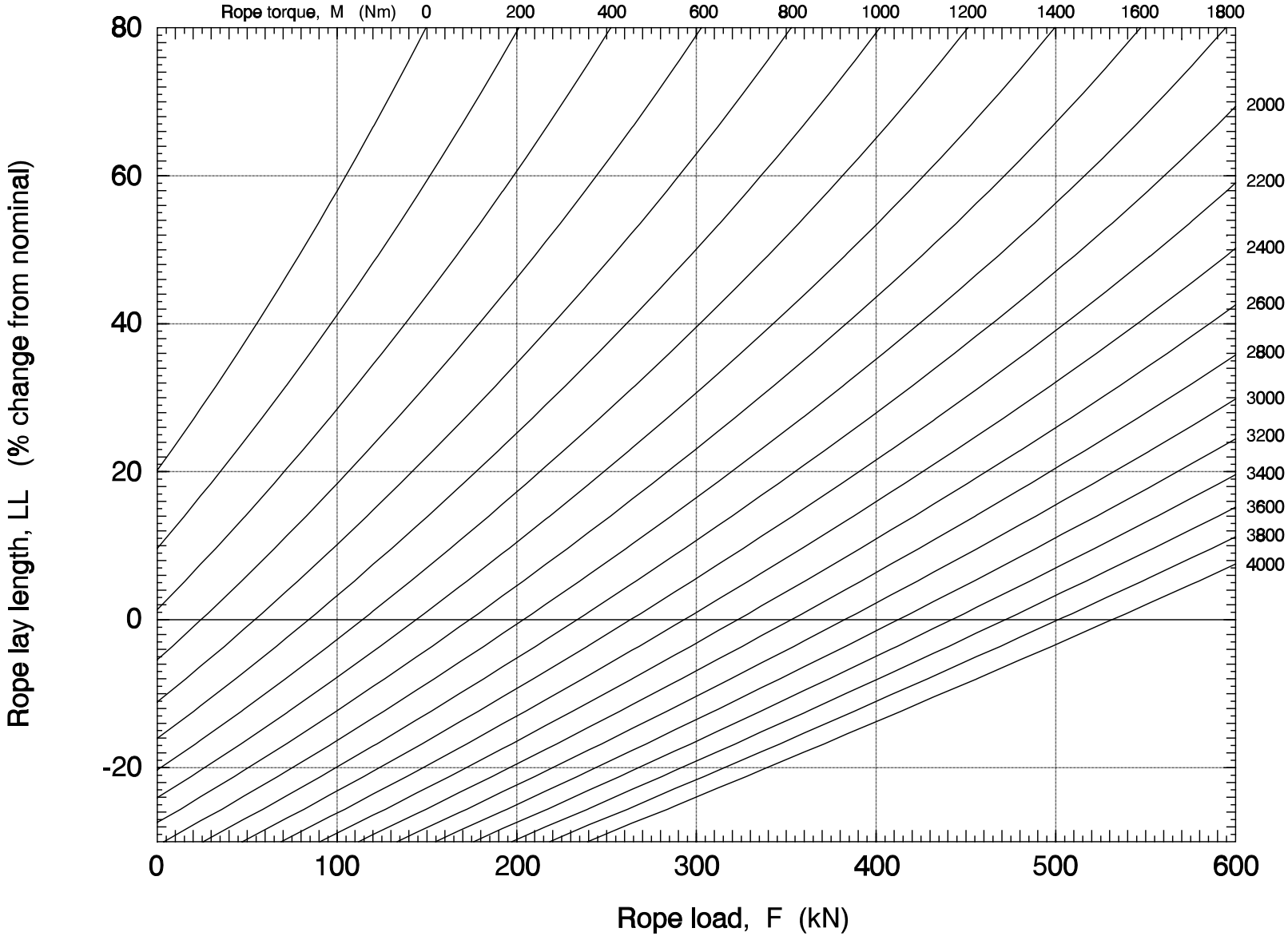

Figure D.11 - Data for graphical lay length solution method, rope T12, 54 mm, 6x32(14/12/6 + 3Δ)/F, 1950 MPa, q = 0,1229 kN/m.

REFERENCES

ALBERT, L., McIVOR, R.A. (1988), *Aluminum mine shaft conveyances at Inco Limited - an overview of problems encountered and solutions*, CIM Bulletin, Vol. 81, No. 916, August 1988, pp 61-65.

ANON., (1972), *Ultra high tensile wire ropes for hoisting from depth*, South African Mining and Engineering Journal, February 1972, pp 19-23.

ANON., (1990), *Kevlar rope eyed for mine-hoist applications*, Coal, Vol. 96, No. 3, March 1990, p 73.

ARCHER, L.G. (1971), *The interpretation of data given on the certificate of test conducted on a winding rope*, The Certificated Engineer, December 1971, pp 263-273

BEAVON, K. (1996), *Johannesburg : 1886-1896*, Article published in the Alumni publication of the University of the Witwatersrand, ARENA, Vol. 3 No. 9, April 1996, pp 12-16.

BEHR, H.C. (1902), *Winding plants for great depths*, Transactions of the Institute of Mining and Metallurgy, Vol. XI, Parts I and II.

BORELLO, M. (1991), *Sixth report on the in-service damage accumulate by wire ropes operating on drum winders*, CSIR Mine Hoisting Metallurgical and Corrosion Services, Report No. MST(91)MC702, April 1991.

CAMPBELL PITT, L.T. (1961), *Winding plant of the gold mines of South Africa*, Transactions of the Seventh Commonwealth Mining and Metallurgical Congress, South African Institute of Mining and Metallurgy, Vol. 3, Johannesburg, 1961, pp 1203-1231.

CANTIN, M.M. et al. (1993), *Experimental analysis and modelisation of the stiffness in torsion of wire ropes*, Proceedings OIPEEC Round Table Conference, Delft, September 1993, pp 11.67-11.77.

CARBOGNO, A., CZAJA, J. (1982), *The testing of double layered hoisting ropes unwinding moment*, Zeszty Naukowe Politechniki Slaskiej, Gornictwo z. 116, Nr kol. 717, pp 95-104 (in Polish).

CARBOGNO, A. (1991), *Hoisting ropes in deep shafts*, Zeszty Naukowe Politechniki Slaskiej, Gornictwo z. 209, Nr kol. 1193, pp 77-116 (in Polish).

CARBOGNO, A., (1995), *Examination of the mechanical properties of flat steel rubber balance ropes manufactured by SAG*, SAG Bulletin No. 3 (8), 1995, pp 1-22.

CHAPLIN, C.R. (1993), *Hoisting ropes for drum winders - the mechanics of degradation*, Proceedings of the Second International Conference, Mine Hoisting 93, Royal School of Mines, London, 28-30 June 1993, pp 12.1.1-12.1.10.

CISKO, G.J., PHILLIPS, J.W. (1986), *A tension torsion loadcell for wire rope*, Experimental Techniques, December 1986, pp 18-20.

COSTELLO, G.A. (1978), *Analytical investigation of wire rope*, Applied Mechanics Reviews, Vol. 31, No. 7, July 1978, pp 897-900.

COSTELLO, G.A., MILLER, R.E. (1980), *Static response of reduced rotation rope*, Journal of Engineering Mechanics, Proceedings of the ASCE, Vol. 106, EM4, August 1980, pp 623-631.

CRAIB, S. (1965), *Winding from deep levels in South Africa*, Fourth International Mining Conference, Paper D2, 1965, pp 1-10.

DAVIS, M.L. (1996), *Financial risks associated with deep level mining*, South African Institute of Mining and Metallurgy Colloquium : Deep Level Mining - The Challenges, Johannesburg, 14 March 1996.

DREHER, F. (1934), *A contribution to the theory of rotation and stress distribution in loaded strands and ropes*, Die Wasserwirtschaft, Vol. 27, No. 7-8, 1934, (in German).

DURAT, P. (1993), *Experience with solid plastic core ropes*, International Aerial Lift Review, 1/1993 p9.

FEYRER, K., SCHIFFNER, G. (1986,1987), *Torque and torsional stiffness of wire rope Parts I and II*, Wire, 36(1986)8, pp 318-320, Wire, 37(1987)1, pp 23-27.

FRITZ, J.T.D. (1982), *The Mine Equipment Research Unit and its contribution towards ensuring safe winding practice*, Paper No. 14, Symposium on Mine Winding Plant, Institution of Certificated Mechanical and Electrical Engineers, Johannesburg, September 1982, pp 1-13.

FULLER, C.N.L, WAINWRIGHT, E.J. (1967), *Recent developments in steel wire ropes for hoisting from great depths*, The South African Mechanical Engineer, June 1967, pp 238-245.

GIBSON, P.T. et al. (1969), *Torsional properties of wire rope*, ASME Design Engineering Division Conference and Exhibit, May 1969, pp. 1-11.

GIBSON, P.T. et al. (1970), *Analysis of wire rope torque*, Wire and Wire Products, November 1970, pp 50-60.

GIBSON, P.T. (1980), *Wire rope behaviour in tension and bending*, Proceedings of the First Annual Wire Rope Symposium, Denver Colorado, Published by the Engineering Extension Service, Washington State University, pp 3-31.

GINDY, S.S. (1985), *Force and torque measurement, a technology overview part II - torque*, Experimental Techniques, July 1985, pp 9-15?.

GIRODO, A.M., SPARG, E.N. (1995), *South African hoisting systems with emphasis on Blair Multi-Rope hoists*, CIM Bulletin, 88(1995)987, Feb 1995, pp 43-49.

GLENDAY, W.B. (1989), *Development of shaft steelwork as applied to deep, circular shafts: design and installation aspects*, South African Institute of Mining and Metallurgy Colloquium : Shaft Sinking - Current Practices and Future Trends, Johannesburg, 20 September 1989.

GLUSHKO, M.F. (1966), *Steel lifting ropes*, Kiev, Technika, 1966, p 327.

GREENWAY, M.E. (1990), *An engineering evaluation to the limits to hoisting from great depth*, International Deep Mining Conference : Technical Challenges in Deep Level Mining, Vol 2, Johannesburg, SAIMM, 1990.

GYNGELL, A.H. (1967), *Hoisting equipment and shaft design in the deep-level South African gold mines*, Presentation made to the 69th Annual General Meeting of the Canadian Institute of Mining and Metallurgy, March 1967, Published in the CIM Bulletin, January 1968, pp 1-11.

HAGGIE RAND (1987), *Steel wire ropes for mine hoisting*, Product Catalogue, November 1987.

HAID, K.D. (1983), *Determination of forces in stranded ropes*, Wire 33(1983)1, 1983, pp 1-5.

HALLER, A. (1989), *Experience with untwisted ropes*, OIPEEC Round Table Conference, Zurich, September 1989.

HANKUS, J. (1993a), *Elongation and contraction of mine hoisting ropes*, Proceedings of the Second International Conference, Mine Hoisting 93, Royal School of Mines, London, 28-30 June 1993, pp 12.5.1-12.5.7.

HANKUS, J. (1993b), *Non-typical process of the progressive weakening of mining hoist rope*, Proceedings OIPEEC Round Table Conference, Delft, September 1993, pp 11.21-11.34.

HANKUS, J. (1995), *Longitudinal and torsion displacements of winding ropes*, Proceedings of the Sixth Underground Operators Conference, Western Australia School of Mines, Kalkoorlie, November 1995, pp 201-205.

HANKUS, J. (1996), *The results of experiments on large diameter winding ropes*, Proceedings of the Mine Hoisting '96 International Conference, Vol. 2, Gliwice, Poland, October 1996, pp 55-58.

HARVEY, T., KRUGER, H.W. (1959), *The theory and practice of electronic testing of winding ropes*, The Transactions of the South African Institute of Electrical Engineers, June 1959, pp 126-181.

HECKER, G.F.K, van ZYL, M.N. (1993), *Drum winder rope test facility : a feasibility study*, CSIR Contract Report MST(93)MC1233, January 1993.

HECKER, G.F.K. (1990), *The safety of hoisting ropes in deep mine shafts*, International Deep Mining Conference : Technical Challenges in Deep Level Mining, Vol 2, Johannesburg, SAIMM, 1990.

HERMES, J.M., BRUENS, F.P. (1957), *The twist variations in a non-non-spin rope of a hoist installation*, Geologie and Mijnbouw (NW. SER.), 19e Jaargang, November 1957, pp 467-476 (in Dutch).

HOTTINGER BALDWIN MESSTECHNIK GMBH (1990), *The proper use of torque transducers*, Darmstadt, Germany, 1990, pp 1-63.

HRUSKA, F. (1953), *Tangential forces in wire ropes*, Wire and Wire Products, May 1953, pp 455-460.

KARAMCHETTY, S.D.S.R. (1980), *Some geometrical characteristics of wires in wire ropes and cables*, Wire Journal, November 1980, pp 98-104.

KOLLROS, W. (1976), *The relationship between torque, tensile force and twist in ropes*, Wire, January/February 1976, pp 19-24.

KUUN, T.C. (1968), *Preliminary design study of a universal winding rope fatigue testing machine*, National Mechanical Engineering Research Institute, CSIR Report No. CN 499, Pretoria, August 1962.

KUUN, T.C. (1993), *Low rotation winding ropes for long lift drum winders,* Unpublished Internal Report, Anglo American Corporation, May 1993, pp 1-7.

KUUN, T.C. (1995), *Practical aspects of rope inspection*, Rope Condition Assessment Training Module for Rope Inspectors, Safety in Mines Research Advisory Committee Project No. GAP054, Johannesburg, November 1995.

KUUN, T.C., WAINWRIGHT, E.J., DOHM, M.A.R., van der WALT, W.P. (1993), *Condition assessment of winding rope*, Proceedings of the Second International Conference, Mine Hoisting 93, Royal School of Mines, London, 28-30 June 1993, pp 6.2.1-6.2.6.

LANE, N.M. (1990), *Constraints on deep level sinking - an engineering point of view*, The South African Certificated Engineer, December 1989/ January 1990, pp 3-9/ pp 7-15.

LANG, J. (1879), *Improvements in the construction of wire ropes*, British Patent Number 138, 13 January 1879.

LAUBSCHER, P.S. (1995), *Rope factors of safety for drum winders - implications of the proposed amendments to the regulations,* GENCOR Group Shaft Safety Workshop, Johannesburg, November 1995.

LAYLAND C.L., RAO, B.E., RAMSDALE, H.A. (1951), *Experimental investigation of torsion in stranded mining wire ropes*, Transactions of the Institution of Mechanical Engineers, M.S. received July 1951, pp 323-336. (Authors affiliated to the Mysore Gold Mining Company (K.G.F), India)

LEE, W.K. et al. (1987), *Helix geometry in wire rope*, Wire Industry, August (1987), pp 461-468.

LEE, W.K. (1991), *An insight into wire rope geometry*, International Journal of Solid Structures, Vol. 28, No. 4, 1991, pp 471-490.

LESNAK, O. (1983), *Ways of improving safety of haulage and balance ropes*, National Coal Board Publication, Numbered G6, March 1983.

LUCHT, W.A., DONECKER F.W. (1981), *Torque balanced wire rope*, SAE Technical Paper Series, 810980, International Off-Highway Meeting & Exposition, Milwaukee, September 1981.

MacDONALD D.H., PIENAAR F.C. (1994), *State of the art and future developments of steel wire rope in sinking and permanent winding operations*, GENCOR GROUP, Shaft Safety Workshop, Magaliesberg, November 1994.

MACHIDA, S., DURELLI, A.J. (1973), *Response of a strand to axial and torsional displacements*, Journal of Mechanical Engineering Science, Vol. 15, No. 4, 1973.

McGRATH, B. (1994a), *Solving a mooring mystery*, Wire Rope News and Sling Technology, August 1994, 29-30 and 34-35.

McGRATH, B. (1994b), *Setting the standard for wire rope aboard research vessels*, Wire Rope News and Sling Technology, August 1994, p23.

McGRATH, B. (1995), *Whitehill Manufacturing Co. : on target with Kevlar rope*, Wire Rope News and Sling Technology, August 1995, pp 36-38.

McKENZIE, I.D. (1987), *The torsional properties of steel wire ropes*, A dissertation in fulfilment of the requirements for registration as a Professional Engineer, University of the Witwatersrand, Johannesburg, July 1987.

McKENZIE, I.D. (1989), *The design of steel wire ropes*, M.Sc. Dissertation, University of the Witwatersrand, Johannesburg, South Africa, July 1989.

McKENZIE I.D., (1990a) *Steel wire hoisting ropes for deep shafts*, International Deep Mining Conference : Technical Challenges in Deep Level Mining, Vol 2, Johannesburg, SAIMM, 1990, pp 839-844.

McKENZIE, I.D. (1990b), *Patent specification : reduced mass rope*, South African Provisional Patent Application No. 89/8857, 21 November 1989, Applicant : Haggie Rand Limited.

MCKENZIE, I.D. (1993), *Haggie can compete with the world's best in steel wire rope*, Mining Mirror, November 1993, pp 41-42.

MILBURN, D.A., RENDLER, N.J. (1972), *Methods of measuring the mechanical behaviour of wire ropes*, Naval Research Laboratory, Washington D.C., Report No. 2459, July 1972.

OPLATKA, G. (1994), *Running wire ropes in rope-ways*, Wire 44(1994)1, pp 95–101.

OPLATKA, G., ROTH, M. (1996), *Endurance of wire ropes under fluctuating tension and twist : influence of rope lay (type)*, OIPEEC Bulletin 71, June 1996.

PENNUCUICK, K. (1963), *A unique wire rope testing device*, Strands, House Journal of the British Rope Group, Vol. 1, No. 3, 1963.

PICKERING, R.G.B. (1996), *Deep level mining and the role of research and development*, Journal of the South African Institute of Mining and Metallurgy, Sep/Oct 1996, pp 173-176.

RAOOF, M., HOBBS, R.E. (1988a), *Torsion tests on large spiral strands*, Journal of Strain Analysis, Vol. 23, No. 2, 1988.

RAOOF, M., HOBBS, R.E. (1988b), *Analysis of multi-layered structural strands*, Journal of Engineering Mechanics, Vol. 114, No. 7, July 1988

RAOOF, M., HOBBS, R.E. (1989), *Torsional stiffness and hysteresis in spiral strands*, Proceedings of the Institution of Civil Engineers, Paper 9455, Part 2, **87**, December 1989, pp 501-515.

RAOOF, M., KRAINCANIC, I. (1994), *Critical examination of various approaches used for analysing helical cables*, Journal of Strain Analysis, Vol. 29, No.1, pp 43-55, ISSN : 0309-3247.

REBEL, G. (1993), *Model of the torque-tension rotation behaviour of a 48 mm triangular strand steel wire rope operating on a drum winder*, B.Sc. Engineering Dissertation, University of the Witwatersrand, Johannesburg, November 1993.

REBEL G. (1995), *Results of preliminary tests to determine the effect of changes in rope specimen lay length on tensile test results*, Unpublished Internal Report, School of Mechanical Engineering, University of the Witwatersrand, December 1995.

REBEL, G. (1996), *Technical and operating manual for the steel wire rope torque-tension testing machine*, Version 1.1, CSIR Mine Hoisting Technology, Cottesloe, Johannesburg, April 1996, pp 1-226 with 33 additional technical reference and product specifications documents.

REBEL G., CHANDLER H.D. (1996), *A machine for the tension-torsion testing of steel wire ropes*, OIPEEC Bulletin No. 71, June 1996, pp 55-73.

REBEL, G., BORELLO, M., CHANDLER, H.D., (1996a) *On the torsional behaviour of triangular strand hoisting rope*, Journal of the South African Institute of Mining and Metallurgy, Vol. 96, No. 6, November 1996, pp 279-287.

REBEL, G., BORELLO, M., CHANDLER, H.D. (1996b), *The torsional behaviour of steel wire ropes for deep level mine hoisting*, Proceedings of the Mine Hoisting '96 International Conference, Vol. 2, Gliwice, Poland, October 1996, pp 5-12.

RIDGE, I.M.L. (1993), *The development of rope*, OIPEEC Bulletin No. 65, June 1993, pp 15-46.

RIDGE, I.M.L. (1996), *Bibliographic review of OIPEEC technical publications 1963–1995*, Reading Rope Research, May 1996.

SCHREMS, K.K. (1994), *Wear related fatigue in wire rope failure*, Journal of testing and evaluation, JTEVA, Vol. 22, No.5, September 1994, pp 490-499.

SHELLY, P.D. (1974), *An analysis of tail rope behaviour*, The South African Mechanical Engineer, Vol. 24, December 1974, pp 1-18 (reprinted).

SPARG, E.N., (1993), *Developments in hoist design technology applied to a 4000 m deep shaft*, Proceedings of the Second International Conference, Mine Hoisting 93, Royal School of Mines, London, 28-30 June 1993, pp 10.2.1-10.2.11.

SYKES D.G., WIDLAKE A.C. (1990), *Reducing rope factors of safety for winding in deep level shafts*, International Deep Mining Conference : Technical Challenges in Deep Level Mining, Vol 2, Johannesburg, SAIMM, 1990.

UTTING, W.S. (1994a), *Survey of literature on the behaviour of steel wire ropes - Part I*, Wire Industry, September 1994, pp 633-635.

UTTING, W.S. (1994b), *Survey of literature on the behaviour of steel wire ropes - Part II*, Wire Industry, November 1994, pp 746-748.

UTTING, W.S. (1995), *Survey of literature on the behaviour of steel wire rope - Part III*, Wire Industry, May 1995, pp 269-270.

UTTING, W.S., JONES, N. (1984) *Survey of literature on the behaviour of steel wire ropes*, Wire Industry, September 1984, pp 623-629.

UTTING, W.S. , JONES, N. (1985), *Tensile testing of a wire rope strand*, Journal of Strain Analysis, Vol 20, No. 3, 1985.

UTTING, W.S. , JONES, N. (1987), *The response of wire rope strands to axial tensile loads*, Parts I and II, International Journal of Mechanical Science, Vol 29, No. 9, 1987, pp 605-619, pp 621-636.

UTTING, W.S. , JONES, N. (1988), *Axial-torsional interactions and wire deformations in a 19-wire spiral strand*, Journal of Strain Analysis, Vol 23, No. 2, 1988.

VAN ZYL, C.J. (1956), *The preparation, test and examination of steel wire rope specimens at the Government Mechanical Laboratory, Cottesloe, Johannesburg*, Journal of the Institute of Certificated Engineers, Vol. 29, March 1956, pp 79-109.

VAUGHAN, J.A. (1918), *Safety in winding operations*, The South African Journal of Science, Nov-Dec 1918, pp 1-12.

VERREET, R. (1986), *The technical properties of the Albert rope, a comparison with modern rope constructions*, Wire 36(1986)1, 1986, pp 13-15.

VERREET, R. (1989), *Wire rope : History of its invention and development*, Wireworld 6-89, 1989, pp 68-76.

VILJOEN, R.P. (1996), *The importance of geology in deep level mining*, South African Institute of Mining and Metallurgy Colloquium : Deep Level Mining - The Challenges, Johannesburg, 14 March 1996.

WAINWRIGHT, E.J. (1990), *Mine hoisting in South Africa*, International Seminar on Shaft Hoisting Technology, Gornictwo z. 193, Gliwice, Poland, 1990, pp 161-172.

WAINWRIGHT, E.J. (1988), *The manufacture and current development of wire rope for the South African mining industry*, International Conference on Hoisting of Men, Materials and Minerals, Canadian Institute of Mining and Metallurgy, Toronto, Canada, June 1988.

WAYMAN, W.T.L. (1973), *Notes on signposts and milestones in hoisting on the Witwatersrand*, Paper No. 1, International Conference on Hoisting of Men Materials and Minerals, The South African Institute of Mechanical Engineers, Johannesburg, October 1973, pp 13-22.

YIASSOUMIS, J.M. (1992), *Torsional behaviour of wire ropes for koepe winders*, M.Sc. Dissertation, University of the Witwatersrand, Johannesburg, South Africa, 1992.